The design and synthesis of novel 17 hydroxysteroid dehydrogenase inhibitors as anti-cancer agents

Springall, Jeremy

Award date:
2012

Awarding institution:
University of Bath

The Design and Synthesis of Novel 17β Hydroxysteroid Dehydrogenase Inhibitors as Anti-cancer Agents

Jeremy Samuel Springall

Volume 1 of 1

A thesis submitted for the degree of Doctor of Philosophy

University of Bath, Department of Pharmacy and Pharmacology

June 2012

Signed…….

Date……..

Abstract

The design, synthesis and biological evaluation of novel steroidal inhibitors of 17 β-Hydroxysteroid dehydrogenase type 1 which converts estrone into the highly potent estrogen, estradiol, is described. This isozyme has been implicated as a new drug target against hormone-dependent tumours which are stimulated by increased levels of estradiol.

Initial targets were planned, around modifications of the steroidal estrone / estradiol core, utilising Mannich, Friedel-Crafts and amide coupling chemistry. When the biological activity of these compounds was evaluated in a cell-based 17β-HSD1 assay, significant inhibitory action was observed. The most potent compound was (13*S*)-3-hydroxy-13-methyl-2-(morpholinomethyl)-7,8,9,11,12,13,15,16-octahydro-6*H*-cyclopenta[a]-phenan-thren-17(14*H*)-one **128** with an IC_{50} of 723 nM, **128** was also shown to be selective for 17βSHD1 over 17β-HSD2 and does not display any cytotoxicity at 50 μM over a 96 hour period in estrogen receptor positive and estrogen receptor negative cells.

A C16 extended linked and reverse amide series were synthesised, for which design was based upon STX1040 **1** the most potent inhibitor in the literature. The most biologically active compound was *N*-(((13*S*,16*R*,17*S*)-2-ethyl-3,17-dihydroxy-13-methyl-7,8,9,11,12,13,14,15,16,17-decahydro-6*H*-cyclopenta[a]-phenan-thren-16-yl)methyl)-2-(pyridin-3-yl)acetamide **186** with a percentage inhibition of 81% at 10 μM. Similar biological activities were observed for the rest of this series, however these values are approximately 20% lower than those observed for STX1040 **1**.

Quantities of H_6-17β-HSD1 were successfully synthesised and purified for use in development of a novel MTS/PES recombinant protein assay, to assess the inhibitory potential of the novel steroidal compounds described and their modes of binding with the active site of 17β-HSD1. For these experiments it can be tentatively concluded that STX1040 **1** acts a mixed site inhibitor for both the E2 and co-factor binding sites and the 2-substituted Mannich compound **127** acts as a competitive inhibitor for the E2 binding site and a non-competitive inhibitor for the co-factor binding site, however further experimentation is required to confirm these preliminary results.

Contents

Contents:

Chemistry Experimental Details

Compounds Synthesised: Chapter 2

Compounds Synthesised: Chapter 3

Compounds Synthesised: Chapter 4

Compounds Synthesised: Chapter 5

Acknowlegements

I would like to take this opportunity to thank Barry Potter and Nigel Vicker for their supervisory guidance and support during the course of this project. Thank you to Sterix-Ipsen for their financial support.

I would also like to thank the following people for their highly valued contribution to this thesis:

- Dr. Gyles Cozier for his general support and assistance with the synthesis, purification and crystallography of H_6-17β-HSD1, and for bearing with me through all of the questions
- Dr. Mark Thomas for the computational chemistry work and continued assistance
- Dr. Tim Woodman for his assistance with the NMR analysis of compounds
- Ms Alison Smith for the HPLC, LRMS data in this thesis
- Dr. Mary Mahon for the X-ray crystallography contained in this thesis
- Prof. Ravi Acharya for the X-ray crystallography of H_6-17β-HSD1
- The Chemistry Department at the University of Bath for their CHN analysis

I am also very grateful to all members of 3.11, 3.17 and 3.30 both past and present, for their continuous help and support throughout this project.

Finally, I would like to thank the Magnificent Flying Boots for providing me with some stories which can never leave the Salamander.

Abbreviations

17β-HSD	17β Hydroxysteroid dehydrogenase
3β-HSD	3β-Hydroxysteroid Dehydrogenase
5α-SR	5α-Steroid Reductase
Ac	Acetyl
ACN	Acetonitrile
AcOH	Acetic Acid
AF	Activation function
AKR	Aldo-keto reductase
Ar	Aryl
AR	Androgen Receptor
BL21 (DE3)	*E.coli* bacterial expression strain
BMS	Bristol Myers Squibb
Bn	Benzyl
br	Broad (spectral)
BSA	Bovine serum albumin
CIP	Calf Intestinal Phosphatase
CNS	Central nervous system
CYP	Cytochrome P450
CYP3A4 BFC	Commercially available high throughput CYP kit
CYP3A4 BQ	Commercially available high throughput CYP kit
d	Doublet (spectral)
DCM	Dichloromethane
DHEA	Dehydroepiandrosterone
DHEA-S	Dehydroepiandrosterone sulphate
DHT	Dihydrotestosterone
DMA	Dimetylacetamide
DMAP	Dimethylaminopyridine

DMF	*N*, *N*-Dimethylformamide
DMSO	Dimethyl sulfoxide
DNA	Deoxyribonucleic acid
E1	Estrone
E2	Estradiol
EBNA	Epstein-Barr virus nuclear antigen
EDTA	Ethylene diamine tetraacetic acid
eq.	Equivalent
ER	Estrogen Receptor
Et	Ethyl
EtOAc	Ethyl acetate
EtOH	Ethanol
Glu	Glutathione
HDBC	Hormone Dependent Breast Cancer
HDPC	Hormone Dependent Prostate Cancer
Hepes	4-(2-Hydroxyethyl)-1-piperazineethanesulfonic acid
HSP	Heat Shock Protein
HRMS	High Resolution Mass Spectrometry
Hz	Hertz
IPTG	Isopropyl β-D-1-thiogalactopyranoside
IC_{50}	Concentration causing 50% inhibition
J	Coupling constant (spectral)
JETSORB	Gel suspension kit
kb	Kilobases
kDa	Kilodaltons
kg	Kilogram(s)
K_i	Inhibition constant
K_M	Michaelis-Menten Constant
K_{Mapp}	Apparent Michaelis-Menten Constant

LB	Luria-Bertani media
LH	Luteinizing hormone
LHRH	Luteinizing hormone releasing hormone
lit.	Literature
LRMS	Low Resolution Mass Spectrometry
Lys	Lysine
m	milli
m.	multiplet (spectal)
M	Moles per litre
M^+	Molecular ion (mass spectrometry)
MDA-MB-231	Human breast epithelial cell line
Me	Methyl
MeOH	Methanol
MHz	MegaHertz
mp	Melting point
n	Nano
NADP(H)	Nicotinamide adenine dinucleotide phosphate (reduced)
NheI	Restriction enzyme
NMR	Nuclear Magnetic Resonance
OD_{600}	Optical density at 600nm
pCEP4	Mammalian expression vector
PEG	Polyethyleneglycol
pET24-a	Bacterial expression vector
PG	Propylene glycol
ppm	Parts per million
PSA	Prostate specific antigen
quart	Quartet (spectral)
QSAR	Quantitative Structure Activity Relationship
RNase	Ribonuclease

r.p.m	rotations per minute
R_{sym}	Differences in the symmetry related reflections
s	Singlet (spectral)
SAR	Structure activity relationship
SDR	Short-chain dehydrogenase /reductase
SDS	Sodium dodecyl sulphate
SDS-PAGE	Sodium dodecyl sulphate – polyacrylamide gel electrophoresis
Ser	Serine
SERMs	Selective Estrogen Receptor Modulators
SOC	Super optimal broth with added glucose
T47D	Human ductal breast epithelial tumour cell line
t	Triplet (spectral)
T	Testosterone
TAE	Tris/Acetate/EDTA buffer solution
TBE	Tris/Borate/EDTA buffer solution
^{t}Bu	tert-butyl
TE buffer	A buffer solution used in biochemistry
TEA	Triethylamine
TEMED	Tetramethylethylenediamine
TFA	Trifluoroacetic Acid
THF	Tetrahydrofuran
TLC	Thin Layer Chromatography
Tris	Tris(hydroxymethyl)aminomethane
Tyr	Tyrosine
V_{MAX}	Constant initial rate of product formation
XhoI	Restriction enzyme
XL10 Gold	High competency cells
δ	Delta (chemical shift)
Δ^4-dione	Androstenedione

Chapter 1

Introduction

1.1 Hormone Dependent Cancers

With the development of new medicines designed to fight off disease and infections, the average life expectancy of people within developed countries has almost doubled since the mid-nineteenth century. Whilst these medical advances have led to an improvement in the quality of life for most people, therefore people being diagnosed with cancer is becoming more common. Cancer occurs predominantly in older people, with 64% of cases diagnosed in people aged 65 and over, and more than a third of cases in people aged 75 and over. In the UK, over 280,000 people were diagnosed with cancer in 2004. Four types; breast, lung, bowel (colorectal) and prostate, account for over half of all new cases of cancer.[1] Of all human cancers, 40% are steroid hormone sensitive, (namely breast, prostate, ovarian and uterine cancers).[1]

1.2 Breast Cancer Statistics

Breast cancer is now the most commonly diagnosed cancer in the UK, with nearly 46000 women and around 300 men diagnosed each year with the disease.[2] One in nine women in the UK will develop breast cancer at some point in their life. Over the last twenty years breast cancer rates have increased by over 50% and over four out of five of all breast cancer cases in the UK are in women over the age of 50, most men diagnosed with breast cancer are over the age of 60.[1,3] It is known that only one in twenty of breast cancers are due to inherited faults in known breast cancer genes, e.g. BRCA2, which lead to a high risk of developing the disease.[2]

1.3 Current Breast Cancer Treatments

Once the staging of the cancer has been determined there are a number of treatment options available for early breast cancer. Local treatments, surgery and radiotherapy, aim to remove the cancer from the breast and auxiliary lymph nodes. Systemic treatments e.g. chemotherapy, endocrine therapy and biological therapies, for example Herceptin, enter the blood stream and circulate throughout the body to destroy any cancer cells which might have metastisised from the original site. Most patients with early breast cancer will be offered surgery. However, sometimes patients have other significant illnesses or conditions that mean surgery is not a

suitable option. In this situation the patient might be offered endocrine or biological therapy.

1.3.1 Endocrine Therapy

Endocrine therapy is usually less toxic than chemotherapy but the patients' response to treatment tends to be slower in onset. Endocrine therapy is appropriate for approximately 70% of patients who have hormone receptor positive advanced breast cancer.[3] To determine this, a clinical pathologist will measure whether or not breast cancer cells are hormone sensitive. This is known as an estrogen receptor (ER) test. Although not used in combination with chemotherapy e.g. cisplatin, endocrine therapy is in certain circumstances combined with biological therapy, although high quality evidence to justify this is lacking. Many patients will have received adjuvant endocrine therapies with either tamoxifen or an aromatase inhibitor for primary breast cancer prior to developing advanced breast cancer and some patients may relapse whilst still taking them. There is currently no evidence on the most appropriate endocrine treatment for patients who have received prior treatment with aromatase inhibitors.[3] Other endocrine therapies include ovarian ablation for pre–menopausal women and fulvestrant (Figure 1) for post–menopausal women.

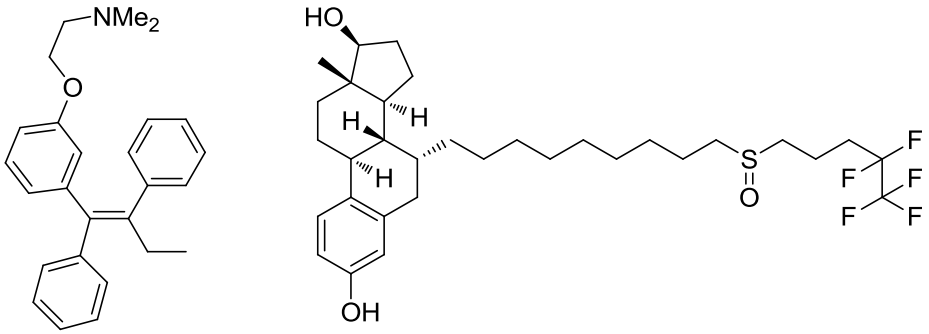

Tamoxifen **Fulvestrant**

Figure 1: Selective Estrogen Receptor modulators that are currently in the clinic

1.4 Estrogen and Androgen Biosynthetic Pathway

The androgen and estrogen biosynthetic pathway is an attractive and challenging area for research into the discovery of potential new medicines to combat the two major hormone dependant cancers: breast and prostate. There are many different enzymes involved in the biosynthesis of both dihydrotestosterone (DHT) and estradiol (E2) from their less active forms, testosterone (T) and estrone (E1). These enzymes

include: steroid sulphatase, 3β-hydroxysteroid dehydrogenase (3β-HSD types 1 and 2), 5α-Steroid reductase (5α-SR types 1 and 2) and several members of the 17β-hydroxysteroid dehydrogenase family.[4] (Figure 2)

3β-HSDs are a group of steroidogenic enzymes. The main steroidogenic isoform, 3β-HSD1, catalyzes the conversion of pregnonolone to progesterone, the conversion of 17-hydroxypregnenolone to 17-hydroxyprogesterone and the conversion of dehydroepiandrosterone (DHEA) to androstenedione (Δ^4-dione). 3β-HSD1 is mainly expressed in the gonads and adrenal cortex.[5]

Human 5α-SR is a NADPH dependent enzyme which occurs as two isozymes with similar molecular weights but only 50% sequence homology. These isozymes exhibit different pH rate profiles: 5α-SR1 predominates in skin and 5α-SR2 predominates in the prostate and genital skin.[6] 5α-Dihydrotestosterone (DHT), formed from testosterone (T) by 5α-SR1 and 5α-SR2, is the main intracellular androgen in the prostate, and stimulates the growth of hormone-dependent prostate tumours via its interaction with the androgen receptor.[7]

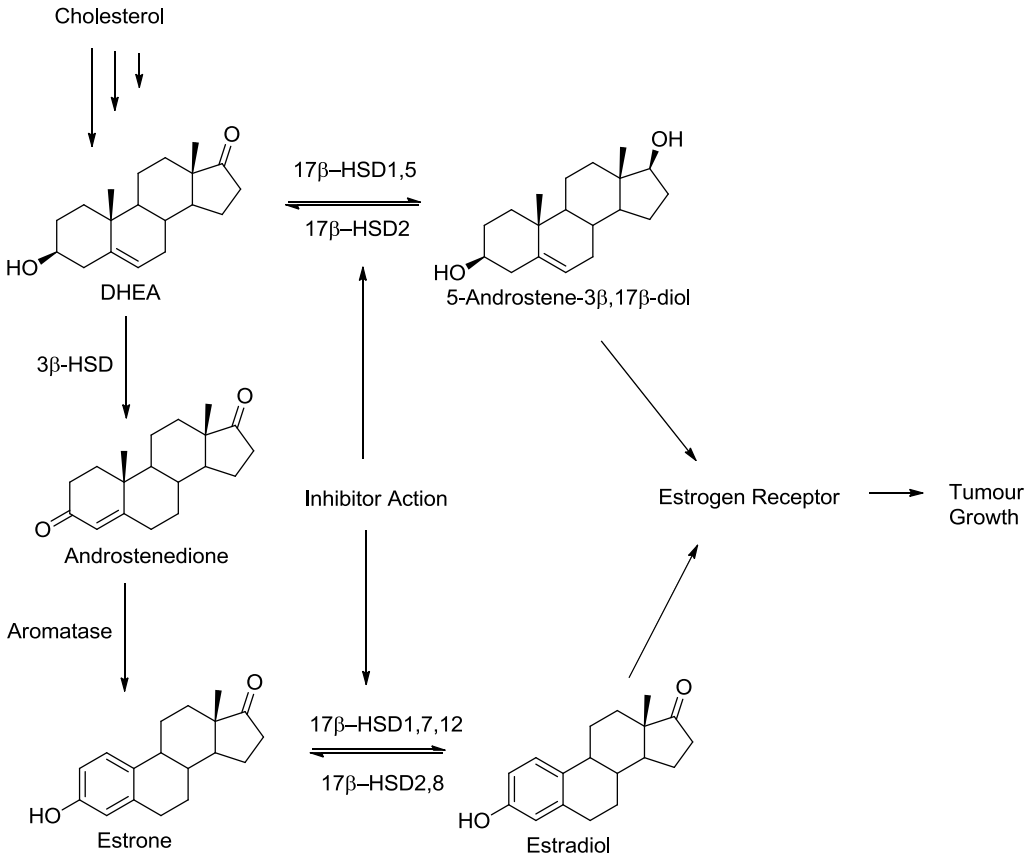

Figure 2: Biosynthetic pathway of Estrogens and Androgens

HSDs play a pivotal role in the local production of steroid hormones in target tissues (intracrine modulation). It has been stated that the intracrine formation of steroid hormones is of relevance to the aetiology of steroid dependent breast and prostate cancer. A number of enzymes play a key role in the local production of estradiol (E2) in the breast. Estrone (E1) is formed from DHEA via a series of enzyme catalysed reactions by 3β-HSD/ketosteroid isomerase (KSI) and cytochrome P450 aromatase (CYP arom).[8] Most of this E1 can be stored locally in the breast as in active estrone sulphate, which can then be converted by estrogen sulphatase back into the weak estrogen estrone.[9] Once this free estrone is formed it will be reduced by 17β-HSD1 into the potent estrogen estradiol which then can interact with the ER to accelerate cell proliferation. The ability of the 17β-HSDs to be able to convert androgens and estrogens to both active and inactive forms makes this particular family of enzymes a very attractive therapeutic target.

1.5 Estrogen Receptor (ER)

Estrogen receptors (ERs) are proteins within breast cancer cells to which estrogen binds and then helps the cancer cells to grow. The ER is a protein that is present in nearly two thirds of breast tumours. The ER is also a protein that integrates signals from numerous cell signalling pathways.[10] Estrogenic hormones act via the ER and this makes the ER the most widely targeted protein in breast cancer therapy. The most well known drugs for targeting the ER are selective ER modulators (SERMs). SERMs are composed of a broad range of compounds. Compounds such as fulvestrant block estrogen action in all tissues, whereas other compounds such as tamoxifen (Figure 1) are mixed agonists–antagonists that show distinctive tissue selectivity in blocking or stimulating estrogen responses.[10] Studies have shown that there are risks associated with long term use of SERMs one of these is that there can be an increased risk of developing endometrial cancer, uterine cancer, strokes and blot clots. However some women are prepared to take this risk as they are far outweighed by the potential benefits of using SERMs for breast cancer treatment. Although SERMs are very useful in breast cancer prevention and treatment they are not effective in all ER positive breast tumours and resistance can often develop as well as undesired side-effects such as venous thromboembolism.

The ER exists in two forms: ER-α and ER-β; these two different forms are encoded by different genes on different chromosomes. Both of these forms belong to the large

nuclear steroid/thyroid hormone receptor family of ligand dependant transcription factors. Like the majority of the other members of the family, the ERs have a modular architecture of four domains, the *N*-terminal A/B domain containing the ligand-independent transcription activation function-1 (AF-1), the C (DNA-binding) domain, the D (hinge) domain, and the C terminal E/F (ligand-binding) domain containing the ligand-dependent transcription activation function-2 (AF-2).[11] While ER-α and ER-β have nearly identical DNA binding domains, these receptor subtypes have only 56% amino acid sequence identity in their hormone binding domains and differ even more markedly (only 21% amino acid identity) in their *N*-terminal activation function-1 (AF1) regions.[10] These differences in identity suggest that there should be different ligands that would have differing levels of potency or efficacy for each of the two ERs. Estrone has only a low affinity for the ER and has to undergo pre-receptor activation by 17β-HSD1 to reduce it to E2 in order to bind with the ER with high affinity (Figure 1).[12] For this reason 17β-HSD1 is a very attractive potential target for the treatment of breast cancer.

1.6 17β-HSDs

It has been reported that there are 15 types of 17β-HSDs known.[13-28] The 17β-HSDs belong to two protein superfamilies: the short-chain dehydrogenase/reductase (SDR) protein superfamily and the aldo-ketoreductase (AKR) protein superfamily. All of the 17β-HSDs with the exception of 17β-HSD5 belong to the SDR protein superfamily and 17β-HSD6 and 9 have only been identified in rodents. Six of the isozymes have been structurally characterised, namely, 1, 4, 5, 10, 11 and 14. Both the oxidative and reductive reactions *in vitro*, *in vivo* they have preferred directionality and can therefore be classified into two categories: a) oxidative enzymes (17β-HSD2, 4, 6, 8, 9, 10, 11, 13 and 14), which catalyse the $NADP^+$ dependent oxidation *in vivo* and therefore the inactivation of steroids, and b) reductive enzymes (17β-HSD1, 3, 5, 7 and 15), which catalyze the NADPH dependent reduction of ligands *in vivo* forming active steroid hormones.[29] Although most of the isozymes are capable of catalysing SDRs constitute a large family of oxidoreductases, present in all forms of life. The SDRs are mainly multimeric enzymes with a monomer molecular mass of ~32 kDa of typically about 250-300 amino acid residues. The enzymes of the SDR family are non-metallo oxidoreductases that exhibit only 15-30% sequence identity.[30-32] Despite low

sequence identity there are two regions present in these enzymes that are highly conserved. The first of these highly conserved regions contains a Tyr-X-X-X-Lys (X is any amino acid) catalytic motif. The second of these regions is an area of alternating α-helices and β-strands, known as a Rossmann fold.[31] The Rossmann fold is responsible for creating the co-factor, nicotinamide adenine dinucleotide (NADPH), binding region.[30] Despite this structural conservation, substrate specificities among family members are diverse and for some 17β-HSDs substrates such as fatty acids or bile acids are preferred over sex steroids. Herein the main points in the literature with regard to 17β-HSD1 and 17β-HSD3 shall be described, as these are the enzymes upon which this research is based.

1.6.1 17β-HSD1

17β-HSD1 is the primary enzyme responsible for catalysing the reduction of the carbonyl at the 17 position (Figure 3) of the in active estrogen E1 to the highly active estrogen E2 using NADPH as a co-factor. 17β-HSD1 is also responsible to a lesser extent for the reduction of androstenedione to testosterone.

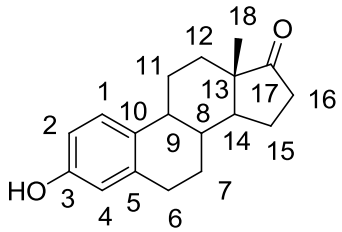

Figure 3: Numbering system of the steroid backbone for E1

17β-HSD1 was the first of the 17β-HSDs to be cloned and have its structure elucidated.[33, 34] The core of the structure is a seven stranded, parallel β-sheet (βA to βG), surrounded by six parallel α-helices (αB to αG), three on each side of the β-sheet. The first structure of 17β-HSD1 has shown that the enzyme has the folding characteristics of a SDR, with Tyr155, Lys159 and Ser142 constituting the catalytic triad of the enzyme.[35] The steroid binding site is a narrow hydrophobic tunnel that shows a high degree of complimentarity to the substrate.[36] In humans, 17β-HSD1 is predominantly expressed in the cytosol of steroidogenic tissue particularly ovaries, breast and placental tissue.[30] The proposed catalytic mechanism is shown in Figure 4 and depicts the transfer of the Pro-*S* hydrogen of the NADPH co-factor to the natural substrate E1 and therefore, forming the natural product E2.

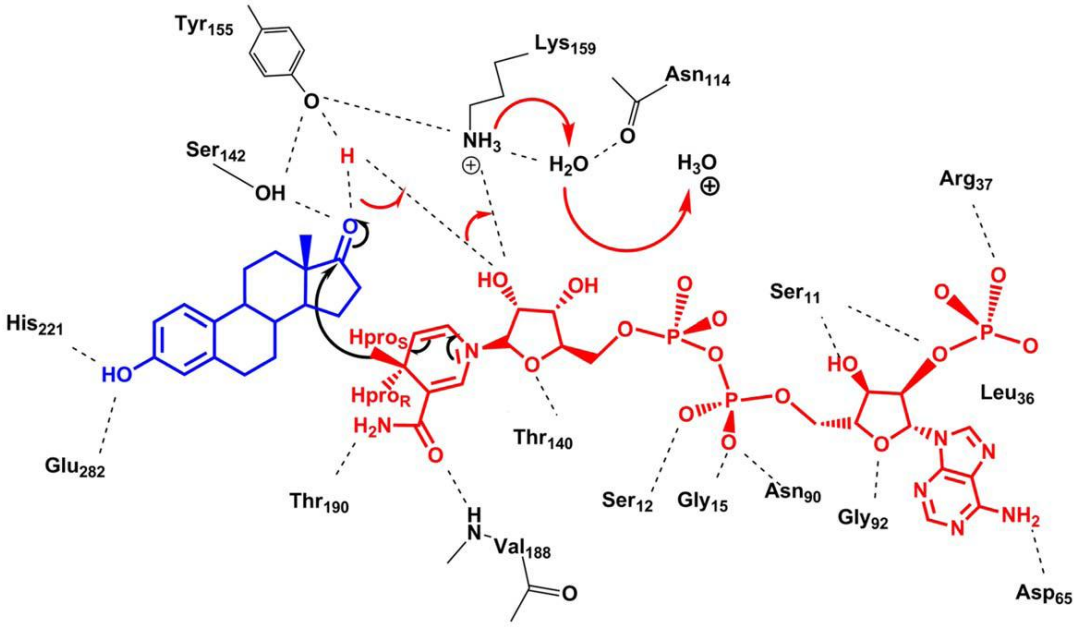

Figure 4: Hypothesised catalytic mechanism of 17β-HSD1. The substrate E1 is in blue, the co-factor NADPH is in red and the amino acids involved in either the stabilization of the ligands or the catalysis of the enzyme are shown in black and the residue is labelled.[37]

Although both 17β-HSD1 and 17β-HSD2 are present in healthy pre-menopausal women, several studies have indicated that the ratio of 17β-HSD1 to 17β-HSD2 is increased in the tumours of post-menopausal patients with hormone-dependent breast cancer.[38, 39] This results in an increased level of E2 which exerts estrogenic effects by binding with the ER, which leads to a proliferative effect, in turn accelerating tumour growth.[6] Hence, a specific 17β-HSD1 inhibitor would potentially lower the levels of E2 present in the mammary gland by competing with the natural substrate E1, and consequently the proliferative effects exhibited on hormone dependent breast cancer. Several studies have indicated that patients with tumours that have high 17β-HSD1 expression have significantly shortened disease free survival.[40-42] There is a lot of research into the discovery of novel inhibitors for this particular enzyme with many reversible and irreversible inhibitors having been reported in the literature.[4, 6, 43-47] It has been shown that the University of Bath drug candidate, STX1040 **1** (Figure 5), inhibited E1 stimulated proliferation of T-47D cells *in vitro* and significantly decreased tumour volumes and plasma E2 levels *in vivo*.[43]

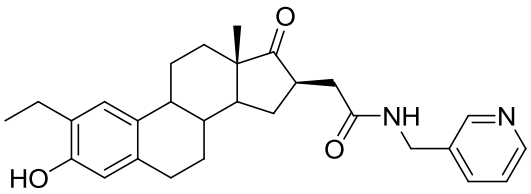

Figure 5: Structure of STX1040, 2-Ethyl-16β-*m*-pyridyl methyl amido methyl estrone **1**

Day *et al.*[48] and Laplante *et al.*[49] have shown that in T-47D cells despite the low level expression of 17β-HSD1 mRNA (~3%), compared to other reductive isoforms 7 and 12 (~50%), is responsible for the high transformation rate of E1 to E2. Laplante *et al.* have also shown that 17β-HSD1 is the only enzyme responsible for the formation of E2 in BT-20 and JEG-3 cell lines, and in HEK-293 cells 17β-HSD1 is the most effective enzyme for the conversion of E1 to E2 with an average 90% transformation after 24 h.[48, 49] Demonstrating that inhibitors designed for 17β-HSD1 and not isoforms 7 or 12 may well have a future in the treatment of hormone dependent breast cancer.

1.6.2 17β-HSD2

17β-HSD2 catalyzes the NADPH dependent conversion of E2, T and 5α-dihydrotestosterone to their less potent forms E1, Δ^4-dione and 5α-androstenedione respectively. Its cDNA encodes for a predicted protein containing 387 amino acids with a molecular mass of 42.8 KDa. It is a member of the SDR protein superfamily and shares a sequence identity of approximately 20% with 17β-HSD1 cDNA.[50] 17β-HSD2 is widely expressed in both adult and fetal tissues such as; placenta, uterus, liver, gastrointestinal and urinary tracts.[51-54] Due to the fact that 17β-HSD2 is expressed in such a wide variety of tissues it has been suggested that its main role is to protect tissues from excessive steroid action.[55]

1.6.3 17β-HSD3

17β-HSD3 catalyzes the NADPH dependent reduction of Δ^4-dione to T in the gonads and is responsible for supplying around 50% of T in the prostate.

The 17β-HSD3 isozyme is membrane bound and consists of 310 amino acids, with a molecular mass of ~34.5 KDa.[35] 17β-HSD3 is bound through an *N*-terminal transmembrane domain to the endoplasmic reticulum, and the hydrophobic nature

has thus far prohibited its structure determination and even soluble expression in cell lines that do not normally express 17β-HSD3.[30] It uses NADH as a co-factor, and the equilibrium favours the reduction of Δ^4-dione to T, which is then converted by 5α-steroid reductase to the most potent androgen, DHT (Figure 2). This reaction occurs in the Leydig cells of the testis under the control of the pituitary hormones.[56] Crystallisation is difficult as the protein has to be removed from the membrane prior to crystallisation, which can alter the tertiary structure. Stabilisation of the protein tertiary structure by adding detergents is a method sometimes used to crystallise such proteins, but to this date this has not been successful for 17β-HSD3.[57]

Currently, little is known about the mechanisms that control the expression of 17β-HSD3 however specific mutations of this enzyme are identified in patients with male pseudohermaphroditism.[30] These patients are phenotypically characterized by the lack of normal development of male reproductive organs,[16, 57] thus proving that 17β-HSD3 plays an essential role in the development of normal male genitalia.

1.6.4 17β-HSD5

The main biosynthesis of T occurs in the testes by 17β-HSD3. However T biosynthesis occurs to some extent in the prostate for which 17β-HSD5 is responsible. 17β-HSD5 is the only 17β-HSD that is a member of the AKR protein superfamily and is also known as AKR1C3, and shows a broad substrate specificity allowing it to display activity for 3α-HSD, 20α-HSD and prostaglandin 11-ketoreductase (prostaglandin F synthase).[58, 59] 17β-HSD5 is highly expressed in the testes and extragonadal tissues such as basal cells of the prostate, adrenals and liver.[60] It preferentially catalyzes the NADPH dependent reduction of Δ^4-dione to T and to a lesser extent DHEA to Δ^4-dione.[61] 17β-HSD5 consists of 323 amino acids with a molecular mass of ~ 30 KDa. The 17β-HSD5 binding site is spacious (~960 $Å^3$ or ~470 $Å^3$ depending on the substrate) and flexible when compared to that on 17β-HSD1 (~340 $Å^3$). This flexibility of the binding site permits the docking of various steroids in different orientations, which in turn encompasses a wider range of activities as described earlier. It has been suggested that 17β-HSD5 is responsible for the biosynthesis of T in females as 17β-HSD3 is not present in the ovary, which is the location of androgen synthesis in women.[62] As 17β-HSD5 is involved in the biosynthesis of androgens, along with 17β-HSD3, it is an emerging therapeutic area for the treatment of prostate cancer. The crystal structure of 17β-HSD5 has been

determined both alone and in complex with a variety of ligands providing an excellent basis for inhibitor development.[29]

1.6.5 17β-HSD7

In humans 17β-HSD7 is expressed in steroidogenic tissues such as the testes or ovaries for non-pregnant women including the uterus, placenta, mammary glands, prostate liver, kidney as well as in neural tissue.[63] It is responsible for catalysing the reduction of E1 to E2, and converts the potent androgen DHT to androstanediol (3β-diol) an ER ligand.[64] Unlike other mammals in which 17β-HSD7 is part of the pregnancy process,[65, 66] its precise role within humans has yet to be determined. Due to its dual enzymatic activity and wide distribution it is believed that 17β-HSD7 acts as an intracrine regulator of steroid metabolism.[67] However, this has yet to be proven and its predominant role *in vivo* is thought to be in cholesterol synthesis.[68]

1.6.6 17β-HSD12

A study from Luu-The *et al.*[27] suggested that 17β-HSD12, originally thought to be exclusively involved in fatty acid elongation may also be an important enzyme responsible for the conversion of E1 to E2.[69] Results from a further study by the same group indicated that it is up-regulated in the tumours of breast cancer patients.[63] It has been shown that 17β-HSD12 is present in steroidogenic tissues such as breast, ovary and prostate but not to the same level of expression as in active lipid metabolizing tissues such as liver, kidney, heart and skeletal muscle as well as in the placenta and testis, further supporting its role as a regulator of fatty acid biosynthesis.[70] Studies by Day *et al.*[48] and Laplante *et al.*[49] confirm that 17β-HSD1 and not 17β-HSD12 is responsible for the high transformation rate of E1 to E2 in a variety of breast cancer cell lines.

1.7 Inhibitors of 17β-HSD1 a Review of the Literature

In recent years there has been a significant increase in the number of patents and publications concerning 17β-HSD1 inhibition, as the pharmaceutical industry has recognised the potential for development of 17β-HSD1 inhibitors as a treatment for hormone dependent breast cancer. The majority of known inhibitors in the literature are based upon modifications of the estrone steroid core. However there has been a concerted effort over the last couple of years in the research of non-steroidal inhibitors. As of this time there are no 17β-HSD1 inhibitors on the market.

Inhibitors of 17β-HSD1 should be selective against 17β-HSD2 and importantly should display no estrogenic effects. Activity against other E1 converting enzymes or antiestrogenic effects can be seen as a desired extra benefit. Good inhibitors should exhibit certain drug-like properties. Lipinski *et al.*[71] describe a series of criteria that an orally active compound should have, these are; no more than five hydrogen bond donors or ten hydrogen bond acceptors. A molecular mass of less than 500 $gmol^{-1}$ and a partition co-efficient (log P) of less than five. If an inhibitor meets these criteria it is theoretically deemed to have the necessary properties required to have sufficient absorption and permeation in biological systems. A good 17β-HSD1 inhibitor will have an IC_{50} value in the low nM range or a high percentage inhibition in μM test concentrations.

In this review inhibitors with modifications of the E1 and E2 steroid core will be discussed first and non-steroidal inhibitors will be discussed afterwards.

1.7.1 Steroidal Inhibitors of 17β-HSD1

Steroids represent a broad class of naturally occurring compounds that play crucial roles in the homeostasis of biological systems. In humans, the different families of steroidal hormones, such as progestins, glucocorticoids, androgens and estrogens all originate from endogenous and exogenous cholesterol. The majority of 17β-HSD1 inhibitors are based upon steroid structures, particularly the natural substrates of 17β-HSD1 E1 and E2. The E1 and E2 scaffold can be conveniently used to investigate how substitution at varying positions of the steroid core affect the binding affinity of inhibitors and can then used to develop structure activity relationships (SAR). The following sections introduce steroidal 17β-HSD1 inhibitors, which are divided into classes based upon the position where the modification is attached to the steroidal core.

1.7.1.1 Derivatives of E1 and E2 Substituted at C2

Substituents at the C2 position of the E1 or E2 core were introduced to try and increase selectivity for 17β-HSD1 over 17β-HSD2 as well as reduce any possible estrogenic effects. Hillisch *et al.*[72] and Gege *et al.*[73] together with Schering have patented a series of 2-substituted E1 and 2-substituted D-homo E1 compounds as selective 17β-HSD1 inhibitors (Figure 6). In a human recombinant 17β-HSD1 assay 2-phenylethynylestrone, **2** and 2-phenylethylestrone, **3** showed good inhibitory

activity with an IC_{50} value of 56 nM and 47 nM respectively, this indicates that bulky substituents at the C2 position are well tolerated by the active site. Other 2-substituted E1 derivatives showed good inhibitory data. The compound, 2-chloroestrone, **4** showed promising activity with an IC_{50} value of 140 nM. The activity of **4** was improved by the addition of either C18 methyl, **5** or C16 fluorine, **6** and **7** group. The stereochemistry of the C16 fluoro group plays an important role in how the inhibitor binds to the active site of 17β-HSD1. When the fluoro group points to the α-face of the steroid core the activity of the inhibitor, **7** marginally increases, however when the fluoro group points to the β-face of the steroid core the IC_{50} increases from 140 nM to 35 nM which is the most potent inhibitor, **6** described amongst the 2-substituted estrone inhibitors.[72]

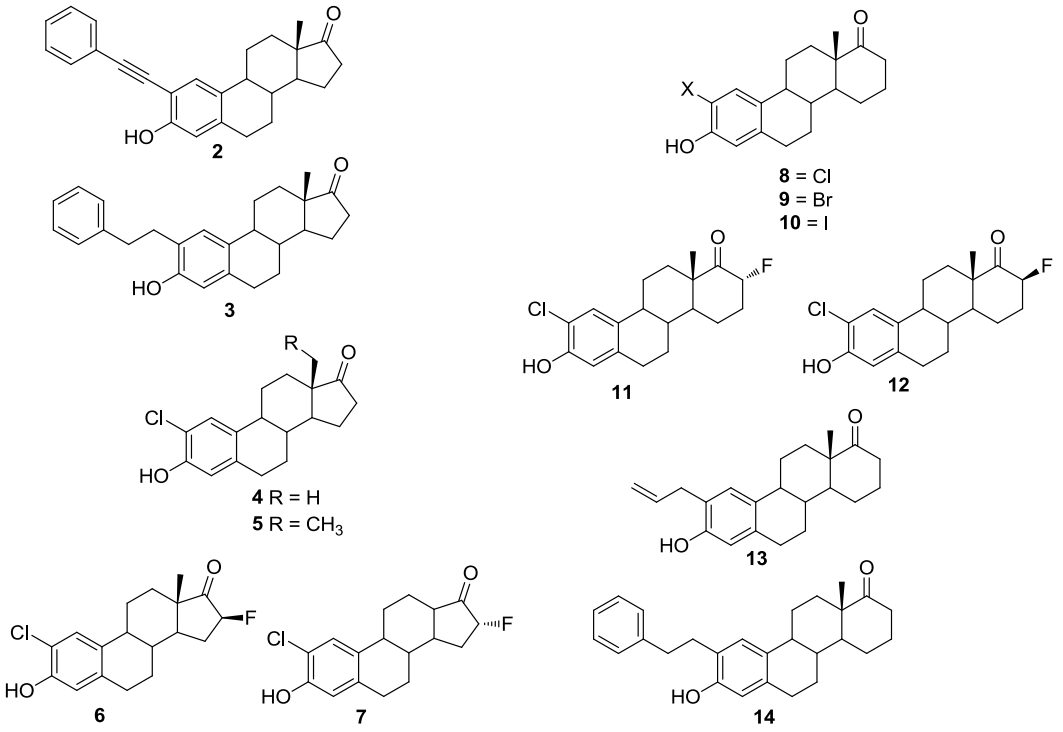

Figure 6: Derivatives of E1 and E2 with varying substitution patterns on C2[72, 73]

Replacing the estrone core with a D-homoestrone core resulted in an increase in activity for the majority of the compounds.[73] The D-homoestrone inhibitors with a halogen in the C2 position are very potent inhibitors, **8-10**. The activity of the C2 halogenated D-homoestrone series shows again that bulky groups are well tolerated within the active site. An interesting observation is that unlike in the native E1 series when a fluoro group is introduced alpha to the carbonyl the 2-chloro-17-β-fluoro compound **12** displays a lower activity and the 2-chloro-17-α-fluoro compound **11**

has a higher activity. This is due to the change of position of the fluoro group within the active site. The best D-homoestrone inhibitors were the 2-substituted, 2-phenylethyl-D-homoestrone **14** and 2-allyl-D-homoestrone **13** with IC_{50} values of 15 nM and 24 nM respectively. For comparison the natural substrate E1 showed an IC_{50} value of approximately 300 nM.

No estrogenicity or selectivity data has been reported for either the E1 or the D-homoestrone series. The C2 substitution is likely to reduce if not prevent any cytochrome P450 (CYP) 1A1, 1A2, 3A4 and 3A7 interaction with these compounds. The 2-position is a well-known major oxidative metabolic pathway, namely by hydroxylation, and the CYP isoforms stated earlier have a uniquely high activity for this position.[74]

1.7.1.2 Derivatives of E1 and E2 Substituted at C6

Several groups have synthesised compounds based upon E1 and E2 with substituents at the 6-position of the steroid core. Allan *et al.*[75] explain that their interest in the 6 position of E1 arose after computational investigation of how E1 binds in the active site of 17β-HSD1 using the crystal structure of 17β-HSD1 with E2 and NADP (PDB code 1FDT).[76, 77] Their investigation suggested that a small hydrogen bond acceptor at the 6 position could potentially capitalise on beneficial interactions with the hydroxyl group of Ser222. They decided that a carbonyl group would be of a sufficient size to make use of this potential interaction and subsequently synthesised 6-oxo estrone **15** and two other oxidised forms **16** and **17** of previously reported potent inhibitors of 17β-HSD1 (Figure 7).[78]

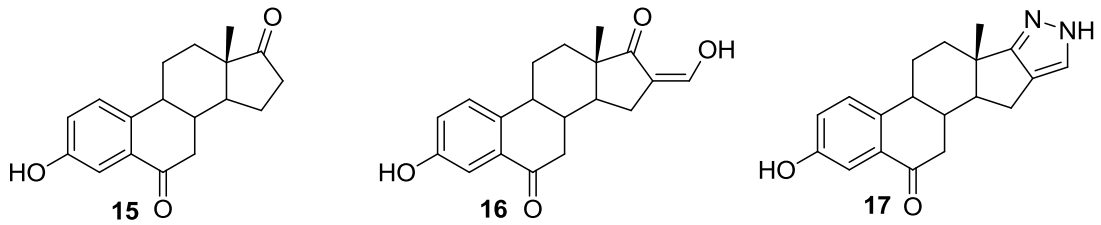

Figure 7: 6-Oxo derivatives of E1[75]

Presence of the 6-oxo substituent does not significantly enhance the activity of the compound compared to that of the natural substrate. These results show that the 6-oxo substituent is well tolerated within the active site of 17β-HSD1 but does not

increase the binding affinity and therefore does not interact with the hydroxyl group of Ser222.

The investigation into position 6 of the steroid core was expanded by the synthesis of oxime derivatives **16**-**17**, with the aim of further investigating the SAR around position 6 by retaining a similar hydrogen bond acceptor. The oxime group was chosen because it could be easily introduced in one step without having to protect the 3-hydroxyl to give the compounds in Figure 8.

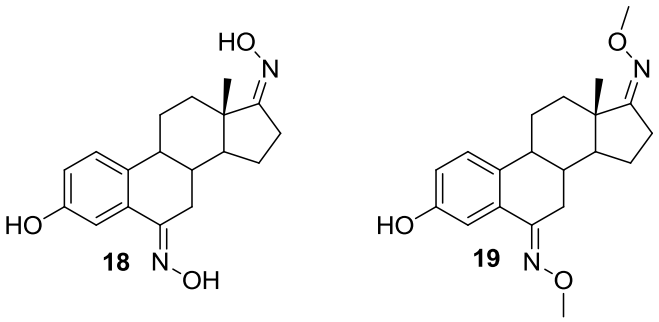

Figure 8: Oxime derivatives of 6-oxo E1

The biological data for the oxime derivatives **18**-**19** shows that the oxime group is not well tolerated in the active site as **18** has an IC_{50} value of 1.90 µM that is 6 fold less active than the natural substrate E1. Compound **19** has a percentage inhibition at 10 µM of 31%. Whether or not this reduction in binding affinity is due to the oxime groups in the 6 position or the 17 position cannot be conclusively determined.

Poirier *et al.* have also reported the synthesis of 6-substituted E2 compounds. In their efforts to design potent inhibitors for 17β-HSD1 they developed a series of E2 based compounds containing a thia-alkanamide side chain at position **6**[79-81] based upon the pure antiestrogen **20**, (Figure 9) which has a very moderate percentage inhibition at 1 µM of 33% for 17β-HSD1 prepared from human placental cytosol.[79]

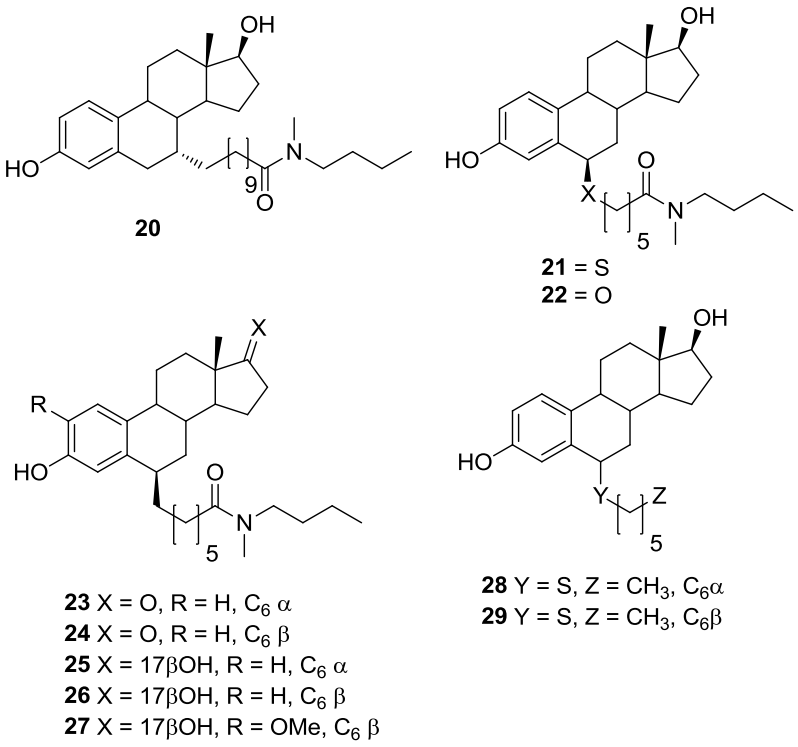

Figure 9: 6-Substituted E1 and E2 derivatives by Poirier *et al*.[83]

By moving the *N*-butyl-*N*-methyl alkyl amide side chain to C6 and optimising the side chain length to have five methylenes **21** instead of nine methylenes, the inhibitory activity was improved to give an IC_{50} value of 0.17 μM, twice as potent as E1. The compound with a 6β-side chain **29** is 70 fold more potent than the compound with a 6α-side chain **28**[79] showing that the orientation of the side chain is a key structural characteristic for the inhibition of 17β-HSD1 and shows that there is steric hindrance in the active site around C6 of the steroid scaffold. Compound **21** was unfortunately shown to display estrogenic activity.[82] It was hypothesised that this activity was due to the instability of the thioether, where if cleaved yields estrogenic E2.[80] From this hypothesis Tremblay *et al.*[80] developed a series of inhibitors **22-27** that potentially would be less liable to undergo modification by metabolising enzymes, by replacing the thioether with an ether. The biological activity of **22** was lower than that of the original thioether inhibitor **21** but the estrogenicity of the compound was considerably reduced. It was also discovered that modifications of the 3-hydroxyl and the amide group of the initial lead compound **21** drastically reduced the biological activity of the inhibitors, therefore showing that the 3-hydroxyl and amide group are key structural characteristics associated with biological activity. With regards to how these modifications altered the estrogenicity

of the compounds, the changing of the amide group did not alter the estrogenicity of the compound, but the alterations of the 3-hydroxyl showed a marked reduction in the estrogenicity of the inhibitors as was expected.[80] Another strategy was developed for trying to reduce the estrogenicity of the lead compound **21**, substitution at C2. Cadot *et al.*[81] had limited success with this strategy due to instability of the thioether and only the 2-methoxy substituted compound **27** was tested. The effect of the group at C17 was also investigated in this work. For the 17-keto compounds it was observed that the biological activity was approximately 30% lower than that of the 17β-alcohols, and the addition of the 2-methoxy group decreased the inhibitory activity by around 20%.[81] Though structurally similar to the antiestogen **20** compound **21** displayed a strong estrogenic effect in T-47D and MCF-7 cell lines.[80, 81] For compounds **22** and **24** the proliferative effect in T-47D cells was only seen at 0.1 μM and 1.0 μM. As proposed the 2-methoxy substituted compound did not display any estrogenic activity on T-47D cells at 1.0 μM but a higher than normal cell growth was observed at lower concentrations.[81]

1.7.1.3 Derivatives of E1 and E2 Substituted at C15

Solvay Pharmaceuticals have patented C15 substituted E1 and 3-methoxy E1 derivatives as 17β-HSD1 inhibitors.[83, 84] These patents cover a series of compounds containing an amide, sulfonamide, urea, carbamate or hydroxyl side chain connected via an alkyl linker to C15 of the steroid backbone, and with additional substitution at C2. The biological activity of these compounds was assessed by using recombinant 17β-HSD1 (rec17β-HSD1).[83, 84] Messinger *et al.*[85] focussed on the synthesis of E1 derivatives based upon the hypothesis that the natural substrate should have a higher binding affinity for the active site of 17β-HSD1 than E2. Their decision to concentrate on C15 substitution was because substitution at C16 displays the undesired side-effect of being estrogenic.[85] After analysis of the 17β-HSD1 X-ray crystal structure complexed with E2 occupying the active site (pdb code 1FDT)[76] it was observed that the enzyme exhibits an opening towards the area located in the proximity of the steroid D ring. This opening is formed via the amino acids; Ser222, Leu219, Met193 as well as Tyr218, Leu96 and Gly198. It was reasoned that the position of these amino acids is highly flexible; due to the flexibility of the protein it is believed that substitutions on C16 can also penetrate the opening.[85]

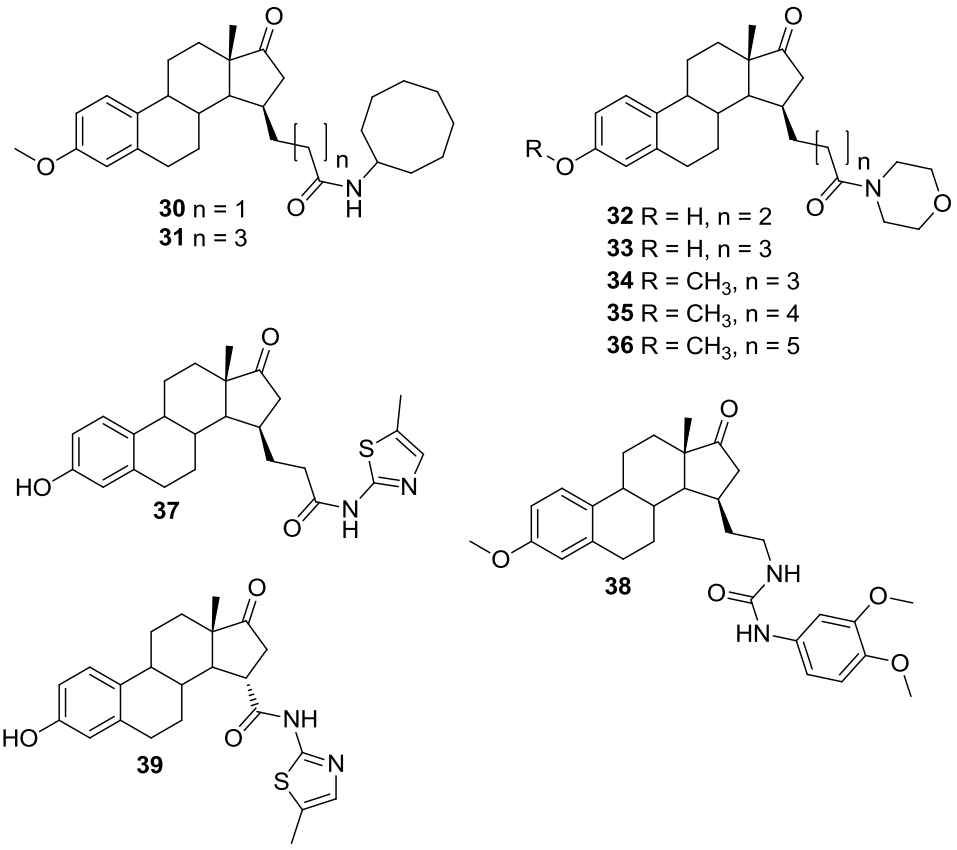

Figure 10: Selected examples of C15 substituted E1 derivatives patented by Solvay Pharmaceuticals[83, 84]

Archetypal inhibitor structures and their rec17β-HSD1 inhibitory activities are shown in Figure 10 and Table 1. The most potent of which is compound **37** displaying 87% and 93% inhibition at 100 nM and 1 µM concentrations respectively and having an IC_{50} of 4 nM. This set of data shows that for these types of inhibitor a large variety of side chains containing groups of differing polarity and size can be tolerated within the active site. Nevertheless some SAR rules can be established; 1) Compounds with a side chain length of 2 – 4 methylene units are generally preferred as demonstrated by the morpholino bearing side chain compounds **32-36**. 2) A hydroxyl group at C3 of the steroid core is not essential for the binding of these inhibitors. 3) 15α substitution can be well tolerated but these inhibitors tend to show a lower biological activity compared to the 15β compounds of a similar structure. The ability of compound **39** to inhibit 17β-HSD1 has been demonstrated *in vivo* in a nude mouse model.[86] Inoculation of the mice with estrogen sensitive MCF-7 breast tumour cells, that expressed human 17β-HSD1 led to the growth of hormone dependent tumours. Subcutaneous administration of compound **32** (5 µM/kg/day) resulted in a 60%

reduction in size of the tumour compared to non-treated control animals. Less polar side chains show a tendency to reveal minor estrogenic activities, identified by estrogen receptor binding and uterine weight tests.[85]

Compound	Recombinant 17β-HSD1		
	% Inhibition at 100 nM	% Inhibition at 1 µM	IC_{50} (nM)
30	89	93	14
31	42	85	
32	19	63	
33	27	79	194
34	12	40	
35	17	68	
36	29	80	
37	87	93	4
38	80	87	14
39	77	89	26

Table 1: C15 substituted E1 derivatives and their recombinant 17β-HSD1 inhibitory activity

1.7.1.4 Derivatives of E1 and E2 Substituted at C16

Interest in the C16 position was initiated by the discovery that E1 and E2 substituted with reactive halogenated functional groups, such as bromoacetoxy, were found to be irreversible inhibitors of 17β-HSD1.[79] The bromoacetoxysteroids are traditionally used to affinity label the target enzyme.[87-89] While such compounds have been extremely useful for the mapping of the active site of 17β-HSD1[90] they are ineffective as therapeutic reagents because of their high reactivity with nucleophiles. Despite the fact that these compounds could not be used for therapy these studies showed that C16 was a good location to introduce a modification for the inhibition of 17β-HSD1. As stated earlier in this report, it was observed that the enzyme exhibits an opening towards the area located in the proximity of the steroid D ring. This

opening is formed via the amino acids; Ser222, Leu219, Met193 as well as Tyr218, Leu96 and Gly198. It was reasoned that the position of these amino acids is highly flexible and therefore expansion from C16 is an attractive option. From docking studies it is hypothesised that there is a possibility that a C16 side chain may interact with the co-factor binding site and therefore produce a dual site inhibitor. Poirier and co-workers had shown that large substituents at C16 of E2 were well tolerated,[91, 92] indicating that there is promise of developing a dual site hybrid inhibitor. The dual site inhibitors are very promising because these inhibitors can potentially interact with both the substrate (E1) and the co-factor (NADPH) binding sites, therefore making use of the binding energy of both moieties to produce an inhibitor that shows a very strong binding affinity for 17β-HSD1. Qui *et al.*[93] were the first group to publish the structure of an E2-adenosine hybrid compound (Figure 11) in 2002.

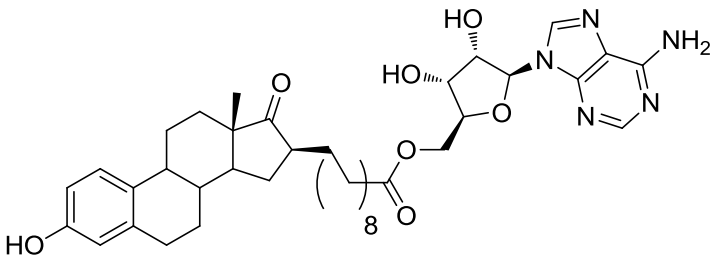

EM-1745 **40**

Figure 11: EM-1745 **40** the first reported E2 adenosine hybrid inhibitor

The E2 adenosine hybrid, EM-1745 **40** show a strong biological activity against 17β-HSD1 with an IC_{50} of 52 nM which was significantly improved over all previously available inhibitors and natural substrates,[93] with the synthesis later described in 2003.[94] To optimise the affinity of each moiety with their respective binding sites, the hydroxyls of the steroid as well as the amine and secondary hydroxyl of the adenosine moiety must be free. Therefore the primary alcohol of the adenosine was retained for the formation of an ester bond with the C16 steroid side chain to give the lead compound EM-1745 **40**. As part of further research into this area Bérubé *et al.*[95] identified the synthesis of simplified hybrid inhibitors of 17β-HSD1 via cross-metathesis and Sonogashira coupling reactions.[95] Showing that hybrid inhibitors can be accessed in an efficient and rapid manner. Poirier *et al.*[96] continued to explore the C16 substitution by investigating whether α / β substitution was optimal for biological activity and what the ideal spacer length was between the steroid and

adenosine moieties. Results from this research (Table 2) show that a β orientation **42-46** is desired for optimal biological activity of the inhibitor with both the steroid and co-factor binding sites. A spacer length of 8 methylenes **46** was determined to be the ideal spacer length for the adenosine residue to interact efficiently with the co-factor binding site.[96]

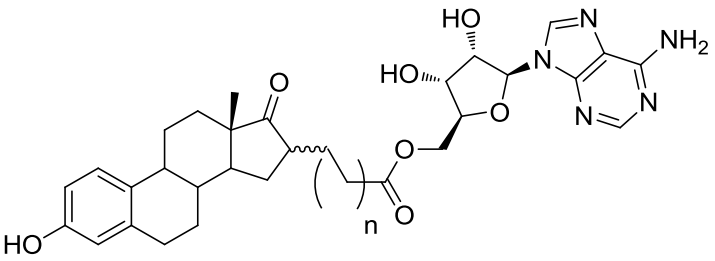

Compound	C_{16} Orientation	Spacer length	IC_{50} (nM)
41	α	10	310
42	β	10	120
43	β	11	1000
44	β	6	430
45	β	7	93
46	β	8	52

Table 2: Modifications of the D ring substituent and their IC_{50} values as determined by a recombinant 17β-HSD1 assay[100]

A protein crystal structure with EM-1745 **40** occupying both the steroid and co-factor binding sites at a resolution of 1.6 Å was reported by Qui *et al.*[97] in 2002 (PDB code 1I5R) and several important observations have been noted: 1) The steroid core and adenine core of EM-1745 **40** bind to 17β-HSD1 in a similar to that observed in the structure of 17β-HSD1-E2-NADP ternary complex. (PDB code 1FDT[76]) 2) The electron density is very strong in the steroid and adenine regions. 3) O17 of the steroid forms strong hydrogen bonds with amino acid residues that are observed in the 17β-HSD1-E2 complex (PDB code 1FDS[80]) (Figure 12).[94]

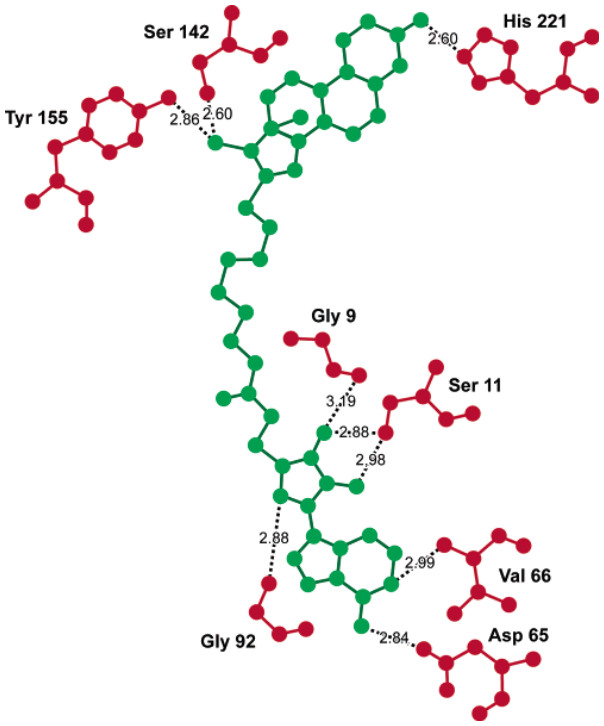

Figure 12: Schematic diagram of the most important hydrogen bonds between EM-1745 **40** (green) and certain amino acid residues (red) of 17β-HSD1. The hydrogen bonds are represented by dashed lines, and their lengths are given in Å.[96]

Two potential major drawbacks when using EM-1745 **40** in intact cell assays or in *in vivo* models were identified and investigated in 2008 by Fournier *et al.*[97] The first of which was that the inhibitor might not penetrate the cellular membrane, and the second was that the inhibitor might be metabolized, at the ester between the steroidal component and the adenosine component of the compound. When EM-1745 **40** was tested in intact HEK-293 transfected cells, for which no exogenous co-factor is required, EM-1745 **40** still retained some inhibiting power, albeit approximately 10 fold lower than that observed in a homogenate of transfected HEK-293 cells at 0.1 μM.[96] Due to the fact that 17β-HSD1 catalyses the formation of E2 from E1 using NADPH as the co-factor the inhibitory activity of EM-1745 **40** was compared using NADPH and NADH as exogenous co-factor in a homogenous cell assay, and as expected the inhibitory activity of EM-1745 **40** was lower when NADPH was used as the co-factor. The conclusions drawn from these experiments were that the lower inhibitory activity of EM-1745 **40** in intact cells compared to a cell homogenate assay was not clear as to whether this could be attributed to the inhibitor being incapable of crossing the cellular membrane or the inhibitor being metabolised. What

could be determined was that EM-1745 **40** is less efficient at inhibiting 17β-HSD1 when NADPH was being used as the cofactor, as would be the case at physiological conditions.[97] Therefore EM-1745 **40** is not a very 'drug like' compound. It is known that E1 is a better substrate when compared to E2 for the reductive activity of 17β-HSD1. It has been reported that the Michaelis-Menten constant (K_M) of E1 is 0.03 μM and 0.36 μM for the cofactors NADPH and NADH respectively. Whilst the K_M for E2 is much greater at 4.6 μM and 1.7 μM for the cofactors $NADP^+$ and NAD^+ respectively,[98] indicating that E1 is a much better substrate for 17β-HSD1. In addition enzyme kinetics analysis of EM-1745 **40** using a Lineweaver-burk plot shows that this inhibitor acts as a typical reversible competitive inhibitor [93] and so by taking this information into account it was hypothesised that a C17 hydroxy analogue **47** of EM-1745 **40** would provide an improved biological activity against 17β-HSD1. When tested against EM-1745 **40** in a homogenated HEK-293 cell assay using NADH as a cofactor, it was discovered that **47** gave a lower percentage inhibition than EM-1745 **40** by approximately 10% at 0.1 μM concentrations.[99] This was unexpected result but after the biological evaluation of a number of other inhibitors differing only at C17 by either a ketone or hydroxyl, this result was once again observed. Nevertheless the biological activity of a larger sample set of inhibitors should be evaluated before any conclusions from this observation can be drawn.

As an expansion of this work and to develop the SAR of C16 substituted inhibitors a series of simplified inhibitors were developed to investigate whether other aromatic groups could be used instead of an adenosine to improve the bioavailability of these inhibitors for 17β-HSD1. These compounds were easily obtained from E1 via an aldol condensation using an aromatic aldehyde, followed by the stereoselective reduction of the carbonyl to an alcohol, and finally the double bond was stereoselectively reduced by catalytic hydrogenation to give **48** with a 16β orientated R group. (Figure 13)

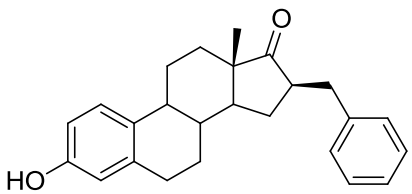

48

Figure 13: A simplified dual site inhibitor[100]

One compound, **48**, synthesised was of particular interest having an IC_{50} of 0.79 – 1.0 μM. When this compound was docked into a 3D structure of 17β-HSD1 complexed with E2, the steroid nucleus was shifted from the steroid binding site to enable the phenyl group to get closer to a hydrophobic pocket formed by Leu96 and Val196.[100] To try and improve the drug like properties of these simplified 17β-HSD1 inhibitors[101] three strategies were utilised to try and reduce the estrogenic activity of these inhibitors. Their strategies were 1) replacing the hydroxyl group at C3 with a hydrogen. 2) Adding a methoxy group at C2, this arose from the use of 2-MeO-E2 Panzem®, which had previously been demonstrated to reduce growth of many cancer cell lines.[102, 103] 3) Adding an alkylamide side chain at C7α known for its anti-estrogenic properties.[105] The chemical structure and inhibitory potency of these compounds are reported in Table 3.

Compound	**Chemical structure**	**% Inhibition at 0.1 / 1 / 10 μM**	**IC_{50} (nM)**
49	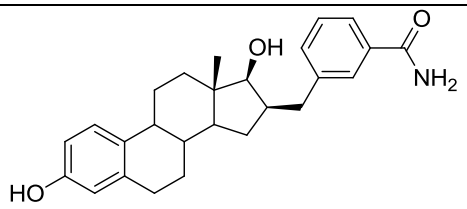	77 / 94 / 96	44 ± 7
50	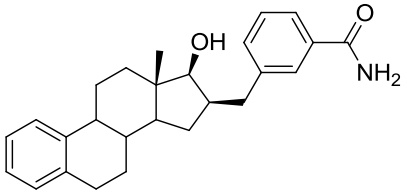	24 / 44 / 79	
51	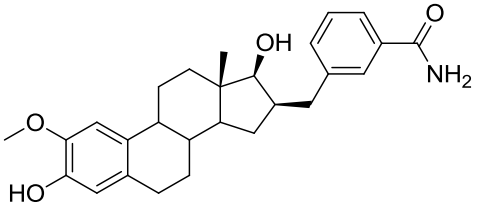	37 / 69 / 81	
52	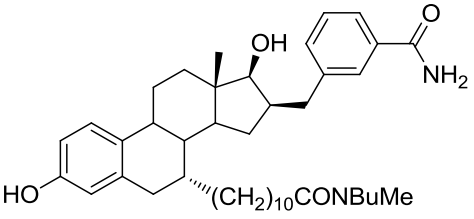	4 / 45 / 61	

Table 3: Inhibitors of 17β-HSD1 and their potency in T-47D intact cells[101]

Results indicate that none of the compounds generated from these strategies were as potent as the parent compound **49** when tested in an intact T-47D cell assay and are noticeably less potent than compound EM-1745 **40**. The estrogenic activities of these compounds were in fact lower than **49** in both T-47D and MCF-7 cell assay which are both ER positive cell lines. Compound **50** and **51** exert 31% and 21% less estrogenic activity than **49** at 0.1 µM. Compound **52** totally inhibits growth at 0.01 µM and even brings cell density under that of the control level for both T-47D and MCF-7 cell lines suggesting that this compound is actually an anti-estrogen that displays some weak 17β-HSD1 activity.[101]

During this period Potter *et al.* were also developing a variety of these hybrid compounds and they started with the addition of substituents of various sizes at C16 conducted in a systematic manner, starting with the incorporation of small substituents such as, nitriles, alkyls and alkenyls. These inhibitors showed promising biological activity (Table 4).[75] These compounds were accessed via condensation reactions of various aldehydes with E1. Ensuing reduction of the C17 ketone followed by hydrogenation of the alkene gave the 16β-alkyl derivatives **55** and **56**.[75, 104]

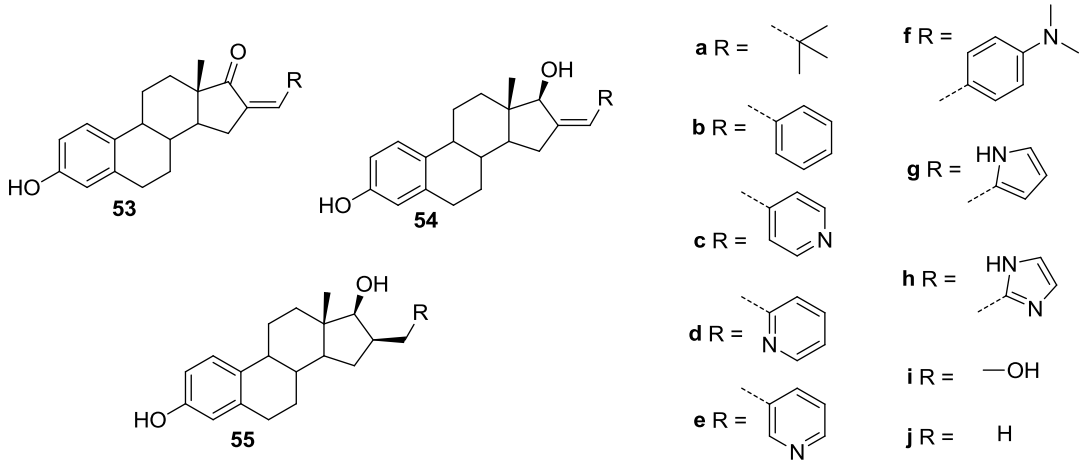

17β-HSD% inhibition at 10 µM[75]							Purified 17β-HSD1[100]		
	53		54		55		53	54	55
R	Type 1[a]	Type 2[b]	Type 1[a]	Type 2[b]	Type 1[a]	Type 2[b]	IC_{50} (µM)[a]	IC_{50} (µM)[a]	IC_{50} (µM)[a]
H	70	10	64	20					

a	82	31	84	27					
b	17	< 10	26	< 10			10-32	3.4-5.6	0.8-1.0
c	34	25	77	< 10	84	37			
d	23	16	55	17	88	11	> 20	9.3-12.6	2.4-5.5
e	44	10	52	43	87	11	8.6-18	7.5-16	3.3-4.2
f	72	13	72	81	41	25	> 40	7.0-14	4.0-5.7
g							1.1-3.4		
h							3.8-4.0		
i					86	17			
j							0.26-0.33	14-32	0.72-1.3

a - Assessed in T-47D cells; b – Assessed in MDA-MB-231 cells

Table 4: Inhibitory activities of various C16 substituted E1 derivatives in a purified 17β-HSD1 assay and T-47D and MDA-MB-231 cancer cell based assays[75, 100]

A wide range of inhibitory activities can be seen in Table 4 although certain compounds showed promising activity against 17β-HSD1 in T-47D cells and selectivity when compared to the percentage inhibition at 10 μM against 17β-HSD2 in MDA-MB-231 cells. (Table 4) Compound **53** (R=H), a known 17β-HSD1 alkylating agent,[106] showed 70% inhibition of 17β-HSD1 at 10 μM and 10% inhibition of 17β-HSD2, compound **53a** showed an improved inhibition of 82% for 17β-HSD1 but was less selective than compound **53** with 31% inhibition of 17β-HSD2. Reduction of the C17 ketone to yield the E2 derivatives **54** gave curious results. Compounds **53a** and **54a** showed similar inhibitory activities and selectivity to each other with this also being the case for compounds **53b** and **54b**. When the alkenyl substituent for compound **54** is changed from a phenyl group to varying pyridyl derivatives the inhibitory activity improves vastly with the largest increase being seen for the *para* substituted pyridyl compound, **54c** 77% for 17β-HSD1 and < 10% for 17β-HSD2. Compound **54c** shows a promising IC_{50} value of 4.1 μM.

Generally the percentage inhibition of 17β-HSD1 was improved by the reduction of the E1 derivatives, **53a-f**, to the E2 derivatives, **54c-f**,**i**. Further investigation of C16 substitution led to the synthesis of a series of C16β substituted compounds, **55**. The results for this series of compounds showed more favourable inhibitory activity against 17β-HSD1 when compared to compounds **53** and **54**, with inhibitions of 84% and over for compounds **55c-e** at 10 μM. These results suggest that some flexibility of the C16 side chain might be important for binding of the inhibitor with the active site of 17β-HSD1. These results also show that bulky aryl substituents can be tolerated by the active site, but optimisation of these systems is needed to obtain a potent inhibitor.[75]

As the biological activities of these compounds was deemed to be promising it was decided that a more flexible, functionalizable substituent at C16 was to be incorporated. To investigate this area of the active site two such linkers were initially investigated: 1) a carboxylic acid, 2) a methyl carboxylic acid. These carboxylic acids could then be readily reacted via an amide coupling reaction with a wide variety of commercially available amines, that were specifically chosen to include a range of electron accepting, electron donating, charge transfer, hydrophobic, hydrophilic and π-stacking properties, with the purpose to explore the SAR in the C16 area of the active site.

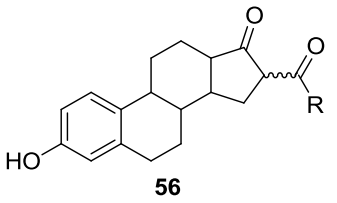

56

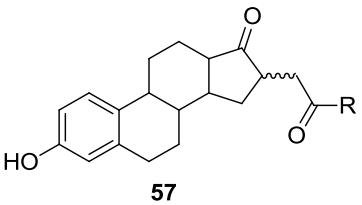

57

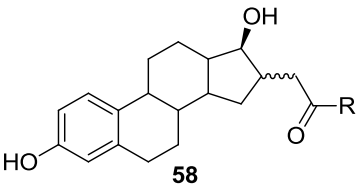

58

Compound		**% Inhibition at 10 μM**						**IC_{50} (μM)**	
		17β-HSD1[a]			17β-HSD2[b]			17β-HSD1[a]	
	R	**56**	**57**	**58**	**56**	**57**	**58**	**56**	**57**
a	OH	39	13	58	< 10	<10	< 10		
b	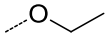		97	67		18	18		0.30
c			90	63		< 10	11		1.5

d	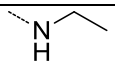		84	76		< 10	13		
e	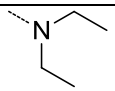		82	79		< 10	14		
f	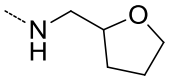	82	91	63	11	21	25		0.38
g	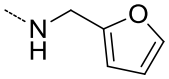	87	85			< 10			
h	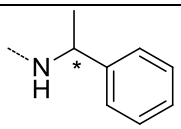	90	83		12	10		0.81	
i	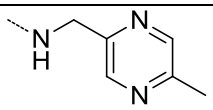	85			< 10				
j	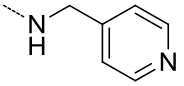	87							
k	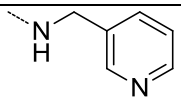	91	95		<10	26		0.51	0.037
l	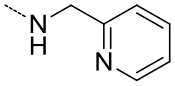		82			< 10			
m	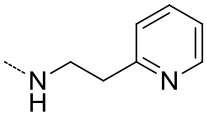		58			14			

a - Assessed in T-47D cells; b – Assessed in MDA-MB-231 cells

Table 5: Biological activities of C16 substituted derivatives of E1 and E2 as determined from T-47D and MDA-MB-231 cell based assays[104]

The biological activities of the carboxylic acid derivatives of E2 based inhibitors, **56-58**, are shown in Table 5. These inhibitors were tested as mixtures of diastereoisomers, for which the ratios of *R* and *S* were undetermined for the majority as it is described that only one set of peaks were observed in the ^{1}H NMR. It can be seen that a large proportion of these inhibitors display good inhibition of 17β-HSD1

at 10 μM. For compounds 5**6g-k** the aromatic amide moieties show greater percentage inhibition than the alkyl amide moieties. Indicating that there is potentially some form of beneficial π-π interaction between the aromatic moiety and the active site of 17β-HSD1. The most potent compound of this series was 5**6k** with an IC_{50} value of 510 nM, all compounds from this series demonstrate good selectivity of 17β-HSD1 over 17β-HSD2.[104]

The percentage inhibition values of 17β-HSD1 for the methyl carboxyl derivatives of E2, **59**, are shown in Table 5. These analogues displayed reduced inhibitory activities when compared to that of the methyl carboxyl derivatives of E1, **58**. Any conclusions made from the results derived from compounds, **58** can only be tentatively concluded as a more comprehensive library of compounds would have to be synthesised including amides with a wider variety of chemical properties.[104]

The methyl carboxyl derivatives of E1 showed very promising inhibitory activity. The amides **57b-h** and **57k-m** showed excellent inhibitory activity of 17β-HSD1 as well as selectivity against 17β-HSD2. From the comparison of the percentage inhibition of **57l** and **57m** it can be deduced that there is an optimum distance for which the pyridyl moiety needs to be for beneficial interaction with the active site of 17β-HSD1. The most potent inhibitor from this series is the compound **57k**, which as reported in a preliminary paper [110] has an IC_{50} of 37 nM, making this compound one of the most potent inhibitors to described at this date.[104]

With a view to reducing the estrogenicity of compound **57k**, synthesis of the 2-methoxy and 2-ethyl analogues, **1** and **59**was undertaken.[104] Several 2-methoxy E1 derivatives have been reported to display lower estrogenic effects when compared to their E1 counterparts[102, 107-108] and 2-substituted E1 derivatives have also shown reduced estrogenicity.[107] Vicker *et al.*[46] described that *in silico* studies using the crystal structure (PDB code 3ERD[109]) of the ligand-binding domain of the human ERα have shown that compounds bearing a C2 substitution of the steroid nucleus do not fit well, as the 2-substituent disrupts key hydrophobic interactions in the ER-α steroid binding site.[46] This therefore gives an *in silico* prediction that compounds **1** and **59** would not be strongly estrogenic, as docking studies of the binding orientation in ER-α have proven predictive in the identification of ER-α selective agonists using the same crystal structure.[110] Compounds **1** and **59** were synthesised

and identified as the most potent and selective inhibitors of 17β-HSD1 (Table 6) and were shown to be selective for 17β-HSD1 over 17β-HSD2.[104]

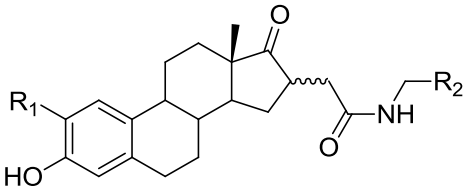

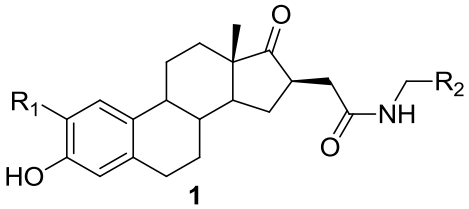

1

Compound	**R_1**	**R_2**	**IC_{50} (nM) against 17β-HSD1[a]**	**% Inhibition 17β-HSD1[a]**	**% Inhibition 17β-HSD2[b]**
57k	H	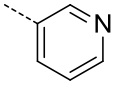	37	97	26
1	Et	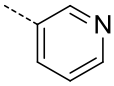	27	99	-5.0
59	OMe	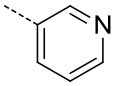	290	96	0

a - Assessed using T-47D cells; b - Assessed using MBA-MD-231 cells

Table 6: A table showing the effect of A ring substitution upon the activity of C16 substituted E1 derivatives as determined in T-47D and MD-MBA-231 cell based assays[104]

When compounds **57k** and **1** were docked into 1FDT[76] with E2 removed it could be seen that the steroid backbones are essentially overlaid, therefore forming the same hydrophobic interactions, with Leu149, Val225, Phe226 and Phe259, as the natural substrate E1. The 2-ethyl group of **1** is able to form an additional hydrophobic interaction with Leu262 and Phe259. It was also noted that the oxygen of the carbonyl in the amide side chain is 3.16 Å from the closest nicotinamide NH, indicating that there may be an interaction between the carbonyl on the 16-amide side chain and the nicotinamide amide moiety. The pyridyl nitrogen of the 16β side chain is 3.16 Å from a phosphate oxygen and could form a hydrogen bonding interaction.[104] These additional interactions between compounds **57k** and **1** and the

co-factor could potentially explain the vastly improved biological activity for 17β-HSD1.

When comparing the inhibitory activity of compounds **60**, **61** and **1**, (Table 7) IC_{50} values of 3.62 μM, 165 nM and 27 nM respectively, and it can be seen that the binding region is sensitive to small changes in the structure of the inhibitor and also indicates the importance of the binding interactions between the inhibitors and the protein and / or co-factor binding sites. This observation is also demonstrated by the approximately 6 fold difference in activity between compounds **61** and **1** in which the nitrogen of the pyridyl ring has been moved from a *meta* to an *ortho* position.

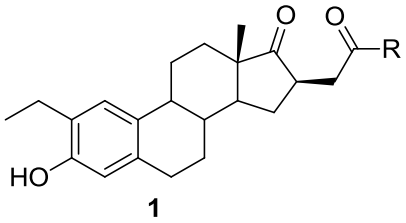

1

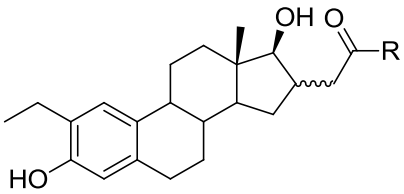

Compound	R	% Inhibition	IC_{50} (μM)
60	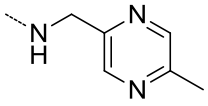	45	3.62
61	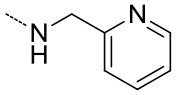	89	0.165
1	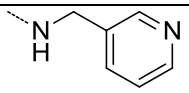	94	0.027

Table 7: A table showing how varying the position and number of nitrogen atoms present in the D ring moiety affects activity as determined in a T-47D cell based assay[104]

This extensive research by Lawrence *et al.*[104] has confirmed that good inhibitory activity and selectivity for 17β-HSD1 against 17β-HSD2 can be obtained for compounds bearing a large and flexible side chain at C16 of E1 and E2. The inhibitory activity of these compounds were assessed using T-47D breast cancer cells, which represent the physiological conditions and show that these inhibitors are able to successfully pass through the cell membrane. 2-((13S,16R)-2-ethyl-3-

hydroxy-13-methyl-17-oxo-7,8,9,11,12,13,14,15,16,17-decahydro-6H-cyclopenta[a]-phenan-thren-16-yl)-N-(pyridin-3-ylmethyl)acetamide, STX1040 **1** is the most potent inhibitor of 17β-HSD1 reported to date and has the lowest reported IC_{50} value of 27 nM obtained from a cell based assay.[43]

1.7.1.5 E ring modified steroids

As an extension of the work by Lawrence *et al.*[104] that led to the discovery of **1**, the C16 position was further explored in combination with modifications at the C17 position in the form of E ring steroidal based inhibitors. These E ring containing inhibitors have the benefit of being able to further explore the chemical space within the active site without the introduction of a chiral centre at the C16 position. It had been previously reported that heterocyclic analogues of E1 with a pyrazole or an isoxazole fused to the 16, 17-position on the D ring were competitive inhibitors of purified placental 17β-HSD1.[111] It was hypothesised that the pyrazole E ring modification acts as a bioisostere for 16-(hydroxymethylene)estrones because of the plausible potential intramolecular hydrogen bonding (Figure 14).

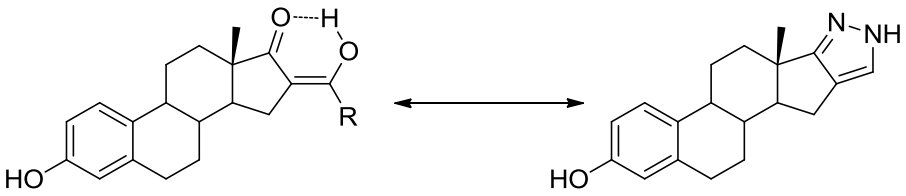

Figure 14: An example of bioisosterism[78]

Besides retaining the carbonyl isostere C=N at C17, the fused pyrazole ring system is also a desirable scaffold for chemical substitution with three different attachment positions for the rapid exploration of chemical space. Fischer *et al.*[78] described the utilisation of the pyrazole based E ring for the synthesis of N1, N2 and C5′ substitiuted compounds as 17β-HSD1 inhibitors. Pyrazoles are attractive targets for synthesis because of the ease of access to a common pyrazole carboxylic acid intermediate for rapid modification. In a T-47D cell based assay the pyrazole compound as a mixture of N1H and N2H tautomers, had an IC_{50} value of 180 nM at 10 µM concentration and displayed a percentage inhibition of 97%. In comparison the corresponding pyrazolone E ring compound[47] and pyridine E ring compound[78] analogues displayed a slightly lower percentage inhibiton of 86 and 78%

respectively. A reduction in activity was also observed for the addition of a C6 carbonyl to 62a.[47] (Table 8)

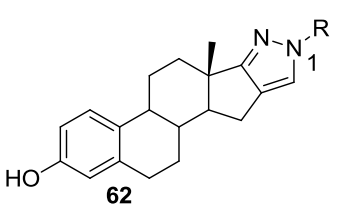

62

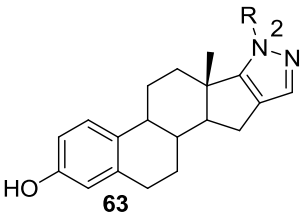

63

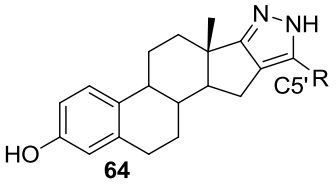

64

	R	% Inhibition at 10 μM (Compound 62)		IC_{50} (μM)	% Inhibition at 10 μM (Compound 63)	
		17β-HSD			17β-HSD	
		Type 1[a]	Type 2[b]	Type 1	Type 1	Type 2
a[c]	H	97	32	0.18		
b	CH_3	94	24	2.75	43	32
c	$CH_2CH(CH_3)_2$	77	61		70	44
d	$CH_2CO_2CH_3$	95	19	0.92	79	30
e	$(CH_2)_2OCH_3$	95	48	0.53	83	55
f	$(CH_2)_2CN$	95	44	0.73		
64a	CO_2Et	94	7	1.85		
64b	CH_2OH	94	-1	0.95		
64c	COOH	32	-6			
64d	CF_3	75	36			

a - Measured in T-47D cells; b - Measured in MDA-MB-231 cells; c - A mixture of N1H and N2H tautomers

Table 8: A table to show how variation in the substitution pattern of the pyrazole affects the biological activity of this class of E ring modified steroids as measured in T-47D and MDA-MB-231 cells

In the *N*-alkylated pyrazole series all the N1 substituted compounds significantly inhibited 17β-HSD1, although the selectivity for 17β-HSD1 over 17β-HSD2 was

shown to be modest for the majority of the inhibitors from this series, for example **62e** has an IC_{50} value of 0.53 μM but displayed only 2 fold greater inhibitory activity for 17β-HSD1 over 17β-HSD2.[78] This shows that the E ring modified scaffold is well tolerated by the active site of 17β-HSD1. A bulky hydrophobic group however was not well tolerated as displayed by **62h**, which had the lowest percentage inhibition of the series. The N2 alkylated derivatives corresponding to their N1 analogues all showed a lower percentage inhibition and so are not as potent as the pyrazole N1 derivatives. The C5' series produced compounds that were highly selective for 17β-HSD1 over 17β-HSD2 and the alkylated compounds from this series demonstrated high percentage inhibition against 17β-HSD1 with compounds **64a** and **64b** both having a percentage inhibition of 94% and IC_{50} values of 1.85 μM and 0.95 μM respectively.[78] Compounds **62d** and **63d**, the *N*-methoxyethyl derivatives, did not show any estrogenic activity up to 100 nM concentration, indicating that it is unlikely to bind to the ER.[78]

As part of further work into the investigation of a pyrazole template as a new scaffold for 17β-HSD1 inhibitors, previous studies had indicated that an amide side chain displayed beneficial interactions with the co-factor, and so this approach was used for the design of a new series of C5' inhibitors (Table 9). By applying this approach to the synthesis of new C5' compounds several new potent inhibitors were developed (Table 9). Compound **65b** was found to be the most potent from this series with an IC_{50} of 300 nM.[47, 78] Other compounds containing a pyridyl moiety in the side chain were found to be potent inhibitors of 17β-HSD1 as well as displaying good selectivity for 17β-HSD1 over 17β-HSD2. Primary aliphatic amides however showed only moderate activity against 17β-HSD1. To try and mimic STX1040 **1** the most potent inhibitor of 17β-HSD1, an ethyl group was substituted onto the 2-position of the steroid core, this led to a 2 fold decrease in activity for compound **66b** compared to the most potent inhibitor **65g** from this series.[46] The addition of a sulfamate group to the 3-OH also led to decrease in activity by approximately 5 fold.

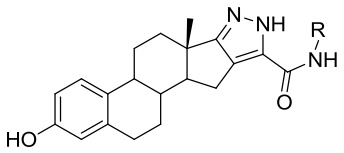

65

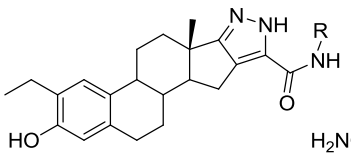

66

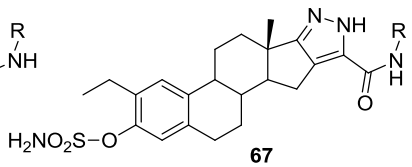

67

Compound	R	% Inhibition of 17β-HSD at 10 µM		IC_{50}[a] (µM)
		Type 1[a]	Type 2[b]	
65a		57	0	
65b	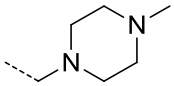	50	-1	
65c	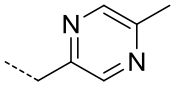	80	61	
65d	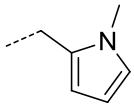	90	-4	2.3
65e	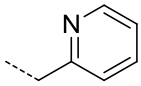	93	9	0.88
65f	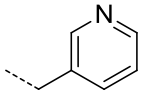	92	28	0.78
65g	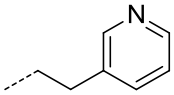	99	3	0.30
66a	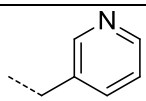			1.97
66b	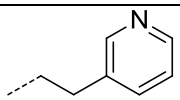			0.7

67a	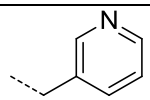	17		
67b	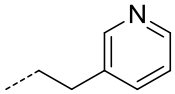	20		

a – Measured in T-47D cells; b – Measured in MD-MBA-231 cells

Table 9: A table to show the biological activities of steroidal E ring based inhibitors as determined in T-47D and MD-MBA-231 cell based assays[113]

A molecular modelling study of compound **65e** and **66b** in the active site of 17β-HSD1-E2-$NADP^+$ complex (PDB code 1FDT[76]) showed that the steroid cores of both compounds in the ligand binding pocket were overlaid and it was seen that they formed the same hydrophobic interactions as E2.[46, 78] The hydrogen bond acceptor group in the side chain are in close proximity to the primary amide group of the nicotinamide group of the co-factor and may form favourable π-stacking interactions with this moiety. In compound **66b** the ethyl group at the 2-position was located in a hydrophobic region and was said to be likely to interact with the amino acid residues; Met147, Leu149, Phe259 and Leu262.[46] The phenol moiety was predicted to interact with His221 which was seen to be 1.8 Å away, this interaction was also observed for the substrate, and the nitrogens present in the pyrazole ring were shown to be 1.9-2.1 Å away from the Pro-*S* of the $NADP^+$. The *meta*-pyridyl moiety positioned itself towards the phosphate backbone between the two ribose rings of the co-factor,[46, 78] and so could potentially form further interactions with the co-factor and protein. This could explain why the compounds **65e-g** bearing a pyridyl side chain are the most potent inhibitors from these series. Compound **62e** was also docked into the crystal structure of the ligand binding domain in human ER-α (PDB code 3ERD[109]). Poor docking scores indicated that **62e** did not fit well in the active site and therefore suggests that this compound is not strongly estrogenic.[78]

1.7.2 Non-Steroidal Inhibitors

The majority of the inhibitors that have been described for 17β-HSD1 are based upon modifications of the E1 and E2 steroid core. There has recently been a concerted effort by several groups to research the potential of non-steroidal inhibitors for activity against 17β-HSD1. Non-steroidal inhibitors have several advantages over

steroidal inhibitors in that non-steroidal compounds could have advantages of ease of synthesis, drug-likeness, selectivity and non-estrogenicity. Non-steroidal inhibitors also have the advantage of enabling a range of different pharmacophores to be assessed for their inhibitory potential for 17β-HSD1. When studying the SAR of steroidal inhibitors some common structural features can be identified which aid binding at the active site. These include a phenol which can undergo bifurcated hydrogen bonding to His221 and Glu282, and a hydrophobic scaffold which inhabits the hydrophobic area in the active site.

1.7.2.1 E1 skeleton mimics

Vicker *et al.*[112] synthesised a series of non-steroidal inhibitors that were designed to be mimics of compound **1** which has an IC_{50} of 27 nM. The reason for designing non-steroidal mimics of this compound was that non-steroidal inhibitors might provide compounds with an improved pharmacokinetic (PK) profile. The search for non-steroidal inhibitors of 17β-HSD1 began with the investigation into which possible scaffolds might be able to replace the E1 steroid core, whilst keeping the phenol and ketone functionalities on the E1 A and D rings, since these moieties are known to be important for binding. An investigation of biphenyl ethanone type systems with different linkers between the phenyl rings showed that those with just a C-C linker showed activity. (Table 10)[112] These compounds were accessed by utilising the Suzuki coupling reaction between a boronic acid and a bromo-substituted aromatic ring.[113] Alignment studies showed that compound **68** is similar in length to E1, and a number of alignment and shape similarity studies were performed to investigate possible scaffolds.

Compound	**Structure**	**% Inhibition of 17β-HSD1 at 10 μM[a]**	**% Inhibition of 17β-HSD2 at 10 μM[b]**	**IC_{50}[a] (μM)**
68	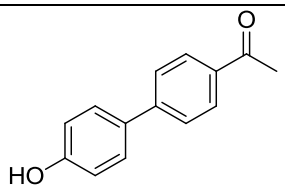	97		3.7

69	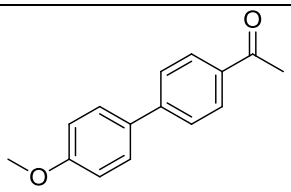	Inactive		
70	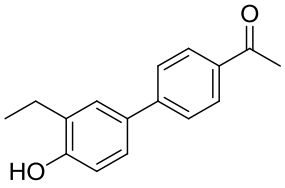	73	51	5.4
71	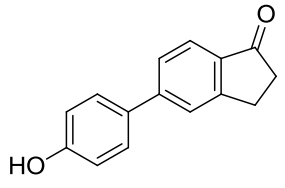	81	17	1.7
72	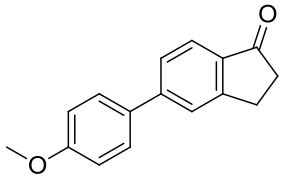	Inactive		
73	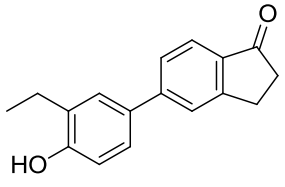	86	48	2.0
74	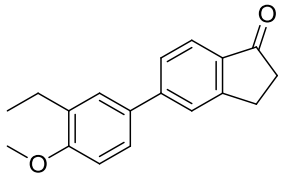	Inactive		
75	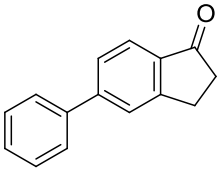	Inactive		
76	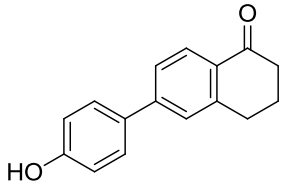	89		15.6

77	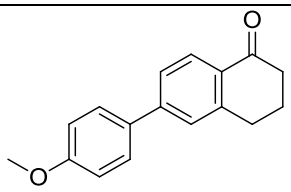	Inactive		
78	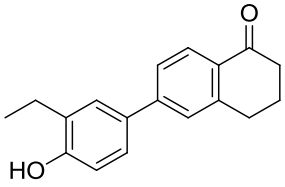	51		
79	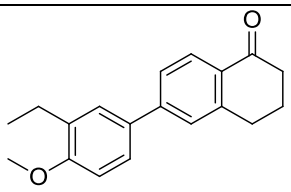	71		8.3
80	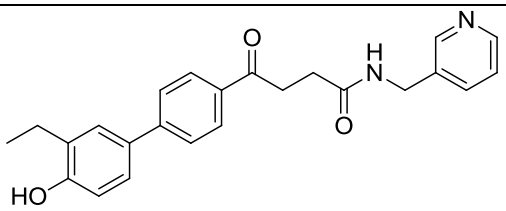	24	12	3.7
81	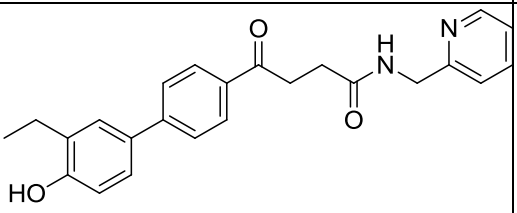	Inactive		
82	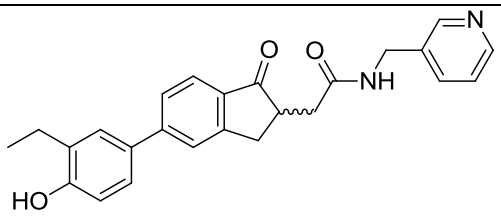	39		4.7
83	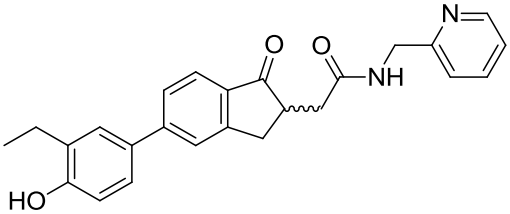	Inactive		

a – Measured in T-47D cells; b- Measured in MD-MBA-231 cells

Table 10: A table to show the biological activities of a series of non-steroidal E1 and E2 mimics as determined from a cell based assay[44]

The compounds shown in Table 10 were assessed for their ability to inhibit 17β-HSD1 using T-47D human breast cancer cells. The results for the biphenyl ethanone series showed promising inhibition of 17β-HSD1, with compounds **68** and **80** showing the best IC_{50} of 3.7 μM. It can be seen for all of the scaffolds that the methylation of the phenol results in the loss of biological activity. The addition of a 2-ethyl group on the A ring was well tolerated for all of these compounds, however the selectivity of these compounds for 17β-HSD1 against 17β-HSD2 was shown to decrease when comparing compounds **68**, **70** and **71**, **73**.[113] The indanone series proved promising, with the most potent compound being the unsubstituted biphenyl indanone **71**, with an IC_{50} value of 1.7 μM and is shown to be selective against 17β-HSD2. The tetralone containing compounds displayed reduced activity compared to the indanone and the acetophenone series. This is a surprising result because the six membered homo D ring 2-substituted E1 derivatives are reported to be at least as active as the E1 scaffold itself.[72, 73] As the acetophenone and indanone scaffolds were shown to be more active than the tetralone scaffold it was then decided that these scaffolds were to be used to synthesise mimics of compound **1**, STX1040, it was decided to incorporate the ethyl substituent immediately, with the idea to avoid estrogenicity from the outset. As with the steroidal series[46] the length of the chain and position of the nitrogen in the pyridyl ring were investigated and as with the steroidal series the *meta* pyridyl compounds, **80** and **82** with IC_{50} values of 3.7 and 4.7 μM respectively displayed the best inhibitory activity compared to the *ortho* pyridyl compounds, **81** and **83**, which were determined to be inactive at 10μM.

These non-steroidal inhibitors are shown to be promising inhibitors of 17β-HSD1, however further investigation and optimisation is required. The inhibitory data for these compounds does indicate that compound **1** is being mimicked in the desired way.

1.7.2.2 Phenylnaphthalene and phenylquinoline derivatives

It was seen that the substrate binding pocket contained a hydrophobic tunnel with polar regions at each end, consisting of the polar amino acids His221 and Glu282 forming hydrogen bonds with the 3-O of the A ring of the steroid and at one end of

the binding pocket Ser142 and Tyr155 forming hydrogen bonds with the 17-O of the D ring of the steroid. In front of the active site is an entry loop comprising of amino acids 188-201. This loop was deemed to be very flexible as these amino acids are not properly resolved in the crystal structure 1FDT[76]. This loop occupies two modes; in mode A the loop closes entry to the substrate binding pocket and in mode B the loop closes entry to the co-factor binding pocket. Bearing this information in mind Hartmann *et al.*[118] synthesised a series of compounds that were designed to mimic the natural substrates E1 and E2. These compounds contained two polar terminal groups that are 10 – 13 Å apart, designed to mimic the 3-O on the A ring of the steroid and 17-O of the D ring of the steroid core. It was determined that to mimic the planar geometry of the steroid phenylnaphthalenes and phenylquinolines would be ideal non-steroidal scaffolds for this and would also satisfy the other criteria stated above.[44]

A series of phenylnaphthalenes were synthesised and the position of the hydroxyls on the naphthalene and phenyl were investigated (Table 11).

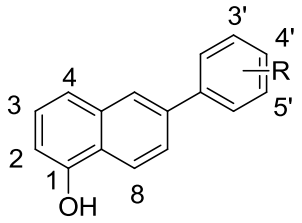

Figure 15: The numbering convention for the core structure of the phenylnaphthalene and phenylquinoline based compounds

When the hydroxyls were located at position 1 on the naphthalene and position 3' and 4' on the phenyl only moderate biological activity was observed. By moving the hydroxyl on the naphthalene to position 2 and the hydroxyl of the phenyl to either position 2', 3' or 4' only compound **84** with the phenyl hydroxyl at position 3' displayed any activity in a recombinant placental 17β-HSD1 assay, with an IC_{50} of 116 nM.[44, 114-115]

Compound	Structure	% inhibition at 100 nM / 1 µM
84	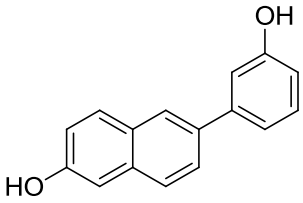	91 / 94
85	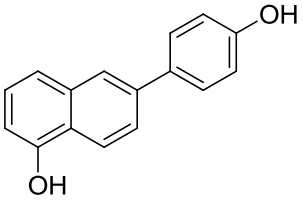	ni / 55
86	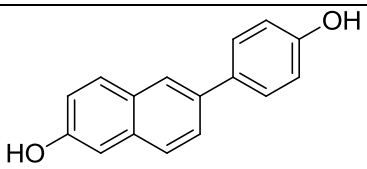	ni / ni
87	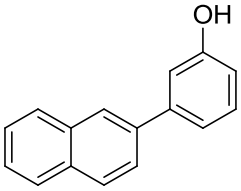	26 / 61
88	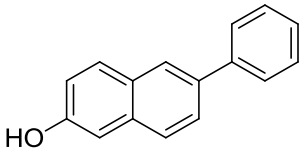	ni / ni
89	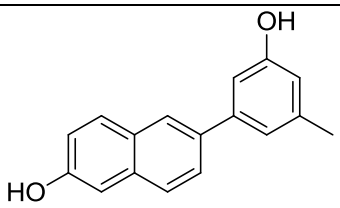	14 / 42
90	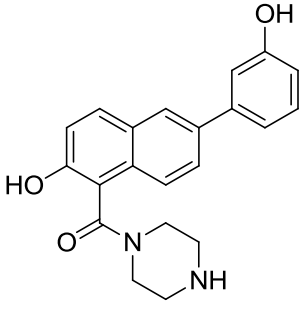	ni / 45

91	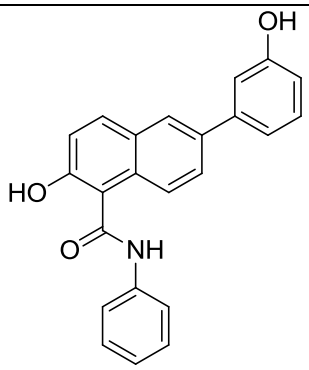	40 / 80
92	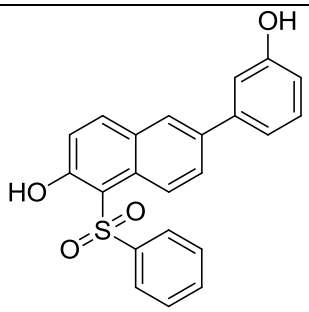	nt / 33
93	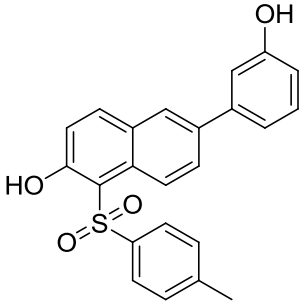	nt / 75
94	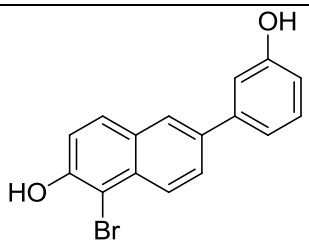	83 / 88
95	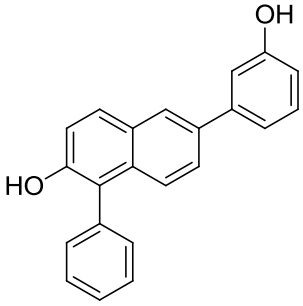	76 / 89

ni – No Inhibition; nt – Not Tested

Table 11: A table displaying the biological activities for a series of phenylnaphthalenes as determined in a recombinant 17β-HSD1 assay[118-120]

Compounds **85** and **86** were inactive, therefore highlighting that the position of the hydroxyls is very important for the inhibition of 17β-HSD1. Removal of the hydroxyl on the naphthalene core to give the monohydroxylated compound **87**, drastically reduced the activity to 26% inhibition at 100 nM. Removal of the hydroxyl of the phenyl moiety resulted in a complete loss of activity,[115] displaying that the presence of a hydroxyl at each end of the compound is very important for biological activity. It was reasoned that this was due to the hydroxyls being very important for the stabilisation of the compound within the active site of 17β-HSD1.

It was hypothesised that substitution at positions 1 and / or 3 with a hydrogen bond acceptor or donor might enable the compounds to interact with the polar amino acids Tyr218 and Ser222. A number of compounds with an amide present at position 1 show only moderate activity, 45% and 80% inhibition at 1 μM for compounds **90** and **91** respectively, compared to 94% for the lead compound **84**. Substitution in position 1 with a sulfone also exhibits moderate activity, 33% and 75% at 1 μM for compounds **92** and **93**, which is lower than that seen for the lead compound **84**.[114] These results for percentage inhibition are all significantly lower than the lead compound **84** and so suggests that substitution at position 1 is not forming any favourable interactions with the active site. Substitution with electron rich moieties such as the halogen bromine **94** and a phenyl group **95** at position 1 gave compounds with an improved activity compared to the lead compound, with IC_{50} values of 40 nM and 20 nM respectively.[114] This increase in activity could be due to π–π stacking interactions, and does demonstrate that there is potential for substitution at position 1 of the naphthalene core. It remains unclear however why **94** is more active than **95** but the electronic effects of the bromine compared to the phenyl are offered as one explaination. These compounds show good selectivity for 17β-HSD1 over 17β-HSD2 and also show low relative binding affinities for the ER-α and ER-β, highlighting their potential as therapeutic agents for hormone dependent breast cancer. It has also been shown that the lead compound **84** displays moderate metabolic stability against CYP1A2, 2B6, 2C9, 2C19, 2D6 and 3A4 in tests using rat liver microsomes, as well as moderate cell permeability in an assay using Caco-2

cells which exhibit the morphological and physiological properties of a human small intestine.[44]

It was hypothesised that the addition of a heteroatom into one of the rings of the compound could establish favourable interactions with the polar amino acids Tyr218 and / or Ser222 which are located close to the C6 position on the B ring of the steroid. To investigate this hypothesis compounds based upon a phenylquinoline core were synthesised. (Table 12)[44, 115] The introduction of a nitrogen into the naphthalene moiety to give a quinolone gave rise to a dramatic decrease in activity, 24% and 14% at 100 nM for compounds **96** and **97** respectively.[120]

Compound	Structure	% Inhibition @ 100 nM/1 µM
96	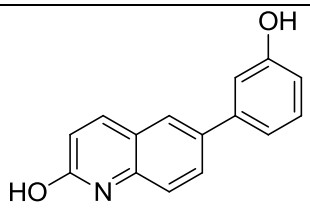	24 / 57
97	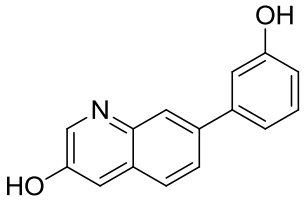	14 / 63

Table 12: A table to show the biological activities of a series of phenylnaphthalenes in a recombinant 17β-HSD1 assay[118,120]

This indicated that the nitrogen of the quinolone is either not forming any favourable interactions with Tyr218 and/or Ser222 or that the basicity of the nitrogen is not well tolerated by the active site. The effect of monohydroxylation on the phenylquinolone series is the same as that which was observed for the phenylnaphthalene series, in that there is either low or no activity observed. It was also highlighted that the position of the nitrogen within the compound has little effect on activity.

1.7.2.3 Bis(hydroxyphenyl) substituted Azoles, Thiophenes, Benzenes and Aza-benzenes

As part of Hartmann's non-steroidal inhibitor research programme, where the rationale for inhibitor design has been described previously, led to the discovery of a

new pharmacophore for the inhibition of 17β-HSD1. Where 1,2- and 1,3-bis(hydroxyphenyl) and tris(hydroxyphenyl) azoles were described as novel ER ligands, of these ligands those bearing two hydroxphenyl moieties did not show any binding affinity to the ERs. As a result of this the bis(hydroxyphenyl) moieties were attached to a heterocyclic core and were used as a starting point for the investigation of these compounds as novel non-steroidal inhibitors of 17β-HSD1.[45, 116]

The nature of the heterocyclic core was investigated with a range of hydrogen bond acceptors and donors used. The substitution pattern on the heterocyclic core was also assessed as well as the position of the hydroxyl groups on the phenyl rings. As well as whether one of the hydroxyls could be substituted with a bioisosteric moiety, with the aim of trying to introduce a variety of different moieties, and still maintain activity against 17β-HSD1. (Table 13)

Compound	**R / R_1 / R_2**	**Structure**	**IC_{50} (µM)**
98		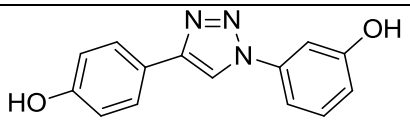	0.84
99		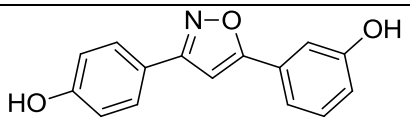	1.61
100		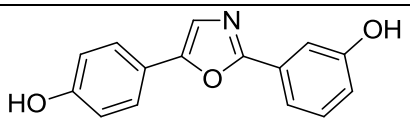	0.31
101	R = CH_3 R_1 = 3-OH R_2 = 3-OH	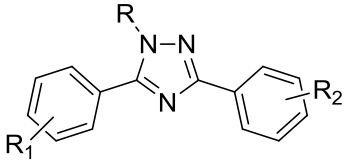	ni
102	R = Ph R_1 = 3-OH R_2 = 4-OH	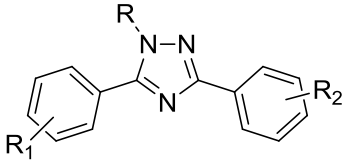	ni

103	R_1 = 3-OH R_2 = 4-OH	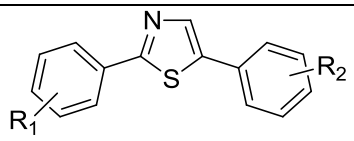	0.05
104	R_1 = 3-OH R_2 = 4-OH	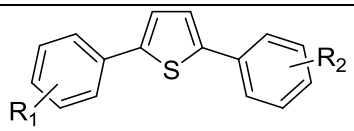	0.069
105	R_1 = 4-OH R_2 = 4-OH	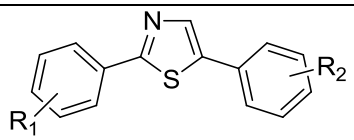	ni
106	R_1 = 3-OH R_2 = 3-OH	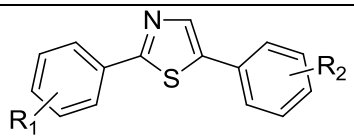	0.243
107	Me	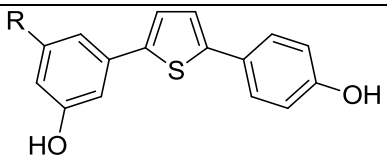	0.629
108	F	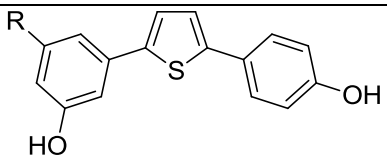	0.042
109	F	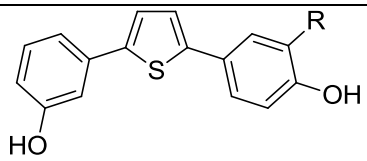	0.008
110		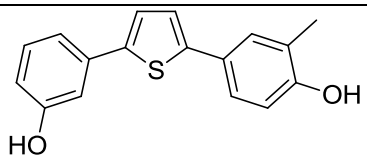	0.046
111		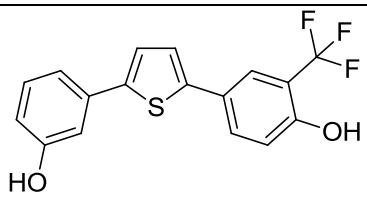	0.038

112	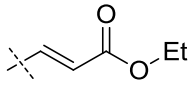	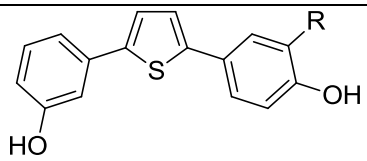	0.130
113	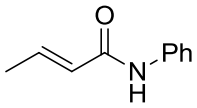	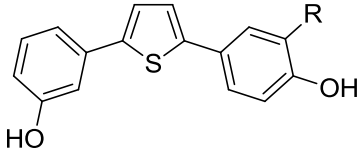	0.427

ni – No Inhibition

Table 13: A table to show the biological activities of a series of bis(hydroxyphenyl) inhibitors as determined in a recombinant 17β-HSD1 assay[121,122]

When looking at the biological results of a recombinant 17β-HSD1 assay it can be seen that compounds from the 5-membered ring series, bearing a heterocycle that acts as a hydrogen bond acceptor (1,2,3-triazoles **98** IC_{50} 840 nM, oxazoles **101** IC_{50} 1.61 μM and isoxazole **106** IC_{50} 310 nM)[45] are active against 17β-HSD1. It was observed however that the 1,2,4-methyl/phenyl substituted triazoles **101** and **102** however were inactive indicating that either the distribution of the nitrogens or the methyl/phenyl substitution are not tolerated by the enzyme.[117] Replacement of the one of the nitrogens present in the heterocyclic core with sulphur gave a compounds with reasonable potency. This led to the investigation of the role of nitrogen in the ring with the synthesis of thiazoles and thiophenes **103**-**109**. In fact the thiazole **103** and thiophene **104** show almost identical potencies, indicating that the nitrogen does not contribute to binding through any obvious hydrogen bond interactions.[116]

The substitution pattern of the two hydroxyl groups of the hydroxyphenyl moieties play an important role in the activity of these compounds with a *para-para* substitution pattern showing low to no activity **105**, whilst compounds bearing a *meta-para* **103**, and *meta-meta* **106** substitution pattern are much more active. It was reasoned that the inactivity of the *para-para* compounds was due to the O-O distance being greater than the 10-13 Å, that was earlier stated as being the optimum distance required for activity.[44, 116]

As stated earlier substitution at position 3 on the heterocycle with either a methyl or phenyl moiety showed a reduction in activity compared to the parent compound.[123] This was also observed for substitution at position 5 on the *meta*-hydroxylphenyl

ring with a methyl **107** IC_{50} = 629 nM, but substitution with a flourine **108** led to an increase in activity IC_{50} = 42 nM. Substitution at position 4 with the same moieties gave a lower activity when compared to substitution at position 5 and the parent compound.[118] *Ortho* substitution was not investigated because substitution at the *ortho* position would force the compounds to become non-planar, and planarity of these compounds was determined to be important for biological activity against 17β-HSD1.[45] Substitution at position 3 on the *para*-hydroxyphenyl ring with a polar or bulky moiety like a hydroxyl or phenyl gave a reduction in activity compared to the parent compound. The introduction of a F at the same position gave the highly potent compound **109** IC_{50} = 8 nM. Substitution with a methyl **110** and CF_3 **111** at the same position also demonstrated an improved activity compared to the parent compound with IC_{50} values of 46 and 38 nM respectively. Functional groups exhibiting a higher degree of flexibility like ethyl acrylate **112** and phenyl acrylamide **113** demonstrated lower activity than the parent compound with IC_{50} values of 130 nM and 427 nM respectively. These results indicate that there is space available for substitution in the active site around the *para*-hydroxy phenyl ring but the nature of the optimum substituent is still to be determined.[118]

All compounds show a low affinity to ER-α and ER-β. In T-47D cells IC_{50} values of 426 nM and 282 nM were observed for compounds **110** and **109** respectively. These results indicate that that the compounds are able to permeate the cell membrane and successfully inhibit the transformation of E1 to E2. Compounds **110** and **109** do demonstrate some biological activity for CYP3A4 with IC_{50} values of 0.50 µM and 0.82 µM respectively. This activity against the hepatic CYP has to be taken into further optimisation of these inhibitors.[118]

To try and introduce variation (Table 14) into these compounds one of the hydroxyl groups was substituted with a bioisostere. The reasoning behind this was that the hydroxyphenyl moiety is susceptible to phase II metabolism.[119] It was previously shown that the *meta*-hydroxyl is important for the activity of these compounds[116] and so was kept in the core structure. Replacement of the *para*-hydroxyl by either a F, NH_2 or SH resulted in a decrease in activity (717 nM vs > 5000 nM). By moving the F to the meta position an improvement in activity was observed (IC_{50} 535 nM **115a** vs IC_{50} 717 nM **114a**) Replacement of the *meta*-Flourine **115a** with a methylsulfonamide **114b** did not result in a change of activity, whilst substitution at

the *meta* position with a bulky substituent like tosylsulfonamide **115c** showed comparable activity to the monohydroxylated thiophene **116** with an IC_{50} value of 350 nM compared to an IC_{50} value of 342 nM indicating that there is room for substitution on one of the phenyl rings but any interactions with amino acids in the active site is not occurring.[118] Some inhibitors bearing one hydroxyl group did display some activity against 17β-HSD1.

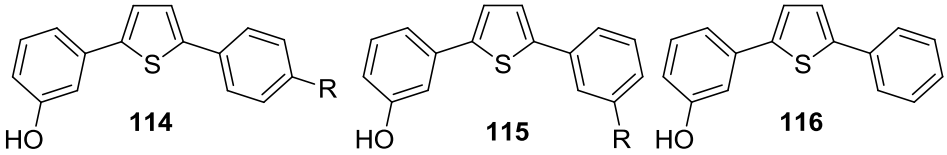

Compound	R	IC_{50} (nM)[a]
114a	F	717
114b	NH_2	>5000
114c	SH	>5000
115a	F	535
115b	$NHSO_2CH_3$	523
115c	Tosylamide	350
116		342

a – IC_{50} determined in a recombinant 17β-HSD1 assay

Table 14: A table displaying the IC_{50} values as determined in a recombinant 17β-HSD1 assay for a series of thiophene modified compounds[118]

As an extension of this work a series of compounds were designed (Table 15) to determine the importance of an aromatic system for these inhibitors. When comparing compounds **117a** and **117b** it can be seen that for compound **117a** the pyridone has a less pronounced aromatic character than the methoxy pyridine **117b** and is inactive compared to an IC_{50} of 690 nM. The reasoning as to why **117b** is more biologically activity when compared to **117a** was that the nitrogen and oxygen of the methoxy pyridine moiety can potentially form hydrogen bonds with the amino acids that form the catalytic centre of the 17β-HSD1 active site. This high activity

was obtained with a *meta-para* substitution on the two hydroxyphenyl groups where the distance between the two electronegative atoms is greater than the 11 Å required determined previously as the ideal distance for activity,[44, 116] and so a series of *meta-meta* substituted compounds were synthesised where the distance between these two electronegative atoms is approximately 11 Å. The most potent of these was compound **118a** with an IC_{50} value of 560 nM. When the chlorine moiety was removed from the compound the activity was reduced, highlighting the importance of the chlorine for the compounds activity. The addition of a nitrogen into the central benzene **118c-e** did not improve the activity and so it can be concluded that the nitrogen is unable to interact with any of the amino acids in the active site. These compounds all show good selectivity for 17β-HSD1 over 17β-HSD2 as well as a low affinity for ER-α and ER-β.[120]

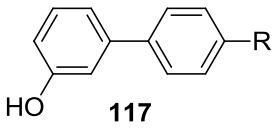

117

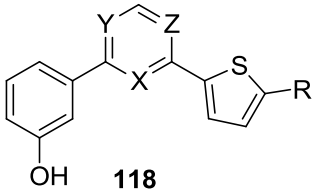

118

Compound	R	X / Y / Z	IC_{50} (nM)[a]
117a	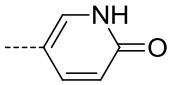		ni
117b	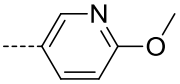		690
118a	Cl	C	560
118b	Ph	C	137
118c	Cl	X = N	139
118d	Cl	Y = N	850
118e	Cl	Z = N	238

ni – No Inhibition a – Measured in a recombinant 17β-HSD1 assay

Table 15: A table to show the biological activities of a series of benzene and azabenzene compounds as determined in a recombinant 17β-HSD1 assay[120]

Even though mid nanomolar activity was observed with compounds bearing only a single hydroxyl group molecular modelling of heterocyclic substituted bihydroxyphenyls showed that linear and non-linear molecules could generate their activity via interactions with the amino acids in the catalytic centre of 17β-HSD1 and a lipohilic sub pocket below the active site. Compounds **119-121** (Table 16) with a ketone moiety and containing two hydroxyphenyls were designed to interact with three distinct areas of the active site shown in Figure 15.

Amongst these the *meta-meta* **119a** and *meta-para* **119d**, but not *para-meta*, substituted hydroxyphenyls showed best activity with an IC_{50} of 22 nM and 33 nM respectively in a human placenta cell free assay,[121] again demonstrating that the *meta*-substituted hydroxyphenyl A ring mimics and *meta*/*para* substituted D ring mimcs are the best substitution pattern for 17β-HSD1 activity.

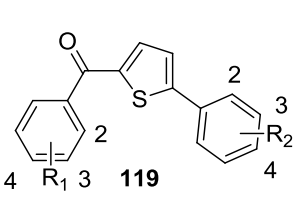

119

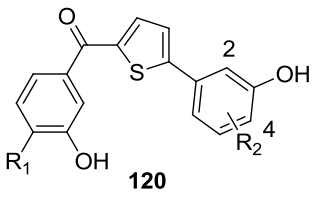

120

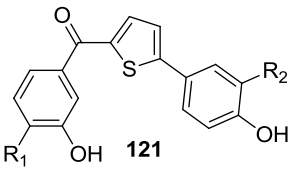

121

Compound	**R_1**	**R_2**	**IC_{50} (nM)[a]**
119a	3-OH	3-OH	22
119b	4-OH	3-OH	368
119c	2-OH	3-OH	945
119d	3-OH	4-OH	33
119e	3-OH	2-OH	95
120a	F		18
120b		2-F	6
120c		4-CH_3	207
121a	F		21
121b		CF_3	16

121c		Cl	5
121d		CH_3	8
121e		F	19

a – Determined in a recombinant 17β-HSD1 assay

Table 16: A table demonstrating the biological activities of a series of thiophene based compounds as determined in a recombinant 17β-HSD1 assay[121]

To try an increase the potential interactions with the active site a series of compounds containing methyl and fluoro substituted compounds were synthesised as it had been previously demonstrated by Bey *et al.*[116] that fluoro substitution can improve the biological activity of the parent compounds. Substitution on either terminal ring with a F can be well tolerated because the biological activity is either similar or improved when compared to the parent compound **121a**, IC_{50} values of 18 nM, 22 nM and 6 nM were obtained for **120a**, **121a**, and **120b** respectively. Methyl substitution though does reduce the activity when substituted on the hydroxyphenyl that is designed to mimic the A ring of E1. Compounds bearing a substitution with a methyl moiety on the D ring mimic of E1 display high activity for 17β-HSD1, but the relative positions of substitution for the methyl and hydroxyl is very important. This can be seen when comparing compounds **120c** and **121d** which have IC_{50} values of 207 nM and 8 nM respectively. To try and combine the inhibitory effects of both the methyl and fluoro substitutions a trifluoromethyl group and its bioisostere chlorine were introduced and these compounds have an IC_{50} value of 16 nM and 5 nM respectively.

When investigating the influence of the centre ring it was observed that the position of the sulphur is very important for activity (Table 17). When comparing compound **122a** and its isomer **122b** there is a marked drop in activity, IC_{50} values of 8 nM and 199 nM respectively. This trend can also be seen when looking at the thiazole isomers where compound **122c** which has the sulphur in the same position as **122a** has the highest IC_{50} value of 35 nM from the thiazole series, **122d** 32% inhibition and **122e** 19% inhibition.

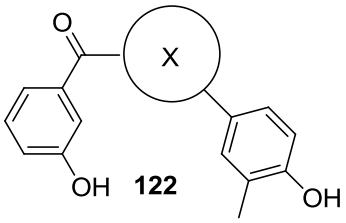

122

Compound	X	IC_{50} (nM)[a]
a	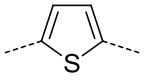	8
b	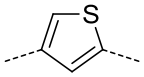	199
c	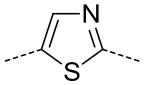	35
d	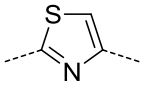	32%[b]
e	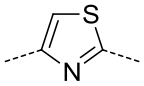	19%[b]

a – Measured in a recombinant 17β-HSD1 assay b – percentage inhibition at 10 μM measured in a recombinant 17β-HSD1 assay

Table 17: A table to show the biological activities for a series of thiophene and azathiophene based compounds as determined in a recombinant 17β-HSD1 assay[127]

When looking at compounds **122a-c** in a T-47D cell assay their activity was similar to that determined in the recombinant 17β-HSD1 assay. It was also shown in human liver microsomes that the most potent compounds **122a-c** are classed in the medium clearance category and none of these compounds have an affinity for ER-α and ER-β.

1.7.2.4 Benzothienopyrimidones

As part of Solvay pharmaceuticals search for therapeutic agents for hormone dependent breast cancer, they investigated non-steroidal small molecules as inhibitors of E2 biosynthesis. Based upon molecular modelling experiments on the active site of 17β-HSD1[122] a small commercial library of compounds were chosen, which were likely to fit into and be complementary to the hydrophobic nature of the

active site of 17β-HSD1 were screened for their inhibitory activity to try and identify potential non-steroidal inhibitors of 17β-HSD1.[123] Compound **123** was identified as a lead compound (Figure 16).[124] Compound **123** has a percentage inhibition of 41 and 99% at 1 µM and 10 µM respectively in a cell based assay.

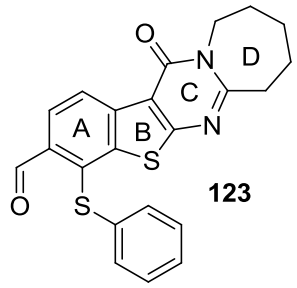

Figure 16: The structure of the lead compound of the benzothienopyrimidone series

To try and improve the biological activity of compound **123** it was decided that modifications were to be made at various positions of the benzothienopyrimidone core. These modifications included the synthesis of derivatives including an aliphatic thioether side chain and an aromatic thioether side chain. These derivatives were evaluated for their biological activity against 17β-HSD1 and 17β-HSD2 (Table 18).

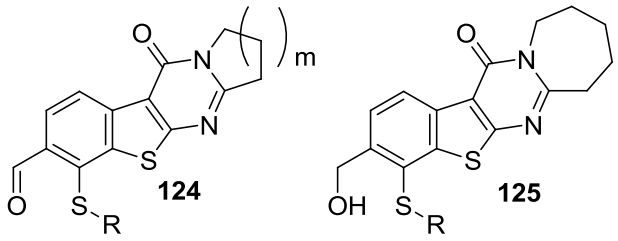

Compound	R	m	% Inhibition of 17β-HSD1 in a cell free assay		% Inhibition of 17β-HSD1 in a cell based assay	
			0.1 µM	1 µM	1 µM	10 µM
124a		3	72	95	66	100
124b	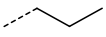	3	73	92	74	100
124c	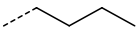	3	68	93	54	100
124d		3	65	93	72	100

124e	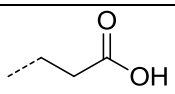	3	0.3	3		
124f	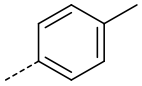	3	63	85	41	99
124g	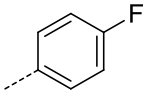	3	87	92	37	77
124h	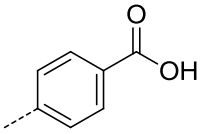	3	4	22		
124i	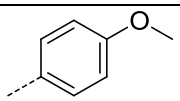	3	89	90	25	72
124j	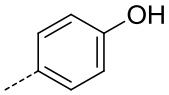	3	59	92	37	77
124k	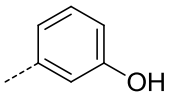	3	94	97	53	84
124l	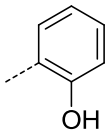	3	86	91	18	90
124m	Pr	1	17	67		
124n	Pr	4	63	75		
125a	Pr		69	86	36	79
125b	Ph		81	88	31	47

Table 18: A table showing the biological activities of a series of benzothienopyrimidones[124]

Most of these compounds showed good to excellent activity against 17β-HSD1. Charged substituents such as carboxylic acids were not well tolerated and their inhibitory activity was lost. The most potent inhibitors were compounds **124g**, **124i**, **124k-l** with inhibitory activities of 94-86% at 0.1 μM concentration. By reducing the

size of the D ring, **124m**, the biological activity was reduced to 17% inhibition at 1 μM compared to the activity of the lead compound **123** with a percentage inhibition of 41% at 1 μM. Similar inhibitory activities were found when the benzylic alcohol **125** substitution was used to replace the aldehyde **124** on the A ring. This indicates that the aldehyde moiety is not essential for the activity of the compounds. It is also stated that the reduction of the aldehyde into the corresponding allylic alcohols maintained the biological activity further supporting this observation. In general all of the compounds based on the benzothienopyrimidine core were selective for 17β-HSD1 over 17β-HSD2 and did not show any undesired estrogenicity in an ER-α or ER-β binding assay.[124]

1.8 Aims of this Work

The aims of this project are to design, synthesise and evaluate novel 17β-HSD1 inhibitors. It is anticipated that inhibition of 17β-HSD1 would block the biosynthesis of the stimulatory sex hormone estradiol and that this could therefore be an effective clinical treatment for breast cancer and other estrogen-dependent diseases. Previous work in the group has already shown that a 17β-HSD1 inhibitor can exhibit positive effects *in vivo*.[43] It is hoped that this project will produce compounds which are potent inhibitors and are selective over other isozymes of the 17β-HSD enzyme family particularly type 2 and that show attractive overall pharmaceutical properties.

This project will utilise many modern medicinal chemistry techniques to introduce functionality at different positions of the steroid core in a step wise manner. In order to do this effectively, a survey of early-stage competitor compounds will be undertaken and from this structure activity relationships can be established. It is hoped that this will provide an effective starting point for synthesis. However, it is also an aim of this project that a multidiscinplinary approach be pursued personally, involving not only synthetic chemistry, but also biological assay development, computational chemistry, enzyme kinetic analysis and potentially protein crystallography. Thus, a very important aim was also the development of a wide skill set within the umbrella of a new area of drug discovery.

The project will use modern computational chemistry techniques to assess the potential of compounds and to establish potential areas of space within the protein target that require further investigation. Several X-ray crystal structures of 17β-

HSD1 are already available with the protein co-crystallised with a variety of ligands. The X-ray crystal structure pdb code 1FDT[76] will be used as both estradiol and $NADP^+$ are present occupying their respective binding sites at a resolution of 2.20 Å. This will enable potentially significant interactions between the enzyme and new inhibitors to be identified.

During this project the compounds synthesised will be assessed for their biological activity against using a whole cell assay developed by colleagues at both Ipsen Paris and Imperial College London. At the start of the third year of this project, Ipsen decided to stop their involvement with this area of research, and so IC_{50} values determined in a cell based assay were not able to be obtained for a number of compounds. To investigate how selected established and new compounds interact with the active site of 17β-HSD1 and the type of inhibition that they display e.g. competitive, uncompetitive and mixed inhibition, production of the recombinant 17β-HSD1 protein in-house will be necessary to provide large enough quantities for both X-ray crystallography, recombinant protein assay and kinetic work. It is envisaged that this will involve the transformation of the 17β-HSD1 gene into an appropriate expression vector followed by subsequent protein expression, purification and characterisation.

Overall, the aim of this multidisciplinary project is to design and synthesise and evaluate novel inhibitors of 17β-HSD1 that ideally exhibit an IC_{50} of below 100 nM, are selective for 17β-HSD1 against other hydroxysteroid dehydrogenases and with good pharmaceutical properties which could ultimately be applied to an unmet clinical need.

Chapter 2

Synthesis, Biological Evaluation and Computation Docking Study of the 2-Substituted Mannich and Friedel-Crafts Series

2.1 Introduction

The following section describes the organic synthesis of novel steroidal 17β-HSD1 inhibitors, where modifications to the steroid core are described in a step wise manner. The IC_{50} determination in a T-47D cell based assay of selected novel steroidal inhibitors was undertaken by collaborators at Ipsen in Paris, and the impact of these findings is evaluated. A computational docking study of the steroidal inhibitors with an X-ray crystal structure of 17β-HSD1 (pdb code 1FDT[76]) was undertaken in collaboration with Dr. M. Thomas who, under instruction by Mr. J Springall (JS) collected the raw data with, interpretation and refinement then being undertaken by JS.

2.2 Design and Synthesis of 2-Substituted Mannich E1 and E2 Derivatives

As stated previously, Hillisch *et al.*[72] and Gege *et al*[73]. introduced substituents at the 2-position of the E1 or E2 steroid core to try and increase selectivity for 17β-HSD1 over 17β-HSD2 as well as to reduce any potential estrogenic effect that might be displayed by these inhibitors. It has been demonstrated that 2-substituted E1 derivatives are potent inhibitors of 17β-HSD1, e.g. **3**, IC_{50} = 47 nM determined in a recombinant protein assay.[7] The compounds described by Hillisch *et al.*[72] and Gege *et al.* [73] have relatively simple modifications and show that 17β-HSD1 inhibition can in principle be obtained with only subtle changes in the steroid core, although no estrogenicity or selectivity data have been reported. These 2-substituted compounds are likely to inhibit any CYP activity, in particular against CYP3A4 as the 2-position lies on a well-known major oxidative metabolic pathway.[74] CYP inhibition might result in the undesired consequence of an increase in pharmalogical effects or toxicity caused by a decrease in drug metabolism. Due to the simplicity of the moieties introduced onto the E1 and D-homo-E1 core there is potential for improving both the activity of the 2-substituted compounds as well as their physico-chemical properties.

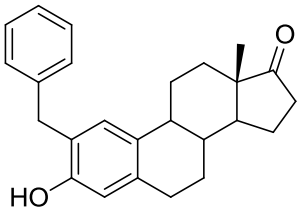

STX2908
126
IC_{50} = 1.0 μM

Figure 17: Structure of 17β-HSD1 inhibitor STX2908 **126**

2.2.1 Synthesis and Biological Results

It is believed that the selective 17β-HSD1 inhibitor, STX2908 **126** (Figure 17) is not particularly soluble in water and therefore it was thought that the introduction of a heteroatom into the 2-substituted moiety might maintain activity whilst also providing the option of forming salts to improve the solubility of these compounds.

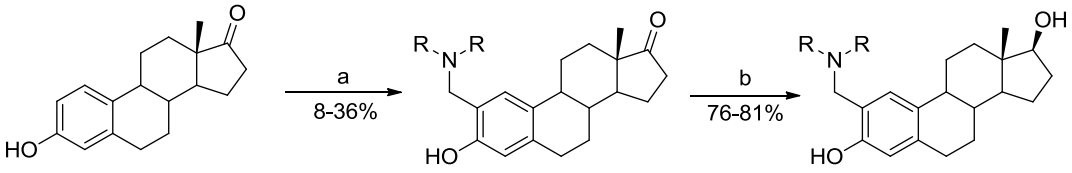

Reaction conditions: a) amine 2 eq, paraformaldehyde, EtOH/Toluene (1/1), reflux, 18 h. b) $NaBH_4$ 1.3 eq, MeOH/THF (1/1), 0 ^oC, 2 h.

Scheme 1: Reaction scheme to show how the 2-substituted Mannich compounds are synthesised from E1

The synthesis of compounds (Scheme 1) containing a nitrogen in the 2-substituted modification came by utilising the Mannich reaction procedure described by Patton *et al.*[125] where a secondary amine is converted into an iminium ion which then readily reacts at the *ortho* position of a phenol. This mechanism is shown below in Scheme 2.

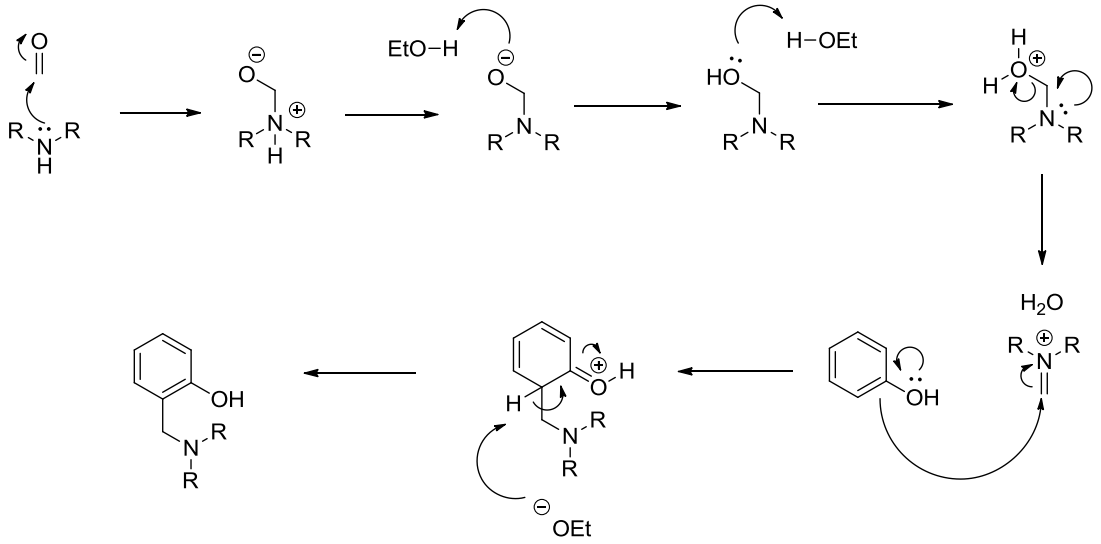

Scheme 2: The mechanism for the Mannich reaction between a secondary amine and phenol

This mechanism can be applied to a wide range of commercially available secondary amines to rapidly access a series of 2-substituted E1 derivatives with the aim of maintaining biological activity against 17β-HSD1, whilst improving the physicochemical properties of the compounds. Figure 18 shows an illustrative example of a HPLC trace for two compounds synthesised in this series, **128** and **129**.

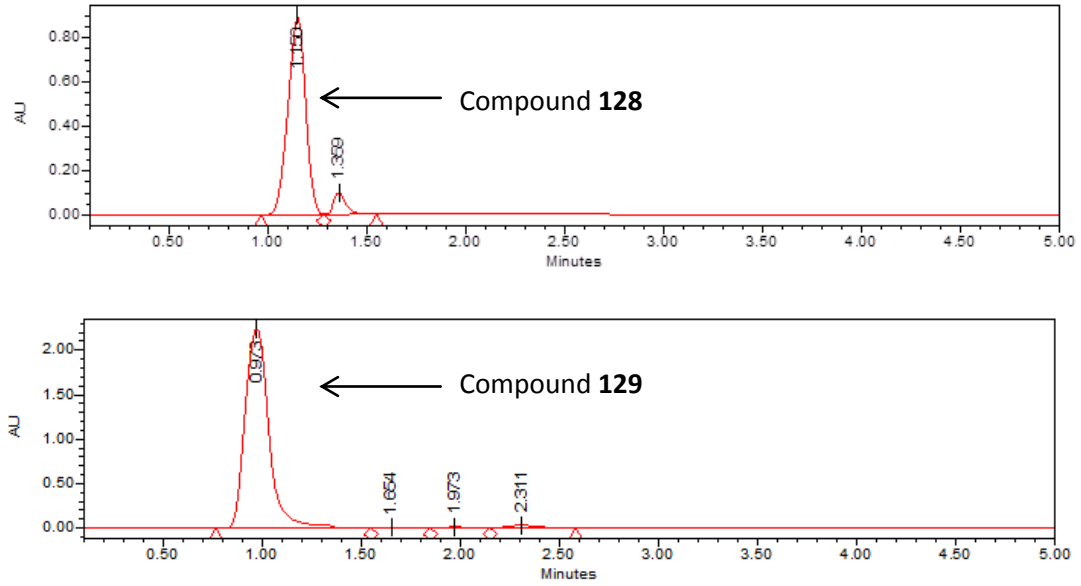

Figure 18: Illustrative examples of HPLC traces for compounds **128** and **129**, (solvent system: 90% acetonitrile in water at 1.0 ml/min), Sunfire C_{18} reverse phase column 4.6 x 150 mm, 3.5 µm pore size

The 2-substituted E1 and E2 Mannich series will also investigate the potential role of aromaticity, ring size, which additional heteroatoms in the 2-substituted moiety can be tolerated and whether having a planar 2-substituent is necessary for activity against 17βSHD1 when compared to compound **126**. The E1 and E2 compounds will be synthesised for each substitution as it is as yet uncertain as to what five membered D ring pattern provides the best inhibitory activity against 17β-HSD1.

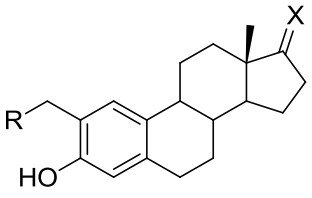

127-129

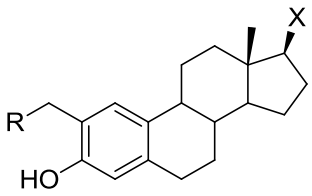

130-132

Compound	R	X	% inhibition at 10 μM[a]	IC_{50} (nM)[a]
127	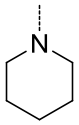	O	28 ± 2	1854 ± 257
128	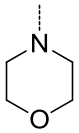	O	96 ± 4	723 ± 138
129	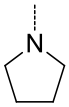	O	93 ± 6	1719 ± 331
130	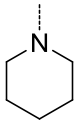	OH	9 ± 0	nt
131	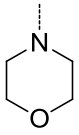	OH	55 ± 1	nt
132	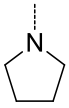	OH	35 ± 7	nt

nt: not tested; a – Measured in a T-47D cell based assay

Table 19: Synthesised 2-substituted Mannich series with biological results against 17β-HSD1 as measured by Ipsen

The data shown in Table 19 shows some interesting results. One of which is that of compound **128** where the substitution at position 2 is that of a morpholine moiety, which displays the best biological activity of this series with an IC_{50} value of 723 nM. This is unexpected because compound **127** has the same ring size as compound **128** but has a significantly lower inhibitory activity against 17β-HSD1 with an IC_{50} value of 1854 nM. This increase in activity could be due to the oxygen of the morpholine moiety forming a beneficial interaction with an amino acid residue within the active site, potentially as an H-bond acceptor. It can be observed that all of the 2-substituted E2 derivatives display lower inhibitory activity against 17β-HSD1 when compared to their 2-substituted E1 counterparts, for example compounds **128** and **131** have percentage inhibition values of 96% and 55% respectively at 10 µM. This demonstrates that for this series, compounds bearing the E1 D ring are best for biological activity. When compared to compound **126** only compound **128** shows an improved activity in a cell based assay with an IC_{50} value of 723 nM compared to 1.0 µM for **126** (unpublished results). This result implies that aromaticity and planarity of the 2-substituent are not key factors for determining the biological potency of the compounds.

Compounds **128** and **129** were sent to the National Cancer Institute USA (NCI) for testing of their inhibitory potential against a variety of different cancer cell lines ranging from leukaemia, K-562; MOLT-4, to renal cancer, RXF393; TK-10 and UO-31. Both compounds **128** and **129** show only minor to no effect against any of the cancer cell lines tested.

2.2.2 Computational Docking Study

Computational bonding interactions

There are several types of non-covalent interaction that are partially responsible for stabilising the position of the compounds in the active site of the protein. These non-covalent interactions are:

Hydrogen bonds

A hydrogen bond is when a dipole is formed between a hydrogen atom, that is covalently bonded to an electronegative atom, and a second electronegative atom e.g. oxygen. Typical hydrogen bond lengths range between 2.6 and 3.5 Å.

Van der Waals

A Van der Waals interaction is where an inductive effect occurs between complimentary partial charges or dipoles in the electron density of adjacent atoms. Typical Van der Waals interactions occur over distances of 2.5 to 4.6 Å.

π-π stacking interaction

A π-π stacking interaction occurs when the p orbitals of two aromatic systems overlap. The π-π stacking interaction occurs at a distance of approximately 3.8 Å.

Hydrophobic interaction

Hydrophobic interactions occur when two non-polar residues are in close proximity, this results in the surface area being exposed to the solvent being reduced. This reduces the entropy of the residues and increases the entropy of all the water present therefore, the formation of hydrophobic interactions is a spontaneous process.

For the docking studies of inhibitors in 1FDT[76] the starting conformations used for receptor docking were generated from an energy minimization performed using the MMFF94s force field, with MMFF94 charges applied, as implemented in Sybyl 7.0. The resulting lowest energy conformer was then used for docking studies using Gold version 2.2 with default parameters. The active site was defined as a 12 Å radius and 30 attempts were computed and scored using Gold score.

The computational docking study provides an insight into how the compounds might bind in the active site of the protein, therefore it is important to bear in mind that any distances reported are only an approximation and not representative of what might be the case in 'real' structures.

After analysis of the compounds through computational docking studies it can be seen that compound **128** has an increased number of interactions with the active site compared to compound **127**. (Figures 19 and 20)

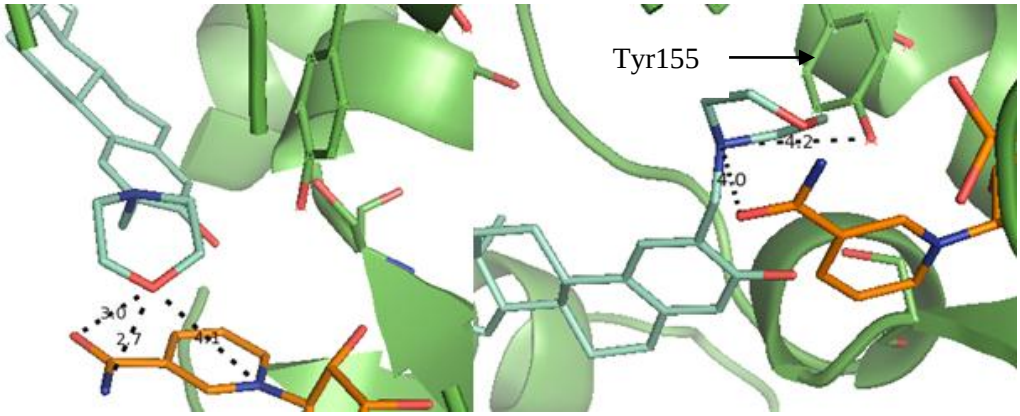

Figure 19: Compound **128** (cyan) docked into 1FDT[76] with NADP (orange) and potential interactions with the morpholine substituent shown

The oxygen of the morpholine substituent in the 2-position displays potential interactions (Figure 19) with the nitrogen and oxygen of the amide from the co-factor at distances of 2.7 Å and 3.0 Å respectively. Additional interactions occur between the nitrogen of the pyridyl ring of the co-factor at 4.1 Å. It was also observed that the nitrogen of the morpholine substituent and the oxygen of the amide present in NADP can potentially interact at a distance of 4.0 Å. The morpholine substituent also exhibits potential hydrogen bonding interactions with the active site of 17β-HSD1 through the hydroxyl of Tyr155 at 4.2 Å. When comparing compound **128** to compound **127**, which has a piperidine substituent at the 2-position, it can be seen from Figure 20, that there are potential hydrogen bond interactions between the 2-substituted piperidine and the active site are with the nitrogen and oxygen of the amide from the co-factor at 3.5 Å and 4.0 Å respectively. This decreased number of potential hydrogen bonding interactions for **127** compared to **128** could explain why **128** is approximately 3 times as potent as **127**. When investigating the ring moiety of the 2-substituent for compound **127** it can be seen in Figure 19 that the morpholine ring of **127** is docked in a boat geometry which is an unstable geometry for a six membered ring to adopt due to steric reasons and bond angles between the carbon atoms within the ring. This indicates that the oxygen of the morpholine moiety is interacting favourably with either the co-factor or a residue within the active site, overcoming the instability of the boat geometry. In comparison compound **128** bearing a piperidine moiety adopts the more stable chair geometry (Figure 20). This

further indicates that the oxygen of the morpholine moiety of compound **127** is forming a favourable interaction with either the co-factor or a residue within the active site of 17β-HSD1.

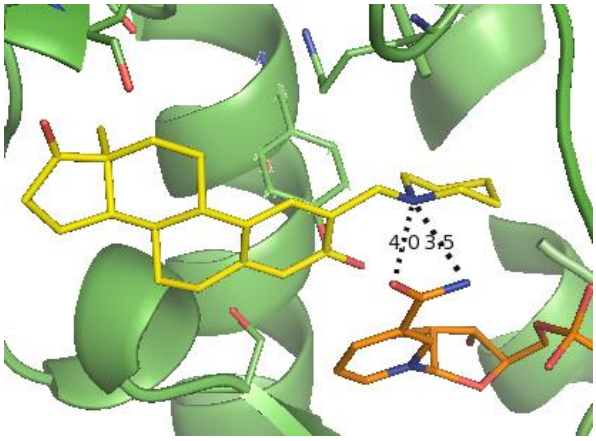

Figure 20: Compound **127** (yellow) docked into 1FDT[76] with NADP (orange) and potential interactions with the piperidine substituent shown

It was observed that, depending on the substituent in the 2-position, the orientation of the compound in the active site changes (Figure 21). This indicates that the active site of 17β-HSD1 is very large and that there is potentially more than one binding orientation for the 2-substituted E1 compounds.

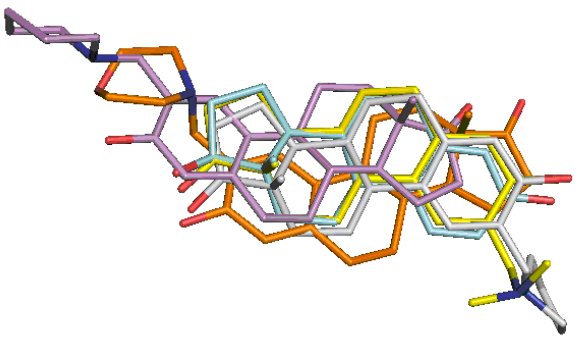

Figure 21: E1 (blue), STX2008 (yellow) a previously synthesised compound bearing a $N(Me)_2$ 2-substituted moiety, **127** (pink), **128** (orange), **129** (white) overlaid in the active site of 17β-HSD1 with the enzyme structure removed

This ambiguity of binding orientation can also be observed from the low resolution X-ray crystal structure obtained of **126** within the active site of 17β-HSD1 (Figure 22), where there is a possible dual confirmation for amino acid residue Phe259. The

electron density of **126** is not entirely resolved, however, there is some electron density which suggests that compound **126** might bind in a mixed orientation and Phe259 shifts accordingly to accommodate the compound. The first orientation consists of the D ring of the steroid core directed towards the $NADP^+$ cofactor binding site, whilst in the second it is observed that the A ring of the steroid points towards the $NADP^+$ cofactor binding site. From studying the available X-ray crystal strucures in the RSCB pdb database it has been observed from the structures for pbd codes 3KLP (Δ^4-diol), 3KMO (3β-diol), 1QYW (androstanedione), 1JTV (T), 3KLM and 3DEY (DHT) that the steroidal ligand binds in the steroidal active site with the D ring pointing away from the $NADP^+$ co-factor binding site (Figure 22). This therefore indicates this observation is not entirely unexpected, although this structure is the first to suggest two competing binding modes.

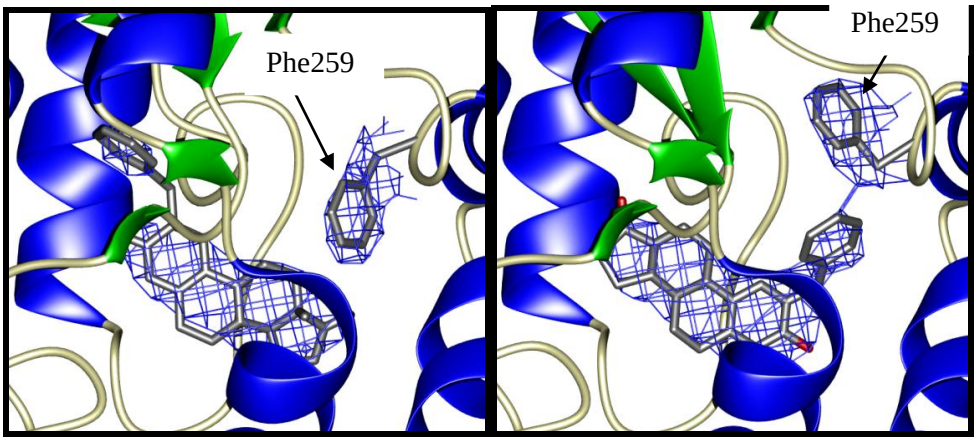

Figure 22: Crystal structure of STX2908 **126** in the active site of 17β-HSD1 at 2.8Å in both binding orientations.

When **129** was docked into the active site of 17β-HSD1 it was observed that it exhibited a different binding orientation to that seen for compounds **127** and **128** (Figure 23) where the D ring points towards the co-factor. This is further evidence that amino acid residues within the active site of 17β-HSD1 can potentially shift to accommodate a variety of compounds.

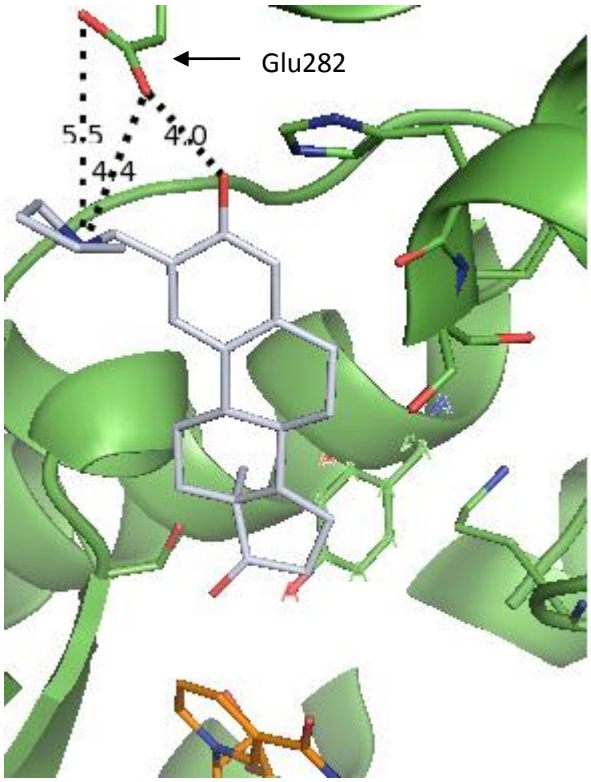

Figure 23: Compound **129** (grey) docked into 1FDT[76] with NADP (orange) and potential interactions with the inhibitors A ring and 2-substituent and the active site shown.

The nitrogen of the pyrollidine substituent from **129** shows potential hydrogen bonding interactions with the oxygen atoms of Glu282 at 4.4 Å and 5.5 Å. The reduced number of interactions with the active site when compared to **128** as well as the change in binding orientation could potentially explain why **129** is not as biologically active as **128**.

These same trends for biological activity against 17β-HSD1 are also observed for the 17β-OH, E2 mimic, compounds. The increased potency of the E1 mimics against 17β-HSD1 compared to the E2 mimics can potentially be explained from the computational docking study as when **128** and **131** are overlaid within the active site of 17β-HSD1 (Figure 24) a change in binding position is observed. The position of **131** moves the morpholine substituent away from the co-factor and therefore moving the morpholine moiety away from the co-factor preventing the formation of any potential intercations that were described previously.

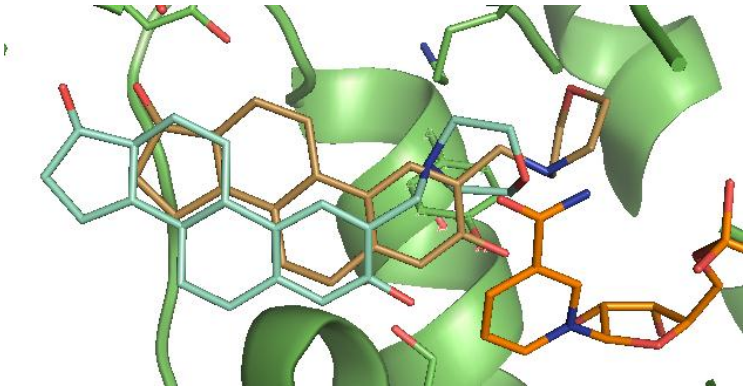

Figure 24: Compound **128** (blue) and **131** (brown) overlaid in the active site of 17β-HSD1 with the co-factor, $NADP^+$ (orange)

The reason for the near comparable activity of compounds **127** and **130** can be theorised as being due to the binding positions of the two compounds being essentially overlaid when determined via computational docking studies (Figure 25).

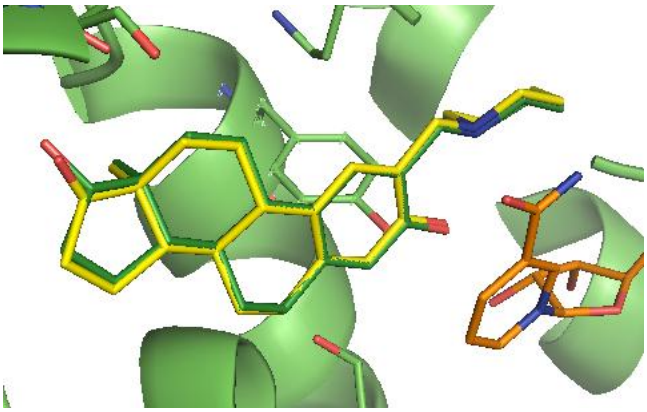

Figure 25: Compound **127** (yellow) and **130** (green) overlaid in the active site of 17β-HSD1 with the co-factor $NADP^+$ (orange).

2.3 Synthesis of Second 2-Substituted Mannich Series

It was hypothesised that, because the morpholine substitution at the 2-position of the steroid core gave the best inhibitory activity against 17β-HSD1, that different 2-substituents containing other heteroatoms might also improve the inhibitory activity against 17β-HSD1 and potentially reduce the estrogenicity of these compounds. However when attempts were made to synthesise other 2-substituted Mannich compounds, the presence of both the 2 and 4-regioisomers was observed in $CDCl_3$ from the ^1H NMR (Figure 26, 27 and Table 20).

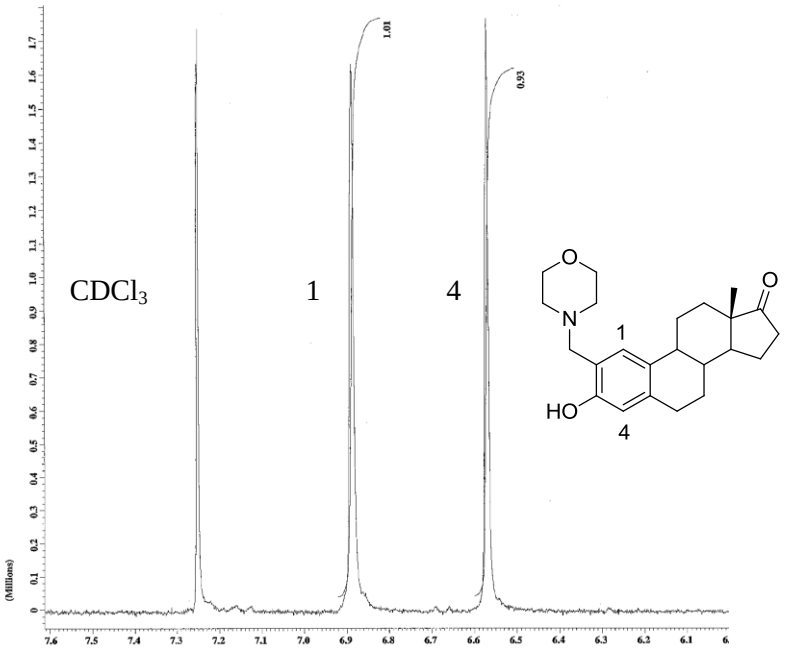

Figure 26: ^{1}H NMR spectrum of compound **128** showing the aromatic hydrogen signals corresponding to the aromatic hydrogens on carbons 1 and 4

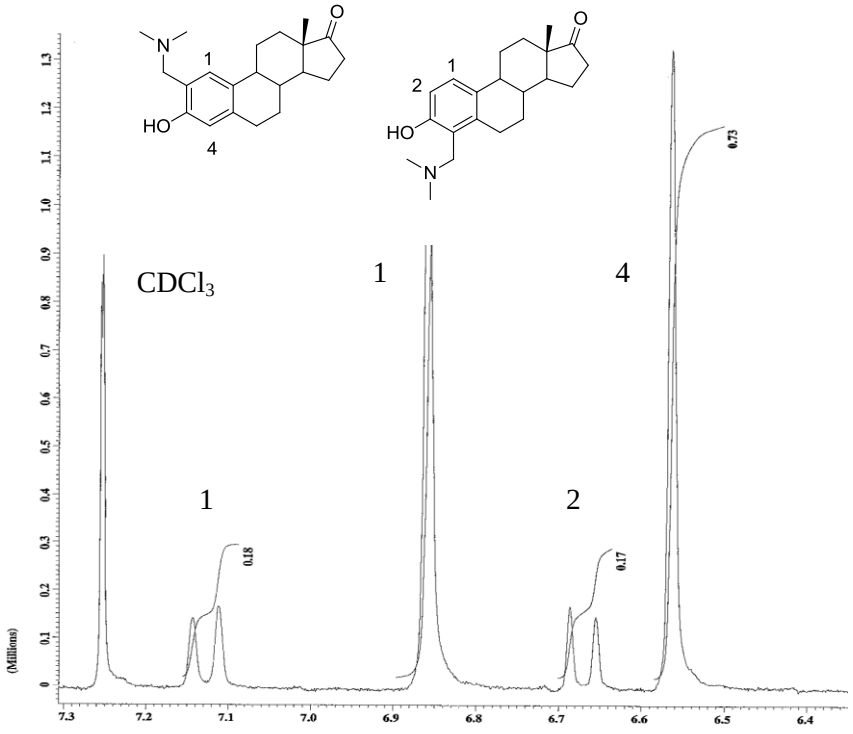

Figure 27: ^{1}H NMR showing the aromatic hydrogen signals indicating that the Mannich reaction occurs at both the 2 and 4-position

Amine	% 2-Substituted E1	% 4-Substituted E1
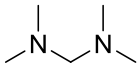	85	15
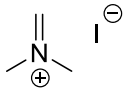 Eschenmoser's salt	80	20
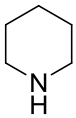 **127**	100	a
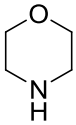 **128**	100	a
 **129**	100	a
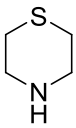	75	25
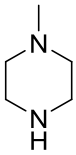	80	20

a – No product detected

Table 20: A table to show which amines were used in the Mannich reaction with estrone and the proportions of the 2 and 4 substituted products of each amine

Following synthesis of the compounds shown in Table 20, attempts were made to try and separate the regioisomers. These regioisomers could unfortunately not be separated by chromatography (HPLC and TLC) or re-crystallisation indicating that the energy required for bond formation at both the 2 and 4-position for the Mannich reaction in this series are very similar and therefore, regioselectivity is specific to the amine being reacted.

When trying to synthesis the *N*-dimethyl-2-substituted E1, the reagent *N*,*N*,*N*′,*N*′-tetramethylmethanediamine was initially used, and when studying the mechanism (Scheme 2) for the Mannich reaction between E1 and a secondary amine, it can be seen that an imine is formed *in situ*. To test whether the mechanism of the Mannich reaction between a secondary amine and E1 proceeded in the manner stated in Scheme 1 Eschenmoser's salt was used without the presence of paraformaldehyde. The reaction between Eschenmoser's salt and E1 provided both the 2 and 4-substituted regiosiomers in the same ratios as was observed for the Mannich reaction using *N*,*N*,*N*′,*N*′-tetramethylmethanediamine, therefore showing that the Mannich reaction between E1 and a secondary amine must proceed with the formation of an imine intermediate in the manner of the mechanism shown in Scheme 2.

2.4 Results of additional biological testing

The most potent inhibitor from the 2-substituted Mannich series compound **128** was selected for further *in vitro* biological evaluation to be carried out by collaborators at Imperial College London. They were able to determine that **128** shows no cytotoxicity in either MCF-7 (ER^+) or MDA-MB-231 (ER^-) cell lines over 96 h for concentrations up to 50μM. MCF-7 and MDA-MB-231 are breast cancer cell lines which account for a large proportion of breast cancer cell studies. They were also able to demonstrate that **128** is selective for 17β-HSD1 against 17β-HSD2.

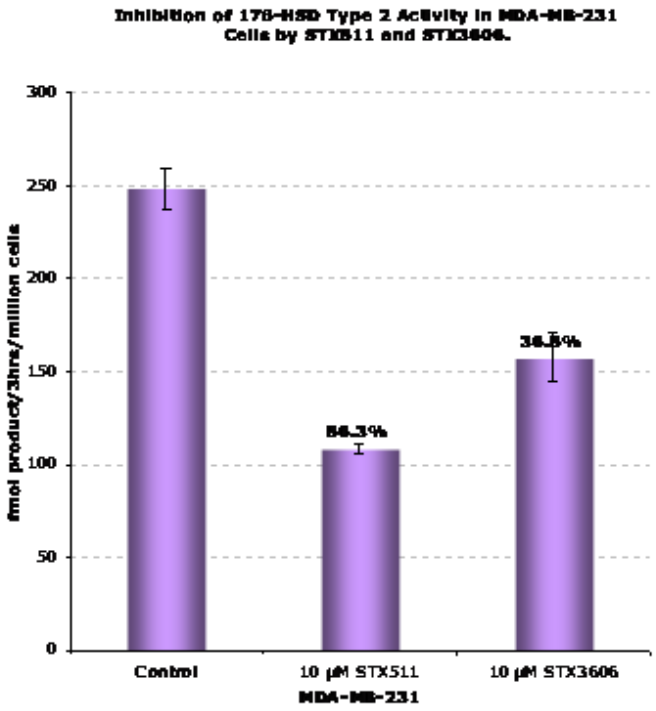

Figure 28: A graph to show the percentage inhibition of 17β-HSD2 activity in MDA-MB-231 cells. STX3606 is compound **128** and STX511 was another compound under investigation as determined by collaborators at Imperial College London in MDA-MB-231 cells

Compound **128** shows 37% inhibition of 17β-HSD2 at 10 μM (Figure 28), but is selective for 17β-HSD1 as it displays a percentage inhibition of 96% at 10 μM, giving **128** a selectivity ratio of approximately 2.6 for 17β-HSD1 over 17β-HSD2.

Due to compound **128** displaying favourable biological results, it was taken forward for testing against certain cytochrome P450s (CYPs), namely CYP3A4 which is primarily associated with metabolism of the 2-position of the steroid core, to assess the metabolic stability of compound **128**. This testing was performed by collaborators at Imperial College London using the commercially available CYP3A4BFC and CYP3A4BQ inhibition kits produced by Becton Dickinson Biosciences, designed to test the metabolic stability of the compounds under investigation.

		IC_{50} (μM)	
Compound	**Compound structure**	**3A4BFC**	**3A4BQ**
E1	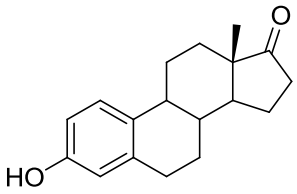	1.5	>100
E2	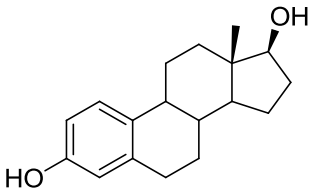	4.4	>100
2-Ethyl E1	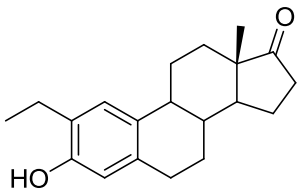	<0.045	1.1
2-Ethyl-3-methoxy E1	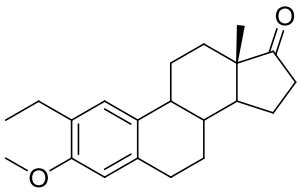	3.8	>100
128	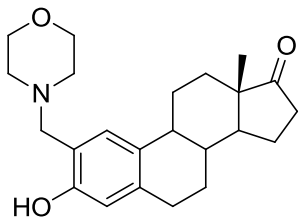	84% @ 10 μM and 70% @ 1 μM	67% @ 10 μM and 65% @ 1 μM

Table 21: Table shows IC_{50} (μM) and percentage inhibition values for steroid-based compounds against specific CYP3A4 using both the CYP3A4BFC and CYP3A4BQ inhibition kits

The compounds used selected in Table 21 were chosen because of their varying activities for CYP3A4 and of these compounds only **129** was synthesised by JS the other compounds had previously been provided to the collaborators at Imperial College London. From the data in Table 21 it can be seen that by having an ethyl

substituent in the 2-position the inhibitory activity against the CYPs is dramatically increased when compared to the natural substrate and product, E1 and E2 respectively. It is also observed that by protecting the oxygen at the 3-position the CYP activity is significantly reduced, IC_{50} 3.8 μM and > 100 μM when compared to IC_{50} values of < 0.045 μM and 1.1 μM for 2-ethyl-3-methoxy E1 compared to 2-ethyl E1 using the CYP3A4BFC and CYP3A4BQ inhibition kits respectively. This substitution pattern is not very useful, however, because as stated earlier substitution at the 3-position can potentially reduce the activity of the compound significantly. When looking at **128** we can see that the percentage inhibition of CYP3A4 is high although this percentage reduces when the concentration is reduced from 10 μM to 1 μM. It is important to bear in mind that these concentrations are much higher than would be seen in a target organ and so can only be used as an approximation of the inhibitory activity of **128** against CYP3A4.

2.5 Design and Synthesis of the 2-Substituted Friedel-Crafts Series

2.5.1 Synthesis and Biological Results

A series of 2-substituted E1 compounds (Table 22) were synthesised utilising the Friedel-Crafts chemistry between commercially available acid chlorides and 3-OMeE1 to provide a series of compounds substituted at the 2-position.

A phenylchloro moiety was chosen for substitution, as in the literature Hartmann *et al.*[116, 121] have shown that compounds substituted with halogens **120b**, **121c** and **121e** can be more potent 17β-HSD1 inhibitors, (IC_{50} values of 6 nM, 5 nM and 19 nM respectively), than the corresponding parent compounds without any halogen substitution being present **119a** and **119d** (corresponding IC_{50} values of 22 nM and 33 nM). This Friedel-Crafts series was designed to investigate whether aromaticity, the presence of a chlorophenyl moiety and length of the 2-substituted moiety are important for the biological activity of these compounds against 17β-HSD1. The 2-substituted Friedel-Crafts series were synthesised (Scheme 3) by methylating the 3-OH of E1, followed by the Friedel-Crafts reaction using the lewis acid aluminium chloride to generate the acylium ion that attacks *ortho* to the 3-OMe. The final step was to de-protect the 3-OMe compounds **134**-**138** by adding a mixture of ammonium hydrochloride and aluminium chloride to a cooled solution before allowing the

reaction mixture to warm to room temperature and then refluxed for two hours before being quenched by pouring slowly onto crushed ice to yield compounds **139-143**.

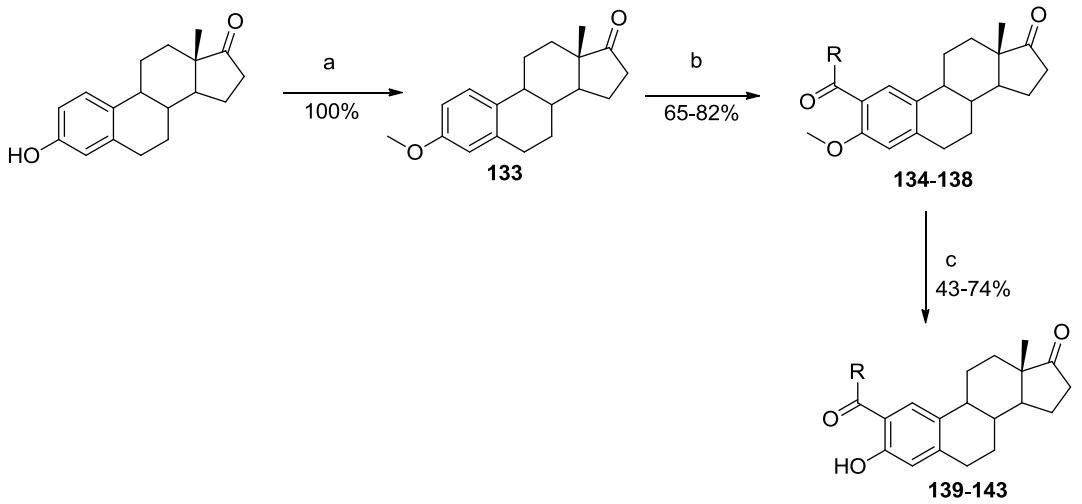

Reaction conditions: a) K_2CO_3 4 eq, MeI 2 eq, DMF, N_2, RT, 2 d. b) Acid chloride 1 eq, $AlCl_3$ 1.1 eq, DCM, 0 ^oC to RT, 15 min. c) $Me_3N.HCl$ 5 eq, $AlCl_3$ 10 eq, DCM, 0 ^oC to RT, 30 min then reflux for 2 h

Scheme 3: The synthetic route followed to access the 2-Friedel-Crafts compounds **139-143**

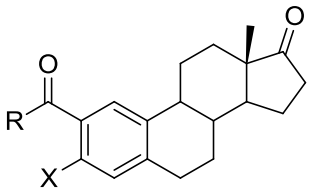

Compound	R	X	% Inhibition at 10 µM
134[a]	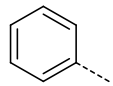	OMe	73 (IC_{50} 1.2 µM)
135	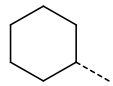	OMe	35 ± 5
136	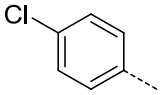	OMe	36 ± 8
137	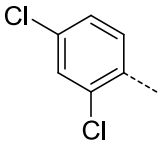	OMe	32 ± 9
138	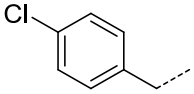	OMe	44 ±3
139[a]	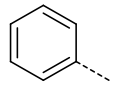	OH	87 (IC_{50} 1.1 µM)
140	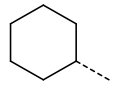	OH	46 ± 1
141	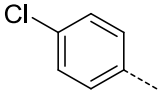	OH	74 ± 2
142	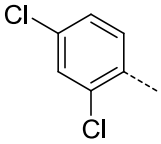	OH	55 ± 4
143	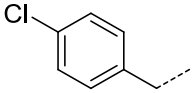	OH	22 ± 10

[a] previously synthesised

Table 22: The biological activities of synthesised compounds **134**–**143** in a T-47D cell based assay as measured by Ipsen

When comparing the 3-OMe and the 3-OH compounds, the 3-OH compounds generally show a higher percentage inhibition, with compound **139** showing the highest percentage inhibition of 74% for the compounds tested. When comparing compound **135** with compound **134** and compound **140**, with compound **139** it is observed that aromatic compounds are moe biologically active than the non-aromatic compounds of the 2-substituted Friedel-Crafts series against 17β-HSD1. It can also be concluded that a chloro moiety is tolerated by the active site but multiple chloro moieties as seen with compounds **137** and **142**, lead to percentage inhibitions of 32% and 55% respectively and are not as well tolerated by 17β-HSD1 as the mono chloro substitution as observed with compounds **138** and **141** which have percentage inhibition values of 36% and 74% respectively. It can also be seen that the distance of the substituent away from the A ring is important for activity. For the 3-OMe compounds the methylene chlorophenyl compound **138** displays a percentage inhibition of 44%, whilst in the 3-OH series its analogue compound **143** has the lowest percentage inhibition of 22%. This is an unexpected result as usually compounds with a free hydroxyl at the 3-position on the A ring are more potent than their protected 3-position derivatives. None of the compounds from the Friedel-Crafts series was assessed for estrogenicity but it is hypothesised that none of these 2-substituted compounds will display estrogenic activity as described previously Vicker *et al*. stated that *in silico* studies using the crystal structure (pdb code 3ERD[114]) of the ligand binding domain of the human ERα have shown that compounds bearing a C2 substitution of the steroid nucleus do not fit well, as the 2-substituent disrupts key hydrophobic interactions in the ERα binding site.

2.5.2 Computational docking study

Through computational docking studies it can be hypothesised that compound **139** can be tolerated by the active site of 17β-HSD1 (Figure 29).

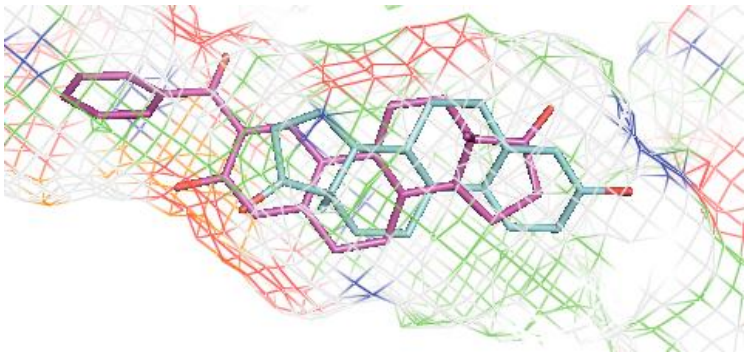

Figure 29: Compound **139** (purple) and E2 (blue) overlaid in the active site of 17β-HSD1.

Only one binding orientation was observed for compound **139** unlike STX2908 **123** (Figure 22) which displays the potential for different binding orientations in the active site. The only difference between compound **123** and compound **139** is that there is a carbonyl between the steroid A ring and the phenyl of the 2-substituent. The carbonyl displays potential interactions with the amide of the $NADP^+$ co-factor at 3.1 Å and 3.8 Å for the oxygen and nitrogen respectively.

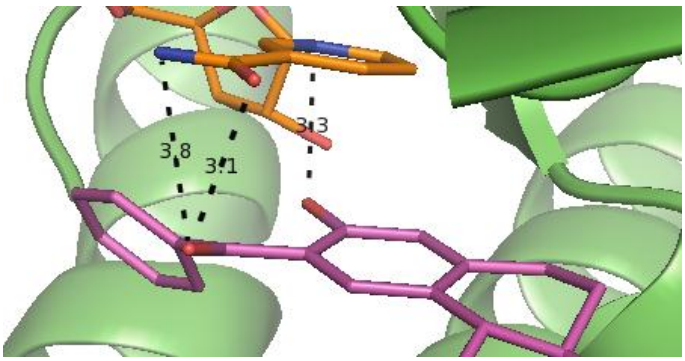

Figure 30: Compound **139** (purple) and NADP (orange) with potential hydrogen bonding interactions shown between the carbonyl of **139** and NADP

The potential interactions between the carbonyl from the 2-substituent of compound **139** and the co-factor doesn't significantly alter the biological activity of compound **139** with comparison to STX2908 **123**, IC_{50} values of 1.1 µM and 1.0 µM respectively. This would imply that the biological activity of these compounds is determined by the moieties present on the ring of the 2-substituent and that the linker

between the A ring and the ring of the 2-substituent does not play a significant role in the binding of these 2-substituted compounds.

When compounds **138**–**143** were docked into the active site of 17β-HSD1 and overlaid (Figure 31) it can be seen that all of these compounds occupy the steroid binding site in the active site of 17β-HSD1. It was observed that compounds **140** and **141** display two binding modes, the first binding mode is where the A ring of the steroid core is orientated towards the co-factor and the second binding mode is where the D ring of the steroid points towards the co-factor this is not surprising due to the similarity of these compounds to STX2908 **123** which has been demonstrated to do the same. Compound **142** displays only the binding mode in which the D ring points towards the co-factor binding site whilst computational docking shows compound **143** binding in an orientation where the A ring is in close proximity to the co-factor.

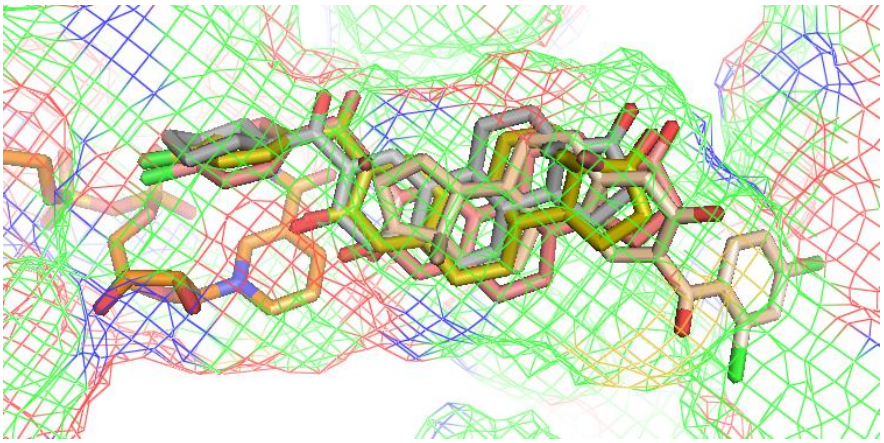

Figure 31: An overlay of compounds **138** (white), **141** (yellow), **142** (pale pink) and **143** (pink) docked into the active site with $NADP^+$ (orange) present.

When looking at compound **141** which displays the highest percentage inhibition, 74.03% it can be seen that the chloro moiety displays a number of potential interactions with the $NADP^+$ co-factor at 3.3, 4.4 and 4.9 Å (Figure 32).

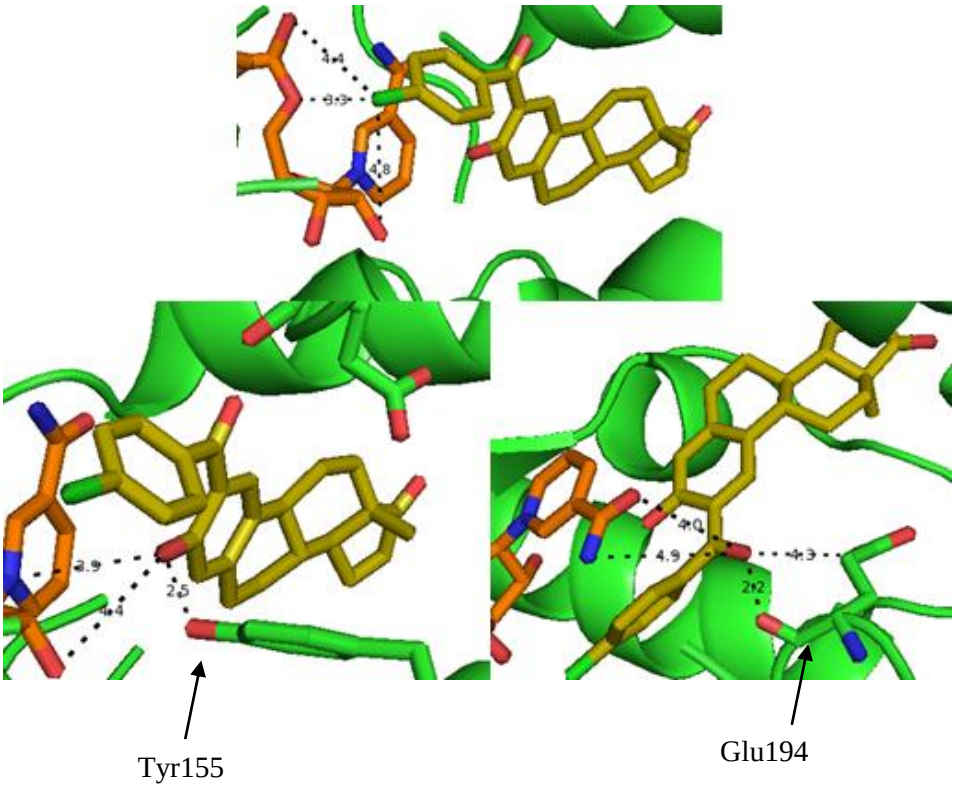

Figure 32: Compound **141** (yellow) with potential interactions shown between the chloro moiety and the co-factor (orange), the hydroxyl on the A ring and the carbonyl linker and the co-factor (orange) and active site amino acid residues Tyr155 and Glu194.

Potential hydrogen bonding interactions were also observed for the hydroxyl present on the A ring and Tyr155 at 2.5 Å as well as the co-factor at 3.9 and 4.4 Å. (Figure 32) Other potential hydrogen bonding interactions were also observed between the carbonyl linker and the amino acid residue Glu194 at 2.2 and 4.3 Å as well as the co-factor at 4.0 and 4.9 Å (Figure 32).

Docking of compound **142** showed that it adopts a binding orientation where the D ring of the steroid core pointing towards the co-factor. Therefore, this compound can form potential interactions with amino acid residues present in the opening of the active site for it to adopt this binding orientation. When looking at the A ring and the 2-substitution of this compound it can be seen that there are several potential interactions between the chloro moieties, the carbonyl linker and the hydroxyl present at the 3-position of the steroid core (Figure 33).

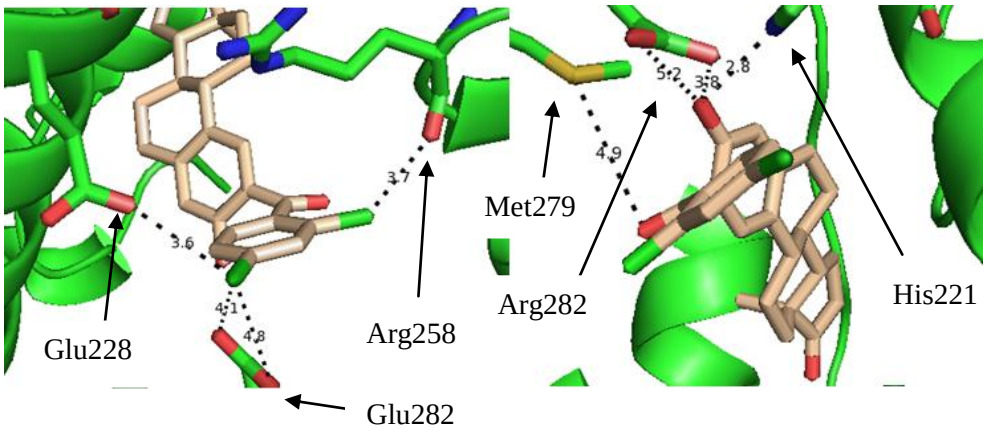

Figure 33: Compound **142** (pale pink) with potential hydrogen bond interactions shown with amino acid residues (green).

The *para* chloro moiety displays potential interactions with the amino acid residues Glu228 at 3.6 Å and Glu282 at 4.1 and 4.8 Å, whilst the *ortho*-chloro moiety shows a potential interaction with Arg258 at 3.7 Å. The carbonyl linker has a potential long distance interaction with Met279 at 4.9 Å. The hydroxyl at the 3-position of the steroid A ring exhibits possible interactions with His221 at 2.8 Å and Arg282 at 3.8 and 5.2 Å. These interactions can explain why compound **142** displays moderate biological activity against 17β-HSD1.

It has been shown that minor modifications in the substituent at the 2-position of the steroid core can play an important role in the biological activity of these compounds against 17β-HSD1. Compound **127** has been identified as the most potent of the compounds described in this series with an IC_{50} value of 723 nM. Compound **127** has also been shown to be selective for 17β-HSD1 over 17β-HSD2 as well as displaying no cytotoxicity for 96 h at 50 µM.

Chapter 3

Synthesis, Biological Evaluation and Computation Docking Study of the 2,4-Substituted Mannich Series

3.1 Synthesis and biological results

To further explore substitution of the A ring it was decided to investigate substitution at the 4-position. The reason for this is that compounds **91-96**,[114] which display a wide variety of substitutions at the 4-position of the A ring mimic, ranging from a bromine in compound **95**, to a phenyl group in compound **96**, have been shown to be

potent inhibitors of 17β-HSD1 with IC_{50} values of 40 nM and 20 nM respectively in a recombinant protein assay. Although compounds **91-96** are of a different class to those being investigated here it does highlight that minor changes in substituent at differing positions of the steroidal A ring can exhibit large effects in inhibitory activity against 17β-HSD1.

To synthesise compounds **147-152** (Scheme 4), E1 was initially methylated at the 3-OH moiety using methyl iodide, followed by regiospecific acetylation at the 2-position using the Friedel-Crafts chemistry that has been previously described to give compound **144**. Compound **144** was deprotected using trimethylamine hydrochloride and aluminium chloride to yield 2-acetyl E1 **145** which was subsequently reduced using H_2 and Pd on carbon for 5 days to give the key intermediate 2-ethyl E1 **146**. Compounds **147-152** were accessed by manipulation of the Mannich reaction described earlier, the reaction was regiospecific because the 2-ethyl moiety prevents attack of the iminium ion at the 2-position, therefore the only position which is accessible for attack is the 4-position. Successively compounds **153-155** were synthesised by reduction using $NaBH_4$ of the C17 carbonyl to the β hydroxyl. This reduction forms only the β orientation and the C18 methyl group prevents attack from the α face.

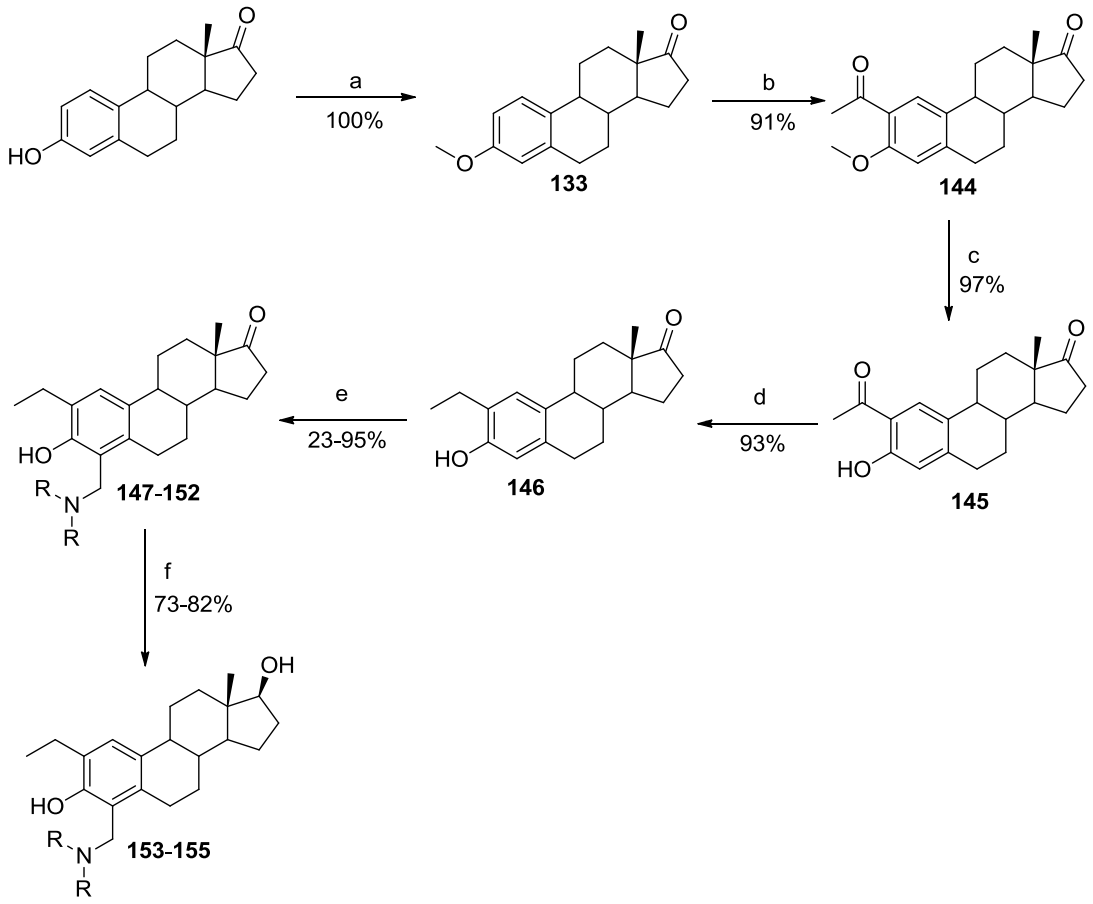

Reaction conditions: a) K_2CO_3 4 eq, DMF, N_2, MeI 2 eq, RT, 2 d. b) acetyl chloride 2.3 eq, $AlCl_3$ 2.5 eq, DCM, 0 ^oC, 50 min. c) $Me_3N.HCl$ 5.5 eq, $AlCl_3$ 11 eq, DCM, 0 ^oC, 40 min, Reflux 3 h. d) 10% Pd(C) 0.037 eq, H_2, 5 d. e) amine 2 eq, paraformaldehyde, EtOH/Toluene (1/1), reflux, 18 h. b) $NaBH_4$ 1.3 eq, MeOH/THF (1/1), 0 ^oC, 2 h.

Scheme 4: The synthetic route used for accessing the 2,4-substituted Mannich series

The added benefit of using the 2-ethyl E1 is that any of the compounds (Table 23) synthesised should not display any estrogenic activity.

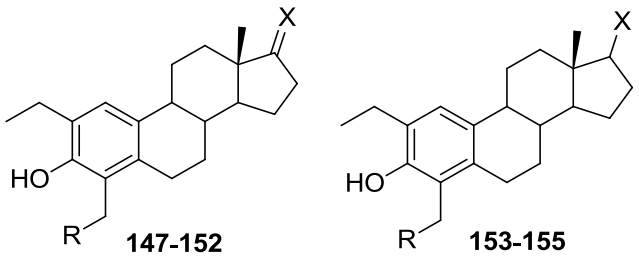

Compound	R	X	% Inhibition at 10 µM
147		=O	43 ± 3 (IC_{50} 4.9 µM)
148	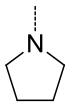	=O	66 ± 6
149	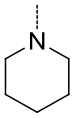	=O	39 ± 5
150	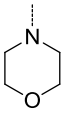	=O	54 ± 4
151	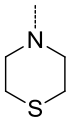	=O	26 ± 4
152	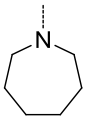	=O	53 ± 6
153		βOH	63 ± 2
154	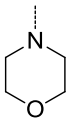	βOH	17 ± 17
155	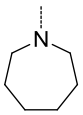	βOH	13 ±13

Table 23: Biological activities of the synthesised 2,4- substituted compounds against 17β-HSD1 in a T-47D cell based assay as measured by Ipsen

From the data in Table 23 is can be seen that the E1 derivatives are more active against 17β-HSD1 than their corresponding E2 derivatives. This was also

demonstrated for the 2-substituted Mannich series described earlier. It can also be observed that it is not the size of the substituent in the 4-position that determines the activity of the inhibitor against 17β-HSD1, as compound **152** with an azepane ring moiety is nearly as active as the compound **148** bearing a pyrolidine ring with percentage inhibition values of 66% and 53% respectively. It can be seen from the biological data for the E1 derivatives bearing a substiuent with a 6-membered ring that the morpholine compound **150** is the most potent with a percentage inhibition of 54%, whilst the piperidine compound **149** which does not contain any additional heteroatoms has a lower percentage activity of 39%, which was also seen for the 2-substiuted E1 Mannich derivatives. From this it could be hypothesised that the thiomorpholine compound **151** would be more biologically active against 17β-HSD1 than the piperidine compound **149**, which is not the case. This could be due to the sulphur atom forcing the six membered ring adopting an unfavourable conformation that is not well tolerated by the active site and therefore, forcing compound **151** to bind in a manner that is not well tolerated by the active site of 17β-HSD1. Interestingly, when comparing compounds **149** and **127** the percentage inhibition of the 2,4-substituted piperidine compound **149** is higher than that observed for the 2-substituted piperidine compound, which is not the case for any of the other 2,4-substituted E1 compounds and their 2-substituted E1 analogues.

When looking at the E2 derivatives, **153** displays the best biological activity, 63% inhibition, with a marked decrease in activity observed for compounds **154** and **155** when compared to their E1 counterparts compounds **150** and **152**, which show very similar percentage inhibitions of 17% and 13% respectively. It is difficult to draw many conclusions for how compounds **154** and **155** interact with the active site of 17β-HSD1 due to the large limits on the percentage inhibition that was measured by collaborators IPSEN. This indicates that when these compounds bear a β-hydroxyl on the D ring they bind in a manner that the size of the 4-substituent plays an increasingly important role in the inhibitory effect of the compounds. In a recombinant protein assay where percentage inhibition is being oberserved in the E2 to E1 direction compound **153** is shown to be acting as a substrate, this has been described in further detail in Section 6.3.5. Overall it appears that the 2,4-substituted E1 and E2 derivatives are moderate to poor inhibitors of 17β-HSD1 and that the nature of the 4-substituent can play an important role in the inhibitory effect of the

compounds against 17β-HSD1. It can also be noted that the substitution of the D ring plays an equally important role in the binding of these inhibitors with the E1 derivatives having a higher affinity for 17β-HSD1 than the E2 derivatives.

3.2 Computational Docking Study

From computational analysis of the 2,4-substituted Mannich compounds docked into the active site of the protein crystal structure of 17β-HSD1 (pdb code 1FDT[76]) it is observed that all of these compounds **147** – **152** fit into the active site (Figure 35).

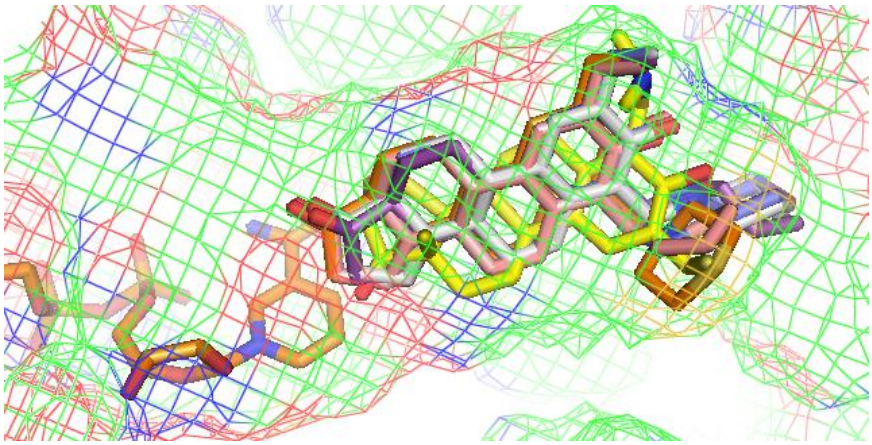

Figure 35: Overlay of compounds **147** (yellow), **148** (pink), **149** (white), **150** (dark blue), **151** (orange), **152** (purple) docked into the active site of 1FDT[76] with the co-factor (orange) shown.

Interestingly, the docking results of compounds **147** – **152** all appear to bind with the D ring of the steroid core in close proximity to the $NADP^+$ co-factor. Only compound **147** the 4-substituted *N*-dimethyl compound positions itself so that the carbonyl present on the D ring at position 17 of the steroid core is in the vicinity of the catalytic triad of Tyr155, Lys159 and Ser142 (Figure 36). It can be observed from Figure 35 that when the 4-substituent is a large ring moiey, the compounds dock into the active site of 17β-HSD1 with the the steroid core rotated through approximately 180º on an axis running through all the rings.

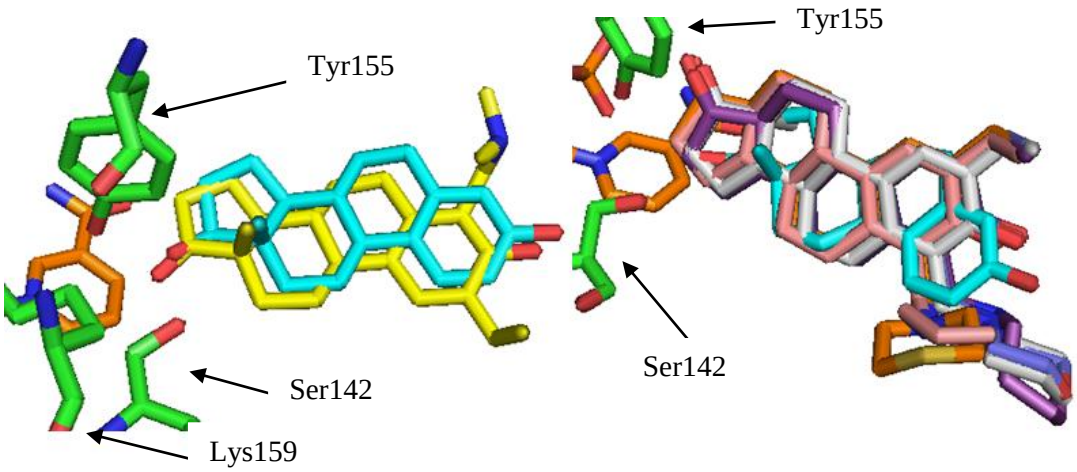

Figure 36: Overlay of compound **147** (yellow) and E2 (blue) with the co-factor (orange) and amino acid residues of the catalytic triad, Tyr155, Ser142, Lys159 shown (green) and an overlay of compounds **148** (pink), **149** (white), **150** (dark blue), **151** (orange) and **152** (purple) with E2 (blue) and co-factor (orange) and amino acid residues (green)

Attempts were made to synthesise a series of 2,4-substituted compounds utilising the Friedel-Crafts approach however, all attempts were unsuccessful. This could be due to steric hindrance around the 4-position of the steroid A ring, preventing attack of the acylium ion intermediate and therefore preventing formation of the desired 2,4-substituted Friedel-Crafts compounds.

It can be seen from the data in Table 23 that the 2,4-substituted Mannich series of inhibitors display poor to moderate inhibition of 17β-HSD1, and are less active than the 2-substituted Mannich series. This implies that to achieve optimum activity against 17β-HSD1 the best position for substitution on the steroid A ring is the 2-position. It can also be concluded that the nature of the substituent plays a very important role in determining the inhibitory potential of the compounds against 17β-HSD1.

Chapter 4

Synthesis, Biological Evaluation and Computation Docking Study of the C17 Amide Series

4.1 Synthesis and Biological Results

It has been shown in the literature[47, 78] that modifications and substitution at the C17 position of E1 can be tolerated by the active site of 17β-HSD1 and that these compounds have the potential to act as inhibitors. The hypothesis behind why these C17 modified compounds act as inhibitors for 17β-HSD1 is because the modification acts as a bioisostere for the hydroxyl at C17 of E2 (Figure 14).

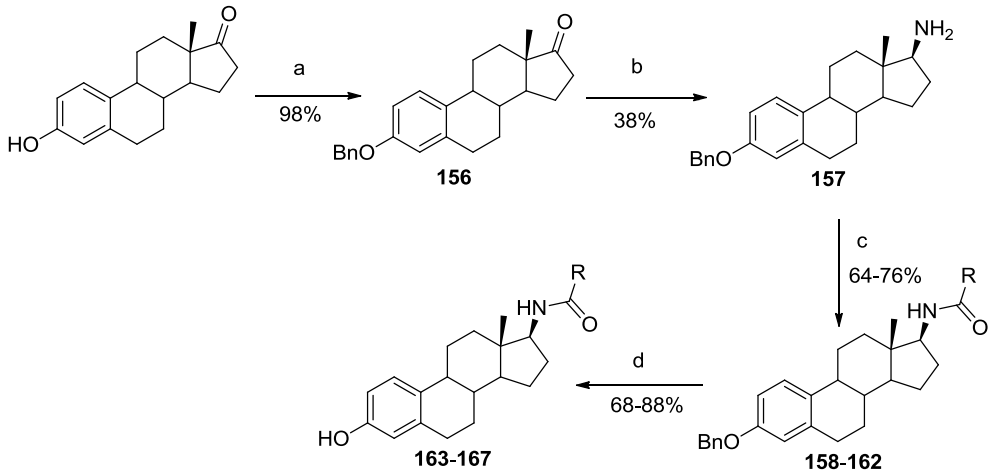

Reaction conditions: a) BnBr 1.2 eq, K_2CO_3 1.2 eq, DMF, RT, 18 h. b) $NaCNBH_3$ 1.2 eq, Ammonium acetate 10 eq, THF/MeOH (200/67), RT, 4 d. c) Acid 0.8 eq, EDCI.HCl 1 eq, DMAP 1 eq, Et_3N 3.3 eq, DCM, RT, 18 h. d) 10% Pd/C 5% mol eq, H_2, MeOH, 18 h.

Scheme 5: The synthetic route for accessing compounds **163-167**

The C17 amine **157** was accessed via a reductive amination between 3-*O*-benzyl E1 **156**, ammonium acetate and sodium cyanoborohydride in THF and methanol at room temperature for four days. Sodium cyanoborohydride was chosen as the reducing agent as it is especially suitable for reductive aminations, since the rate for the reduction of iminium ions is much faster than the rate observed for ketones. The C17 amine adopts a β stereochemistry because the sodium cyanoborohydride attacks from the α face of the steroid core due to the steric hindrance from the β C18 methyl group. The mechanism for this reduction is shown in scheme 6.

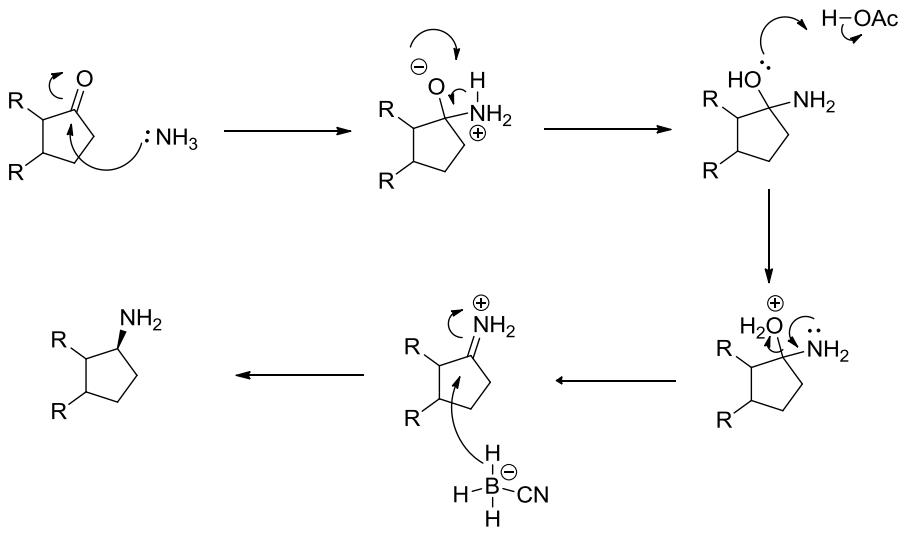

Scheme 6: Reductive amination mechanism for the formation of compound **157**

The C17 amine **157** was then reacted with a series of commercially available benzoic acids using EDCI.HCl, DMAP and triethylamine as an amide coupling reagents to yield the desired C17 amides **158-162**, before the final deprotection of the 3-hydroxyl via a palladium catalysed de-benzylation **163-167**. This amide coupling reaction was initially attempted with a series of benzoic acid chlorides as it was thought that the increased reactivity of the acid chloride would provide higher yields when compared to the EDCI.HCl coupling route. However, these reactions provided the compound in relatively low yields and were troublesome to purify by flash chromatography.

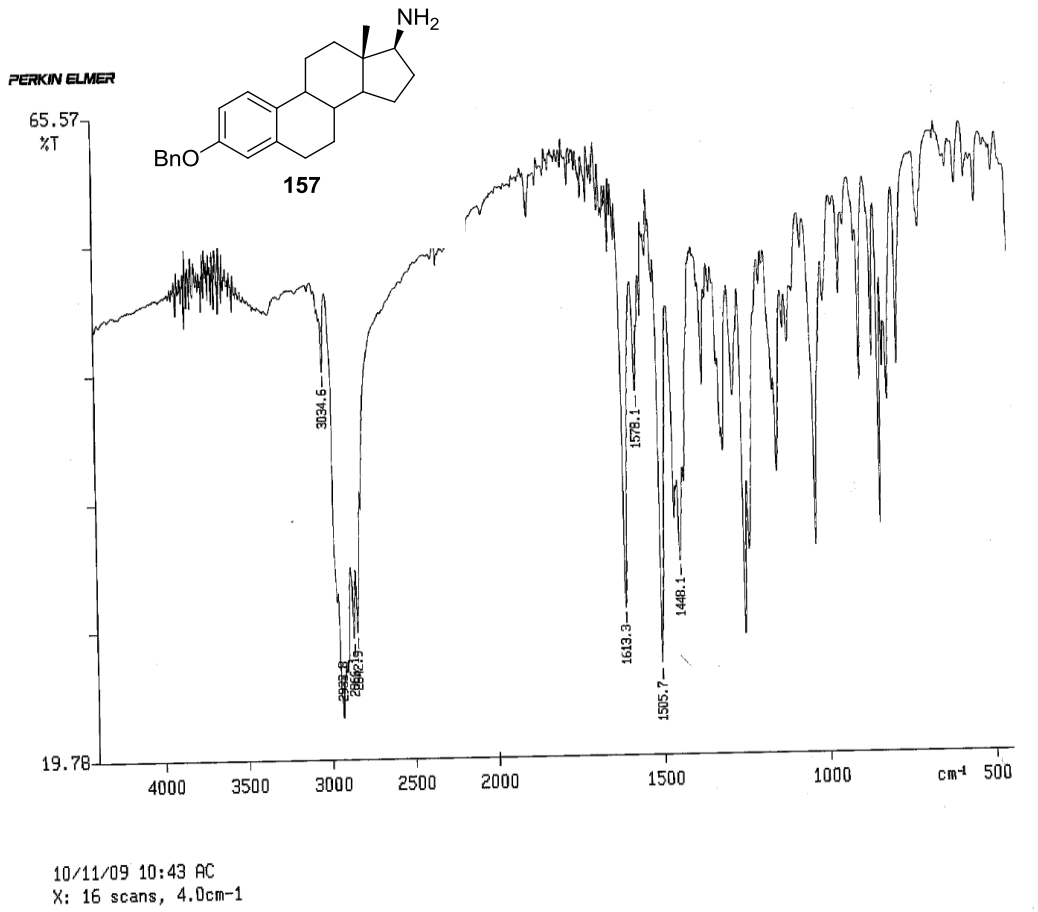

Figure 37: FT-IR of compound **157**, showing that the signal corresponding to the carbonyl stretch is no longer present confirming the synthesis of compound **157**

It was hypothesised that these compounds would bind in the active site with the D ring pointing towards the $NADP^+$ co-factor and the A ring towards the opening of the active site. A methoxy substitution on the benzoic acid moiety was decided upon as this group is an electron donating group and so would provide information about the electronic effects of this region of the active site as well as if there is any size limitation in this region.

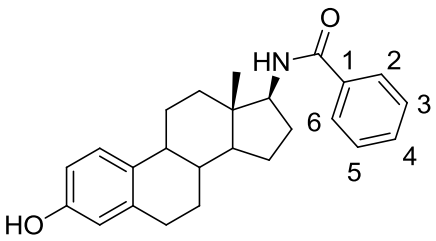

Compound	Substitution					% Inhibition at 10 µM
	2	3	4	5	6	
163	H	H	OMe	H	H	19 ± 11
164	OMe	H	OMe	H	H	27 ± 3
165	OMe	OMe	H	H	H	5 ± 2
166	OMe	H	H	OMe	H	16 ± 3
167	OMe	H	OMe	OMe	H	65 ± 3
168[a]	H	H	H	H	H	15

a – Previously synthesised

Table 24: Biological activities of the synthesised C17 amide compounds **163**-**168** in a T-47D cell assay measured by IPSEN

It can be seen from Table 24 that **166** is the most active compound of the methoxy substituted compounds with a percentage inhibition of 65%. When looking at how the percentage inhibition of these compounds varies with the position of the methoxy substituent it can be seen that having a methoxy moiety in the 4-position the compounds **163** and **164** provide moderate activity against 17β-HSD1 with percentage inhibitions of 19% and 27% respectively. Other compounds **166** and **167** bearing a methoxy moiety at the 2-position are tolerated by the active site and demonstrate moderate to good activity against 17β-HSD1. However, **165** with a methoxy substituent present in the 2 and 3-position shows the lowest activity of all this series of compounds with a percentage inhibition of 5%. The percentage inhibition of **165** is lower than that of **168** which does not bear any substitution of the phenyl ring, indicating that compounds bearing electron donating groups in both the

ortho and *meta* positions are not well tolerated by the active site. Interestingly **166** shows approximately three times the percentage inhibition of that displayed by **165**, 16% and 5% respectively, showing that *meta* substitution of the phenyl ring can be accepted by the active site, so long as the *ortho-meta* substitution pattern is present on opposing sides of the phenyl ring. Compound **166** shows a similar percentage inhibition to **168** signifying that the 2,5-methoxy substitution is as biologically active as the non-substituted phenyl ring. When combining the inhibitory effects of 2,4,5-methoxy substitution in a single compound an increase in percentage inhibition of approximately 3 fold is observed for compound **167** compared to **163**, **164** and **166**.

4.2 Computational Docking Study

Results from a computational docking study of compounds **163-167** docked into the protein crystal structure 1FDT[76] shows that all of these compounds are tolerated by the active site (Figure 38).

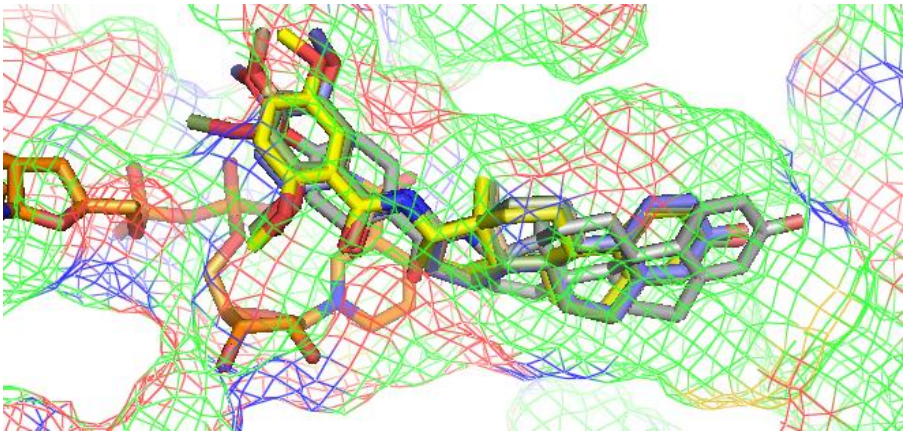

Figure 38: Overlay of compounds **163** (grey), **164** (pink), **165** (green), **166** (yellow), **167** (blue) docked into the mesh protein crystal structure 1FDT with co-factor (orange) shown.

The majority of compounds that belong to the C17 amide series display low inhibitory activity against 17β-HSD1 in a T-47D cell based assay. Due to this it can be concluded that this series of compounds can be tolerated by the active site, however the interactions that are formed are not entirely favourable and so an in depth compoutational docking study was not undertaken for the C17 amide series.

Chapter 5

Synthesis, Biological Evaluation and Computation Docking Study of the 16-Substituted Extended Linker and Reverse Amide Series

5.1 Introduction

It has been shown by Pelletier *et al.*[91, 92] that large substituents at C16 of E2 are well tolerated by the active site of 17β-HSD1. Allan *et al.*[43] have also demonstrated that the Bath drug candidate STX1040 **1** (Figure 5) inhibited E1 stimulated proliferation of T-47D cells *in* vitro and significantly decrease tumour volumes and plasma E2 levels *in* vivo[43]. Further research into the SAR of compounds bearing a C16 substituent is an attractive proposition. To develop the SAR two strategies were devised, the first being the moving of the pyridine substituted amide side chain of the C16 substituent, of STX1040 **1**, one carbon away from the steroid core to investigate what the optimum linker length for these C16 substituted compounds is; the second approach being the reversal of the amide orientation of STX2109 **169** (Figure 39), 103% inhibition at 1 μM and an IC_{50} value of 75 nM, which is designed to investigate whether the same biological activity can be obtained as that seen for STX2109 **169** despite a minor change in structure and therefore providing an insight into how these compounds bind in the active site of 17β-HSD1.

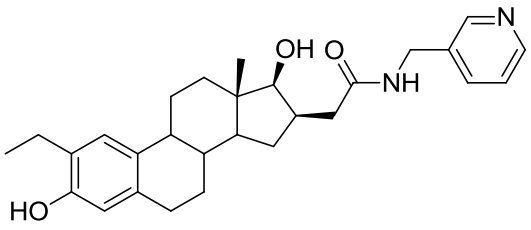

STX2109 **160**

Figure 39: Structure of University of Bath compound STX2109 **160**

We thus decided to synthesise compounds of the following structures:

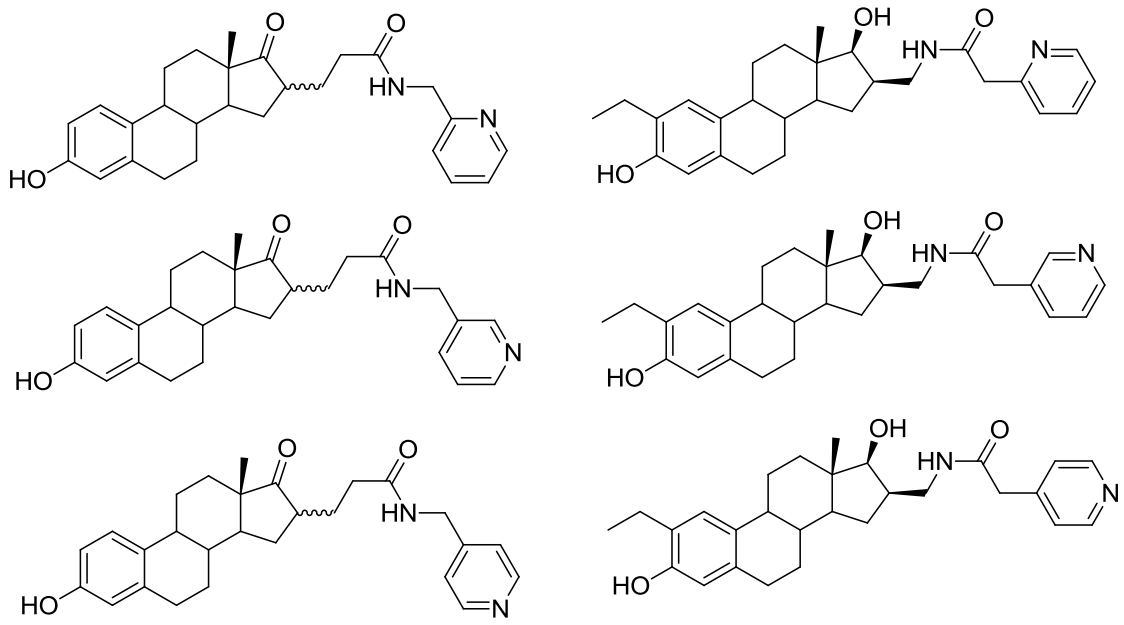

Figure 40: The C16 substituted target compounds

5.2 Design, Synthesis and Biological Evaluation of C16 Extended Linker Series

5.2.1 Synthesis and Biological Results

It has been shown in the literature that by extending the length of the C16 linker that biological activity towards 17β-HSD1 can be increased. This can be seen by comparing compounds **57k** which contains a linker length of 3 atoms and **58k** containing a linker length of 4 atoms, which have IC_{50} values of 0.51 μM and 0.037 μM respectively.[75] By extending the linker length to five atoms we can easily determine what the optimum linker length is for this series of 17β-HSD1 inhibitors.

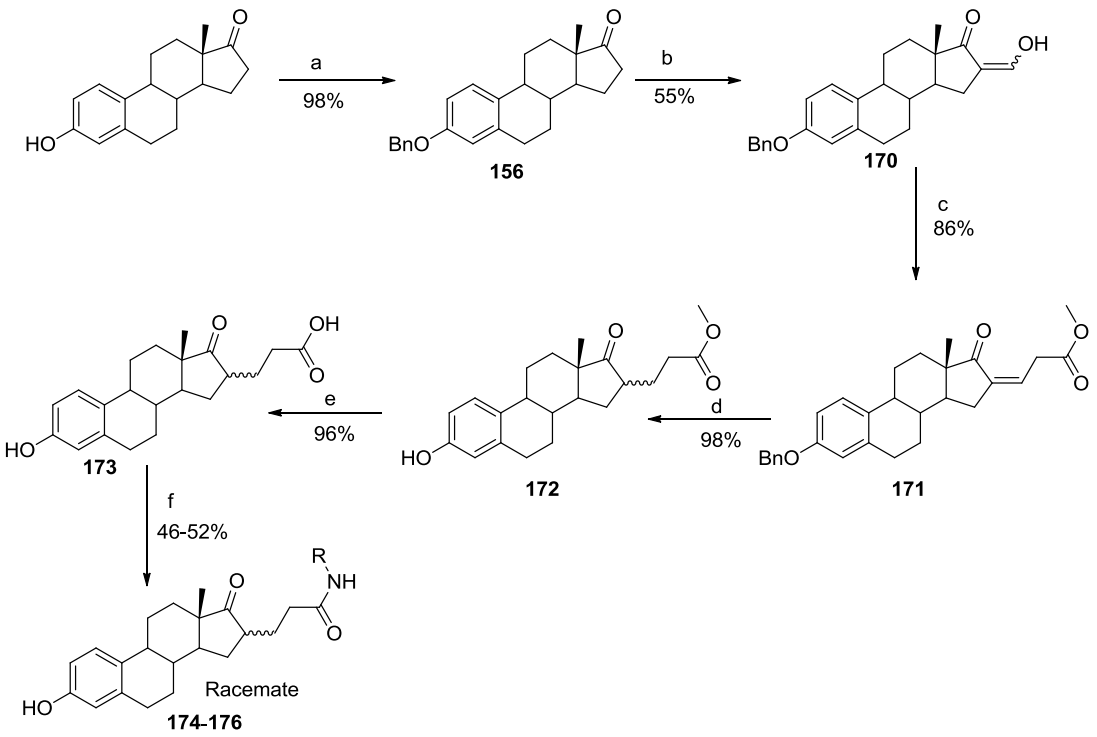

Reaction conditions: a) BnBr 1.2eq, K_2CO_3 1.2 eq, DMF, RT, 18 h. b) ^tBuOK 3eq, Ethyl formate 7eq, Toluene, RT, 2.5 h. c) Ph_3PCHCO_2Me 1eq, $CHCl_3$ RT 18 h. d) 10% Pd/C 0.1eq, MeOH / THF (1/1), RT, 18 h. e) 3M $NaOH_{(aq)}$, 100 ^oC, 2 h. f) Et_3N 3.3eq, EDCI.HCl 1eq, DMAP 1eq, Amine 1eq, DCM, RT, 18 h.

Scheme 7: Reaction scheme for how to access compounds **174-176**.

Compounds **174-176** were accessed by a condensation reaction between ethyl formate and 3-*O*-benzyl E1 **156**, followed by a Wittig reaction with a stabilised phosphoylide to give **171**. The driving force behind the Wittig reaction is the formation of the very stable triphenylphosphine oxide; it is believed that the zwitterionic betaine intermediate rapidly closes to form a cyclic four membered oxaphosphetane which then, depending on the whether the ylide used is a stabilised, or destabilised ylide reacts to give the *E* or *Z* alkene respectively (Scheme 8).

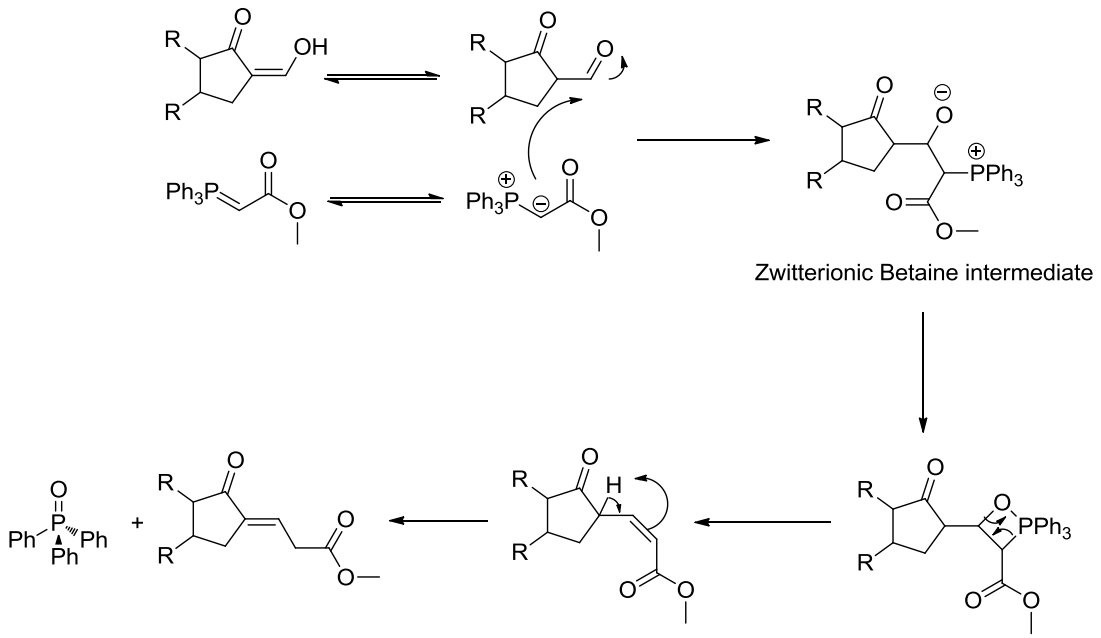

Scheme 8: Wittig mechanism for the formation of compound **171**

Formation of the C16 alkene present in compound **171** can be confirmed by looking at the ^{1}H NMR spectrum in Figure 41 where a doublet is observed at approximately 3.3 ppm which corresponds to a CH_2 bonded to the C16 alkene and the carbonyl. If the double bond formed a single bond further away from the C16 then two doublets would be observed at a higher ppm of approximately 6 ppm to 6.5 ppm. A quartet would also be observed for the C16 CH at approximately 2.5 ppm to 3 ppm which is not the case.

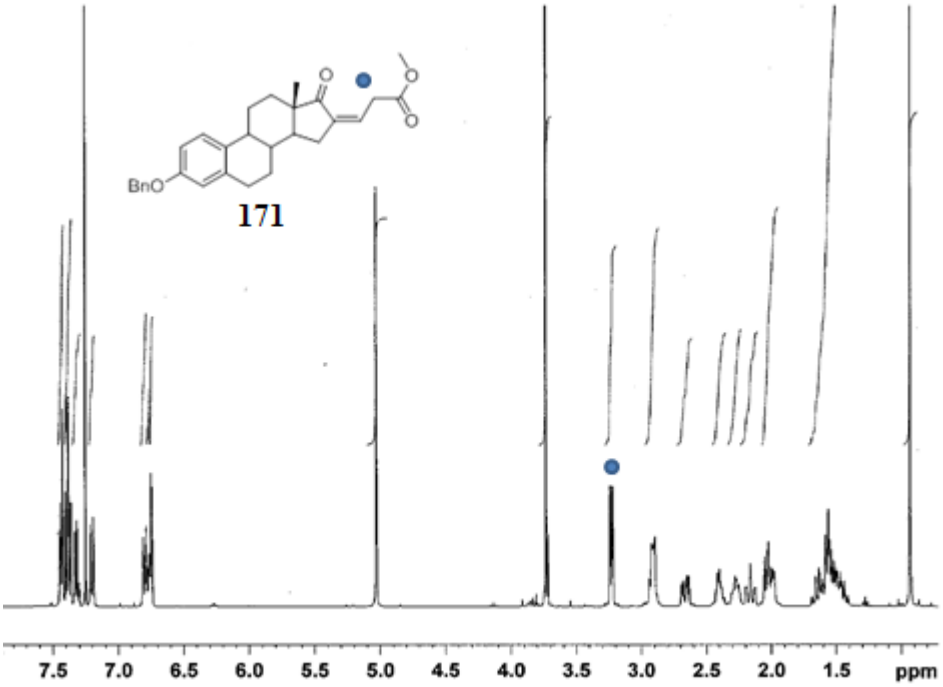

Figure 41: ^{1}H NMR demonstrating the formation of compound **171**, with a CH_2 signal highlighted to show that the oxaphosphetane reacts in the manner shown in Scheme 3

The ensuing reduction of the alkene and deprotection of the 3-*O*-benzyl group yielded compound **172**. Subsequent saponification of compound **172** gave the key intermediate, the ethyl carboxylic acid compound **173**. An amide coupling reaction between a variety of pyridyl amines using EDCI.HCl, DMAP and triethylamine as amide coupling re-agents yielding the desired compounds **174**-**176** (Scheme 4). The biological results for these compounds can be seen in Table 25.

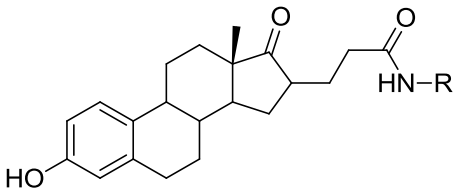

Compound	R	% inhibition at 10 µM
174	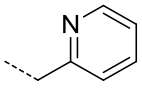	63 ± 3
175	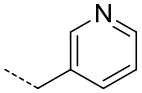	68 ± 1

176	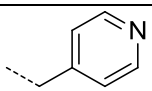	49 ±13

Table 25: Biological results of the synthesised compounds **174-176** in a T-47D cell assay as measured by Ipsen

These inhibitors were tested as mixtures of diastereoisomers, for which the ratio of *R* and *S* was undetermined as only one set of peaks was observed in the ^{1}H NMR spectrum. It can be seen that these compounds display moderate to good inhibition of 17β-HSD1 at 10 μM. As stated earlier, the position of the nitrogen in the pyridyl moiety plays an important role in the biological activity of these compounds. This series of compounds again highlights this observation with the *N-para* pyridyl compound **176** displaying the lowest percentage inhibition of 49%, which is approximately 14% lower than the *N-ortho* pyridyl compound **174** and approximately 19% less than that observed for the most active *N-meta* pyridyl compound **175**. The most active compound having the nitrogen in the *meta* position is not unexpected, as compounds bearing this substitution pattern have been previously shown to be the most active compounds of their series.[75, 104]

5.2.2 Computational Docking Study

From computational docking studies it can be seen that compounds **174-176** are all well tolerated by the active site of 17β-HSD1 and adopt the same binding orientation where the C16 substituent is pointing towards the co-factor binding site which is the proposed binding orientation for STX1040 **1** when it is docked into 17β-HSD1. It was also observed that the steroid cores of compounds **174-176** all occupy the same space as the E2 steroid core of 1FDT[76] (Figure 42).

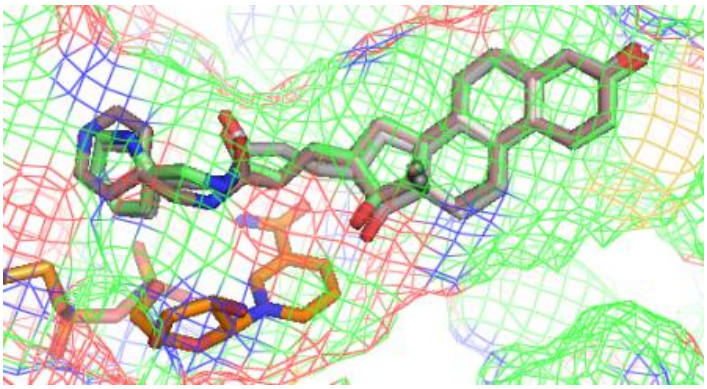

Figure 42: Compounds **174-176** docked into 1FDT[76] with the co-factor (orange), highlighting that they all appear to bind in the same orientation and occupy the same site

Several potential interactions between **174** and both the active site of 17β-HSD1 and the co-factor were identified (Figure 43). These include interactions between the nitrogen of the amide present in the C16 extended linker and a hydroxyl of the ribose linker at a distance of 4.1 Å, and the nitrogen of the pyridyl moiety at a distance of 4.7 Å, as well as the oxygen of the amide present in the C16 extended linker and the nitrogen of the amide present on the pyridyl moiety at a distance of 4.5 Å.

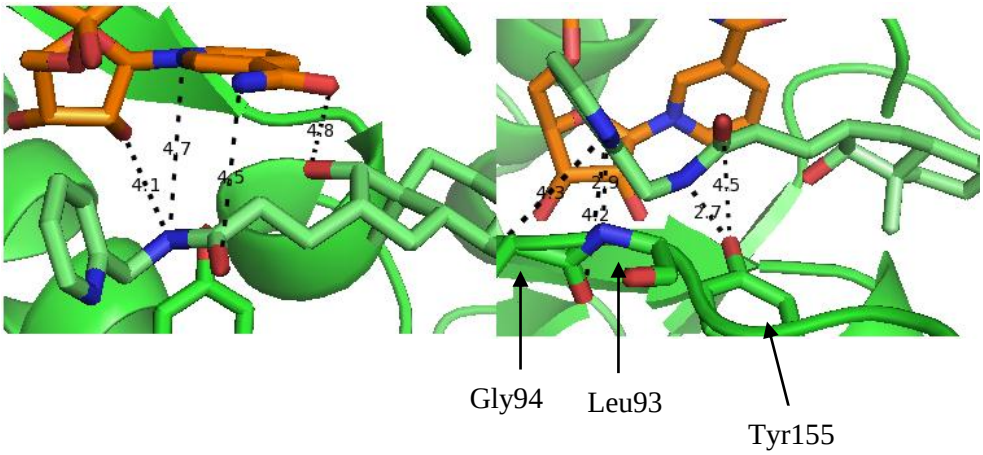

Figure 43: Compound **174** (green) docked into 1FDT[76] with all potential interactions with the co-factor (orange) and amino acid residues (green) shown

Compound **174** displays potential interactions with certain amino acid residues present in the active site of 17β-HSD1, consisting of Tyr155 interacting with both the nitrogen and oxygen of the amide present in the extended C16 linker at distances of 2.7 Å and 4.5 Å respectively. The nitrogen of the pyridyl moiety of compound **174**

looks to have some potential interactions with the oxygen and nitrogen of Leu93 and the nitrogen of Gly94 at distances of 4.2 Å, 4.3 Å and 2.9 Å respectively.

When compound **175** was docked into the active site of 17β-HSD1 (1FDT[76]) potential interactions were observed with both the co-factor and amino acid residues present in the active site. The interactions with the co-factor consist of the nitrogen in the pyridyl ring of compound **175** interacting with oxygen atoms present in the co-factor backbone at distances of 2.7 Å and 2.9 Å, as well as the nitrogen of amide present in the C16 extended linker displaying potential interactions with a hydroxyl present on the ribose at a distance of 4.4 Å and the nitrogen of the pyridyl of the co-factor at a distance of 4.5 Å and with the nitrogen of the amide of the co-factor at a distance of 4.3 Å (Figure 44).

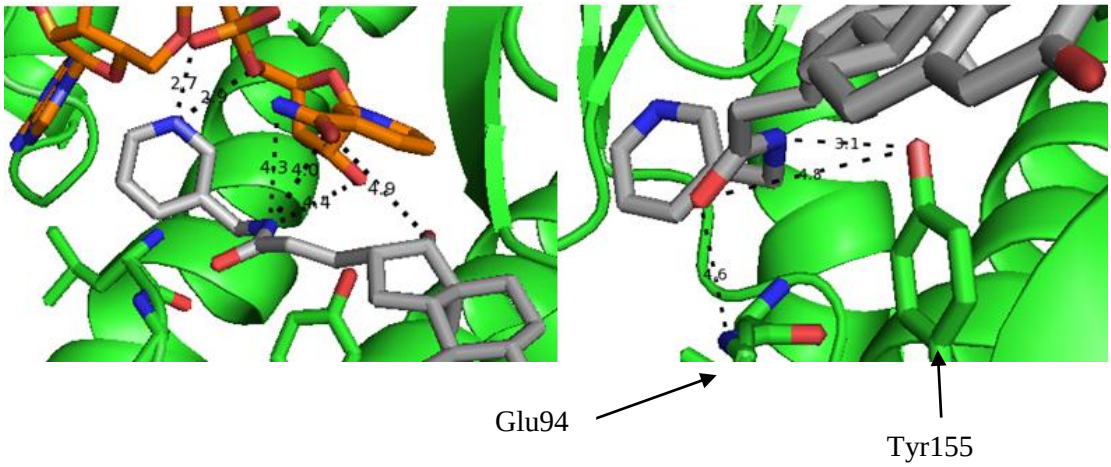

Figure 44: Compound **175** (grey) docked into 1FDT[76] with all potential interactions with the co-factor (orange) and amino acid residues (green) shown

Interactions with amino acid residues Gly94 and Tyr155 were observed (Figure 44). The oxygen of the C16 extended amide linker of **175** displays a potential interaction with the nitrogen of Gly94 at a distance of 4.6 Å, as well as an interaction with the oxygen present in Tyr155 at a distance of 4.8 Å. The nitrogen of the C16 extended amide also interacts with the oxygen of Tyr155 at a distance of 3.1 Å. All of these interactions with both the co-factor and amino acid residues are very similar for both compounds **174** and **175**, which was expected considering their very similar percentage inhibitions of 17β-HSD1 at 10 µM which are 63% and 68% respectively.

A computational docking investigation of compound **176** the least biologically active compound from the extended C16 linker with a percentage inhibition value of 49%

identified similar interactions to those observed for compounds **174** and **175** between the compounds and both the co-factor and amino acid residues Gly94 and Tyr155 (Figure 45). The interactions with the co-factor are between the nitrogen of the amide present in the C16 extended linker and a hydroxyl of the ribose linker at a distance of 4.0 Å, in addition to the nitrogen of the pyridyl of the co-factor at a distance of 4.1 Å, as well as the nitrogen of the amide present in the co-factor at a distance of 4.3 Å. An interaction between the C17 carbonyl of compound **176** and the oxygen of the amide present on the pyridyl ring of the co-factor exists at a distance of 4.8 Å. It appears that unlike compounds **174** and **175**, the oxygen of the amide from the C16 extended linker for compound **176** does not form any potential interactions with the co-factor. This could be one reason why compound **176** displays a lower percentage inhibition when compared to compounds **174** and **175**.

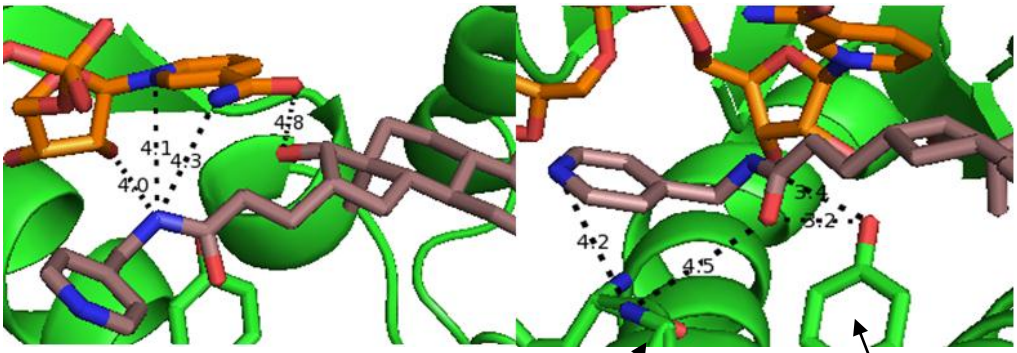

Figure 45: Compound **176** (brown) docked into 1FDT[76] with all potential interactions with the co-factor (orange) and amino acid residues (green) shown

Similarly to compounds **174** and **175** potential interactions between compound **176** and amino acid residues Gly94 and Tyr155 were observed. The nitrogen of the pyridyl E ring of compound **176** can interact with the nitrogen of Gly94 at a distance of 4.2 Å. The oxygen of the amide present in the C16 extended linker can interact with the same nitrogen of Gly94 at a distance of 4.5 Å as well as the oxygen of Tyr155 at a distance of 3.2 Å. The nitrogen of the amide present in the C16 extended linker appears to be able to interact with the same oxygen of Tyr155 at a distance of 3.4 Å. It was noted that no potential interactions with Leu93 were observed for compound **176** when compared to **174** and **175** which again could explain why

compound **176** is the least biologically active compound from the C16 extended linker series.

When comparing the biological activities of this series of compounds **174**-**176** to those observed for compounds **1**, **57j**-**k** and **58k**-m,[109,110] it can be seen that all of the compounds containing a linker length of five atoms **58m** and **174**-**176** display similar percentage inhibition values in the range of 50 – 70%, whilst compounds **57j-k**, **58k-l** bearing a linker length of three or four atoms show percentage inhibition values of approximately 90% and compounds **58k**-**l** depending on the position of the nitrogen in the pyridyl ring. This implies that a linker length of 3-4 atoms is the optimum number of atoms for biological activity against 17β-HSD1. A reason as to why compounds **58m** and **174**-**176** bearing a linker containing five atoms displaying lower percentage inhibitions than compounds with a linker of 3-4 atoms is that the extension of the linker forces the pyridyl ring further into the co-factor binding site, therefore displacing the pyridyl ring away from the optimum binding position.

5.3 Design and Synthesis of the C16 Reverse Amide Series

5.3.1 Synthesis and Biological Results

To access compounds designed from the second SAR strategy 2-ethyl-3-OMe-16-CHOH E1 **177** was reacted with **179** a source of electrophilic nitrogen which was synthesised by reacting hydroxylamine and trifluoroacetic acid anhydride at reflux under anhydrous comditions by a preparation described by Pomeroy *et al.*[126] to give the 2-ethyl-3-OMe-16-CN E1 compound **180**. The proposed mechanism for this reaction is shown in Scheme 9.

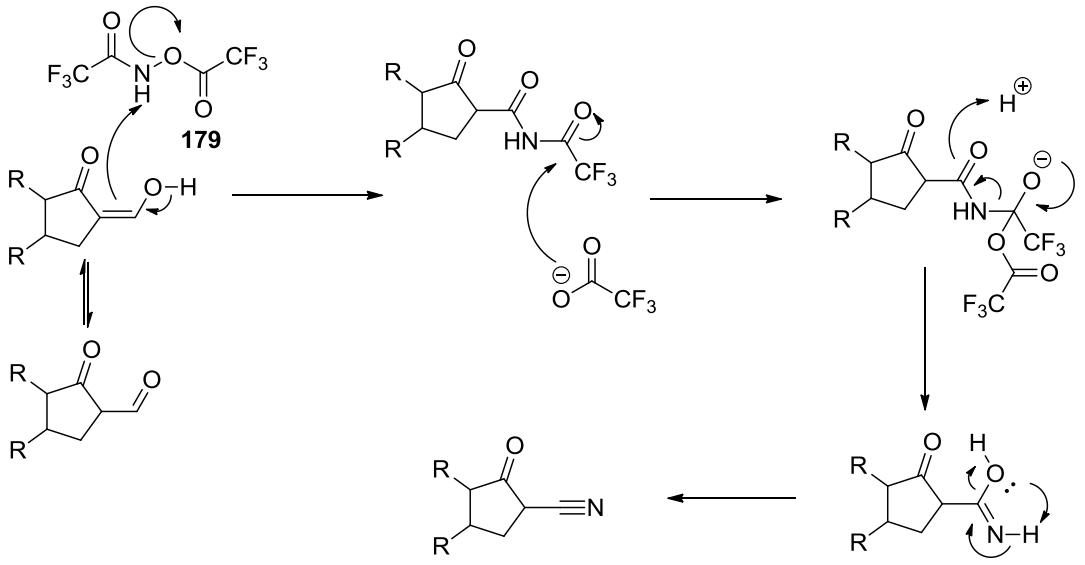

Scheme 9: Proposed mechanism for the formation of compound **179**

It is proposed that the alkene of compound **178** attacks the electrophilic nitrogen of **179** to form the electrophilic amide intermediate that would readily react with the trifluoroactate anion to form an imine intermediate and trifluoroacetic anhydride. The lone pair of the hydroxyl is then thought to attack the proton of the imine and therefore use the formation of the cyano moiety as he driving force for the reaction and giving water as a by product.

A single X-ray crystal structure of this diastereoisomer, compound **180**, shows that it is triclinic and adopts the P1 unit cell. The X-ray crystal structure (Figure 46) confirms the stereochemistry of the 16 and 17 positions of the diastereoisomer **180** as β at both centres. Compound **180** was then reduced with $LiAlH_4$ to give the 16β-methyl amine-17β-hydroxyl diastereoisomer **181**. The amine **181** was then reacted with an aromatic acid chloride to yield the 3-OMe protected desired compound. Reacting the diastereoisomer **181** with the acid chloride was not regiospecific and provided both the 16-*N*-substituted and 17-*O*-substituted compounds. It was thought that this lack of regiospecificity could be avoided because the pKa of the amine is higher than that of the hydroxyl therefore making it a better nucleophile and more likely to attack the electrophilic centre present in the acid chloride. To make the substitution regiospecific for the amine an amide coupling approach was adopted where EDCI.HCl was used in conjunction with DMAP and triethylamine to give compounds **182**-**184**. Demethylation of the resulting compounds with BBr_3 yielded the desired final compounds **185**-**187** (Scheme 10).

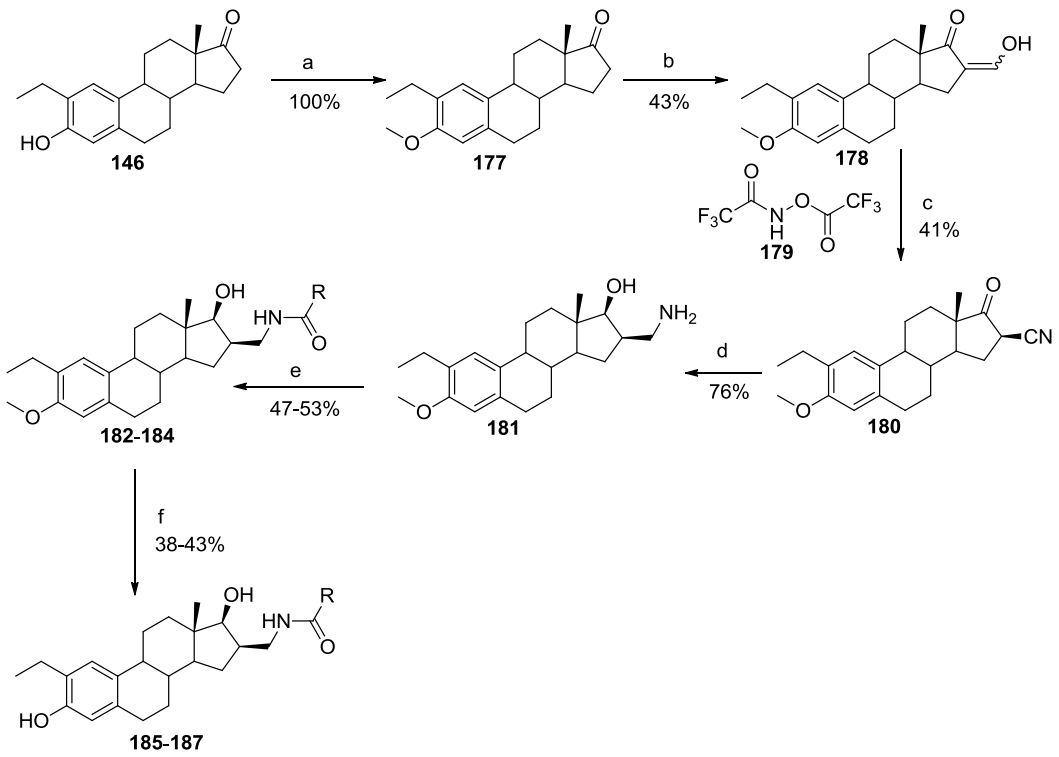

Reaction conditions: a) MeI 1.2eq, K_2CO_3 1.2 eq, DMF, RT, 18 h. b) ^tBuOK 3eq, Ethyl formate 7eq, Toluene, RT, 2.5 h. c) *O,N*-Bis-(trifluoroacetyl)-hydroxylamine 3eq, Pyridine 5.5eq, Toluene, Reflux 3 h. d) $LiAlH_4$ 3eq, THF, 0°C to RT, 18h. e) Acid 1.7eq, TEA 3.5eq, EDCI HCl 1.5eq, DMAP cat. DCM, RT, 18 h. f) BBr_3 3eq, DCM, -78 °C to RT 18 h.

Scheme 10: Reaction scheme for the synthesis of compounds **185-187**

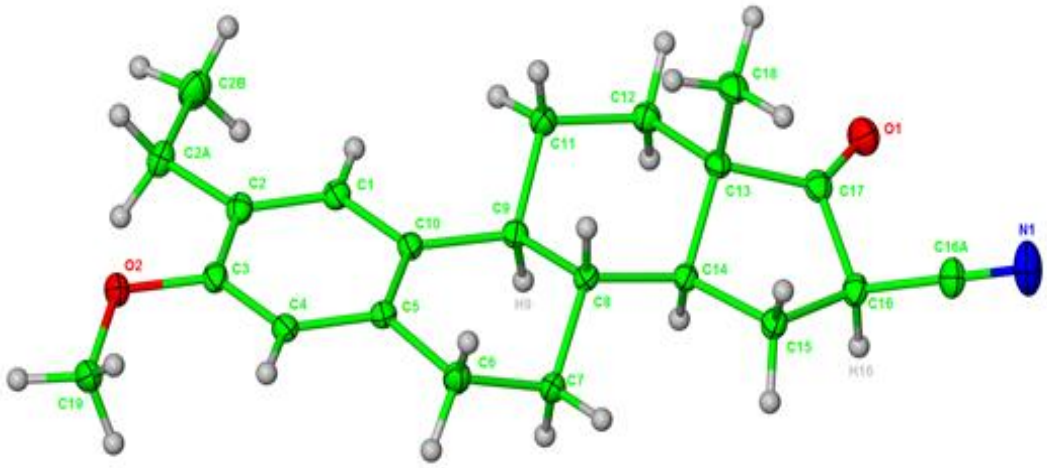

Figure 46: X-ray crystal structure for compound **180** demonstrating the stereochemisty at C16

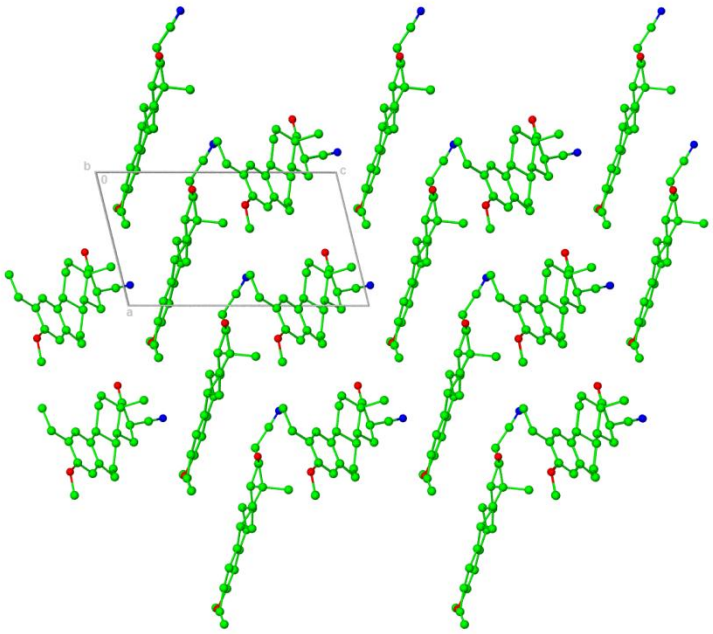

Figure 47: X-ray packing diagram of the diastereoisomer **180**

The $LiAlH_4$ reduction [132] of both the cyano and carbonyl to the corresponding amine and alcohol of compound **181** can be easily monitored by observing the stretches of the corresponding functional groups by FT-IR to ensure that the reaction has proceeded to completion. See Figure 48 and 49 for the FT-IR spectra of compounds **180** and **181**.

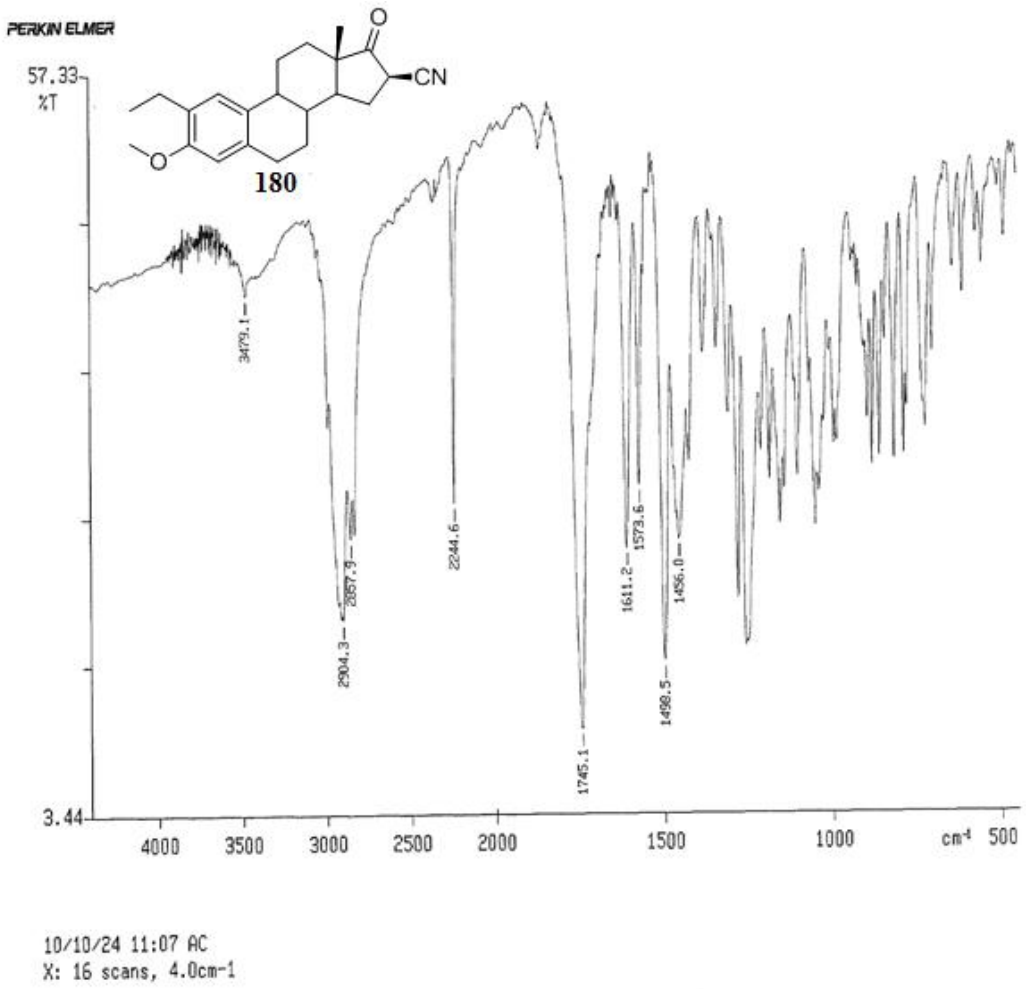

Figure 48: FT-IR spectrum of compound **180** showing the formation of the cyano moiety by the cyano signal at a frequency of 2244.6 cm^{-1}

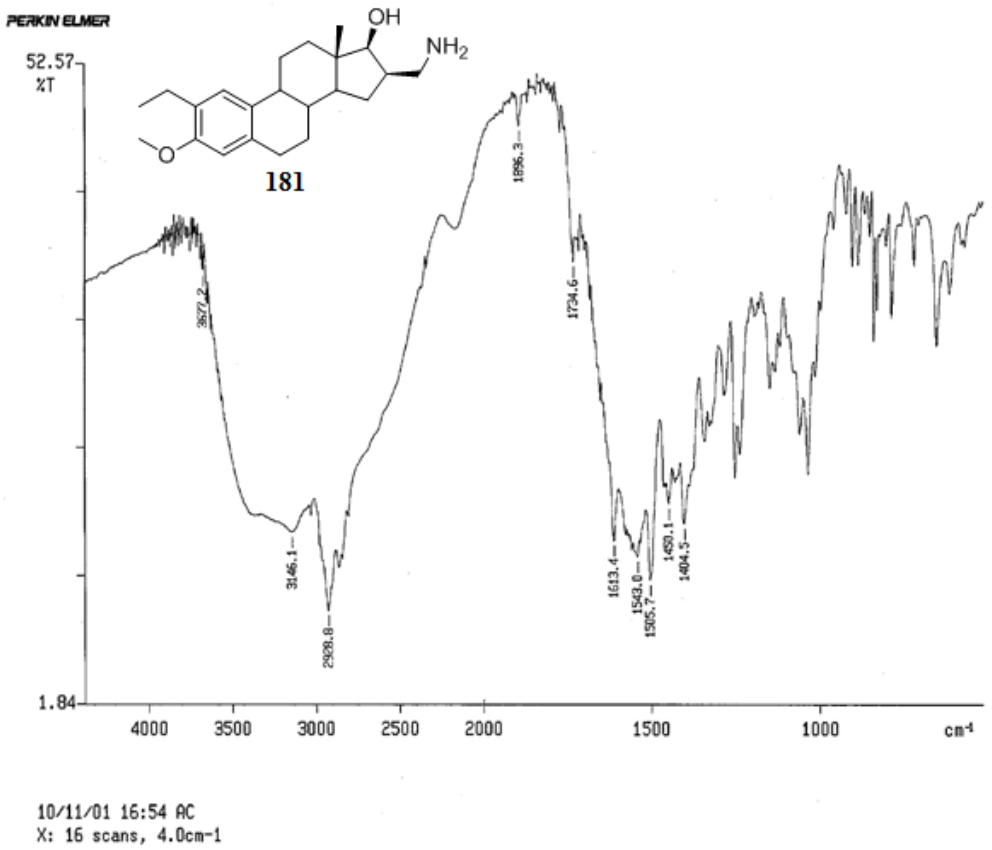

Figure 49: FT-IR spectra of compound **181** with iillustrating that the $LiAlH_4$ reduction has occurred by the loss of signals corresponding to the cyano and carbonyl moities.

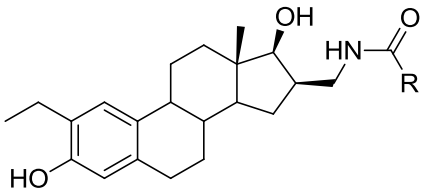

Compound	R	% Inhibition at 10 µM
185	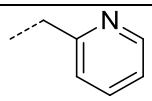	45 ± 3
186	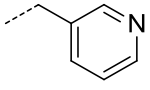	81 ± 1
187	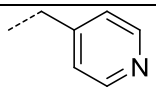	41 ± 1

Table 26: Percentage inhibition data for synthesised compounds **185-187** against 17β-HSD1 at 10 µM concentrations in a T-47D cell assay measured by IPSEN

It can be seen that these compounds display moderate to good inhibition of 17β-HSD1 at 10 μM (Table 26). As previously stated, the substitution pattern of the nitrogen in the pyridyl ring plays an important role in the biological activity of these compounds. This series of compounds again highlights this observation with the *N-para* pyridyl compound **187** displaying the lowest percentage inhibition of 41%, which is very similar to the 45% inhibition observed for the *N-ortho* pyridyl compound **185**. The percentage inhibition of both these compounds **185** and **187** is approximately two fold lower than that observed for the most active *N-meta* pyridyl **186** compound, displaying a percentage inhibition of 81%. The most active compound being that having the nitrogen in the *meta* position is not unexpected as compounds bearing this substitution pattern have been previously shown to be the most active compounds of their series.[75, 104]

5.3.2 Computational Docking Study

From computational docking studies it can observed that compounds **185-187** all fit into the active site and adopt the same binding orientation with the C16 moiety pointing towards the co-factor binding site (Figure 50), which is the hypothesised binding mode for STX1040 **1**. It can also be seen that the steroid core of compound **185-187** all overlay the steroid core of E2 very closely.

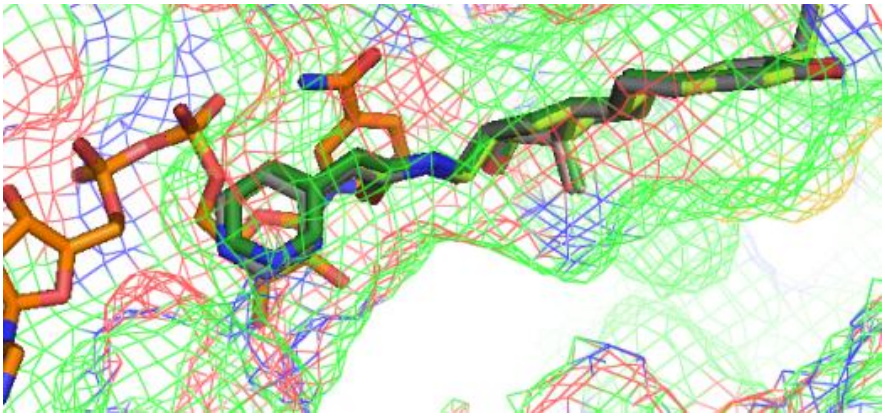

Figure 50: Compounds **185-187** docked into 1FDT[76] with the co-factor (orange), showing that they all appear to bind in the same orientation and occupy the same binding site

The similar biological activities of compounds **174-176** and **185-187** against 17β-HSD1, an be explained as the compounds **186-187** are shown to adopt a very similar binding mode (Figure 51) in the active site of 17β-HSD1 and display similar

potential interactions with the co-factor and amino acids residues present in the active site of 17β-HSD1 as that observed for compounds **174-176**.

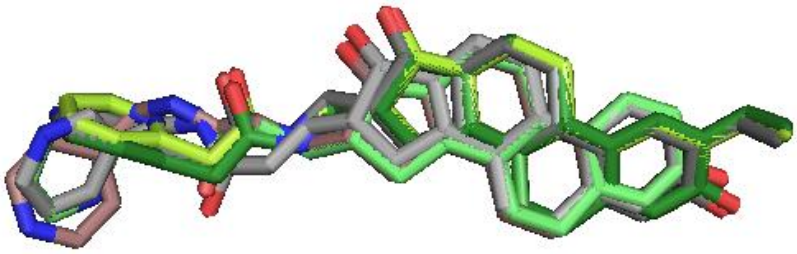

Figure 51: Compounds **174-176** and **185-187** overlaid in their determined docking orientation with the protein structure removed

When compound **185** was docked into the active site (Figure 52) of the protein crystal structure of 17β-HSD1 (pdb code 1FDT[76]) potential interactions were observed with the co-factor; these include the nitrogen of the pyridyl E ring interacting with a hydroxyl from the ribose linker at a distance of 4.4 Å. The carbonyl of the amide present in the C16 linker interacts with a hydroxyl of the ribose linker, the nitrogen of the pyridyl ring of the co-factor and the nitrogen of the amide moiety attached to the co-factor pyridyl ring at a distances of 3.6 Å, 3.1 Å and 3.9 Å respectively. The nitrogen of the amide present in the C16 linker shows a potential interaction with the oxygen present in the amide moiety attached to the pyridyl ring of the co-factor at a distance of 4.0 Å.

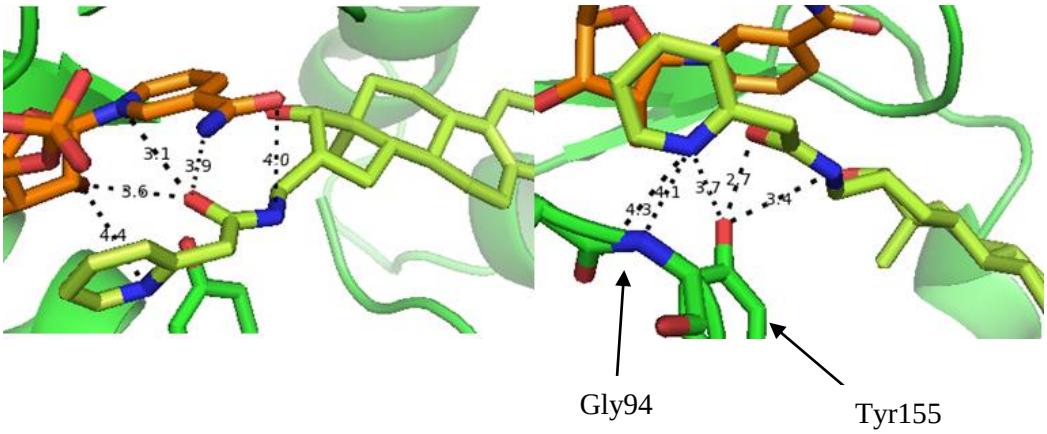

Figure 52: Compound **185** (yellow) docked into 1FDT[76] with all potential interactions with the co-factor (orange) and amino acid residues (green) shown

Compound **185** also displays potential interactions with amino acid residues Leu93, Gly94 and Tyr155. The nitrogen present in the pyridyl E ring of compound **185** interacts with the oxygen present in Leu93 at a distance of 4.3 Å, the nitrogen present in Gly94 at a distance of 4.1 Å and the oxygen of Tyr155 at a distance of 3.7 Å. The carbonyl oxygen of the amide present in the C16 linker can interact with the hydroxyl present in Tyr155 at a distance of 2.7 Å. The hydroxyl of Tyr155 can also interact with the nitrogen of the amide present in the C16 linker over a distance of 3.4 Å.

Compound **186** displays potential interactions with the co-factor as well as amino acid residues Leu93, Gly94 and Tyr155 (Figure 53). When looking specifically at the interactions between the co-factor and compound **186** it can be seen that the nitrogen in the pyridyl E ring can form long distance interactions with the two hydroxyls present on the ribose linker at distances of 5.4 Å and 5.5 Å. The oxygen present in the amide of the C16 linker can form potential interactions with the nitrogen of the co-factor pyridyl ring, the nitrogen and oxygen of the amide present on the co-factor pyridyl at distances of 3.2 Å, 3.5 Å and 3.8 Å respectively. The nitrogen of the amide present in the C16 linker can interact with the oxygen of the amide moiety present on the co-factor pyridyl ring at a distance of 4.0 Å.

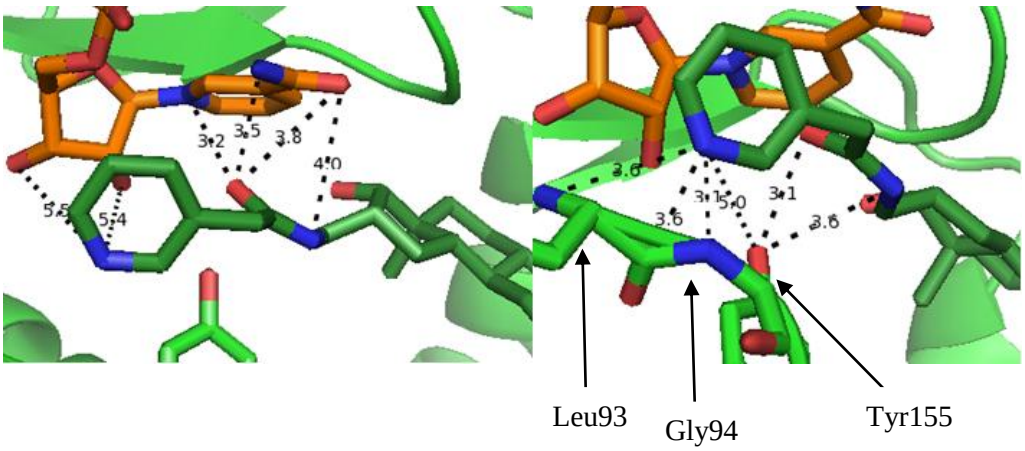

Figure 53: Compound **186** (dark green) docked into 1FDT[76] with all potential interactions with the co-factor (orange) and amino acid residues (green) shown

As stated earlier, compound **186** also interacts with amino acid residues present in the active site of 17β-HSD1. These interactions include the nitrogen of the pyridyl E ring of compound **186** forming potential interactions with both the nitrogen and

oxygen of Leu93 at a distance of 3.6 Å, as well as interacting with the nitrogen of Gly94 at a distance of 3.1 Å. The same nitrogen also can form a long range interaction with the hydroxyl of Tyr155 at a distance of 5.0 Å. The amino acid residue Tyr155 can also form potential interactions with the oxygen and nitrogen of the amide moiety of the C16 linker at distances of 3.1 Å and 3.6 Å respectively. This large number of potential interactions can be used to explain why compound **186** is the most biologically active compound from the reverse amide series.

Computational docking studies of compound **187** shows that similar interactions to those observed for compounds **185** and **186** between the co-factor and amino acid residues are present in the active site. The interactions between compound **187** (Figure 54) and the co-factor include those between the nitrogen of the pyridyl E ring of compound **187** and a hydroxyl of the ribose linker at a distance of 4.9 Å as well as an oxygen atom present in the co-factor backbone at a distance of 3.7 Å. The oxygen of the amide present in the C16 linker can form potential interactions with the nitrogen of the pyridyl ring of the co-factor and both the nitrogen and oxygen of the amide moiety of the pyridyl ring of the co-factor at distances of 3.1 Å, 3.7 Å and 4.2 Å respectively. The nitrogen of the amide present in the C16 linker of compound **187** interacts with the oxygen of the amide present on the pyridyl ring of the co-factor at a distance of 4.0 Å.

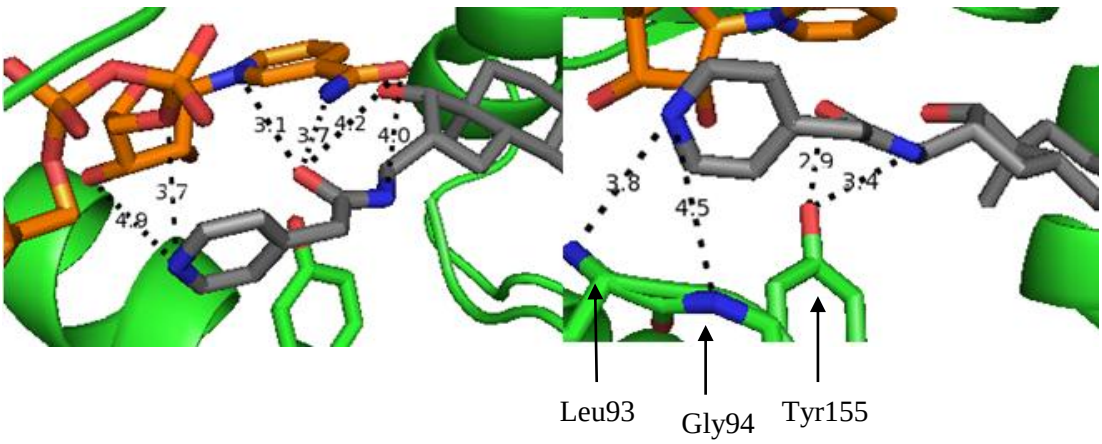

Figure 54: Compound **187** (grey) docked into 1FDT[76] with all potential interactions with the co-factor (orange) and amino acid residues (green) shown

The nitrogen of the pyridyl E ring of compound **187** also forms interactions with the nitrogen of the amino acid residue Leu93 and the nitrogen of Gly94 at distances of 3.8 Å and 4.5 Å respectively. The hydroxyl of Tyr155 can form interactions with

both the oxygen and nitrogen of the amide of the C16 linker at distances of 2.9 Å and 3.4 Å respectively.

The combination of the biological data and the computational docking study indicates that compounds **174-176** and **185-187** adopt a similar binding orientation to that hypothesised for STX1040 **1**, where the steroid core binds in the steroid binding site. From the computational docking study it can be concluded that the co-factor binding region is large enough to accommodate both the C16 side chain and the co-factor, which allows interactions between the C16 side chain and the co-factor. It can be seen from the percentage inhibition values in Tables 24 and 25 that these C16 substituted inhibitors are moderate to good inhibitors of 17β-HSD1, with compound **187** being the most potent from this series with a percentage inhibition of 81%. When comparing compounds **174-176** and **185-187** against STX1040 **1** and STX2109 **169** it can be observed that they display a lower inhibitory activity and this therefore indicates that STX1040 **1** and STX2109 **169** has the optimum linker length of four atoms between the steroid core and the pyridyl ring, and the preferred orientation of the amide for 17β-HSD1 activity. From studying the biological data and computational docking study it can be concluded that compounds **174-176** and **185-187** can potentially act as "dual site" inhibitors, however the nature of the inhibition can not be determined from the computational docking study alone. Enzyme kinetics analysis has been further described in Section 6.3.4.

Chapter 6

Biological Evaluation

6.1 Aims

The objective of this part of the overall project was to synthesise and obtain large enough quantities of both the His tagged (H_6) and un-tagged forms of 17β-HSD1 for use in protein crystallography trials and developing an in house recombinant protein assay to study the inhibitory effect of novel steroidal ligands whose synthesis has been previously described. The recombinant protein assay will also be used to investigate how selected synthesised compounds are inhibiting 17β-HSD1.

6.2 Expression and Purification of 17β-HSD1

To do this it is necessary to express the human form of the 17β-HSD1, then isolate and purify the protein. 17β-HSD1 has been previously expressed by our group in a mammalian cell line, but unfortunately the low level of expression makes it difficult to undertake crystallographic studies. The mammalian system used is the gene for 17β-HSD1 cloned into the pCEP4 vector (Figure 55) and protein is then expressed in 293-EBNA cells. Collaborators from Imperial College London have managed to gain access to constructs of both the untagged and His-tagged versions of 17β-HSD1.

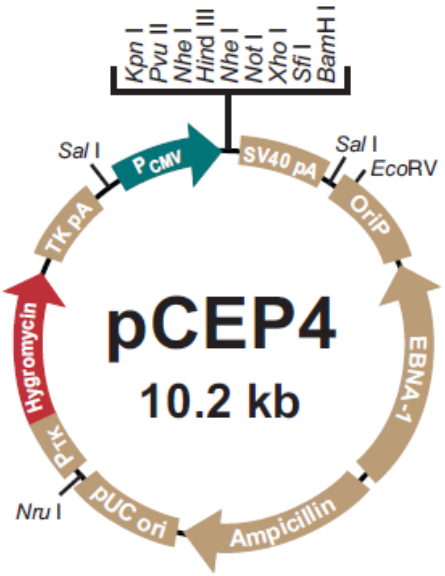

Figure 55: pCEP4 vector map displaying the restriction enzyme site and gene for antibiotic resistance

Therefore, a bacterial expression system was developed to try and attain larger quantities of the protein. The first step in expressing the protein was to clone both the His-tagged and untagged forms of the 17β-HSD1 gene from the mammalian expression vector pCEP4 into a bacterial expression vector pET-24a (Figure 56).

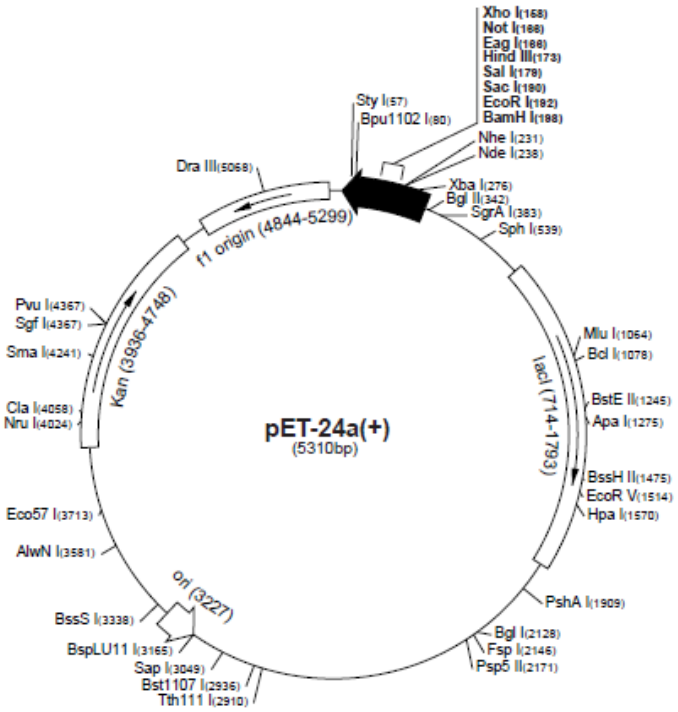

Figure 56: A map of the pET24a bacterial expression vector displaying the restriction enzyme site and gene for kanamycin resistance

To do this the restriction enzymes Nhe1 and Xho1 were used to remove the required gene from pCEP4 mammalian expression vector and to digest the pET-24a bacterial vector. An agarose gel was run to identify the restriction enzyme products for 17β-HSD1 and pCEP4, the band corresponding to 17β-HSD1 gene was removed from the agarose gel and then purified using a QIAquick gel extraction kit. The pET-24a restriction enzyme digest product was purified using the Qiagen PCR purification kit, followed by use of CIP alkalinephosphatase to prevent re-ligation of the bacterial expression vector with itself by removing the terminal phosphates, followed by a final purification step, a Qiagen purification kit was used to remove any unwanted enzymes and buffers that are present to ensure that only the desired fragment of pET-24a isolated. The next stage was to ligate the extracted gene for 17β-HSD1 into the pET-24a bacterial expression vector using a New England Biolabs Quick Ligation Kit to form the desired vector that codes for 17β-HSD1 (Figure 57).

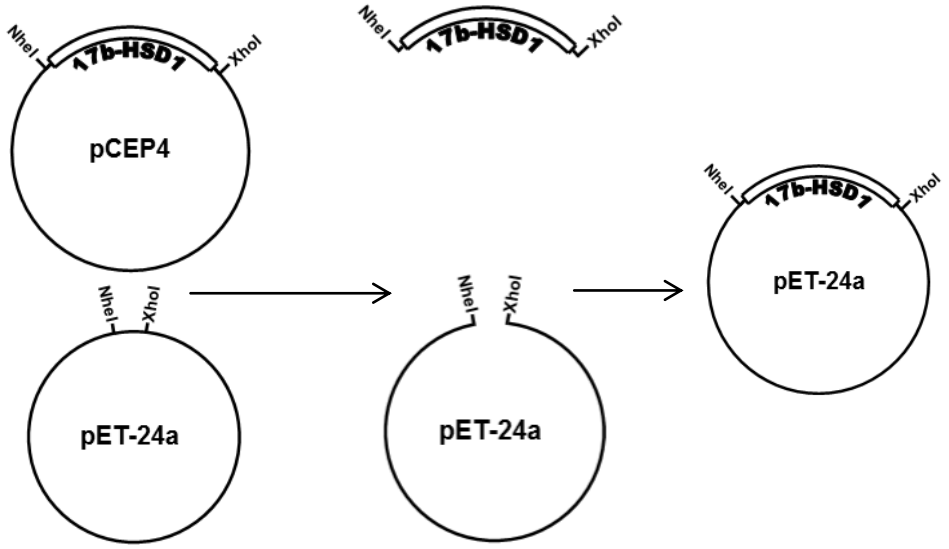

Figure 57: Schematic representation of the insertion of the 17β-HSD1 gene into the pET-24a bacterial expression vector from the mammalian pCEP4 expression vector

This process was repeated for the H_6-17β-HSD1 gene. To be able to amplify the ligated vector the ligation products were transformed into competent cells. The XL10 Gold cells were chosen as they are highly competent, therefore increasing the chances that the ligated vector will enter the cells. The XL10 Gold cells are able to do this as they have what is termed to be a 'leaky' membrane, meaning they can easily incorporate new vectors within themselves. As only the fully ligated vector and the pET-24a bacterial expression vector contains antibiotic resistance to kanamycin, the XL10 Gold cells that incorporate the fully ligated vector will survive in the LB agar plates that contain the antibiotic kanamycin. Therefore only the colonies growing in the LB agar plates are the XL10 gold cells containing the fully ligated vector. For the untagged 17β-HSD1/pET-24a plate one colony was observed, whilst for the H_6-17β-HSD1/pET-24a plate four colonies were seen. The next step was to pick these colonies onto a fresh LB agar plate and grow up a 10 ml culture of each and purify the DNA using a QIAquick mini-preparation kit. Additional NheI and XhoI double digests were then undertaken to help successfully identify two bands of the correct size corresponding to the pET-24a (5.3 Kbp) and the 17β-HSD1 gene (1.2 Kbp) by agarose gel electrophoresis, staining with ethidium bromide and analysing by UV visualisation of the gel. Once successful clones were identified, by agarose gel electrophoresis, they needed to be transformed into an *E.coli* bacterial

expression strain, in this case BL21(DE3) pLysS, and then expression of the protein induced.

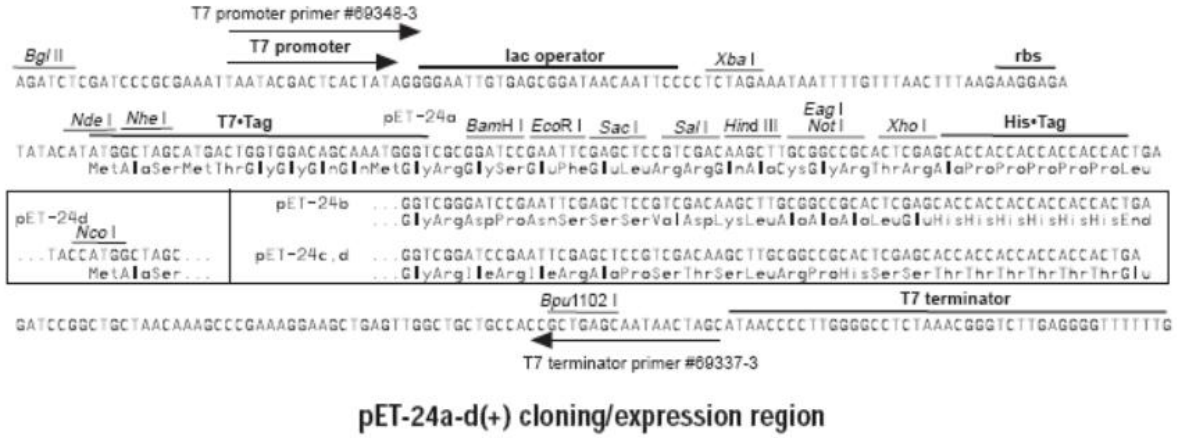

Figure 58: The protein cloning expression region of pET-24a with the lac operon region and NheI and XheI region identified

Protein expression is induced by using a compound called isopropyl β-D-1-thiogalactopyranoside (IPTG) which brings about a chemical response within the cell which starts the process of protein expression. The *lac* operon is an operon responsible for the transport and metabolism of lactose in *E. coli*. The *lac* operon utilises a two part control mechanism to ensure that the cell only expends energy in producing the gene that is encoded for after the *lac* operon only when necessary. It achieves this with the *lac* repressor, which halts protein production in the absence of lactose. When lactose is present, a lactose metabolite called allolactose, binds to the *lac* repressor causing a change in its shape and therefore preventing the repressor from binding to the operator and allowing the RNA polymerase (RNAP) to transcribe the genes located after the operon and so leading to encoded proteins. IPTG acts as an allolactose mimic (Figure 59) and so triggers transcription of the *lac* operon.

In the pET-24a bacterial expression vector being used for this section of the project, the cloning/ expression region is shown in Figure 59, there is a T7 promoter sequence code before the *lac* operator sequence and a T7 terminator sequence after the pET-24a cloning/ expression region. The T7 RNAP is an RNAP from the T7 bacteriophage that catalyses the formation of the RNA in the 5' → 3' direction. The

T7 RNAP is extremely promotor and terminator specific and only transcribes DNA after a T7 promoter sequence and transcription is halted DNA at the T7 terminator sequence. These T7 RNA polymerase regions define the region for protein expression within the pET-24a bacterial expression vector being used. By using the restriction enzymes NheI and XhoI the 17β-HSD1 gene is inserted between the T7 promotor, *lac* operator sequence and the T7 terminator sequence, therefore if the 17β-HSD1 gene is ligated successfully into the pET24a bacterial expression vector, 17β-HSD1 will be expressed.

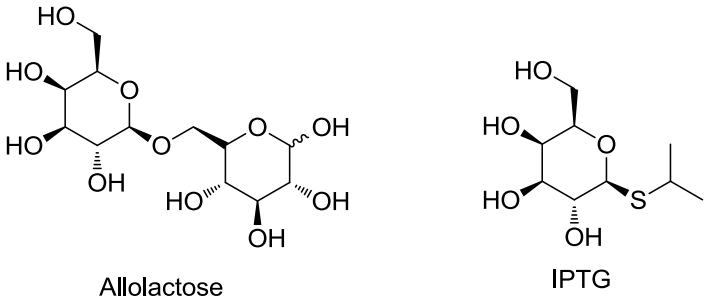

Figure 59: Structures of Allolactose and its mimic IPTG, which is used to induce protein expression

BL21(DE3)pLysS was the first bacterial expression strain to be tried because it multiplies very quickly and is a standard bacterial expression strain. Disappointingly, the protein was not overly expressed using this particular strain as can be seen in the SDS PAGE protein gels below (Figure 60).

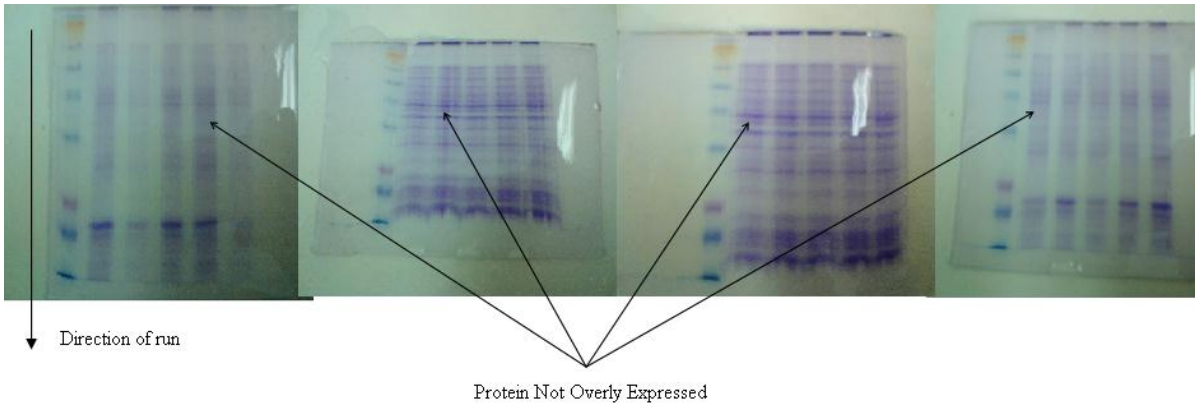

Figure 60: Protein gels showing that the (H_6-) 17β-HSD1 enzyme has not been overly expressed. The arrows indicate the position at which the band for over expression of 17β-HSD1 is expected to be seen

One possible reason as to why the *E. coli* bacterial expression strain BL21(DE3) pLysS did not overly express the protein is that the codons used for amino acids are not preferred for the bacteria *E. coli* but are for humans. For this reason a new *E. coli* bacterial expression strain, Rosetta 2 was used. Rosetta 2 are BL21 derivatives designed to enhance the expression of eukaryotic proteins that contain codons rarely used in *E.coli*. This particular strain codes for specific human t-RNAs for the rare codons; AGA, AGG, AUA, CUA, GGA, CCC and CGG coding for the amino acids arginine, leucine, isoleucine and proline. Once the transformation into Rosetta 2 has taken place and enough of the strain has been grown, the next step was to induce protein expression.

After leaving the culture to express the protein overnight, the culture is centrifuged and the supernatant and pellet are separated. The supernatant consists of mainly the LB broth that the cells were grown in, and the pellet is the desired fraction as this contains the Rosetta 2 cells with the desired protein. After re-suspending the pellet we have to break open the Rosetta 2 cells and further centrifuge the solution to separate the desired soluble protein from the insoluble fraction which contains the cell debris and other insoluble proteins. To see if the protein had been overly expressed using the Rosetta 2 strain a SDS PAGE protein gel was run (Figure 61) and, as can be clearly seen the protein has been overly expressed both in the soluble and insoluble fractions. Although the majority of the protein is insoluble, enough of the protein is present in the soluble fraction for further use. To increase the amount of soluble protein that can be harvested a series of investigations into how the amount of IPTG, the temperature at which the culture is left, and the time period for which the culture is left to express affects the expression were undertaken. IPTG concentrations of 250 µM, 50 µM, 25 µM and 12.5 µM were used to investigate what is the optimum concentration of IPTG to be used for the expression of 17β-HSD1 in the soluble fraction. From the SDS PAGE gels that can be seen from Figures 61 and 62 it can be seen that the lower concentration of 12.5 µM provides the best expression of H_6-17β-HSD1 in the soluble fraction when compared to the 250 µM IPTG concentration. It was also found from these experiments that to obtain the largest quantity of soluble protein the culture has to be left overnight and at a temperature of 16 ºC. Figure 62 shows the H_6-17β-HSD1 form of the protein was

expressed at higher levels than the untagged protein and so it was decided to try and puify the H_6-17β-HSD1 first.

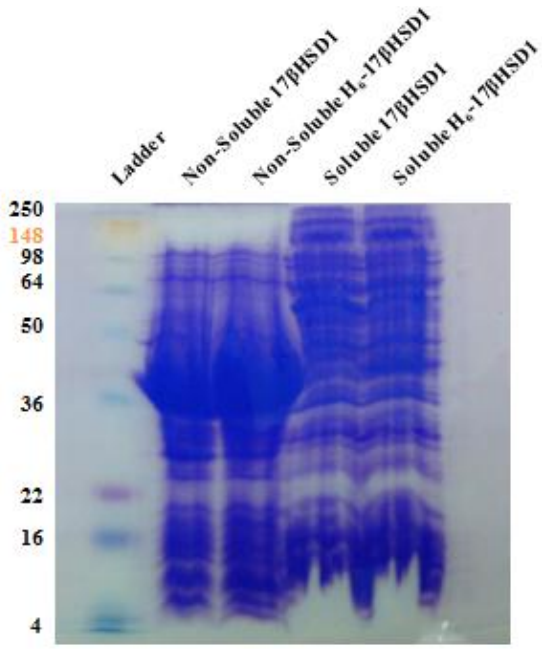

Figure 61: SDS PAGE gel displaying the increased expression of (H_6-) 17β-HSD1 in the non-soluble fraction using 250 µM IPTG.

Once the protein was overly expressed in the soluble fraction the next stage was to isolate and purify the protein (Figure 62). The reason for using the H_6-17β-HSD1 form of the protein is that the His tag enables affinity purification to occur and therefore making the purification process much more efficient as any proteins that do not specifically interact with the nickel can be eluted from the His-bind column using low concentrations of imidazole before the His tag protein is eluted with a higher concentration of imidazole. Initially, batch elution of the protein was undertaken with 500 mM imidazole. This, however, did not provide the protein in a high enough purity and therefore stepwise elutions using 50 mM, 100 mM, 200 mM and 500 mM imidazole were utilised. This step wise approach did improve the purity of the eluted protein.

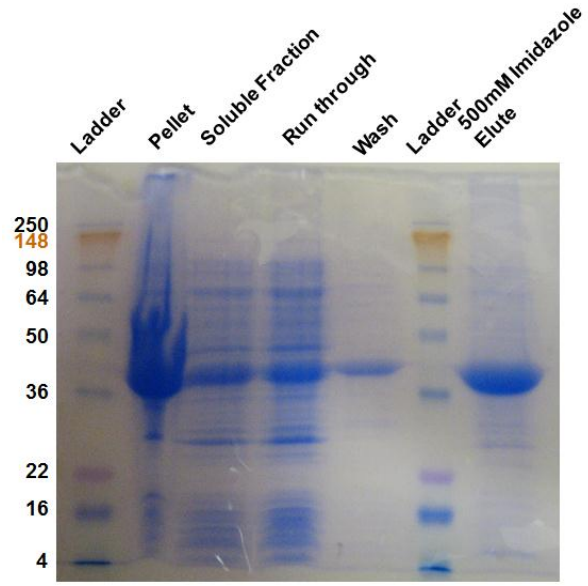

Figure 62: SDS PAGE gel showing the results for the batch elution at 500 mM imidazole after expression at 12.5 µM IPTG

However, to make the purification process more controllable and reproducible it was decided to use an AKTA FPLC. The FPLC purification was undertaken using a single His-Bind column with an elution gradient of 20-500 mM imidazole (Figure 63). The eluted protein was of an acceptable purity, but for protein crystallography the protein used must be of a very high purity. Therefore, to further improve the purity of the protein a Q-sepharose column purification step with a NaCl elution was used (Figure 64).

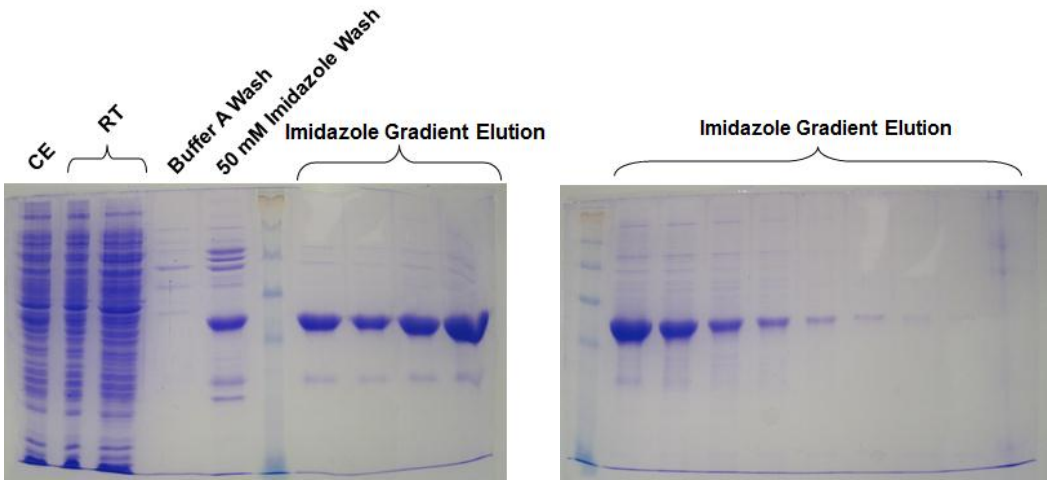

Figure 63: SDS PAGE gel showing the purification of H_6-17β-HSD1 using a His bind column with imidazole elution

After purification the protein underwent dialysis to reduce the concentration of imidazole that was present. This dialysis step was followed by concentration of the protein to the desired concentration for use in either biological assays or crystallisation trials. The addition of a His-tag should not affect the structure or activity of the protein due to its small size and low immunogenicity as well as the fact that the tag is located on the exterior of the protein and so should not hinder the entry of compounds into the active site. If, however, the presence of the His-tag does impact upon the co-crystallisation with the inhibitor or activity of the enzyme in a recombinant protein assay, it is possible to cleave the tag from the protein before use by using an enterokinase kit supplied by Novagen, as an enterokinase cleavage site is coded for between the his tag and the start codon at the start of the protein coding sequence present in the 17β-HSD1 gene being used.

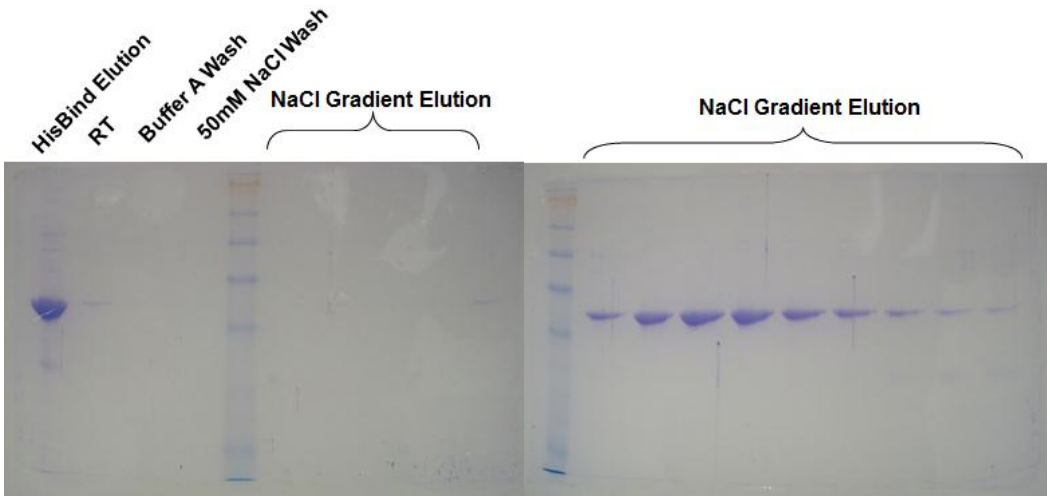

Figure 64: SDS PAGE gel showing the purification of (H_6-)17β-HSD1 using a Q-sepharose NaCl elution

6.3 Enzyme Kinetic Analysis

Having successfully synthesised and purified the protein, it was important to prove that it was active and therefore could be used for enzyme kinetic analysis and X-ray protein crystallography. To do this an enzyme kinetics assay was developed based on an absorbance assay from Mazza *et al.*[128] This assay measures the change in absorbance of NADPH at 340 nm (Figure 65).

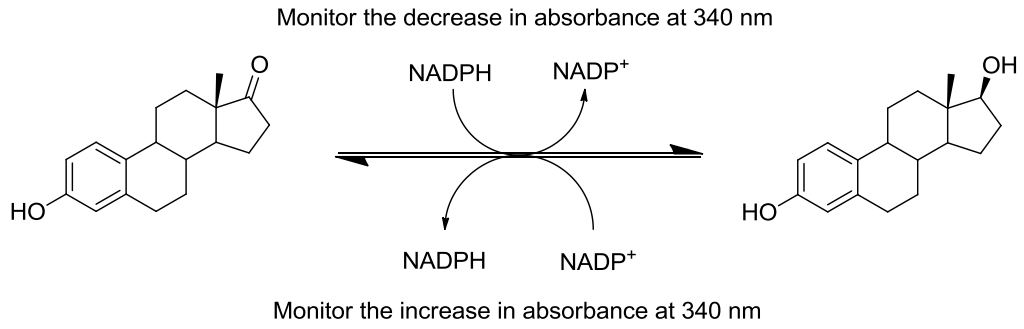

Figure 65: The reversible reaction of the conversion of E1 to E2 and what change in absorbance is being monitored at 340 nm

The assay conditions can be found in the Experimental section of this report.

6.3.1 UV Cuvette Assay

The activity of 17β-HSD1 can be measured in either direction depending on the conditions used. This shows that the activity of the enzyme is reversible. It was decided to use the E2 to E1 direction as this means going in the NADP to NADPH direction. If trying to measure the rate of the reaction in the opposite direction (E1 to E2) NADPH is being converted to NADP. As NADPH can be reduced to NADP in solution without having the enzyme present, a background rate is observed, which makes it more difficult to get accurate results from running the assay.

When undertaking enzyme kinetic studies the first results determined are the V_{MAX} and Michaelis-Menten constant, the K_M for the assay conditions used.

Experimental studies of enzyme kinetics are typically conducted by monitoring the initial rate of product formation in a solution in which the substrate is present at an excess to the enzyme. The principle features of many enzyme-catalysed reactions are:

1. For a given initial concentration of the substrate, $[S]_0$, the initial rate of product formation is proportional to the total concentration of the enzyme, $[E]_0$.
2. For a given $[E]_0$ and low values of $[S]_0$, the rate of product formation is proportional to $[S]_0$.

3. For a given $[E]_0$ and high values of $[S]_0$, the rate of product formation becomes independent of $[S]_0$, reaching a maximum value known as the maximum velocity, V_{MAX}, which in this case is where the enzyme active site is saturated with substrate.

The Michaelis-Menten mechanism accounts for these principle features. According to this mechanism, an enzyme-substrate complex is formed and either the substrate is released unchanged or after modification to form products.

$$E + S \leftrightarrow ES \quad k_a, k'_a \qquad \text{Eqn1}$$

$$ES \rightarrow P \quad k_b \qquad \text{Eqn2}$$

The rate of product formation according to this mechanism is:

$$v = k_b[ES] \qquad \text{Eqn3}$$

The concentration of the enzyme-substrate complex can be obtained by applying the steady state approximation, and therefore writing:

$$\frac{d[ES]}{dt} = k_a[E][S] - k'_a[ES] - k_b[ES] = 0 \qquad \text{Eqn4}$$

It therefore follows that:

$$[ES] = \left(\frac{k_a}{k'_a + k_b}\right)[E][S] \qquad \text{Eqn5}$$

Where [E] and [S] are the concentration of the free enzyme and substrate, respectively.

To express the rate law in terms of the concentration of the free enzyme and substrate added it is noted that $[E]_0 = [E] + [ES]$. As the substrate is typically in a large excess relative to the enzyme, the free substrate concentration is approximately

equal to the initial substrate concentration and so it can be written that $[S] = [S]_0$. It then follows that:

$$[ES] = \frac{[E]_0}{1 + \left(\frac{k'_a + k_b}{k_a}\right)\frac{1}{[S]_0}} \qquad \text{Eqn6}$$

By substituting this result into Equation 3, we obtain the Michaelis-Menten equation for the rate of an enzyme-catalysed reaction:

$$v = \frac{k_b[E]_0}{1 + \left(\frac{k'_a + k_b}{k_a}\right)\frac{1}{[S]_0}} \qquad \text{Eqn7}$$

The constant $(k'_a + k_b) / k_a)$ is characteristic of a given enzyme acting on a given substrate; it is called the Michaelis-Menten constant (K_M). It is also possible to express the Michaelis-Menten constant as $K_M = [E][S] / [ES]$. It therefore follows that the K_M has the units of concentration. For practical purposes the K_M is the concentration of substrate that achieves half V_{MAX}.

The K_M is a way of quantifying the affinity of an enzyme for its substrate. If the enzyme has a low affinity for its substrate we obtain a large K_M value and if the enzyme has a high affinity we obtain a low K_M value. As we are dealing with a two substrate / two product reaction, K_M is actually K_{Mapp} and V_{MAX} is actually V_{MAXapp}. Using our assay conditions we showed that the bacterially expressed H_6-17β-HSD1 was active (Figure 66) and we were able to plot a Michaelis-Menten graph (Figure 67) from the data that was obtained.

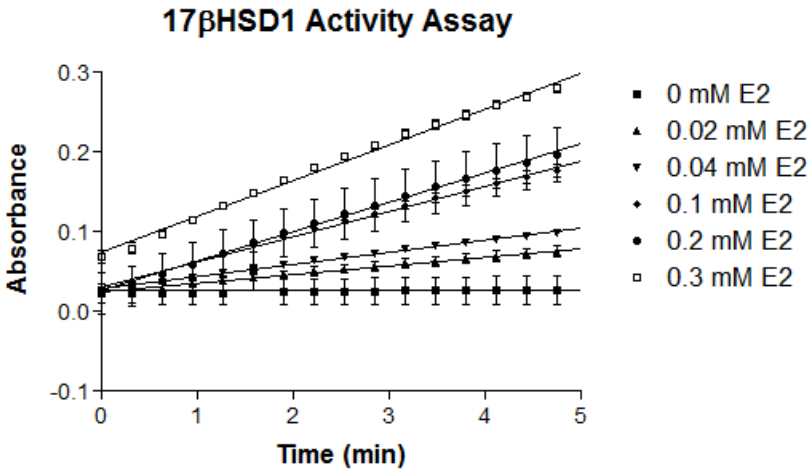

Figure 66: A plot showing the activity of H_6-17β-HSD1 from the UV cuvette assay

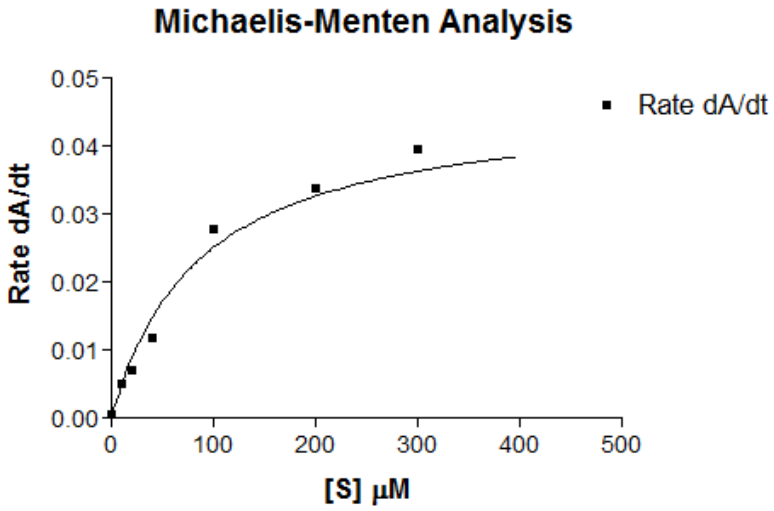

Figure 67: Michaelis-Menten plot for 17β-HSD1, V_{MAXapp} = 0.046 ΔAbs/min and K_{Mapp} = 87 µM at 100 µM NADP and 96 µM H_6-17β-HSD1

There are other methods for determining the K_M value of 17β-HSD1 from experimental data, the most common of which is the Lineweaver-Burk and Eadie Hofstee plots (Figure 68).

In accordance with experimental observations:

1. When $[S]_0 << K_M$ the rate is proportional to $[S]_0$:

$$v = \left(\frac{k_a k_b}{k_a' + k_b} \right) [S]_0 [E]_0 \qquad \text{Eqn8}$$

2. When $[S]_0 >> K_M$ the rate reaches its maximum value and is independent of $[S]_0$:

$$v = V_{MAX} = k_b [E]_0 \qquad \text{Eqn9}$$

Substitution of K_M and V_{MAX} into equation 8 gives:

$$v = \frac{V_{MAX}}{1 + \frac{K_M}{[S]_0}} \qquad \text{Eqn10}$$

Equation 10 can be re-arranged into a form that allows data analysis via linear regression to be able to take place in the form of the Lineweaver-Burk equation (Equation 11):

$$\frac{1}{v} = \frac{1}{V_{MAX}} + \left(\frac{K_M}{V_{MAX}} \right) \frac{1}{[S]_0} \qquad \text{Eqn11}$$

A Lineweaver-Burk plot is a double recipricol plot of 1/v versus $1/[S]_0$ which gives a straight line with a slope of K_M/V_{MAX}, a y-intercept at $1/V_{MAX}$ and an x-intercept at $-1/K_M$.

Equation 10 can also be re-arranged to allow data analysis via a different linear regression called the Eadie-Hofstee equation:

$$v = -K_M \frac{v}{[S]_0} + V_{MAX} \qquad \text{Eqn12}$$

The Eadie-Hofstee plot is a plot of v versus $v/[S]_0$ which yields a straight line with a slope of $-K_M$, a y-intercept of V_{MAX} and an x-intercept of V_{MAX} / K_M.

Both the Lineweaver-Burk and Eadie-Hofstee plots have their positives and negatives. The Lineweaver-Burk plot provides good precision of the V_{MAX} and K_M, however as it is a double recipricol plot it places undue weighting on the data points at lower concentrations of $[S]_0$. The Eadie-Hofstee plot does not place undue weighting on the lower concentrations of $[S]_0$; however, it has the disadvantage that the dependent variable, v, is used on both axis and so results in the lower precision of the V_{MAX} and K_M values.

Analysis by using the Lineweaver-Burk and Eadie Hofstee equations give values of K_{Mapp} = 62.5 and 94.7 μM and V_{MAXapp} = 0.035 and 0.047 ΔAbs/min respectively. These data show similar values to the non-linear regression from the Michaelis-Menten plot, and all the values are easily within an order of magnitude of each other. The K_{Mapp} value also shows that the enzyme has a high affinity for the substrate as is expected. The plot that is preferred is the non-linear Michaelis-Menten graph; as can be seen from the plot, the points fit the curve much better than is observed in the linear regression plots shown in Figure 68. This means that the most accurate K_{Mapp} value for 17β-HSD1 from this assay is 87 μM. However, it can be observed from both the Lineweaver-Burk and Eadie Hofstee plots that the data does not fit the Lineweaver-Burk and Eadie Hofstee derivations of the Michaelis-Menten equation.

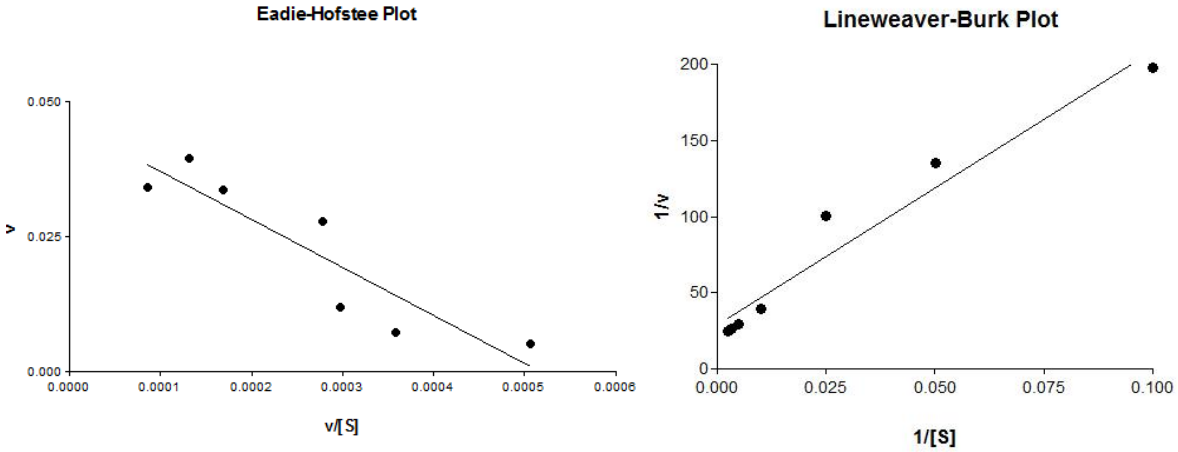

Figure 68: Eadie Hofstee and Lineweaver Burk plots. An alternative way of analysing enzyme kinetic data

It is also very important to prove that our inhibitors are not acting as a substrate for the enzyme. This can sometimes be the case when inhibitors are designed to be very

similar in structure to the natural substrate (Figure 69) and can lead to the inhibitor being metabolised in a very similar manner to the natural substrate, potentially leading to off target effects.

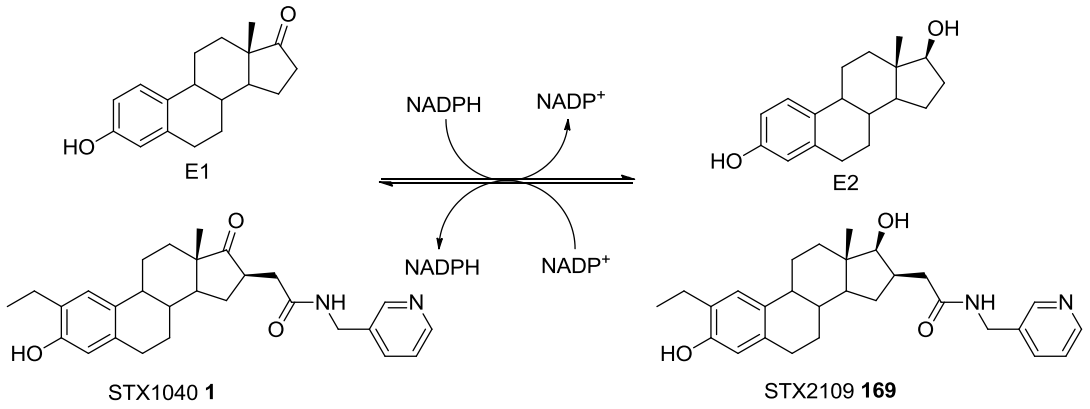

Figure 69: A schematic representation of why STX2109 **169** is being used to see if this series of steroidal ligands act as substrates for 17β-HSD1 in the UV absorbance assay

This was tested by running an assay with an inhibitor, in this case STX2109 **169**, present in place of the natural substrate. A control assay comprising of the enzyme with the substrate, E2, and co-factor, NADP, with no inhibitor present was also run to provide a maximum expected rate. An assay containing just the enzyme in the presence of the co-factor without either the natural substrate, E2, or an inhibitor being present was also run to provide a controlled minimum rate (Figure 70). The reason for using STX2109 **169** instead of STX1040 **1** in this experiment was because STX2109 **169** is designed to be an E2 mimic (Figure 69) and so would give the best representation as to whether this class of inhibitors would act as substrates towards 17β-HSD1 in an assay measuring the conversion of E2 to E1.

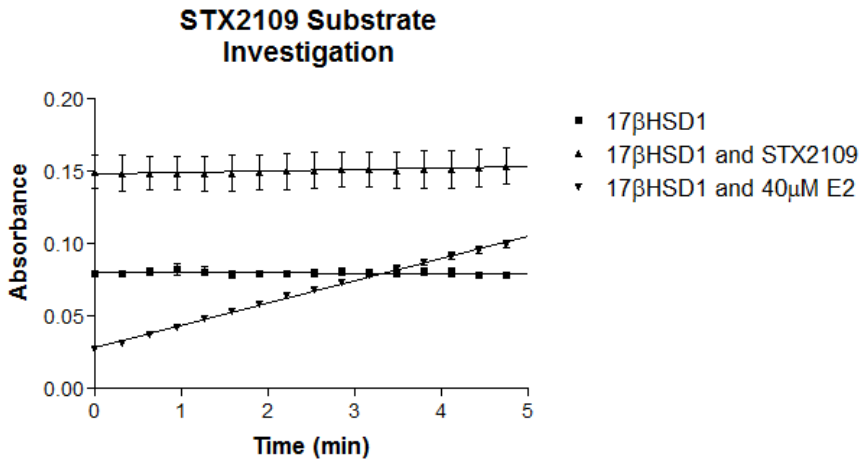

Figure 70: A plot to show that STX2109 **169** does not act as a substrate for 17β-HSD1

Assay	Rate dA/dt	P value	Significantly Different
17β-HSD1	-0.0002128	0.5043	No
17β-HSD1 and STX2109 **169**	0.001008	0.5315	No
17β-HSD1 and E2	0.01528	<0.0001	Yes

Table 27: Results showing that STX2109 **169** does not act as a substrate for 17β-HSD1

The data obtained from the substrate investigation study (Table 27) assay show that the rate for 17β-HSD1 without the natural substrate, E2, compared to the rate observed for 17β-HSD1 with the inhibitor, STX2109 **169** are not statistically significantly different. The statistical analysis was performed using the graph fittig software Prism. A P value of less than 0.05 shows that the null hypothesis, in this case that there is no difference between two selected sets of data, is not correct. This shows that the inhibitor STX2109 **169** is not acting as a substrate for 17β-HSD1. The rate for when the E2 is present with the enzyme is notably different (approximately 15 fold greater) than that of 17β-HSD1 with the inhibitor STX2109 **169** and 17β-HSD1 without the natural substrate E2.

6.3.2 Microplate Reader Assay

The decision was made to change the method of analysis for the assay from using a UV cuvette based method which was very time consuming and laborious to one which used a Molecular Devices Versamax tunable microplate reader and 96 well plates. The decision for this change was to reduce the amount of time it was taking to perform the enzyme kinetic analysis. As the microplate reader is able to analyse multiple wells simultaneously, this therefore saves time on preparation of the assay conditions and overall time taken to perform the analysis.

To assess the capabilities of the absorbance assay as a tool for studying how inhibitors act with the active site of 17β-HSD1, an inhibitor was selected to test the assay. It has been stated earlier that STX1040 **1** is a highly potent inhibitor of 17β-HSD1 with an IC_{50} value of 47 nM in a cell based assay and this therefore makes STX1040 **1** a good candidate to use for the testing of the assay. For the reaction direction of 17β-HSD1 that is being used for this assay STX1040 **1** cannot act as a substrate due to the carbonyl present on C17. Therefore, any rate observed when using STX1040 **1** will be entirely due to the conversion of E2 to E1.

The modifications made to the assay described by Mazza *et al.*[133] involved changing the solvent that was used to dissolve the inhibitor compounds. This was done as THF was dissolving the 96 well plates that were being used, and so affecting the ability to record the rates that were being obtained from the assay. The new solvent that was selected had to have the ability to dissolve compounds that were highly hydrophobic, because if the compounds are insoluble an accurate measurement of the rate cannot be obtained. This inaccuracy can lead to a misinterpretation of how the inhibitor is interacting with the enzyme. To decide upon which solvent is the best for the assay, a solubility study of the inhibitor being used, STX1040 **1**, was undertaken. A series of solvents was selected that were known to be good at dissolving compounds that were relatively insoluble. The solvents used were MeOH, a mixture of DMSO/isopropanol (50/50 v/v) and DMSO. The solvent that was best for dissolving STX1040 **1** was DMSO and so was used here in for the enzyme kinetics experiments.

To characterise the interaction of H_6-17β-HSD1 with the inhibitor, STX1040 **1**, the assay can be used to work out IC_{50} values of STX1040 **1** at varying concentrations of our substrate E2. STX1040 is used for this experiment as it has been shown to be our most potent inhibitor of 17β-HSD1. The IC_{50} value is the concentration of inhibitor that provides 50% inhibition of a maximum possible biological function. In this case the biological function is the rate at which the enzyme uses the substrate. The reason for doing this is so that we can show that the inhibitor STX1040 **1** does in fact act as an inhibitor of the enzyme 17β-HSD1 using this assay. An IC_{50} curve (Figure 71) is effectively a dose-response curve where we are examining the effect of different inhibitor concentrations on the rate of the enzyme being tested, where in this case the rate observed is for the conversion of E2 to E1 by the enzyme.

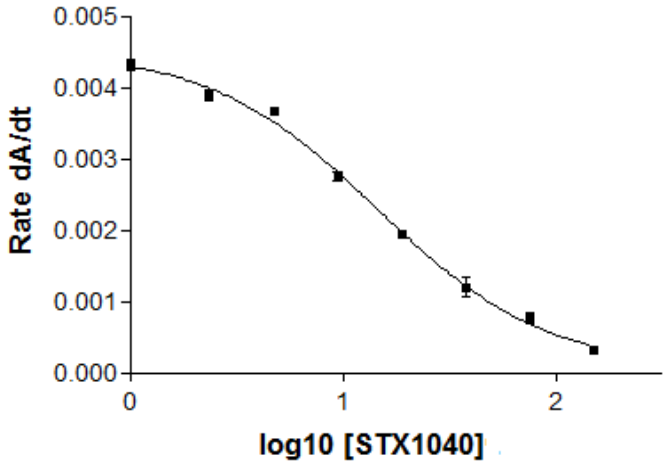

Figure 71: IC_{50} plot at 200μM E2 for STX1040 **1**

Using plots as shown in Figure 72 it is possible to obtain IC_{50} values; in the example shown this is 14.5 μM for STX1040 **1**. This value is much higher than that stated earlier for the IC_{50} of STX1040 **1** in the cell-based assay; this is because a different assay is being used to gain the IC_{50} values and so they are non-comparable. As can also be clearly seen the inhibitor STX1040 **1** is actively inhibiting the enzyme 17β-HSD1.

The next stage is to determine what type of inhibitor STX1040 **1** is: competitive, non-competitive, or un-competitive. A competitive inhibitor binds to the enzyme and forms an enzyme-inhibitor complex in the active site, preventing any natural substrate from binding in the active site. A non-competitive inhibitor binds to the

enzyme but not at the active site, potentially changing the tertiary structure of the enzyme and preventing the natural substrate from binding to the active site of the enzyme. An un-competitive inhibitor binds the complex formed when the substrate is bound in the active site of the enzyme and prevents the release of the product. One method for determining the type of inhibitor STX1040 **1** is by using a graphical representation called a Dixon Plot (Figure 73). A Dixon Plot is a graph of the reciprocal of the rate of conversion of E2 to E1 by the enzyme, versus the inhibitor concentration at varying concentrations of substrate. The type of inhibitor is determined by where the linear regressions intersect. For a competitive inhibitor or mixed site inhibitor the linear regressions would intersect above the x-axis, for a non-competitive inhibitor they would intersect on the x-axis and for un-competitive inhibitors they would run parallel with each other. Other information that can be determined from a Dixon Plot is K_i, the inhibition constant. From the Dixon Plot one obtains the K_i value by dropping a vertical line from where the lines intersect down to the x-axis.

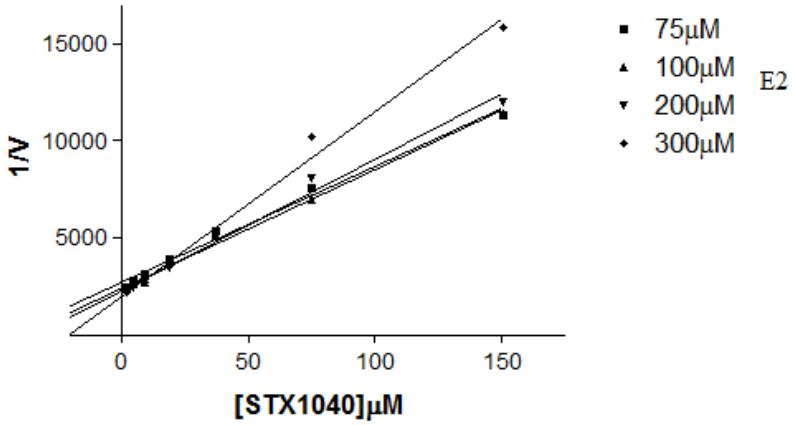

Figure 72: A Dixon Plot of the reciprocal of the rate versus the concentration of STX1040 **1**

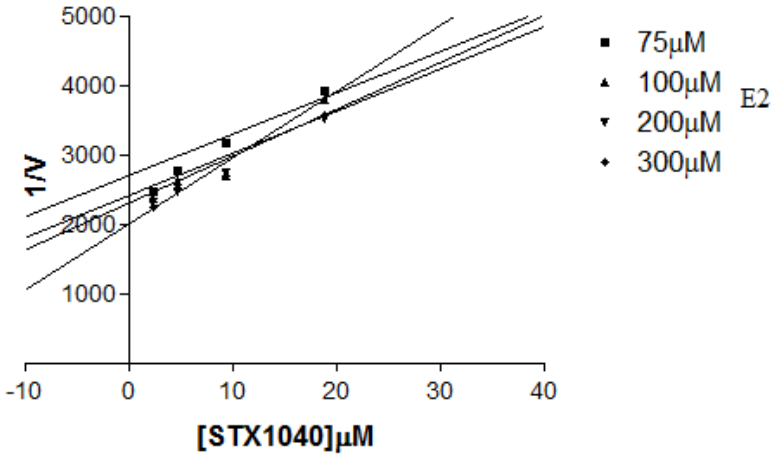

Figure 73: The expanded region of the Dixon plot identifying where the linear regressions intersect

From Figures 72 and 73 we can see that all the linear regressions intersect above the x-axis; however, they do not all intersect at the same point with each other. Therefore this data can not be used to conclusively prove that STX1040 **1** is acting as a competitive inhibitor.

6.3.3 MTS/PES Microplate Reader Assay

6.3.3.1 Introduction

The results obtained for the Dixon plot (Figure 72) using the microplate reader assay occured over a small absorbance range. To obtain more accurate and reproducible results an assay with a larger absorbance range is required. It was hypothesised that the low absorbance response, due to the extinction co-efficient of NADPH, from the assay was the reason as to why the data did not fit the Dixon plot model. To increase the detected absorbance of the assay a literature search revealed that electron carrier agents can be used to provide an increased absorbance.[129] NADPH has a high molar extinction co-efficient (ε) at the λ_{MAX} of 259 nm, 16900 $M^{-1}cm^{-1}$. However, at this wavelength it is difficult to accurately monitor this compound in physiological and biochemical systems, because cell-free extracts contain several components (NADP, and most proteins) with absorption maxima at λ = 260 nm. Consequently NADPH is usually monitored at its secondary absorption maximum of 339 nm where the ε value is much lower, 6220 $M^{-1}cm^{-1}$. This is very important to

note as when considering the Beer-Lambert law (Equation 13), the lower the ε value the lower the value generated for the absorbance.

$$T = \frac{I}{I_0} = 10^{-\varepsilon lc} \qquad \text{Eqn13}$$

Where T = transmittance, I = intensity, ε = molar absorptivity, l = path length and c = concentration.

When considering the transmittance expressed in terms of absorbance Equation 13 can be written as:

$$A = -log_{10}\left(\frac{I}{I_0}\right) = \varepsilon lc \qquad \text{Eqn14}$$

Where A = absorbance, I = intensity, ε = molar absorptivity, l = path length and c = concentration. Equation 14 implies a linear relationship between absorbance and concentration.

Therefore, it can be difficult to quantify the amount of NADPH as reaction products generated in cell-free extracts. This difficulty can be greatly reduced by coupling the formation of NADPH to the formation of a dye or other coloured substance which has an absorbance in the visible region of the spectrum, 450-700 nm. Formazan / tetrazolium couples represent an approach used for some cell proliferation assays. Formazans of these compounds e.g. MTT are insoluble in aqueous solutions and therefore are not useful in cell-free activity assays coupled to the generation of NADPH. Fortunately, the formazan MTS (Figure 74) is aqueous soluble and also exhibits a broad absorption band, 450-580 nm) giving a considerable λ range in which it may be usefully measured, therefore making MTS a useful indicator of the NADPH produced in physiological buffers.[129] To enable conversion between the tetrazolium salt and formazan an electron coupling reagent is required.

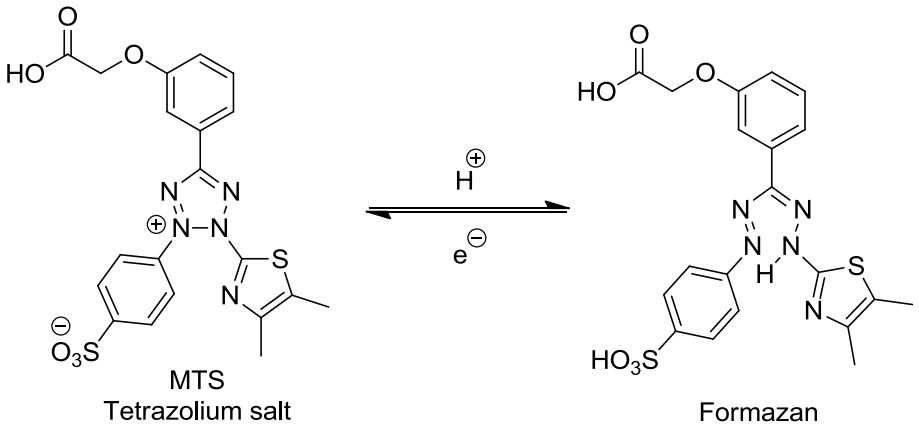

Figure 74: The structures of the tetrazolium salt MTS and the corresponding formazan

Traditionally, phenazine methosulfate, PMS is used as the electron coupling reagent. However more recently phenazine ethosulfate has been used as it is more chemically stable and so does not expire as quickly. Figure 75 shows the redox pathway for the conversion of $NADP^+$ to NADPH and the roles in which MTS/PES plays.

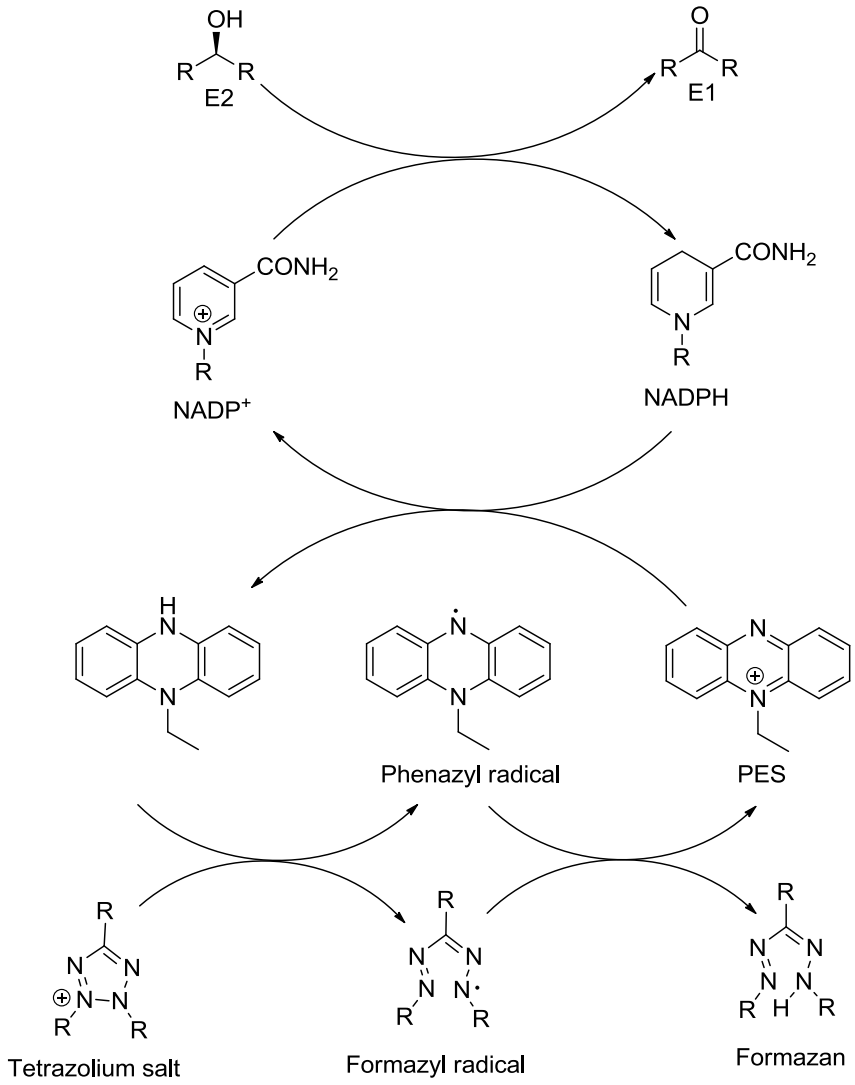

Figure 75: Redox pathway for the formation of formazan from the tetrazolium salt[129]

6.3.3.2 Assay Development

6.3.3.2.1 Michaelis-Menten Analysis

By using MTS/PES it is proposed that an increase in absorbance will be observed compared to the absorbance assay previously described.

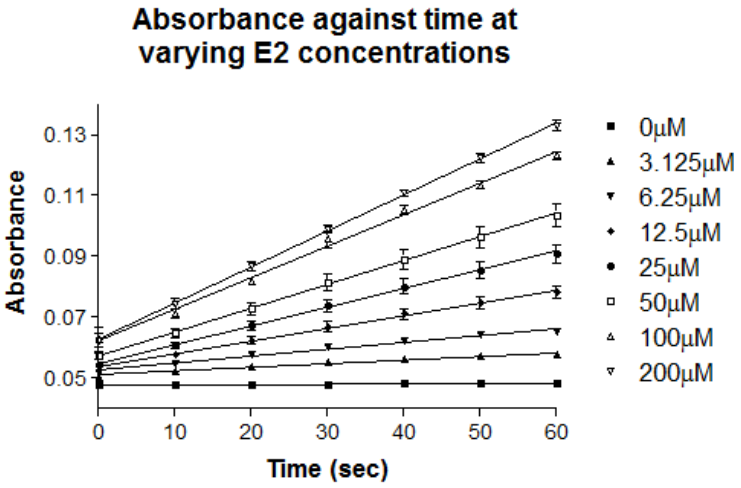

Figure 76: A plot showing the change in absorbance due to the conversion of E2 to E1 using the MTS-PES assay

By applying the Michaelis-Menten equation to the data obtained for the conversion of E2 to E1 a K_{Mapp} value for E2 was determined as 30.99 µM and a V_{Maxapp} of 1.94 ΔAbs/min.

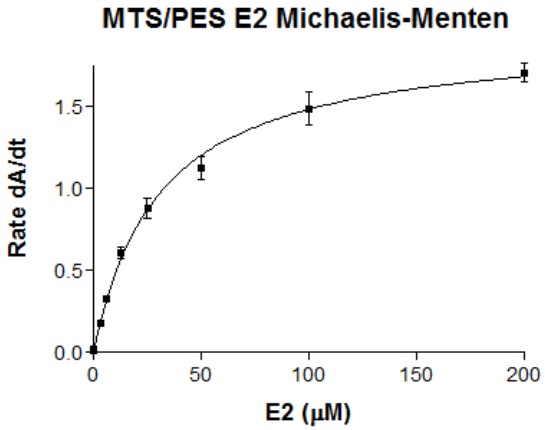

Figure 77: Michaelis-Menten plot for the rate of conversion for E2 to E1 assessed over 60 s

From the plot (Figure 77) it was calculated that the data fits the Michaelis-Menten model for ligand binding with reasonable accuracy, an R^2 value of 0.9793 was determined.

To aid in assessing how well the data fit the Michaelis-Menten model, residual plots can be used. A residual plot is a way of showing if the regression being used for analysis is suitable. The residuals plot shows the variance of the data points from the

curve in the y-axis. For the regression to be suitable for the data being analysed a random scattering of the points should be observed above and below the x-axis. When this random scattering is not observed it implies that another type of regression would better fit the data. The residuals plot for the Michaelis-Menten model does not show a random scattering through the plot as all but one point above the x-axis. (Figure 78)

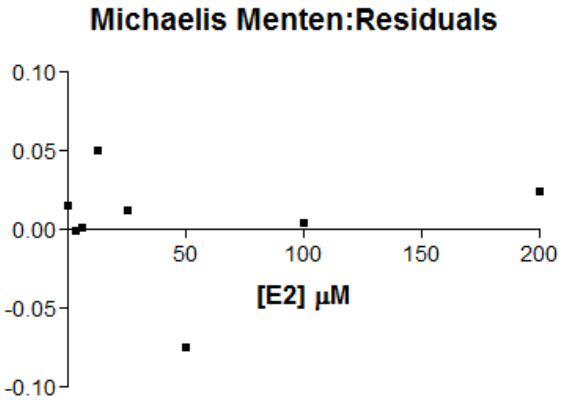

Figure 78: The residuals plot for the Michaelis-Menten analysis shown in Figure 83

Non-linear Michaelis-Menten analysis (Figure 79) of the observed rate for the conversion of E2 to E1 at varying concentrations of $NADP^+$ provides us with information about the K_{Mapp} of $NADP^+$, which in this assay is 23.71 µM and has a V_{Maxapp} of 2.525 ΔAbs/min.

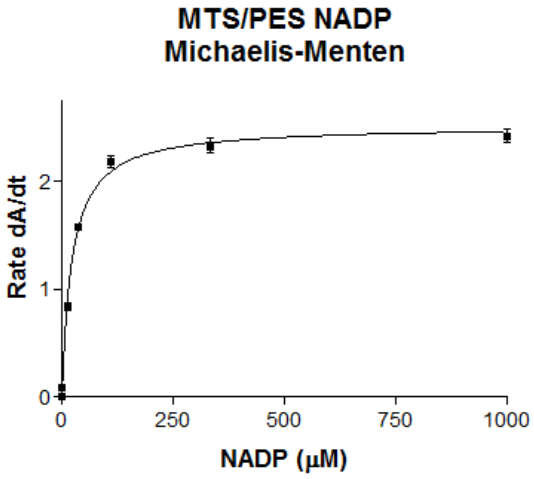

Figure 79: Michaelis-Menten analysis for the $NADP^+$ binding site

The residuals plot (Figure 80) for the Michaelis-Menten model displays a random scattering pattern, indicating that this ligand binding model can be used for the

binding of $NADP^+$ with 17β-HSD1. An R^2 value 0.9489 was determined for the Michaelis-Menten model, indicating the data fits the non-linear regression with reasonable accuracy.

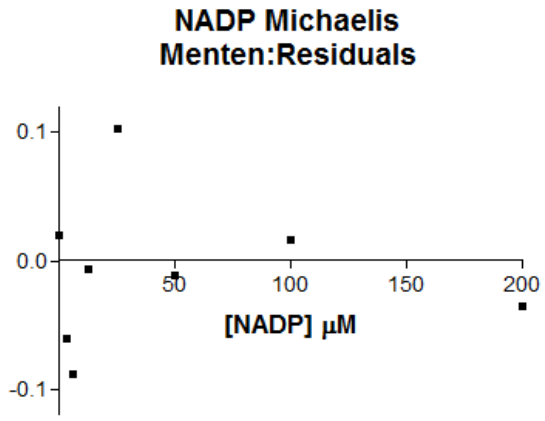

Figure 80: The residuals plot for the Michaelis-Menten analysis shown in Figure 85

In order to be able to use the MTS/PES assay for inhibitor experiments certain parameters have to be determined to ensure that the data obtained is representative of how the enzyme operates at optimum conditions.

The first of these is the effect of temperature upon the enzyme. It is expected that the best temperature to use would be 37 ºC as this is human body temperature. An assay was run at both 37 ºC and room temperature, 22 ºC and as expected a temperature of 37 ºC was found to be the optimum temperature for the assay to be run at. This is because an increased rate was observed for all concentrations of E2 (Figure 81). Therefore when undertaking inhibitor studies any small changes in rate at low concentrations of E2 will be observed and not over looked. The temperature of 37 ºC was then used for all future assays.

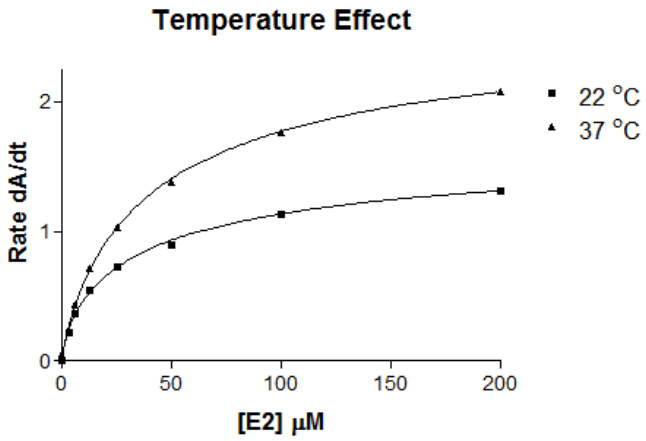

Figure 81: A plot to show the effect of temperature upon the rate of conversion of E2 to E1

When analysing the assay data using the Michaelis-Menten model the residuals plot (Figure 82) shows a very interesting result.

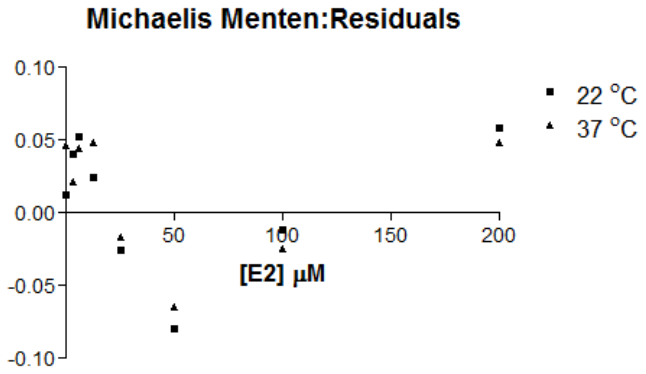

Figure 82: The residuals plot for the Michaelis-Menten analysis for the effect of temperature on the assay

For the Michaelis-Menten analysis a clear trend can be seen from the residuals plot where the points adopt an upside down 'U' shape. This upside down 'U' is a clear indication that this particular curve fitting model is not the most suitable for this set of data, therefore implying that 17β-HSD1 does not obey Michaelis-Menten kinetics.

The choice of buffer for running of these assays is very important. To assess which buffer out of those that have been reported in the literature both 0.1 M Tris pH 7.5 and 0.05 M Potassium pyrophosphate pH 9.2 were analysed (Figure 83).

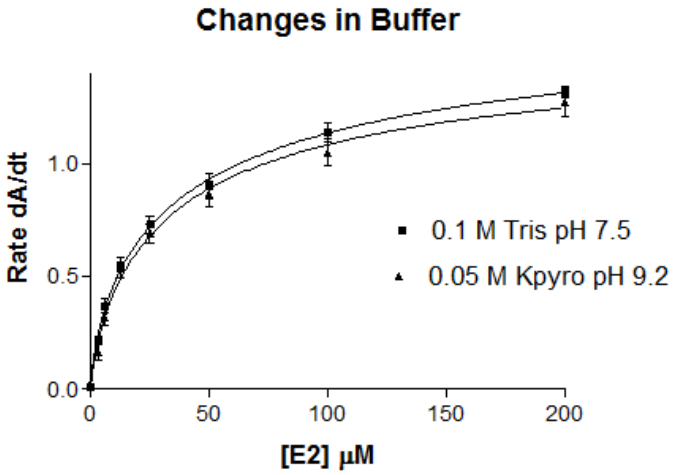

Figure 83: A plot to show how changing buffer alters the rate of conversion of E2 to E1

From the plot it can be seen that both buffers have very similar curves at all concentration of E2. The K_{Mapp} values determined are 42.73 µM and 36.93 µM and V_{MAXapp} values of 1.760 and 1.590 ΔAbs/min for 0.1 M Tris pH 7.5 and 0.05 M potassium pyrophosphate pH 9.2 respectively.

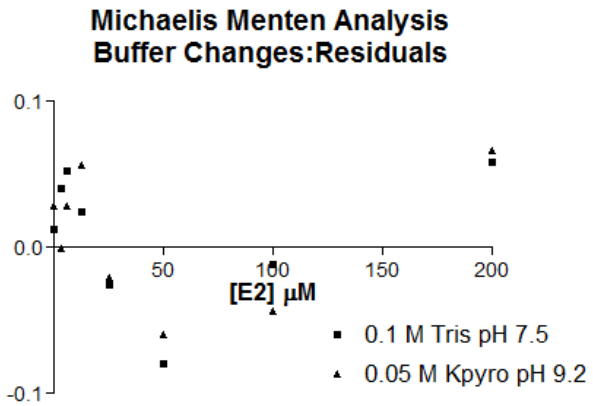

Figure 84: The residuals plot for the effect of Buffer on the MTS/PES assay

The residuals plot (Figure 84) for both the Michaelis-Menten model is shown above. It can be clearly seen that there is a trend within the data and that some other non-linear regression would be better suited to the data. It was decided that the 0.1 M Tris pH 7.5 would be used for future assays as this was the buffer used in the UV absorbance assay previously described.

The concentration of 17βSHD1 used in the assays is an important factor to consider because the aim is for the assay to provide a large enough maximum rate so that any

inhibition of this rate can be observed against a large response, but the rate should not be too large so that large quantities of inhibitor are required to bring about a reduction in the response, and therefore any potential low affinity inhibitors can not be identified.

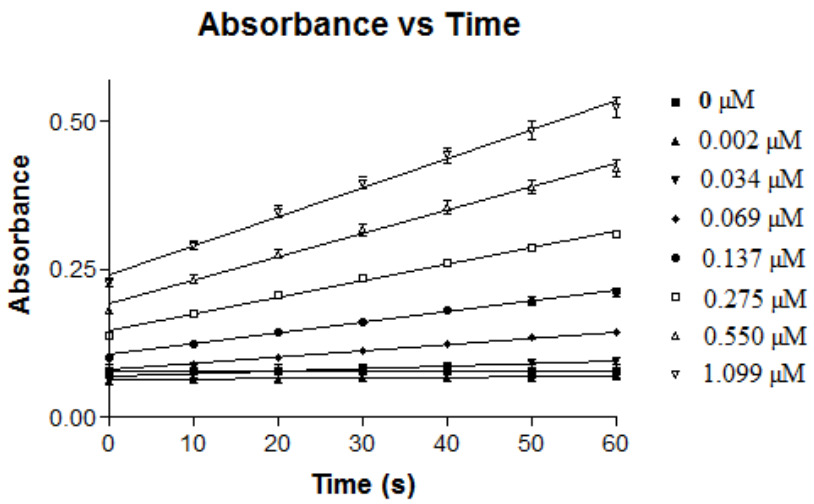

Figure 85: A plot to show the change in absorbance against time for varying concentrations of 17β-HSD1

From Figure 89 it can be seen that the relationship between the absorbance observed for the conversion of E2 to E1 against time is a linear one at all concentrations of 17β-HSD1 tested. The R^2 values are all in the range of 0.9198 to 0.9825 for all concentrations of 17β-HSD1 (Table 28), suggesting that the data strongly fits a linear regression analysis model.

[17β-HSD1] (µM)	**R^2 value**
0.002	0.9198
0.034	0.9686
0.069	0.9671
0.137	0.9705
0.275	0.9825
0.550	0.9639
1.099	0.9652
Mean	0.9625
SD	0.02
% RSD	2.06%

Table 28: R^2 results for various concentraions of 17β-HSD1 being investigated

The % RSD shown in Table 28 is less than 5% indicating that the experiment is linear for all of the concentrations of 17β-HSD1 used enabling the choice of 17β-HSD1 concentration that best suits the experiment.

To further assess what concentration of 17β-HSD1 should be used for the MTS/PES assay it was decided to select three concentrations of 17β-HSD1 and undertake an enzyme kinetics analysis (Figure 86), in this case 0.002, 0.034 and 0.069 µM were selected, as these concentrations provide a good change in absorbance due to the conversion of E2 to E1.

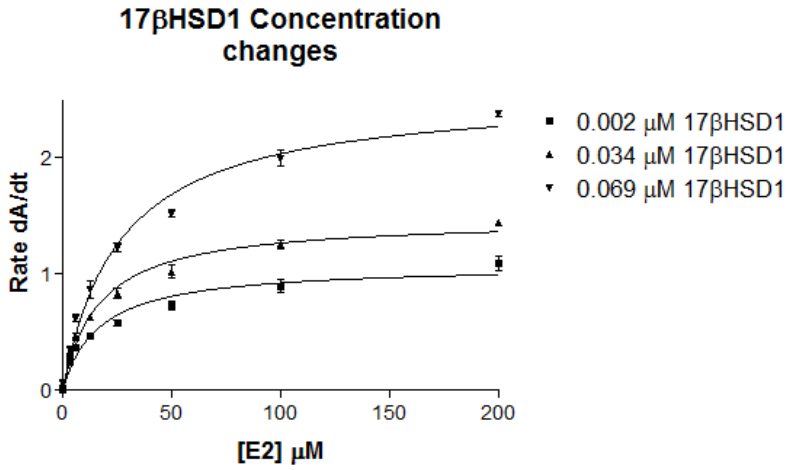

Figure 86: Michaelis-Menten analysis to show the effect of 17β-HSD1 concentration on the rate of conversion of E2 to E1

The results above show that as expected as the concentration of 17β-HSD1 increases so does the V_{MAXapp}. To decide what concentration of the enzyme to use the K_{Mapp} values were compared alongside the R^2 values. K_{Mapp} values of 16.57 µM, 24.54 µM and 28.91 µM and R^2 values of 0.9347, 0.9895 and 0.9901 were determined respectively for 0.002, 0.034 and 0.069 µM. Due to the closeness in results for 0.034 µM and 0.069 µM for K_{Mapp} and R^2 the V_{MAXapp} is what the choice is based upon. In this case it was decided that a larger V_{MAXapp} value was desirable and so 0.069 µM of 17β-HSD1 was used for all future assays. The concentration of 0.002 µM was not chosen because of the low V_{MAXapp} and low K_{Mapp} value in comparison to the other 17β-HSD1 concentrations.

As some of the inhibitors under investigation have poor solubility in water, DMSO was added to the assay to help make them soluble and therefore aid in getting a true

understanding of their effects on 17β-HSD1. Therefore it was decided that the optimum amount of DMSO to add to the assay was an important factor to determine as potentially DMSO could have a negative effect upon 17β-HSD1. Figure 87 shows the effect that DMSO has upon the conversion of E2 to E1.

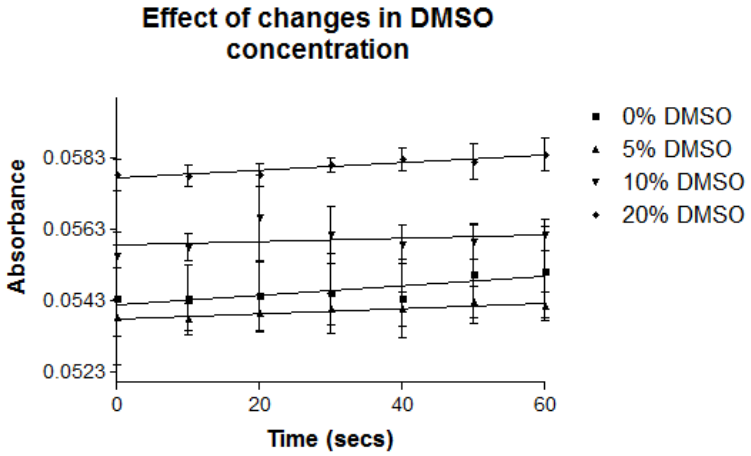

Figure 87: A linear plot to show that concentrations of up to 20% DMSO have no negative impact upon the rate of conversion of E2 to E1 compared to 0% DMSO

From the data that generated Figure 87 and the slopes calculated for this data in Table 29 it can be concluded that the amount of DMSO added up to and including 20% does not deviate from the 0% control data.

% DMSO	Slope of linear regression
0	$1.298\times10^{-5} \pm 7.615\times10^{-4}$
5	$7.262\times10^{-6} \pm 7.615\times10^{-6}$
10	$4.881\times10^{-6} \pm 1.131\times10^{-5}$
20	$1.048\times10^{-5} \pm 6.135\times10^{-6}$

Table 29: Results showing the slopes of the linear regressions at varying DMSO concentrations

Due to all DMSO concentrations investigated providing similar results, any of the concentrations investigated could be used. It was decided that 20% of DMSO was to be used for the MTS/PES inhibitor assay investigations as 20% DMSO would ensure that both E2 and the inhibitors would stay in solution for the duration of the assay.

The final parameter that was assessed was the concentration of MTS/PES that would be used for the assay. As this is the electron carrier agent and is therefore responsible for the absorbance generated from the conversion of E2 to E1 it is a very important parameter to assess.

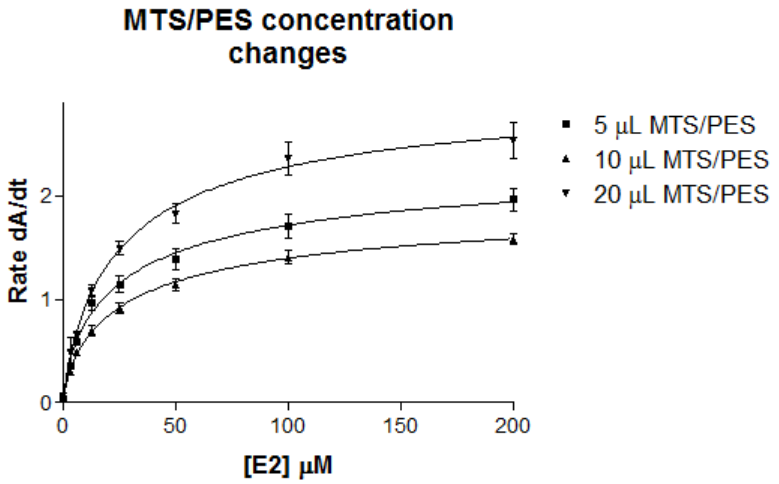

Figure 88: Michaelis-Menten analysis of the effect in changing the MTS/PES concentration in the assay

From Figure 88 it can be seen that the V_{MAXapp} increases, 2.003 to 2.758 ΔAbs/min for 5 µL and 20 µL respectively, as the concentration of MTS/PES increases this was as expected and it is assumed that at higher concentrations of MTS/PES the V_{MAXapp} will eventually remain constant. However, it was not viable to undergo experiments at these concentrations as this would have had a significant effect on the concentration of E2, 17β-HSD1 and the inhibitors under investigation. The large V_{MAXapp} is desirable for the assessment of inhibitors, however a small volume of MTS/PES is required so as to enable suitable amounts of E2, NADP and the inhibitor to be used and so therefore 10 µL of MTS/PES was used for all future assays.

Residual plot analysis (Figure 89) of the Michaelis-Menten model for the MTS/PES data indicates that a trend was observed, where the points adopt an upside down 'U' shape. This upside down 'U' is a clear indication that this particular curve fitting model is not the most suitable for this set of data.

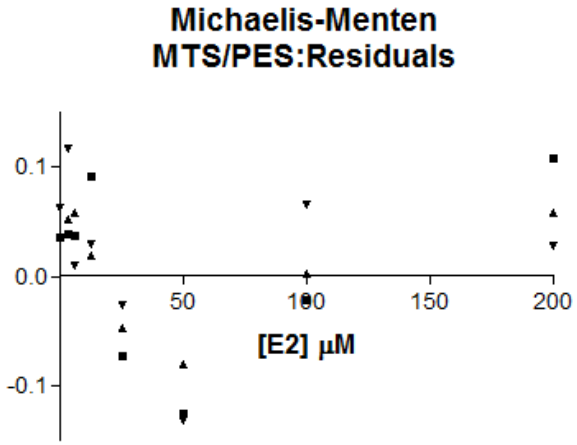

Figure 89: The residuals plot for the Michaelis-Menten analysis for the effect in changing the MTS/PES concentration

6.3.3.2.2 Hill analysis

It was observed from the residual plots that some of the data does not fit the Michaelis-Menten model, because of this it was decided to analyse the data using the Hill co-efficient (H) as well. The Hill co-efficient (H) provides a quantitative method for determining binding co-operativity, where if H > 1 then positive cooperativity is observed, which means that binding of a ligand at one site increases the binding affinity of a ligand at another site within the macromolecule. If H < 1 then negative cooperativity is observed, meaning that the binding of a ligand at one site decreases the binding affinity of a ligand at another site within the macromolecule. Puranen *et al*.[130] published results stating that 17β-HSD1 exists as a homodimer[131] consisting of two non-covalently bound subunits. It was also stated that substitution directed at the hydrophobic dimer interface resulted in inactive aggregates of the protein, indicating an exceptionally strong association between the monomers. As 17β-HSD1 exists as a homodimer analysis using the Hill model is acceptable. For all of the experiments described previously the data was also analysed using the Hill model to ascertain which model is best for the analysis of the data.

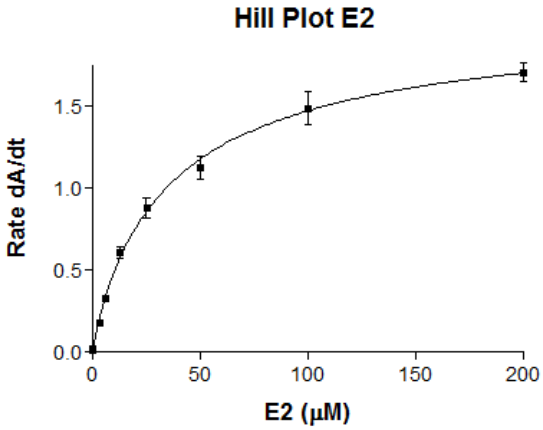

Figure 90: A Hill plot for the analysis of E2 conversion to E1 in the MTS/PES assay

It can be seen that the data fits the Hill model (Figure 90) for ligand binding reasonably well, an R^2 value of 0.9803 was determined. From the Hill model a K_D value of 37.47 µM, V_{MAXapp} of 2.081 ΔAbs/min, which are very similar to those calculated from the Michaelis-Menten model, and an H value of 0.8948 were calculated. This means that analysis using the Hill model, 17β-HSD1 acts in a negatively cooperative manner towards other binding subunits within the macromolecule after E2 has bound.

The residuals plot for the Hill model shows a random scattering, this confirms that the Hill model fits the data better than the Michaelis-Menten model. (Figure 91)

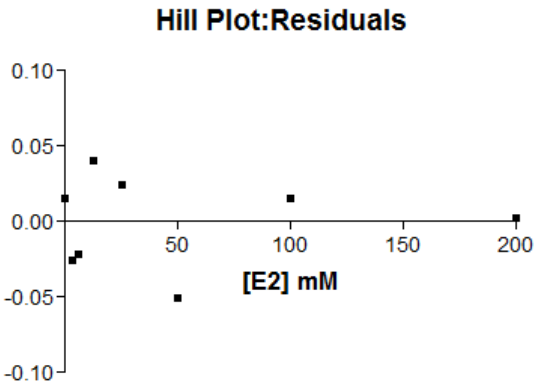

Figure 91: The residuals plot for the Hill analysis of the conversion of E2 to E1

Hill analysis for the binding of $NADP^+$ (Figure 92) provides very similar data to that observed for the Michaelis-Menten model, a K_D of 19.46 µM and a V_{MAXapp} of 2.752 ΔAbs/min were determined. A H value of 1.174 is calculated this suggests that

binding of $NADP^+$ to 17β-HSD1 results in positively cooperative manner towards the other subunits within the macromolecule.

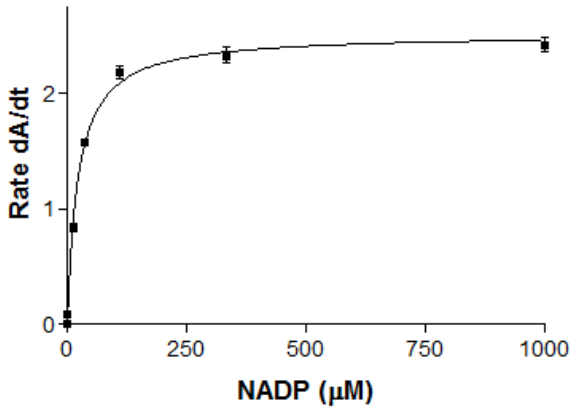

Figure 92: A Hill plot for the analysis of the conversion of $NADP^+$ NADPH

The residuals plot (Figure 93) for the Hill model displays a random scattering pattern, indicating the Hill model is suitable to use for the analysis of $NADP^+$ to 17β-HSD1. An R^2 value of 0.9509 is observed for the Hill model.

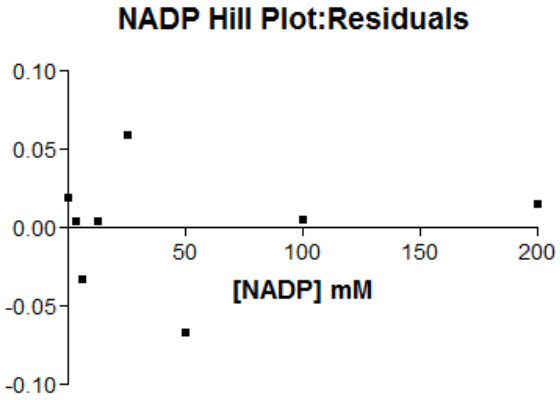

Figure 93: Residuals plot for the determination of the K_D for $NADP^+$ by Hill analysis

For analysis of the effect of temperature by the Hill model (Figure 94) very similar curves are obtained to those observed by the Michaelis-Menten analysis, however there are key differences in the residual plots (Figure 95).

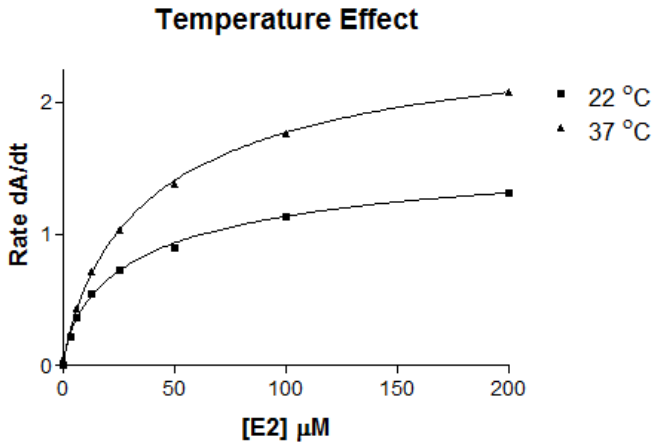

Figure 94: A Hill plot to show the effect of temperature upon the rate of conversion of E2 to E1

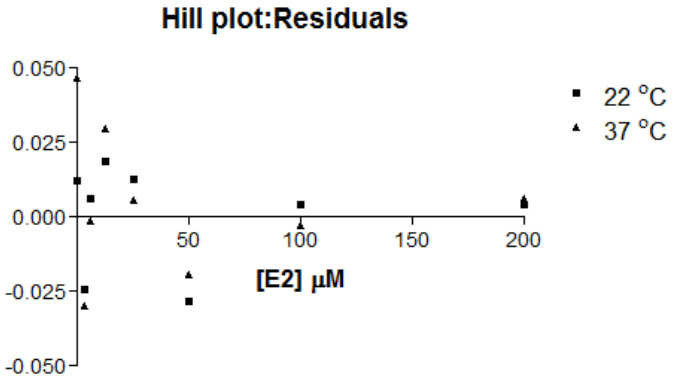

Figure 95: Residuals plot for the Hill analysis for the effect of temperature upon the rate of conversion of E2 to E1

For the Michaelis-Menten analysis a clear trend was observed in the residuals plot where the points adopt an upside down 'U' shape, whilst the Hill analysis is a random scattered plot, suggesting that analysis of the conversion of E2 to E1 by 17β-HSD1 should be determined using the Hill model.

The analysis for determining which buffer was used for running the assay using the Hill analysis (Figure 96) provided similar results to those obtained from the Michaelis-Menten analysis.

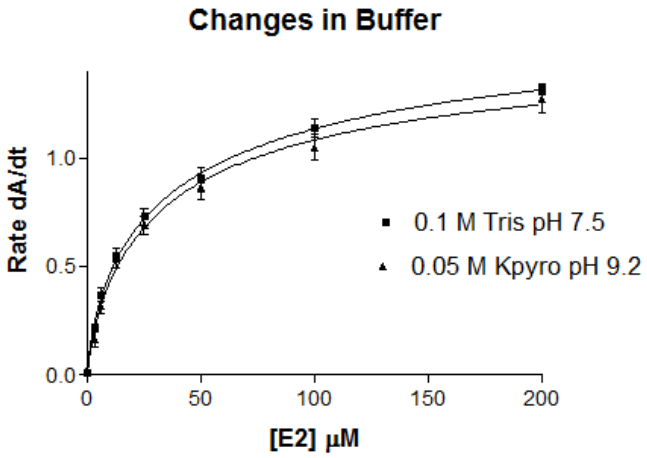

Figure 96: A plot to show how changing buffer alters the rate of conversion of E2 to E1

The K_D values determined are 42.73 µM and 36.93 µM and V_{MAXapp} values of 1.760 and 1.590 ΔAbs/min for 0.1 M Tris pH 7.5 and 0.05 M potassium pyrophosphate pH 9.2 respectively.

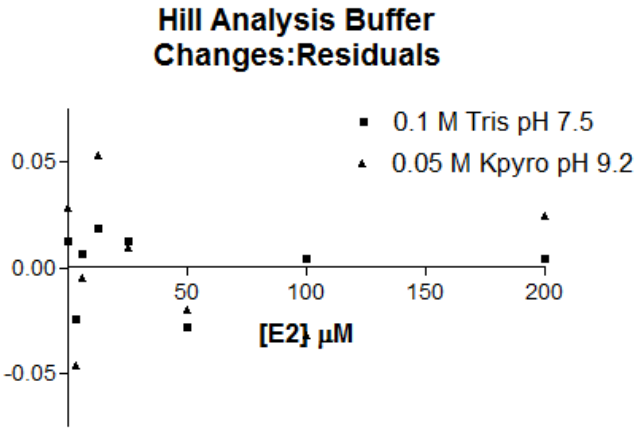

Figure 97: Residuals plot for the Hill analysis for the effect of buffer upon the rate of conversion of E2 to E1

It was observed from the Michaelis-Menten residuals plot that there is a trend within the data and that some other non-linear regression would be better suited to the data. The residuals plot (Figure 97) for the Hill model shows a random scattering and therefore this non-linear regression fits the data.

Hill analysis of the concentration of MTS/PES (Figure 98) to be used displays similar curves to those seen when analysis by the Michaelis-Menten model was undertaken.

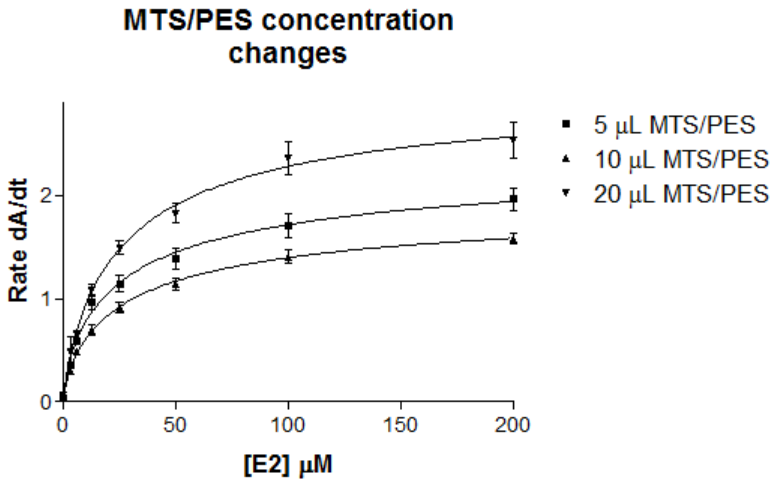

Figure 98: A plot to show how changing the MTS/PES concentration alters the rate of conversion of E2 to E1

Residual plot analysis (Figure 99) of the Hill model for the MTS/PES data shows a random scattering of the data points, again suggesting that the data should be analysed using the Hill model.

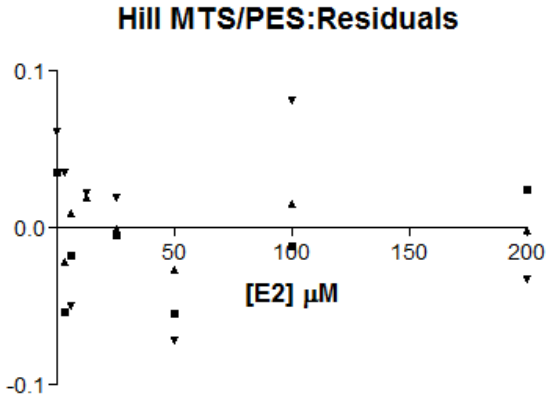

Figure 99: Residuals plot for the Hill analysis for the effect of MTS/PES concentration upon the rate of conversion of E2 to E1

Further work is however, required to further clarify which non-linear regression should be used for the analysis of the data obtained. The final conditions for the MTS/PES inhibitor assay have been determined to be:

Condition	Final conditions	Volume per well
Temperature	37 ºC	
Buffer	0.1 M Tris pH 7.5	10 µL
17β-HSD1 concentration	0.069 µM	5 µL
E2 concentration	30 µM (~ K_M)	10 µL
MTS/PES volume	10 µL	10 µL
NADP concentration	25 µM (~ K_M)	10 µL
Inhibitor concentration	Varying concentrations	10 µL
Water		45 µL
	Total well volume	100 µL

Table 30: The final conditions that were determined for the MTS/PES assay

E2 and the inhibitors under investigation were dissolved in DMSO to improve the solubility of the compounds within the assay, therefore giving a final volume of DMSO being added of 20 µL (20%).

6.3.4 Enzyme-Inhibitor Study

6.3.4.1 Assay Comparison

It was decided to test the MTS/PES assay as a predictive tool for inhibitory activity of the compounds against 17β-HSD1 by comparing the percentage inhibitions determined using the rec17β-HSD1 MTS/PES assay to that determined from a cell based assay for a variety of compounds featuring a number of different substitution patterns (Table 31).

	MTS/PES recombinant protein assay	**T-47D cell assay[a]**
Compound	**% inhibition @ 10 µM**	**% inhibition @ 10 µM**
STX670	65 ± 3	100
STX1040 **1**	80 ± 2	99
STX2818	26 ± 1	119
127	11 ± 3	28 ± 2
128	10 ± 1	96 ± 4
132	-6 ± 9	35 ± 7

135	10 ± 2	35 ± 5
137	1 ± 10	32 ± 9
141	20 ± 6	74 ± 2
143	17 ± 1	22 ± 10
154	6 ± 2	17 ±18
155	38 ± 6	13 ± 13
164	-7 ± 15	27 ± 3
165	6 ± 0	5 ± 2
166	4 ± 8	16 ± 3
167	1 ± 3	65 ± 3
174	31 ± 3	63 ± 3
175	27 ± 1	68 ± 1
176	17 ± 1	49 ± 13
185	5 ± 2	45 ± 3
186	7 ± 4	81 ± 1
187	10 ± 8	41 ± 1

a – Cell based assay results were measured by Ipsen

Table 31: Comparison of the percentage inhibition values from the MTS/PES assay and a cell-based assay

It can be clearly observed that the MTS/PES assay does not provide the same sensitivity as the cell based assay. There are, however agreements between the two assays. When comparing the two sets of data it can be seen that the compounds that have low percentage inhibition values (< 60%) in the cell based assay also display a low percentage inhibition in the MTS/PES assay. Examples include compounds **128**, **135**, **168** and **175** with percentage inhibitions of 28%, 35%, 49% and 41% respectively in the cell based assay and percentage inhibitions of 11%, 10%, 17% and 10% respectively in the MTS/PES assay. For compounds displaying greater than 60% inhibition in the cell based assay, these also display higher than average percentage inhibition in the MTS/PES assay at 10 µM. However, these compounds will need to be tested at 200 µM to further prove this. Examples of these compounds include STX1040 **1**, **166**, **167** which display percentage inhibition values of 99%,

63% and 68% respectively in the cell based assay and percentage inhibition values of 91%, 65% and 65% respectively in the MTS/PES assay. There are a couple of exceptions to this, compounds **152** and **174** which display either high percentage inhibition in the cell based assay and then low percentage inhibition in the MTS/PES assay or low percentage inhibition in the cell based assay and high percentage inhibition in the MTS/PES assay.

Therefore, it can be concluded that the MTS/PES assay can be used to assess the potency of 17β-HSD1 inhibitors. The limitations of the MTS/PES assay when compared to the cell based assay include: lower sensitivity, no information is gathered with regards to membrane permeability and the MTS/PES assay is using 17β-HSD1 in the reverse direction and therefore the inhibition data obtained is only a rough approximation of the biological activity of the compounds. Advantages of the MTS/PES assay when compared to the cell based assay are; the inhibitory effect is solely due to the effect of the compounds upon the enzyme, the assay is quick to run and the assay can be used to determine whether compounds can act as substrates.

6.3.5 Inhibitor Substrate Study

It is important for further drug design to understand how the compounds interact with the active site of the target protein. One important thing to know is whether or not the compound acts as a substrate. Figure 100 shows that when varying concentrations of compound **129** are present with NADP and 17β-HSD1 in the absence of E2 no rate is observed for the conversion of NADP to NADPH, therefore indicating that compound **129** does not act as a substrate for 17β-HSD1.

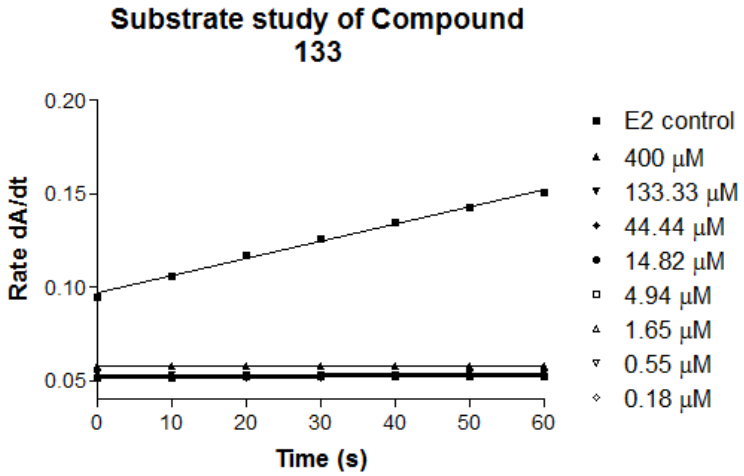

Figure 100: A linear plot demonstrating that compound **129** does not act as a substrate for 17β-HSD1

As compound **150** gave an enhanced rate at both 10 µM and 200µM in the recombinant 17β-HSD1 MTS/PES assay, in collaboration with Dr. G. Cozier a variety of compounds that were potent in the cellular assay were tested to see if they could potentially act as substrates for 17β-HSD1 (Table 32).

Compound	Rate (ΔAbs/min)	% Activity
No Inhibitor	0.0006 ± 0.00002	0.0 ± 0.06
E2	0.0369 ± 0.00003	100.0 ± 0.08
STX1040 **1**	0.0022 ± 0.00001	4.3 ± 0.03
141	0.0037 ± 0.00007	8.5 ± 0.20
153	0.1062 ± 0.00009	291.4 ± 0.24
167	0.0066 ± 0.00003	16.4 ± 0.07
174	0.0020 ± 0.00001	3.8 ± 0.02
175	0.0013 ± 0.00001	1.9 ± 0.04
186	0.0020 ± 0.00001	3.9 ± 0.03

Table 32: Inhibitor substrate investigation results

It can be concluded that **153** can potentially act as a very good substrate, the fact that **153** can act as a substrate and, therefore binds well to 17β-HSD1, means it will appear as an inhibitor in the cell based assay, which measures the amount of radio-active E1 that is converted rather than the amount of NADP. However, by using the MTS/PES assay which measures the conversion of NADP to NADPH it can be

determined that compound **153** acts as a substrate. It can also be stated that **167** can also potentially act as a substrate, but not a very good one. However, further work would be required to confirm this. From the data obtained for the other compounds assessed in Table 31 it can be stated that they do not to act as substrates for 17β-HSD1.

6.3.6 Type of Inhibitor Investigation

Compound **128** was selected for further biological evaluation with the use of the MTS/PES assay; the reason for this is that compound **128** is known to be a moderate inhibitor of 17β-HSD1 in a cell based assay as well as not acting as a substrate as previously described, therefore making it a good candidate to investigate whether the MTS/PES assay can be used to determine IC_{50} values. Figure 101 displays the IC_{50} curve that was determined. An IC_{50} value of 70 ± 1.2 µM was calculated for compound **128** using the MTS/PES assay. This is different to the IC_{50} value of 723 ± 138 nM that was determined using a cell based assay one reason for this is that the MTS/PES assay is being conducted at concentrations that are much higher than those observed at the cellular level. In a cell based assay the compounds can potentially be metabolised inside the cell and these metabolism products can potentially be responsible for the inhibitory effect. Taking these factors into account makes it very difficult to compare results between cell based and recombinant protein based assays.

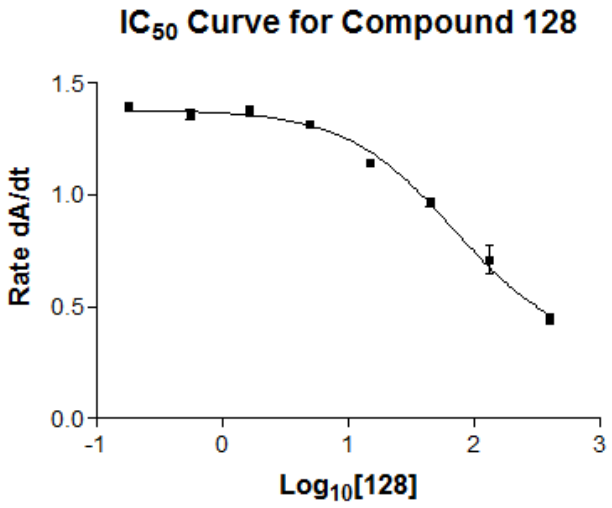

Figure 101: IC_{50} curve for compound **128**

A better way of interpreting IC_{50} values between assays, is to look at relative IC_{50} values (Table 33) giving a better representation of the inhibitory activity of the compounds. The IC_{50} plots of STX1040 **1** and **127** can be found later in this report.

Compound	**T-47D Cell based assay IC_{50} (nM)**	**Cell based assay relative IC_{50}**	**MTS/PES assay IC_{50} (µM)**	**MTS/PES assay relative IC_{50}**
STX1040 **1**	47		3 ± 0.4	
127	1854 ± 257	39	59 ± 11	21
128	723 ± 138	15	70 ± 20	25

Table 33: A table showing the relative IC_{50} values for both the MTS/PES and cell-based assays

The relative IC_{50} values do not follow the same trend between the two assays. An explaination for this is that the IC_{50} curves for compounds **127** and **128** lack the section of the curve that corresponds to the maximum inhibition therefore, the IC_{50} values for compounds **127** and **128** are estimates and could change if IC_{50} curves were produced with high enough inhibitor concentrations to reach the maximum inhibition. For the highly active compound STX1040 **1** this is not particularly an issue because the IC_{50}**,** had already started to tail off at the higher STX1040 **1** concentrations and so would not make much difference to the IC_{50} value determined.

6.3.6.1 Compound 127

It is hypothesised that the most potent inhibitor STX1040 **1** against 17β-HSD1, in a cell based assay with an IC_{50} value of 47 nM binds in both the substrate and co-factor binding sites and therefore acts as a "dual site" inhibitor. By using carefully designed enzyme kinetic experiments the mode of binding of STX1040 **1** can potentially be determined. To do this a compound that is not hypothesised to interact with the co-factor binding site compound **127** was used as a control for STX1040 **1**.

To determine whether the compounds are competitive inhibitors for the E2 and NADP binding site IC_{50} values were determined at varying concentrations of E2 and NADP. The E2 concentrations used were approximately half of the K_{Mapp} (15 µM), the K_{Mapp} (30 µM) and four times the K_{Mapp} (120 µM). If the compounds act as competitive inhibitors for the E2 binding site then an increased IC_{50} value should be observed for each increasing E2 concentration used. This is because as the

concentration of E2 is being increased, it makes it more difficult for the compound to outcompete the natural substrate for the binding site within the enzyme. If no change in IC_{50} value is observed then it can be concluded that the compound does not interact with the specified binding site.

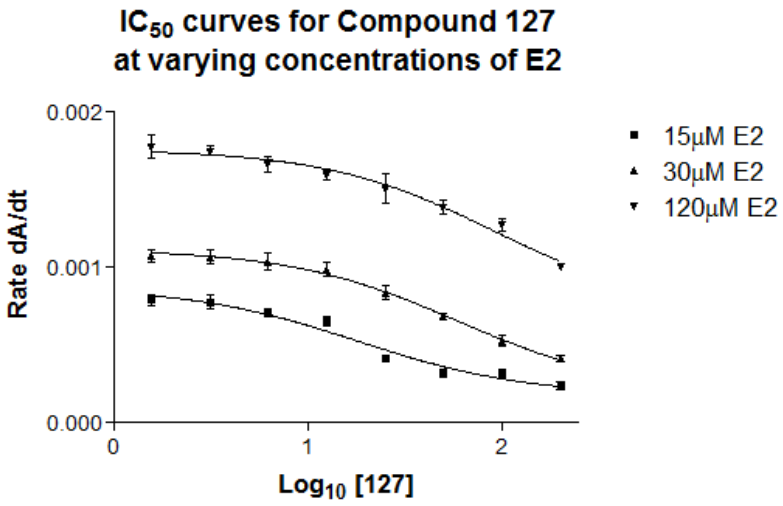

Figure 102: IC_{50} curves for **127** at varying concentrations of E2

For compound **127** IC_{50} values of 18.19 ± 8.1 µM, 59.21 ± 11.0 µM and 90.46 ± 15.3 µM were determined for 15 µM, 30 µM and 120 µM of E2 respectively (Figure 102), therefore indicating that compound **127** does as hypothesised interact with the E2 binding site of 17β-HSD1.

The same principle can be applied to the NADP co-factor binding site where approximately half the K_{Mapp} (12.5 µM), K_{Mapp} (25 µM) and five times the K_{Mapp} (125 µM) of NADP were used to determine whether or not the compounds interact with the co-factor binding site.

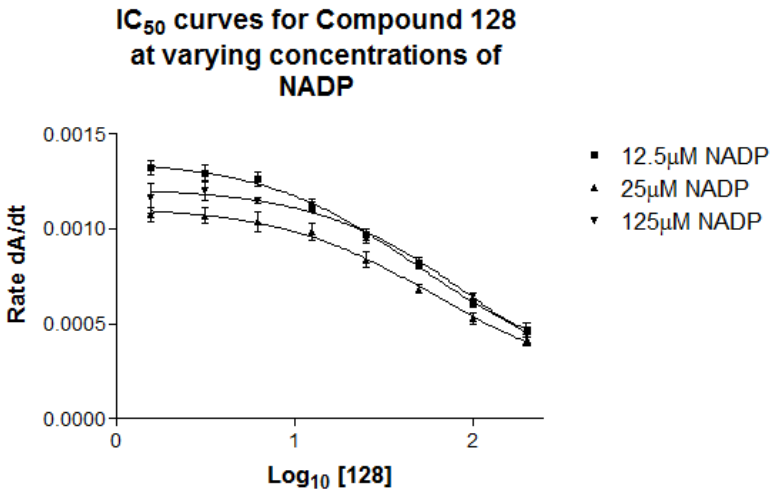

Figure 103: IC_{50} curves for **127** at varying concentrations of NADP

For compound **127** IC_{50} values of 47.94 ± 1.2 µM, 59.21 ± 1.3 µM and 97.95 ± 1.4 µM were determined for 12.5 µM, 25 µM and 125 µM of NADP respectively (Figure 103), therefore indicating that compound **127** interacts with the NADP binding site of 17β-HSD1. However, as the IC_{50} curves lack the section corresponding to maximum inhibition, the IC_{50} curves obtained are ony estimates and could change if IC_{50} curves were produced with high enough inhibitor concentrations. One way of determining what type of interaction the compound has with the active site of the protein is to use a Dixon and Cornish-Bowden plots. The Dixon plot has been described earlier in section 6.3.2. The Cornish-Bowden plot is a graphical representation where substrate concentration over the rate is plotted on the y-axis and the inhibitor concentration is plotted on the x-axis and the linear regressions correspond to the different substrate concentrations used. Like the Dixon plot the type of inhibitor is determined by the position at which the linear regressions intersect. For a competitive inhibitor the linear regressions run parallel to each other and do not intersect, for a mixed action inhibitor the linear regressions intersect below the x-axis and the x value of this intersection corresponds to the K_i value. Unlike the Dixon plot the Cornish-Bowden plot can be used to determine the K_i of an un-competitive inhibitor, un-competitive inhibition is characterised by the point of intersection taking place above the x-axis, and the K_i value is obtained by dropping a vertical line from the point of intersection to the x-axis.

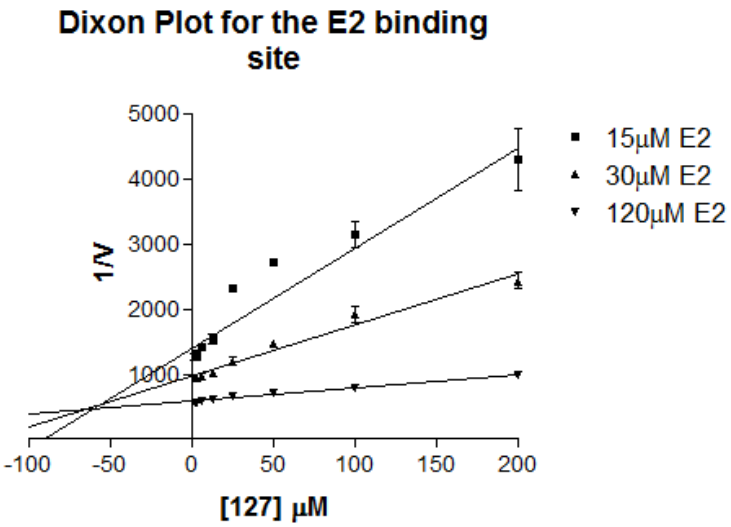

Figure 104: Dixon plot for **127**, where each linear regression corresponds to a different E2 concentration

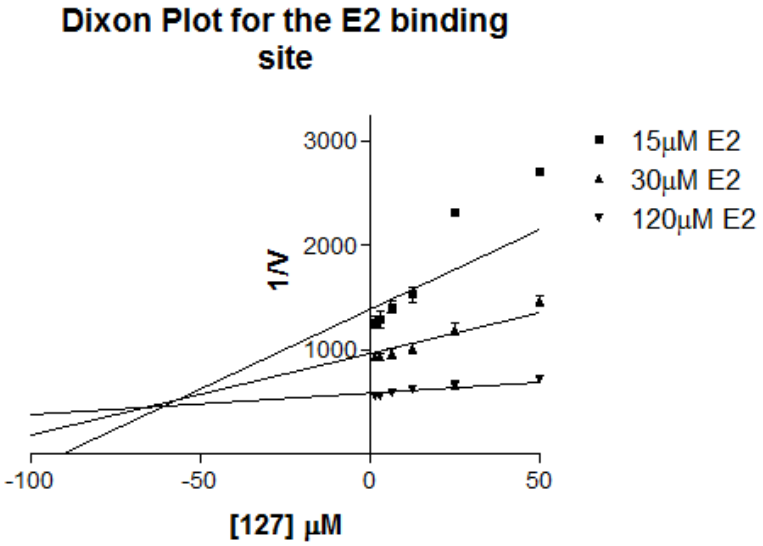

Figure 105: Expanded region from the Dixon plot of **127**, demonstrating that **127** is a competitive inhibitor against E2

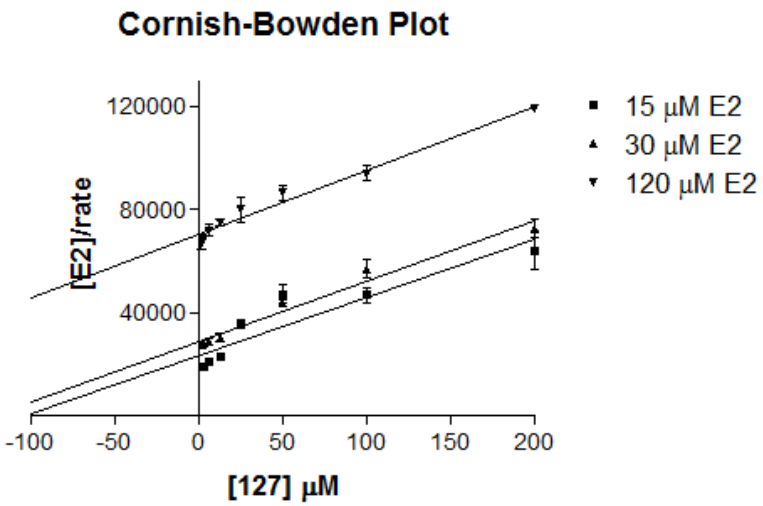

Figure 106: Cornish-Bowden plot for **127**, demonstrating that **127** is acting as a competitive inhibitor for the E2 binding site

From the Dixon plots in Figure 104 and 105 and the Cornish-Bowden plot in Figure 106 it can be determined that **127** acts as a competitive inhibitor of the E2 binding site as in the Dixon plot the linear regressions intersect above the x-axis and from the Cornish-Bowden plot the lines run parallel to each other. This result agrees with the hypothesis determined from computational docking studies that compound **127** binds in the steroid binding site. From the Dixon plot a K_i value of approximately 60 µM is determined.

When looking at the NADP binding site it can be tentatively be concluded that **127** acts as an un-competitive inhibitor as the Dixon plot in Figure 107 shows the linear regressions run parallel to each other, however they do intersect indicating that this form of modelling does not give the best representation of the mode of action of compound **127**. From the Cornish-Bowden plot in Figure 108 it can be seen that the linear regressions intersect on or at a point just above the x-axis, corresponding to a K_i value of approximately 110 µM, therefore agreeing with the results determined from the Dixon plot in saying that compound **127** is acting as a non-competitive inhibitor of the NADP binding site of 17β-HSD1.

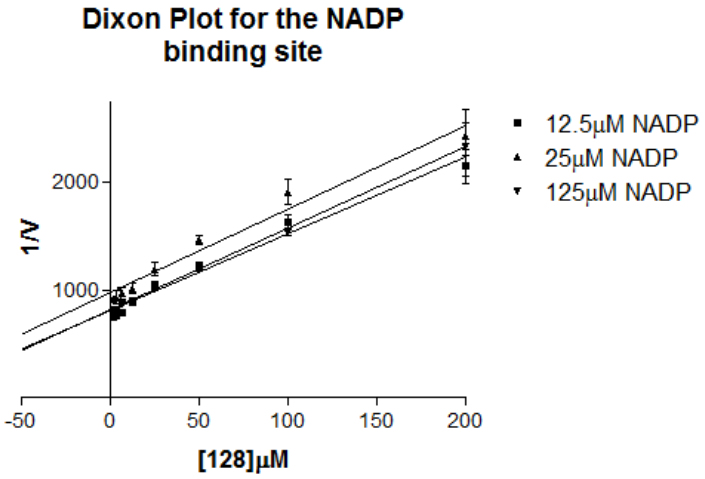

Figure 107: Dixon plot for **127** at varying concentrations of NADP

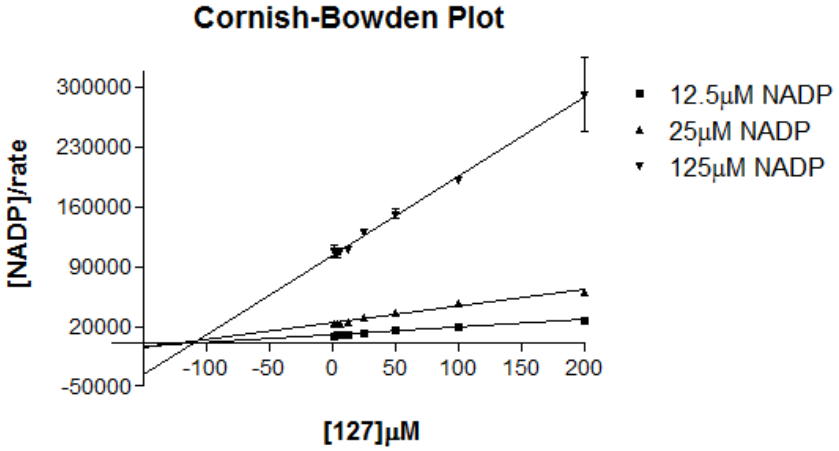

Figure 108: Cornish-Bowden plot for **127** at varying concentrations of NADP demonstrating the un-competitive inhibition for the NADP binding site

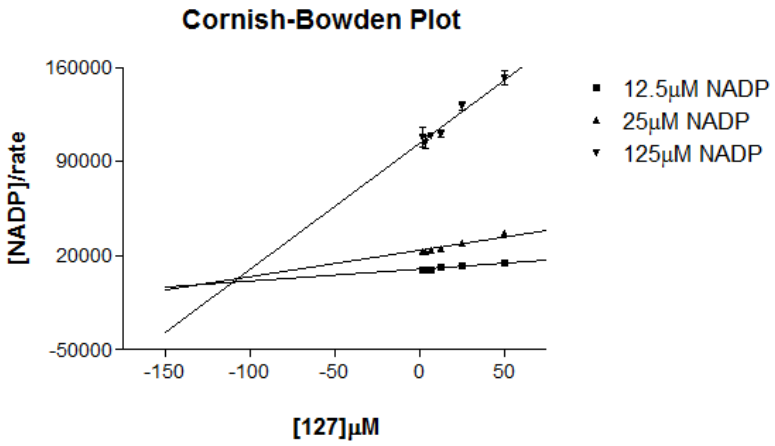

Figure 109: An expanded view of the Cornish-Bowden plot for **127**, highlighting the position at which the linear regressions intersect

However, the linear regressions for the Dixon plot and Cornish-Bowden plots do not fit the data very well for both the variable E2 and variable NADP concentrations. Therefore, these results indicate that 17β-HSD1 does not obey the Michaelis-Menten model. However, as 17β-HSD1 is a two substrate two product reaction mechanism, analysis using the ternary complex and substituted enzyme mechanisms might provide a better insight into how 17β-HSD1 behaves. This has been discussed in more detail in Section 6.4.

6.3.6.2 STX1040 (1)

It is hypothesised from the use of compoutational docking studies that STX1040 **1** acts as a "dual site" inhibitor where the C16 moiety interacts with the active site of the co-factor. It is hypothesised that STX1040 **1** acts as a competitive inhibitor for both the steroid and co-factor binding site of 17β-HSD1. The reason for this hypothesis is that the X-ray crystal structure (pdb code 1I5R) of compound EM-1745 **40** with 17β-HSD1 shows the inhibitor occupying both the steroid and co-factor binding sites. Therefore STX1040 **1** which also displays a C16 substituted moiety that is designed to be a NADPH mimic, coupled with the highly potent IC_{50} value of 47 nM should theoretically bind in the same manner. When the principle to determine whether the compounds are competitive inhibitors for the E2 and NADP binding site, by determining IC_{50} values at varying concentrations of E2 and NADP, is applied to investigate how STX1040 **1** binds in the active site of 17β-HSD1 IC_{50} values of 1.78 ± 0.2 μM, 2.82 ± 0.4 μM and 4.90 ± 1.0 μM for 15 μM, 30 μM and 120 μM of E2 respectively (Figure 110). This therefore indicates that as hypothesised, STX1040 **1** acts as a competitive inhibitor in the E2 binding site of 17β-HSD1.

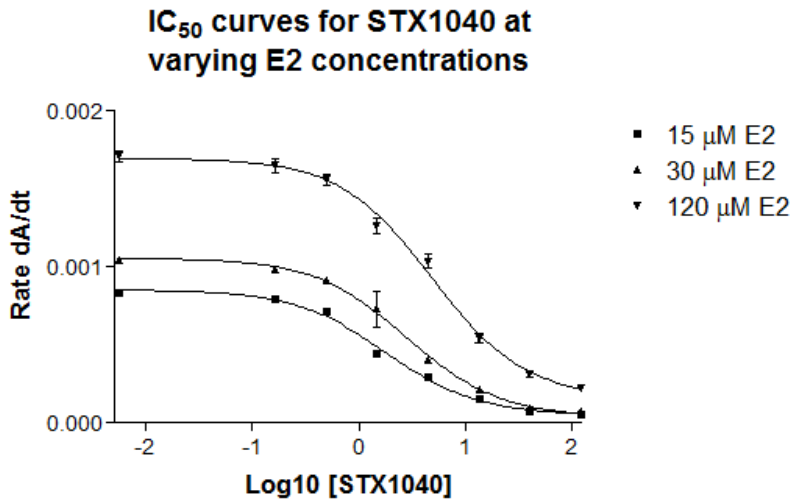

Figure 110: IC_{50} plots for STX1040 **1**, at varying concentrations of E2

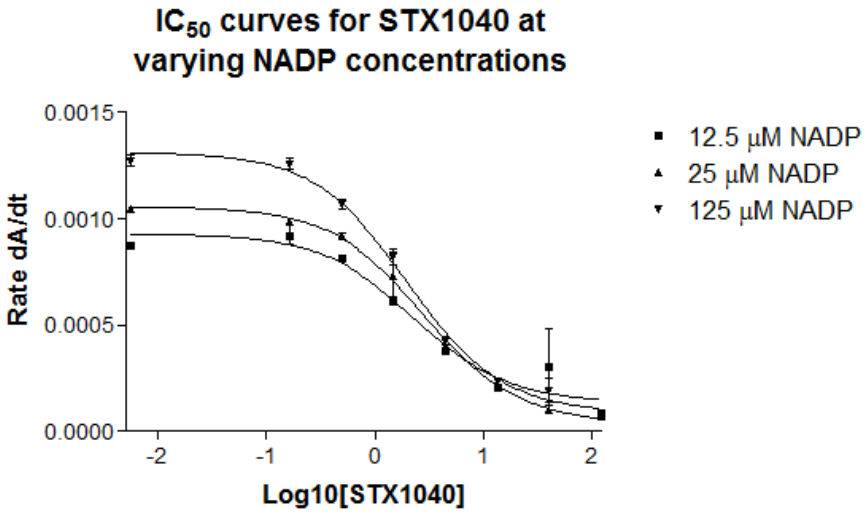

Figure 111: IC_{50} plots for STX1040 **1**, at varying concentrations of NADP

However, IC_{50} values of 2.27 ± 1.2 µM, 2.82 ± 0.8 µM and 2.00 ± 0.5 µM are determined for 12.5 µM, 25 µM and 125 µM of NADP respectively (Figure 111). These IC_{50} values are very similar and so suggest that STX1040 **1** does not act as a competitive inhibitor of NADP, therefore disproving the hypothesis that STX1040 **1** acts as a competitive "dual site" inhibitor. However, it cannot be said that the C16 moiety of STX1040 **1** does not interact with the co-factor binding site in a different capacity, so Dixon and Cornish-Bowden plots were produced to investigate the type of inhibition that STX1040 **1** displays against 17β-HSD1.

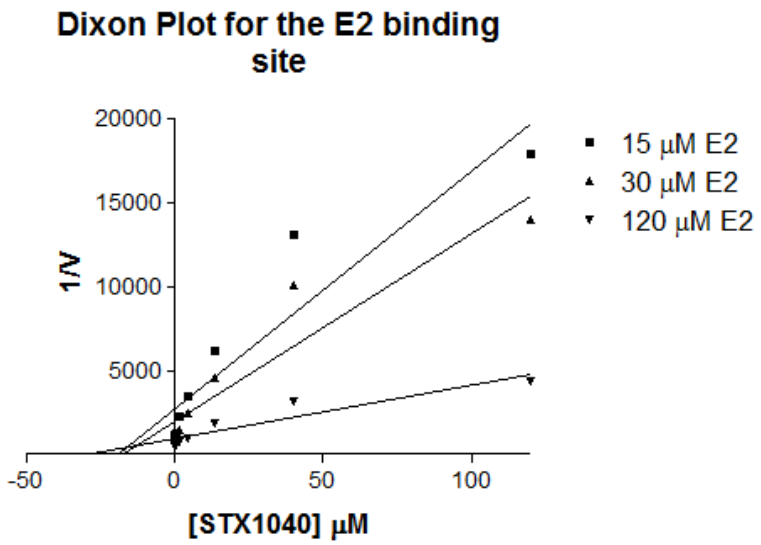

Figure 112: Dixon plot for STX1040 **1**, the linear regressions correspond to varying E2 concentrations

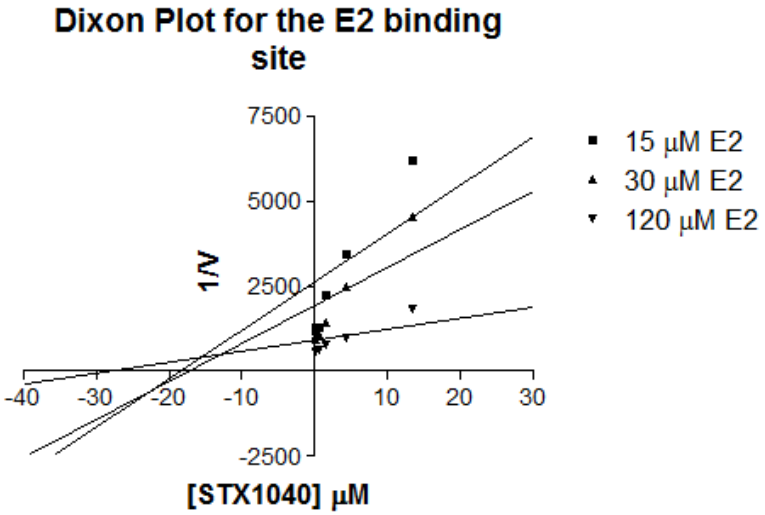

Figure 113: An expanded view of the Dixon plot for STX1040 **1**, highlighting the points at which the linear regressions intersect

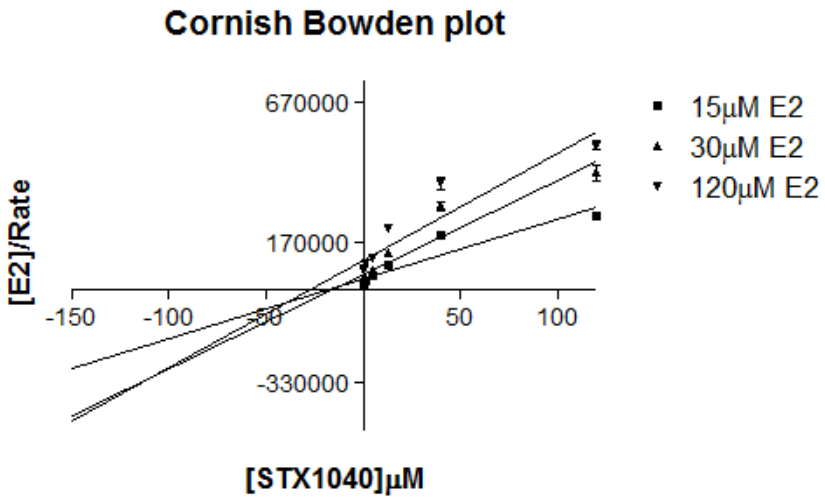

Figure 114: Cornish-Bowden plot for STX1040 **1**, demonstrating that STX1040 **1** is potentially a mixed action inhibitor

From Figures 112 and 114 it can be determined that STX1040 **1** is acting as a mixed action inhibitor. This can be observed from the Cornish-Bowden plot as the point of intersection for the linear regressions lies below the x-axis, however it is observed there is more than one point of intersection indicating that STX1040 **1** is behaving in a manner that cannot be fully explained by these plots alone and further investigation is required.

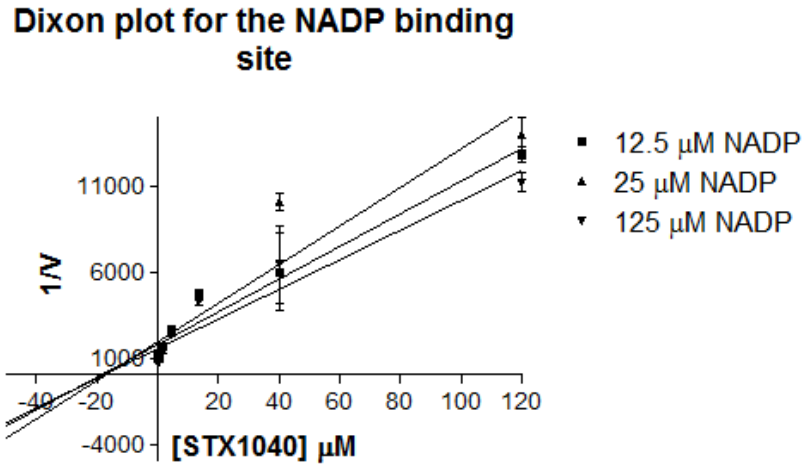

Figure 115: Dixon plot for STX1040 **1**, the linear regressions correspond to different concentrations of NADP

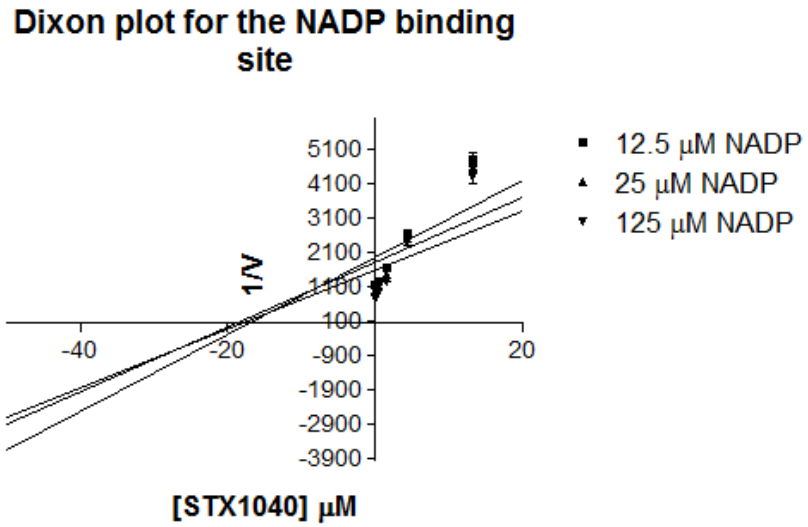

Figure 116: An expanded view of the Dixon plot for STX1040 **1** highlighting the position at which the linear regressions intersect, suggesting STX1040 **1** acts as a mixed action inhibitor.

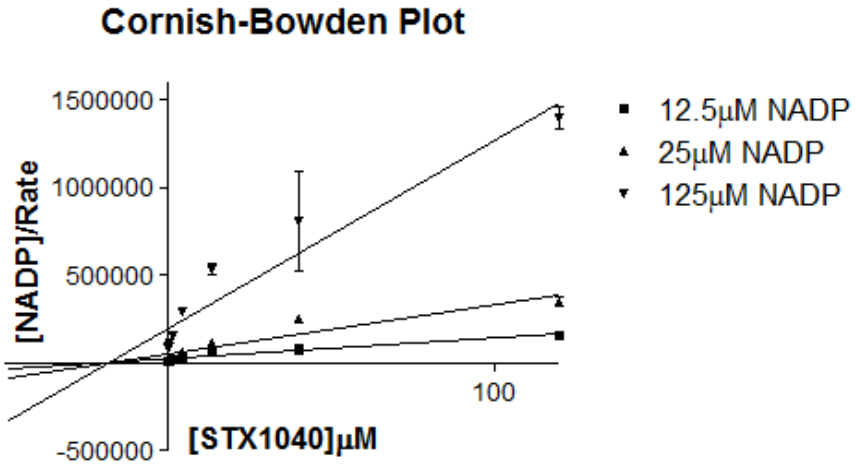

Figure 117: Cornish-Bowden plot for STX1040 **1**, with the linear regressions corresponding to different NADP concentrations

From Figures 115 and 117 the data suggests that STX1040 **1** in the variable NADP concentration experiments acts as a mixed inhibition compound. Using the Cornish-Bowden plot shown in Figure 117 it can be seen that the linear regression intersect on the x-axis, giving a K_i value of approximately 20 µM, this result is confirmed by the Dixon plot (Figure 115). Further experimentation is required to conclusively prove these preliminary results.

The Dixon and Cornish-Bowden plots are simple linear regression plots based upon there being a single substrate and single product, however 17β-HSD1 is a two substrate two product enzyme and this is further confirmed as the linear regressions do not accurately fit the data obtained for both **128** and STX1040 **1**. Therefore further work is required before any non-preliminary conclusions can be made about the mode of inhibition utilised by these inhibitors against both the steroid and co-factor binding sites of 17β-HSD1.

6.4 Two Substrate Two Product Enzyme Mechanisms[132]

There are two main classifications of the two substrate two product models; the ternary complex mechanism, so called because it contains the enzyme and both substrates in a single complex, and the substituted enzyme mechanism, where the enzyme is modified by conversion of the substrate to the product, therefore enabling the second substrate to bind and be converted to the second product (Figure 118).

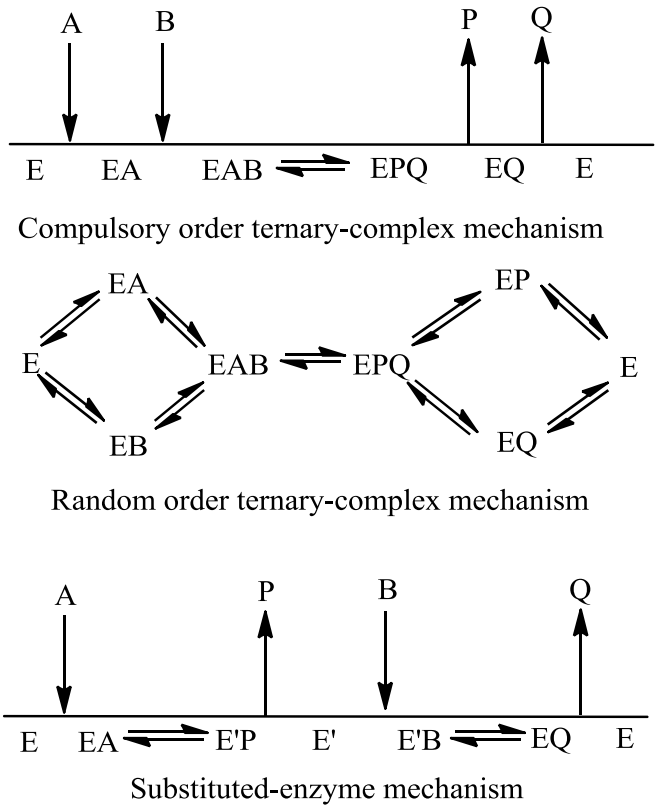

Figure 118: Schematic representations of the three principle two substrate two product enzyme mechanisms

A and B represent the substrates, P and Q represent the products. Written below the line is the role of the enzyme and the complexes formed during the enzyme reaction

mechanism. The arrows represent the addition and release of the substrates and products respectively.

6.4.1 Ternary Complex Mechanism

6.4.1.1 Ordered-Ternary Complex Mechanism

The ternary complex mechanism can proceed in one of two ways, ordered and random. For the ordered ternary complex mechanism, it is generally accepted that the structures of both the enzyme and substrate can be altered on binding. This gives the enzyme the ability to preferentially bind one substrate over another during the initial stages of the enzyme reaction, or that no binding site exists on the enzyme for one of the two substrates until the other has bound. Once the required substrate has bound this then changes the affinity of the enzyme for the second substrate, or a structural change takes place in the enzyme upon binding of substrate, A, resulting in the formation of the binding site for substrate, B, resulting in the formation of the ternary complex, followed by a stepwise release of the products.[132]

6.4.1.2 Random Ternary-Complex Mechanism

The random ordered ternary complex mechanism occurs where either of the substrates, A and B, can form an enzyme-substrate intermediate complex leading to the formation of the ternary complex and the subsequent formation and release of the two products.

6.4.2 Substituted Enzyme Mechanism

For the substituted enzyme mechanism there is only one mechanistically reasonable order for the enzyme reaction to proceed and so no random order alternative is possible. The substituted enzyme mechanism involves the binding and conversion of substrate A to product P and during this process the enzyme is modified in a manner that allows the binding and conversion of substrate B to product Q, which prior to the release of product P was not possible. It is not anticipated that 17β-HSD1 follows the substituted enzyme mechanism because the conversion of E1 to E2 involves the transfer of the Pro*S* hydride from the NADPH co-factor, and not the enzyme converting the co-factor to its oxidised form followed by the binding of the steroid E1 and the subsequent reduction to E2. This is further supported by the X-ray crystal

structure displaying both the steroid and co-factor occupying their respective binding sites (pdb code 1FDT[80]).[132]

It can be hypothesised that 17β-HSD1 follows a random order ternary complex based upon the X-ray structures of the protein in complex with steroidal ligands and co-factor ligands. Work by Negri *et al.*[37] further supports this hypothesis, however further enzyme kinetic experiments are required to conclusively prove this.

6.4.3 Dead End Complexes

The formation of dead end complexes can occur for any of the mechanisms described above. The formation of a dead end complex is when the incorrect substrate or one of the products, occupies the binding site for substrate, A, preventing the change in affinity or structural change of the enzyme taking place and therefore, the catalytic action of the enzyme proceeding (Figure 119).This makes determining the mechanism by which the enzyme operates a very complex and time consuming process, which was beyond the scope of this project.

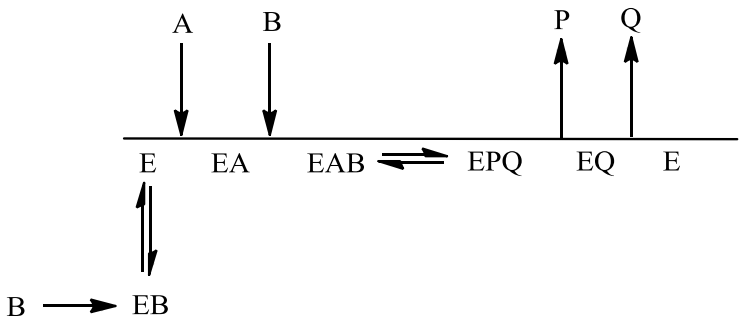

Figure 119: An example of the formation of a dead end complex, and how this can affect the enzyme mechanism, in this example an ordered ternary-complex mechanism

6.5 Design of Experiments to Determine the Two Substrate Two Product Reaction Mechanism

6.5.1 Determination Between a Ternary-Complex and Substituted Enzyme Mechanism[132]

Initially K_{Mapp} values for the two substrates should be determined. At each concentration of constant substrate, B, the variable substrate, A, concentration should range from approximately 0.2 to about 10 times its K_{Mapp}. This is then repeated with the substrate A concentration remaining constant and varying the concentration of

substrate B. Plots of these data will provide information as to which mechanism the protein adopts. For example a plot of substrate A concentration/rate on the y-axis versus substrate A concentration on the x-axis for a ternary complex will show the linear regressions intersecting below the x-axis, where the x-axis value corresponds to $-K_{iA}$ and the y-axis value corresponds to $(K_{MA} - K_{iA})$/rate. The same plot for a substituted enzyme mechanism would show the linear regressions intersecting on the y-axis, corresponding to a value of K_{MA}/rate.

6.5.2 Determination Between an Ordered Ternary-Complex and Random Order Ternary-Complex Mechanism[132]

Product inhibition studies are a very useful tool for determining the order of binding of substrates and release of products, providing that only one product is added to the reaction mixture. The question of whether a particular product acts as a competitive, un-competitive or mixed inhibitor is dependent upon which substrate concentration is considered to be variable.

Table 34 shows the type of inhibition expected for each combination of the product and variable substrate. The arrows indicate the tendency to modify the type of inhibition at saturating concentrations of the constant substrate. For example if mixed inhibition is observed for substrate A and product P with a tendency towards a un-competitive inhibition being observed at saturating concentrations of the constant substrate, B, this would indicate that an ordered ternary-complex order mechanism is adopted by the enzyme under investigation. However, if competitive inhibition is observed then a random ordered ternary complex mechanism is adopted by the enzyme.

Product	**Variable Substrate**	**Type of inhibition observed**	
		Ordered ternary-complex mechanism	Random ordered ternary-complex mechanism
P	A	Mixed → un-competitive	Competitive
P	B	Mixed	Competitive
Q	A	Competitive	Competitive
Q	B	Mixed → no inhibition	Competitive

Table 34: Product inhibition in the three principal two substrate two product mechanisms[132]

In order to prove conclusively that STX1040 **1** and **128** behave in the manner described previously, full enzyme kinetic analysis will need to be undertaken so that a better understanding of the mode of action for the conversion of the substrates to products can be gained. This will enable the design of inhibitor experiments that can fully investigate how these compounds behave with both substrate binding sites present in 17β-HSD1.

Chapter 7

Protein Crystallography

7.1 Literature Structures

When searching the RSCB pdb database 21 X-ray crystal structures of 17β-HSD1 were found. All of these crystal structures occupy a C2 space group, but vary in resolution and structure of ligand(s) that has been co-crystallised in the active site.

The earliest reported X-ray crystal structure is of the apoenzyme at a resolution of 2.20 Å. (pdb code 1BHS[33]). This first structure was closely followed by one from Housset *et al.*[76] who provided the first X-ray crystal structures of 17β-HSD1 complexed with a steroidal ligand, E2 and E2 co-crystallised $NADP^+$ (pdb codes 1FDS[80] and 1FDT[76]) at resolutions of 1.70 Å and 2.20 Å (Figure 120) respectively.

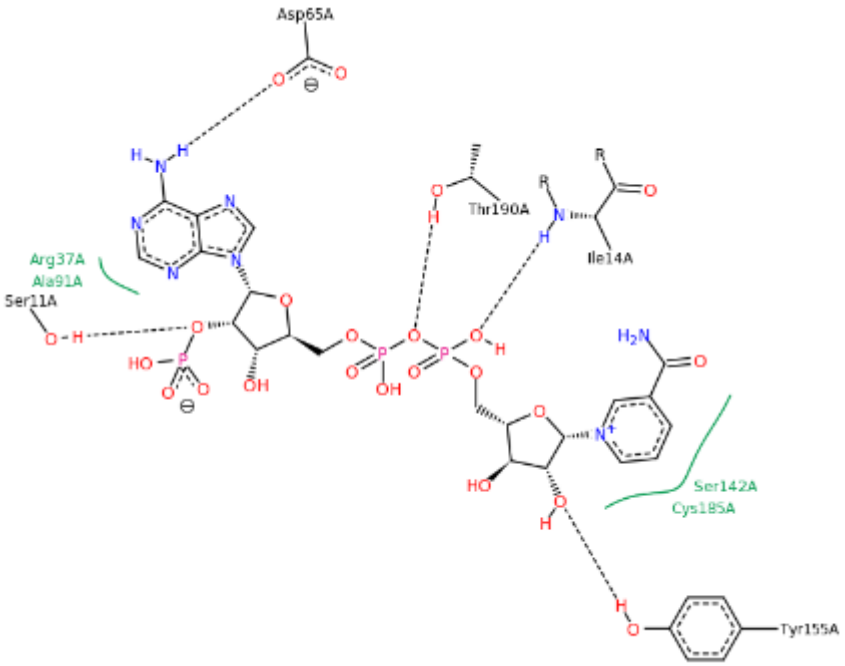

Figure 120: A schematic representation of how the cofactor $NADP^+$ binds in the active site of 17β-HSD1 (pdb code 1FDT[76])

Other steroidal ligands have been co-crystallised with 17β-HSD1, these include DHT,[133] dehydroepiandrosterone,[134] equilin[131], T,[135] Δ^4-dione,[136] and E2B.[137] From all of these X-ray crystal structures it can be seen that the steroidal ligands all occupy the same binding site within the active site of 17β-HSD1 (Figure 121).

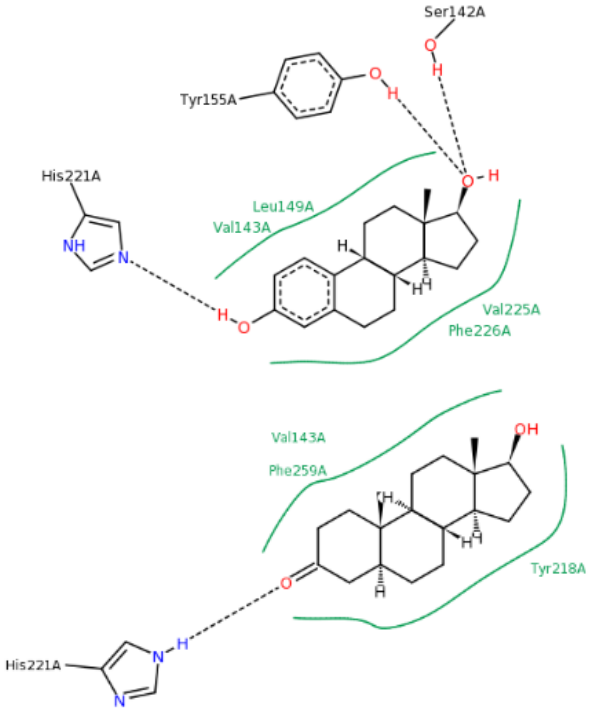

Figure 121: Schematics of the key interactions between different steroidal ligands, E2 (pdb code 1FDS) and DHT (pdb code 1DHT), and amino acid residues within the active site of 17β-HSD1

It has been observed from the structures for pbd codes 3KLP (Δ^4-diol), 3KMO (3β-diol), 1QYW (Δ^4-dione), 1JTV (T), 3KLM and 3DEY (DHT) that the steroidal ligand binds in the steroidal active site orientated with the D ring pointing away from the $NADP^+$ co-factor binding site (Figure 122). This implies that the active site of 17β-HSD1 is large and that the moieties present on the A ring play an important role in determining the binding orientation of the steroidal ligand within the active site.

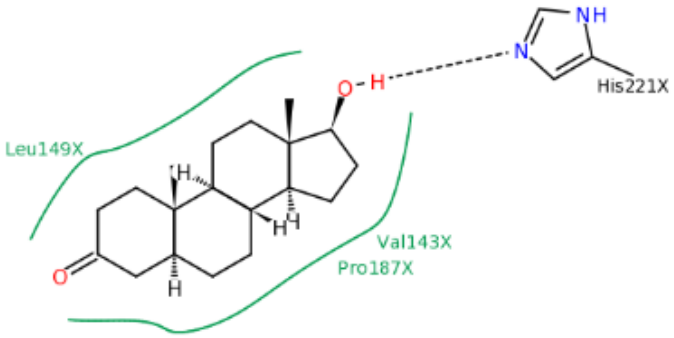

Figure 122: A schematic representation of how the steroidal ligand DHT binds in the active site of 17β-HSD1 (pdb code 3KLM)

There have also been X-ray crystal structures (pdb codes 1I5R and 3HB4) which depict how C16 substituted steroidal inhibitors bind in the active site of 17β-HSD1 (Figure 123). Both of these ligands bind with their C16 substituents positioned towards the $NADP^+$ co-factor binding pocket with EM1745 **40** (pdb code 1I5R) displaying how the C16 substituent occupies the $NADP^+$ cofactor binding site.

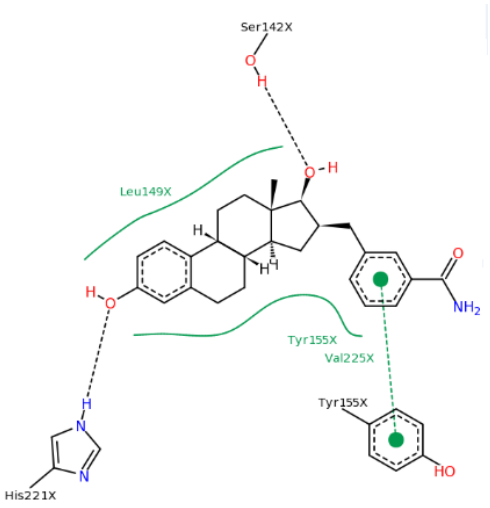

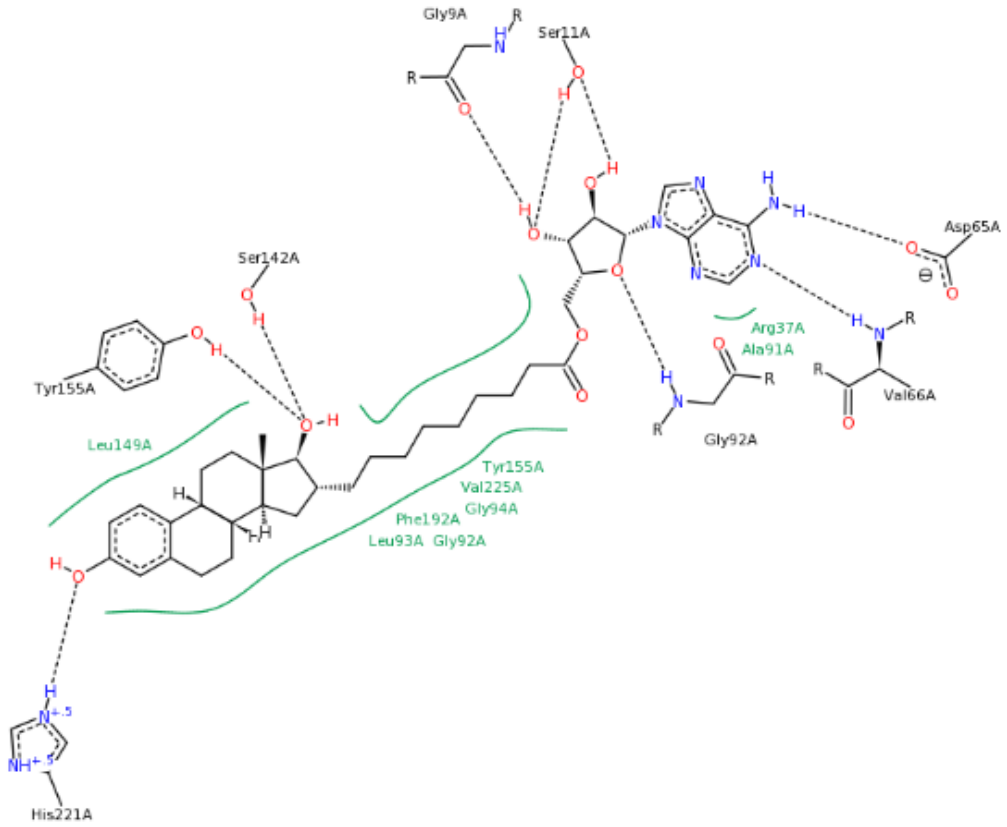

Figure 123: A schematic representation of how the steroidal inhibitors E2B (pdb code 3HB4) and EM1745 (pdb code 1I5R) binds in the active site of 17β-HSD1

7.2 X-Ray Protein Crystallography

As stated previously, it has been hypothesised that inhibitors bearing a C16 substituent of which STX1040 **1** is the most potent, IC_{50} value of 47 nM from a cell based assay, interact with both the substrate and co-factor binding sites in the active site of 17β-HSD1. To prove this hypothesis attempts were made to obtain an X-ray crystal structure of the protein co-crystallised with the inhibitor STX1040 **1** in the presence of and without NADP.

Once a large enough quantity of protein had been obtained, crystallization studies were started in collaboration with Dr. G. Cozier. The initial conditions used to start the crystallography trials were a series of conditions which have been previously used in the literature to crystallise the protein.[133] In the case described in the literature the vapour diffusion technique was used for crystallisation. The reservoir contained 0.15 M $MgCl_2$, 0.1 M Hepes, (*N*-(2-hydroxyethyl) piperzine-*N*'-2-ethanesulfonic acid) pH 7.5 and 28% polyethyleneglycol (PEG) 4000 as the

precipitant. Hanging drops of concentrated protein and glycerol were used. Initially, it was decided to try and crystallise the apoenzyme without the co-factor or the inhibitors being present as well as co-crystallisation with inhibitors STX1040 **1** and STX2109 **169** with and without the presence of the co-factor $NADP^+$. The rationale behind this was that if a set of crystallization conditions could be established then it would be easier to start co-crystallising the protein with some steroidal inhibitors as many of the reported structures were obtained when the compounds had been soaked into the forming crystals of the apoenzyme. Initial trials at crystallising the bacterially expressed protein utilised a range of PEG4000 concentrations at varying $MgCl_2$ concentrations. Using these crystallization conditions as well as others that were similar in counter-ion concentration and polymer concentration, a starting point was established for trying to crystallise the protein. Some very small needle and urchin like crystals were found to have grown under these conditions initially. Although these crystals could not be used for X-ray crystallography, they did provide some information about the concentration of PEG4000 that should be used in the trials. Needle / urchin like crystals formed when lower concentrations of PEG4000 were used.

As crystallization of the protein proving difficult, based on the conditions reported in the literature,[128] it was decided that the best course of action would be to set up screens to look for other suitable conditions. A Phoenix nano-litre drop dispensing crystallography robot was used to set up a series of 96 well plates using the Molecular Dimensions Ltd structure screen 1 and 2 and the PACT structure screen. There were several hits from the screens, most notable of which were: 0.2 M Magnesium Acetate and 0.1 M Sodium Cacodylate pH 6.5 against 20% PEG8000 (1:2 ratio of protein to well buffer) and 1.6 M Sodium Citrate pH 6.5 (2:1 ratio of protein to well buffer). From these initial hits a series of optimised conditions were set up. These were 0.05 M - 0.4 M Magnesium acetate with 0.1 M sodium cacodylate against 15–37.5% PEG8000, as well as 1.3 M–1.8 M Sodium citrate pH 6.5. The best crystals were obtained with 0.2 M Magnesium Acetate, 0.1M sodium cacodylate pH 6.5 with 20% PEG8000 (Figure 124). However, these crystals were not large enough to use on the home source X-ray diffractor, the X-ray diffraction data was collected by Prof. R. Acharya at the synchrotron radiation source (Diamond U.K.). Data were indexed and reduced with DENZO and SCALEPACK modules of

the HKL suite[138] in the C2 space group. The structure was determined by Dr. G. Cozier using the molecular replacement method using pdb code 1FDT[76] as the search model with the programme Phaser[139] from the CCP4i programme suite. Refinement was performed using Refmac[140] from the programme package CCP4i in addition to the manual model building using the programme COOT.[141]

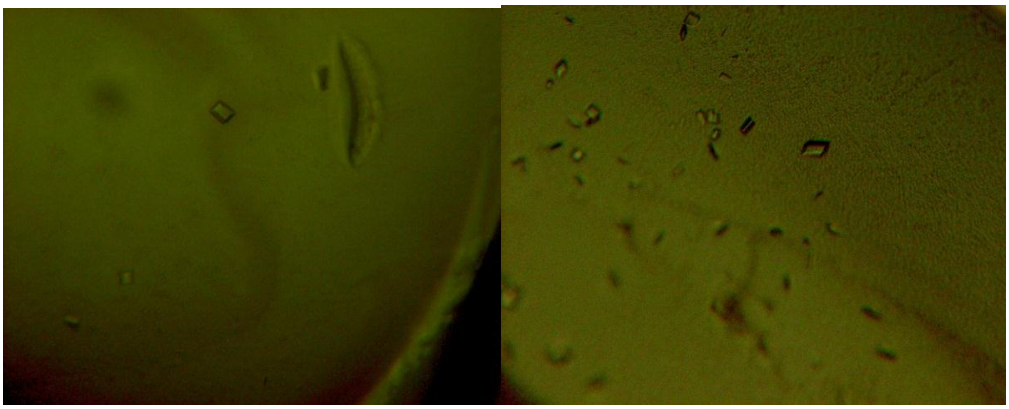

1 2

1) 0.2M Mg Acetate + 0.1M Na Cacodylate pH 6.5 + 20% PEG 8000

2) 1.6M Na Citrate pH 6.5

Figure 124: Single crystals of H_6-17β-HSD1 and the conditions under which they were grown

The Data collection results can be seen below in Table 35 and are very similar to results which have been previously published for 17β-HSD1.

Data Collection	
Space Group	C2
Unit cell	A = 122.386 b = 43.755 c = 60.705Å α = 90.00 β = 99.35 γ = 90.00°
Resolution (Å)	30.19 – 2.46
Completeness for range (%)	97.70
Measured Reflections	51953
Number of Unique Reflections	11478
I / σ_I[a]	15.7 (outermost shell 2.55-2.46Å I/σ = 11.4)
Rsym	0.040 (outermost shell 2.55- 2.46Å Rsym 0.091)

Table 35: Data collection results for diffraction of H_6-17β-HSD1

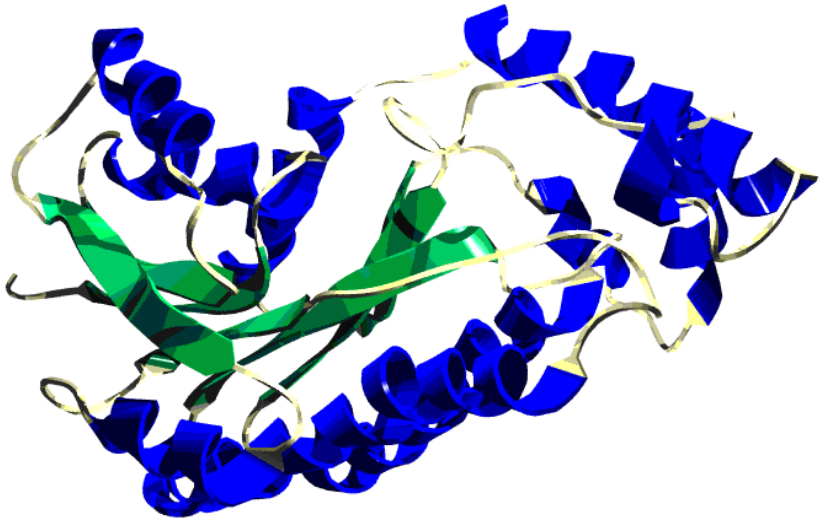

Figure 125: 17β-HSD1 protein structure derived from X-ray crystallography. α-Helices are shown in blue and β-sheets are shown in green

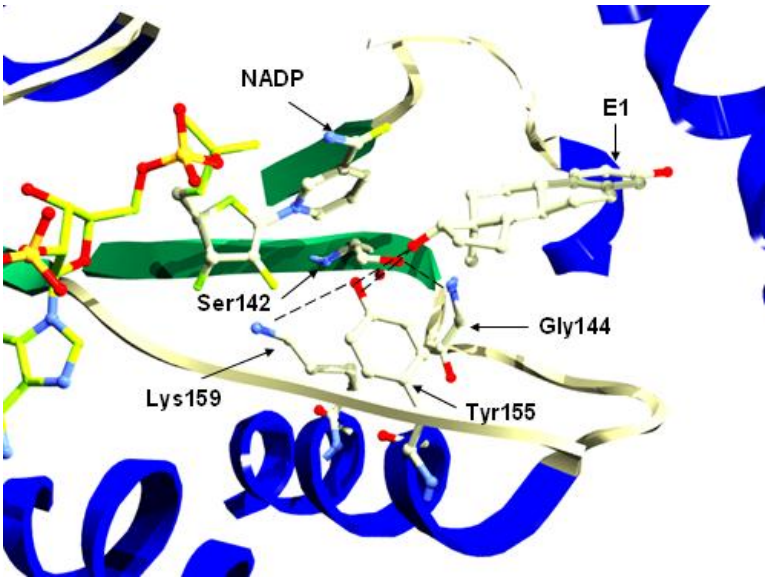

Figure 126: Active site of 17β-HSD1 with some secondary structure removed for clarity and catalytic residues highlighted with hydrogen bonds represented by dashed lines

Figure 125 shows the solved structure of the apo-enzyme crystal that was diffracted at Diamond in Oxford. Figure 126 shows the overlaid structures of E1 and NADP in the active site of the solved structure of 17β-HSD1. The key catalytic residues Ser142, Gly144, Tyr155 and Lys159 that are used in the reduction mechanism of E1 to E2 are shown.

An X-ray crystal structure of STX2908 **127** co-crystallised with 17β-HSD1 at a resolution of 2.8 Å was obtained (Figure 22). It was observed that the inhibitor **127** can potentially bind in two different orientations within the steroid binding site of 17β-HSD1. The first orientation consists of the D ring of the steroid core directed towards the $NADP^+$ cofactor binding site, whilst in the second it is observed that the A ring of the steroid points towards the $NADP^+$ cofactor binding site. As stated previously from studying the available X-ray crystal strucures in the RSCB pdb database it has been observed from the structures for pbd codes 3KLP (Δ^4-diol), 3KMO (3β-diol), 1QYW (Δ^4-dione), 1JTV (T), 3KLM and 3DEY (DHT) that the steroidal ligand binds in the steroidal active site with the D ring pointing away from the $NADP^+$ co-factor binding site. This therefore shows that this observation is not entirely unexpected, although it is believed that this structure is the first to suggest two competing binding modes.

Chapter 8

Conclusions

This project set out to explore the design and inhibitory potential of compounds against 17β-HSD1, with the long-term and overarching aim of developing a new molecule that could be clinically significant for treatment for hormone dependent breast cancer. Although the latter aim is likely to be many years away, this project has identified some potentially significant compounds, that will likely require further optimisation and development.

Initial targets were planned, based around modifications of the steroidal estrone / estradiol core, utilising the Mannich and Friedel-Crafts reaction. Over 20 compounds substituted at C2 and C4 of the steroid core were synthesised and display biological activites ranging from 9-96% inhibition at 10 μM for the Mannich series and 22-74% inhibition at 10 μM for the Friedel-Crafts series in a 17β-HSD1 cell-based assay. From the data described earlier it is observed that compounds displaying modifications of the E1 core are more biologically active than their E2 counterparts. The most potent compound in this series is (13*S*)-3-hydroxy-13-methyl-2-(morpholinomethyl)-7,8,9,11,12,13,15,16-octahydro-6*H*-cyclopenta[a]-phenan-thren-17(14*H*)-one **128** with an IC_{50} of 723 nM; **128** is also shown to be selective for 17βSHD1 over 17β-HSD2 and does not display any cytotoxicity at 50 μM over a

period of 96 hours in estrogen receptor positive and estrogen receptor negative cells. Similar biological activities are observed for compounds substituted at the C2 and C4. The wide range of biological activity observed indicates that the optimum substitution at these positions has still not yet been identified and so there is scope for further improvement of these compounds.

Modifications of the steroid core at the C17 position gave a series of compounds where a bioisostere was introduced in place of the C17 carbonyl group, enabling expansion from this position. Six compounds were synthesised and display poor to moderate biological activity against 17β-HSD1, with percentage inhibition values of 5-65% at 10 μM. The most potent compound in this series is *N*-((13*S*,17*S*)-3-hydroxy-13-methyl-7,8,9,11,12,13,14,15,16,17-decahydro-6*H*-cyclopenta[a]-phenanthren-17-yl)-2,4,5-trimethoxybenzamide **167**, with a percentage inhibition of 65% at 10μM. Further modification of this series of compounds is required to provide a fully coherent SAR for the effect of substitution at this position. Results have been observed for compounds bearing a C17 E ring moiety[113] that can be used in conjunction with the results obtain within the project to build an early stage SAR.

Further research into the SAR of compounds bearing a C16 substituent is an attractive proposition, because the most biologically active compound observed in the literature STX1040 **1** with an IC_{50} of 47 nM from a cell-based assay, has been shown to inhibit E1 stimulated proliferation of T-47D cell *in vitro* and significantly decreases tumour volumes and plasma E2 levels *in vivo*.[49] Two strategies were therefore devised to develop the SAR for this position of the steroid core, the first being extending the C16 linker length to investigate what is the optimum linker length for biological activity; the second being the reversal of the amide orientation present in the C16 linker to investigate what effect minor changes of STX1040 **1** might have on the biological activity of the compounds. Six compounds were synthesised and display moderate to good inhibition of 17β-HSD1. Percentage inhibition values range from 41-81% inhibition at 10 μM. The most potent compound being *N*-(((13*S*,16*R*,17*S*)-2-ethyl-3,17-dihydroxy-13-methyl-7,8,9,11,12,13,14,15,16,17-decahydro-6*H*-cyclopenta[a]-phenan-thren-16-yl)methyl)-2-(pyridin-3-yl)acetamide **186** with a percentage inhibition value of 81% at 10μM. Both series of compounds designed to investigate the SAR of the C16 position display lower biological activity to that observed for STX1040 **1**, indicating

that STX1040 **1** exhibits the optimum linker length and preferred amide orientation present in the C16 linker. Further optimisation can be performed by changing the 2-substitution from an ethyl moiety to one that has been shown to be active from the 2-substituted Mannich series described in this project. This will result in an increase in relative molecular mass, however the introduction of an amine can be utilised to form a quaternary ammonium salt and so potentially increase the solubility of these compounds in aqueous media. All of the synthetic and SAR studies were underpinned by molecular modelling studies, using the established X-ray crystal structure 1FDT of 17β-HSD1. Results showed that E1 derivatives are more biologically active than their corresponding E2 derivatives, and that compounds bearing a 3-OH moiety are more biologically active than their corresponding 3-OMe derivatives. It can also be concluded that for 2-substituted compounds aromaticity is important for biological activity, however, this can be overcome by the addition of an electronegative atom e.g. oxygen. Compounds with large 2-substituted moieties are well tolerated by the active site of 17β-HSD1 but further investigation is required to determine the optimum substitution at this position. Substitution at the 4-position is tolerated by the active site however, does no provide good biological activity. Results show that by substituting the carbonyl at C17 with an amide these compounds are not as well tolerated by 17β-HSD1. It has been determined that a C16 linker length of 3 / 4 atoms is the optimum linker length for inhibitory activity against 17β-HSD1 and that reversing the amide orientation is also detrimental to biological activity for this series of C16 substituted compounds.

Another aim was to explore in-house the interaction of synthetic compounds with the enzyme by both structural and kinetic evaluations. Sufficient quantities of the His-tagged H_6-17β-HSD1 protein, were successfully synthesised and purified. The H_6-17β-HSD1 was shown to be active, therefore permitting an in house MTS/PES recombinant protein assay to be developed so as to enable the study of the inhibitory effect of novel steroidal ligands against 17β-HSD1. The MTS/PES assay was shown to give similar trends for biological activity against 17βSHD1 when compared to the cell-based assay that was used for obtaining the percentage inhibition values. The MTS/PES assay was used to investigate how two compounds **127** and STX1040 **1**, for which it is hypothesised interact in different manners with the binding sites of 17β-HSD1. It can tentatively be concluded that compound **127** acts as a competitive

inhibitor for the E2 binding site with a K_i value of approximately 60 μM and as a non-competitive inhibitor for the $NADP^+$ binding site with a K_i value of approximately 110 μM. In addition it can also be tentatively be concluded that STX1040 **1** acts as a mixed action inhibitor for both the E2 and $NADP^+$ binding sites. Further experimentation is required to conclusively prove or disprove these preliminary results.

As ample quantities of H_6-17β-HSD1 were obtained protein X-ray crystallography trials were also able to be undertaken and resulted in an X-ray crystal structure of the apo-enzyme being obtained at a resolution of 2.46 Å using the hanging drop diffusion technique. The data collection results are very similar to results which have been previously published for 17β-HSD1.[36] A X-ray crystal structure of STX2908 **126** co-crystallised with 17β-HSD1 at a resolution of 2.8 Å was obtained. It was observed that the inhibitor **126** can potentially bind in two different orientations within the steroid binding site of 17β-HSD1. The first orientation consists of the D ring of the steroid core directed towards the $NADP^+$ cofactor binding site, whilst in the second it is observed that the A ring of the steroid points towards the $NADP^+$ cofactor binding site. From studying the available X-ray crystal strucures in the RSCB pdb database it has been observed for pbd codes 3KLP (Δ^4diol), 3KMO (3β-diol), 1QYW (androstanedione), 1JTV (T), 3KLM and 3DEY (DHT) that the steroidal ligand binds in the steroidal active site with the D ring pointing away from the $NADP^+$ co-factor binding site. This therefore shows that this observation is not entirely unexpected, although it is believed that this structure is the first to suggest two competing binding modes.

It is fair to note that to gain a better understanding of how these inhibitors interact with the steroid and co-factor binding sites of 17β-HSD1 an in depth study into the mechanism of action for the enzyme is required. However, the use of biological assays can provide useful preliminary data as to how these compounds may achieve their biological activity. This will all help bring the project closer to the development of a potential safe, effective clinical treatment for hormone dependent breast cancer and other estrogen-dependent diseases and disorders to augment the range of endocrine therapy currently available. Progress on this project overall was unfortunately curtailed at the start of the third year of work, when the industrial

funder Ipsen decided to stop all work in this and related areas and therefore became unable to assay further compounds synthesised in this work.

To date, there are no named development compounds from any group for 17β-HSD1 as a new cancer target. These are therefore very early days for the concept explored here. However, the *in vivo* activity for STX1040 **1** published by our group in a cancer model augurs well for this approach.

Chapter 9

Experimental Details: Chemistry

All chemicals were purchased from Aldrich Chemical Co. (Gillingham, UK) or Lancaster Synthesis (Morecambe, U.K.). All organic solvents of A. R. grade were supplied by Fisher Scientific (Loughborough, U.K.). Reactions using anhydrous solvents were carried out under nitrogen. Thin-layer chromatography (TLC) was performed on precoated plates (Merck TLC aluminum sheets silica gel 60 F254). Product(s) and starting material(s) were detected by either viewing under UV light and/or treating with a suitable staining system, for example vanillin followed by heating. Flash column chromatography was performed on silica gel (Sorbsil/Matrex C60) or using Argonaut prepacked columns with a Flashmaster II. IR spectra were recorded on a Perkin Elmer Spectrum RXI FT-IR in KBr discs and peak positions are expressed in cm^{-1}. ^{1}H NMR (400 MHz) and *DEPT* edited ^{13}C NMR (101 MHz) spectra were recorded with a Varian Mercury VX 400 NMR spectrometer, and chemical shifts are reported in parts per million (ppm). HPLC analyses were performed on a Waters Millenium 32 instrument equipped with a Waters 996 PDA detector using either a Waters Radialpack C18 reversed phase column (8 × 100 mm), or a Symmetry C18 reverse phase column (4.6 × 150 mm) eluting with the solvent system specified at 1.0 mL/min. FAB low and high-resolution mass spectra were recorded at the Mass Spectrometry Service Centre, University of Bath, using *m* nitrobenzyl alcohol (NBA) as the matrix. ESI and APCI low resolution mass spectra were obtained on a Waters Micromass ZQ. Elemental analyses were performed by the Microanalysis Service, University of Bath. Melting points were determined using an Optimelt block and are uncorrected.

(13*S*)-3-Hydroxy-13-methyl-2-(piperidin-1-ylmethyl)-7,8,9,11,12,13,15,16-octahydro-6*H*-cyclopenta[a]-phenan-thren-17(14*H*)-one (Compound 127), $C_{24}H_{33}NO_2$, MW 367.25,

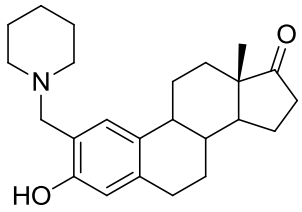

127

To a solution of estrone (2.00 g, 74 mmol) in EtOH/toluene (1/1, 60 mL) was added piperidine (1.26 g, 150 mmol) and paraformaldehyde (227 mg). The reaction mixture was heated to reflux for 18 h and then cooled to room temperature. The reaction mixture was concentrated *in-vacuo* to approximately 10 mL. The reaction mixture was diluted with water (50 mL) and extracted with diethyl ether (2 × 50 mL), the organic phase was separated and washed with brine (20 mL), dried ($MgSO_4$), filtered and evaporated *in-vacuo*. The crude product was re-crystallized from EtOH to give the title compound **127** (717 mg, 26%) as white crystalline needles. m.p. 195-198 °C, HPLC: t_r 1.12 min (90% Acetonitrile in Water) 95%, ^{1}H NMR (400 MHz, $CDCl_3$): δ 0.90 (3H, s, 18-CH_3), 1.46–1.53 (11H, m), 1.91-2.23 (6H, m), 2.31-2.53 (6H, m), 2.83-2.86 (2H, m, 6-CH_2), 3.56-3.67 (2H, m, 2-CCH_2), 6.56 (1H, s, ArH) and 6.86 (1H, s, ArH), ^{13}C NMR (101 MHz, $CDCl_3$): δ 13.87 (18-CH_3), 21.57, 24.02, 25.86 (2 × CH_2), 26.02, 26.61, 29.25, 31.60, 35.88 (CH_2), 38.42, 43.94 (CH), 48.02 (C), 50.43 (CH), 53.90 (2 × CH_2), 62.21 (2-CCH_2), 115.81 (ArCH), 119.23 (ArC), 125.30 (ArCH), 130.09, 136.72, 155.84 (ArC) and 221.10 (CO), LRMS (ESI) calcd for $C_{24}H_{34}NO_2$ [M+H$^+$]: *m/z* = 368.3, found *m/z* = 368.3, HRMS (ESI) calcd for $C_{24}H_{34}NO_2$ [M+H$^+$]: *m/z* = 368.2511, found *m/z* = 368.2584, Anal. calcd. for $C_{24}H_{33}NO_2$: C 78.43, H 9.05, N 3.81%, found C 78.40 H 9.09, N 3.67%. Data obtained for melting point identical to that in the literature. [125]

(13*S*)-3-Hydroxy-13-methyl-2-(morpholinomethyl)-7,8,9,11,12,13,15,16-octahydro-6*H*-cyclopenta[a]-phenan-thren-17(14*H*)-one (Compound 128), $C_{23}H_{31}NO_3$, MW 369.50,

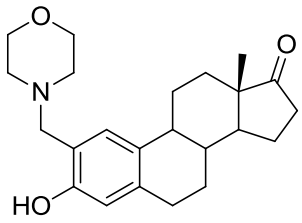

128

To a solution of estrone (1.00 g, 37 mmol) in EtOH/toluene (1/1, 60 mL) was added morpholine (0.65 g, 74 mmol) and paraformaldehyde (227 mg). The mixture was heated to reflux for 18 h and then cooled to room temperature. The reaction mixture was concentrated *in-vacuo* to approximately 10 mL. The reaction mixture was diluted with water (50 mL) and extracted with diethyl ether (2 × 50 mL), the organic phase was separated and acidified with saturated aqueous citric acid (30 mL), the neutralised with 1 M $NaHCO_3$. The crude products were extracted with EtOAc (2 × 50 mL), washed with brine (20 mL), dried ($MgSO_4$), filtered and evaporated *in-vacuo*. The crude product was re-crystallized from EtOH to give the title compound **128** (91 mg, 35%) as white crystalline needles. m.p. 205-209 °C, HPLC: t_r 1.15 min (90% Acetonitrile in water) 93%, ^{1}H NMR ($CDCl_3$, 400 MHz): δ 0.90 (3H, s, 18-CH_3), 1.38-1.65 (7H, m), 1.92-2.20 (5H, m), 2.34-2.38 (1H, m), 2.46-2.56 (4H, m), 2.83-2.86 (2H, m, 6-CH_2), 3.61-3.74 (6H, m), 6.58 (1H, s, ArH) and 6.89 (1H, s, ArH). ^{13}C NMR (101 MHz, $CDCl_3$): δ 13.83 (18-CH_3), 21.55, 25.98, 26.54, 29.22, 31.56, 35.84 (CH_2), 38.35, 43.89 (CH), 47.97 (C), 50.38 (CH), 52.91 (2 × CH_2), 61.90 (2-CCH_2), 66.78 (2 × CH_2), 115.93 (ArCH), 118.19 (ArC), 125.67 (ArCH), 130.59, 137.28, 155.20 (ArC) and 220.96 (CO), LRMS (ESI) calcd for $C_{23}H_{32}NO_3$ $(M+H)^+$: *m/z* = 370.2, found *m/z* = 370.1, HRMS (ESI) calcd for $C_{23}H_{32}NO_3$ $(M+H)^+$: *m/z* = 370.2304, found *m/z* = 370.2372. Anal. calcd. for $C_{23}H_{31}NO_3$: C 74.76, H 8.46, N 3.79%, found C 74.40, H 8.48, N 3.76%. Data obtained for melting point identical to that in the literature. [125]

(13*S*)-3-Hydroxy-13-methyl-2-(pyrrolidin-1-ylmethyl)-7,8,9,11,12,13,15,16-octahydro-6*H*-cyclopenta[a]-phenan-thren-17(14*H*)-one (Compound 129), $C_{23}H_{31}NO_2$, MW 353.50,

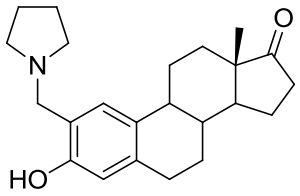

129

To a solution of estrone (2.00 g, 74 mmol) in EtOH/toluene (1/1, 60 mL) was added pyrrolidine (1.07 g, 150 mmol) and paraformaldehyde (227 mg). The mixture was heated to reflux for 18 h and then cooled to room temperature. The reaction mixture was concentrated *in-vacuo* to approximately 10 mL. The reaction mixture was diluted with water (50 mL) and extracted with diethyl ether (2 × 50 mL), the organic phase was separated and washed with brine (20 mL), dried ($MgSO_4$), filtered and evaporated *in-vacuo*. The crude product was re-crystallized from EtOH to give the title compound **129** (204 mg, 8%) as white crystalline needles. m.p. 160-163 °C, HPLC: t_r 1.12 min (90% Acetonitrile in water) 99%, ^{1}H NMR (400 MHz, $CDCl_3$): δ 0.91 (3H, s, 18-CH_3), 1.38-1.67 (4H, m), 1.82 (4H, quin, *J* = 3 Hz) 1.92-2.21 (7H, m), 2.35-2.39 (1H, m), 2.46-2.53 (1H, m), 2.62 (4H, br. s), 2.83-2.86 (2H, m, 6-CH_2), 3.69-3.84 (2H, m, 2-CCH_2), 6.56 (1H, s, ArH), 6.88(1H, s, ArH). ^{13}C NMR (101 MHz, $CDCl_3$): δ 13.85 (18-CH_3), 21.54, 23.62 (2 × CH_2), 25.97, 26.59, 29.22, 31.58, 35.85 (CH_2), 38.38, 43.92 (CH), 47.99 (C), 50.40 (CH), 53.50 (2 × CH_2), 58.87 (2-CCH_2), 115.72 (ArH), 120.01 (ArC), 124.63 (ArCH), 129.96, 136.66, 155.75 (ArC) and 221.08 (CO), LRMS (ESI) calcd for $C_{23}H_{32}NO_2$ $(M+H)^+$: *m/z* = 354.2, found *m/z* = 354.2. HRMS (ESI) calcd for $C_{23}H_{32}NO_2$ $(M+H)^+$: *m/z* = 354.2355, found *m/z* = 354.2419. Anal. calcd. for $C_{23}H_{31}NO_2$: C 78.15, H 8.84, N 3.96%, found C 77.90, H 8.92, N 3.78%. Data obtained for melting point identical to that in the literature. [125]

(13*S*,17*S*)-13-Methyl-2-(piperidin-1-ylmethyl)-7,8,9,11,12,13,14,15,16,17-decahydro-6*H*-cyclopenta[a]-phenan-threne-3,17-diol (Compound 130),
$C_{24}H_{35}NO_2$, MW 369.54,

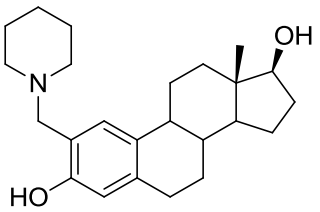

130

Prepared by modification to the literature procedure. [142]

Sodium borohydride (40 mg, 1.06 mmol) was added portion-wise to a solution of (13*S*)-3-hydroxy-13-methyl-2-(piperidin-1-ylmethyl)-7,8,9,11,12,13,15,16-octahydro-6*H*-cyclopenta[a]-phenan-thren-17(14*H*)-one (300.0 mg, 0.82 mmol) **127** dissolved in MeOH/THF (1/1, 6 mL) at 0 °C. The resulting solution was stirred for 2 h and then treated with water (5 mL). The crude products were extracted with ethyl acetate (2 × 5 mL), washed with brine (5 mL), dried ($MgSO_4$), filtered and evaporated *in-vacuo* to give the title compound **130** (244 mg, 81%) as a white foam. m.p. 98-101 ºC, HPLC: t_r 1.29 min (90% Acetonitrile in water) 93%, ^{1}H NMR ($CDCl_3$, 400 MHz): δ 0.77 (3H, s, 18-CH_3), 1.14-1.52 (6H, m), 1.61-1.73 (6H, m), 1.82-1.88 (3H, m), 2.07-2.17 (3H, m), 2.21-2.32 (1H, m), 2.47-2.78 (4H, br. s), 2.79-2.83 (2H, m, 6-CH_2), 3.56-3.66 (2H, quin, *J* = 14 Hz, 2-CCH_2), 3.70-3.74 (1H, t, *J* = 9 Hz, 17-CH), 6.54 (1H, s, ArH) and 6.86 (1H, s, ArH). ^{13}C NMR ($CDCl_3$, 101 MHz): δ 11.06 (18-CH_3), 23.12, 24.04, 25.86 (2 × CH_2), 26.40, 27.31, 29.38, 30.63, 36.73 (CH_2), 38.89, 43.24 (CH), 43.90 (C), 50.04 (CH), 53.91 (2 × CH_2), 62.24 (2-CCH_2), 81.95 (17-CH), 115.77 (ArCH), 119.05 (ArC), 125.31 (ArCH), 130.70, 136.97 (ArC) and 155.63 (ArC). LRMS (ES) calcd for $C_{24}H_{36}NO_2$ $(M+H)^+$: *m/z* = 370.3, found *m/z* = 370.2. Anal. calcd. for $C_{24}H_{35}NO_2$: C 74.76, H 8.46, N 3.79%, found C 74.40, H 8.48, N 3.76%. Data obtained for melting point is identical to that in the literature.[125]

(13*S*,17*S*)-13-Methyl-2-(morpholinomethyl)-7,8,9,11,12,13,14,15,16,17-decahydro-6*H*-cyclopenta[a]-phenan-threne-3,17-diol (Compound 131), $C_{23}H_{33}NO_3$, MW 371.51,

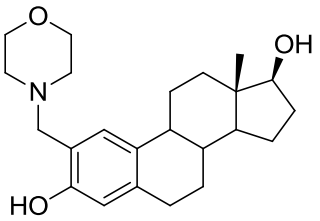

131

Prepared by modification to the literature procedure.[142]

Sodium borohydride (40.0 mg, 1.06 mmol) was added portion-wise to a solution of (13*S*)-3-hydroxy-13-methyl-2-(morpholinomethyl)-7,8,9,11,12,13,15,16-octahydro-6*H*-cyclopenta[a]-phenan-thren-17(14*H*)-one (300.0 mg, 0.81 mmol) **128** dissolved in MeOH/THF (1/1, 6 mL) at 0 °C. The resulting solution was stirred for 2 h and then treated with water (5 mL). The crude products were extracted with ethyl acetate (2 × 5 mL), washed with brine (5 mL), dried ($MgSO_4$), filtered and evaporated under reduced pressure to give the title compound **131** (247 mg, 82%) as a white foam. m.p. 164-168 °C, HPLC: t_r 1.01 min (90% Acetonitrile in water) 99%, ^{1}H NMR ($CDCl_3$, 400MHz): δ 0.77 (3H, s, 18-CH_3), 1.12-1.73 (8H, m), 1.83-1.96 (2H, m), 2.04-2.18 (2H, m), 2.22-2.31 (1H, m), 2.43-2.64 (4H, br. s), 2.76-2.82 (2H, m, 6-CH_2), 3.58-3.76 (7H, m), 6.56 (1H, s, ArH) and 6.91 (1H, s, ArH). ^{13}C NMR ($CDCl_3$, 100MHz): δ 11.06 (18-CH_3), 23.11, 26.39, 27.26, 29.38, 30.62, 36.70 (CH_2), 38.85, 43.23 (CH), 43.87 (C), 50.03 (CH), 52.94 (2 × CH_2), 61.96 (2-C*C*H_2), 66.83 (2 × CH_2), 81.91 (17-CH), 115.90 (ArCH), 118.03 (ArC), 125.69 (ArCH), 131.22, 137.55 (ArC), 155.04 (ArC), LRMS (ESI) calcd for $C_{23}H_{34}NO_3$ $(M+H)^+$: *m/z* = 372.3, found *m/z* = 372.1. HRMS (ESI) calcd for $(M+H)^+$: *m/z* = 372.2460, found *m/z* = 372.2528.

(13*S*,17*S*)-13-Methyl-2-(pyrrolidin-1-ylmethyl)-7,8,9,11,12,13,14,15,16,17-decahydro-6*H*-cyclopenta[a]-phenan-threne-3,17-diol (Compound 132), $C_{23}H_{33}NO_2$, MW 355.51,

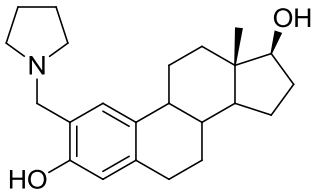

132

Prepared by modification to the literature procedure.[142]

Sodium borohydride (28.0 mg, 0.74 mmol) was added portion-wise to a solution of (13*S*)-3-hydroxy-13-methyl-2-(pyrrolidin-1-ylmethyl)-7,8,9,11,12,13,15,16-octahydro-6*H*-cyclopenta[a]-phenan-thren-17(14*H*)-one (200.0 mg, 0.57 mmol) **129** dissolved in MeOH/THF (1/1, 6 mL) at 0 °C. The resulting solution was stirred for 2 h and then treated with water (5 mL). The crude products were extracted with ethyl acetate (2 × 5 mL), washed with brine (5 mL), dried ($MgSO_4$), filtered and evaporated under reduced pressure to give the title compound **132** (153 mg, 76%) as a white foam. m.p. 77-80 ºC, HPLC: t_r 0.97 min (90% Acetonitrile in water) 99%, ^{1}H NMR ($CDCl_3$, 400 MHz): δ 0.78 (3H, s, 18-CH_3), 1.14-1.52 (6H, m), 1.65-1.73 (2H, m), 1.82-1.87 (6H, m), 2.08-2.17 (2H, m), 2.25-2.30 (1H, m), 2.63-2.79 (4H, br. s, 2 × CH_2), 2.81-2.83 (2H, m, 6-CH_2), 3.70-3.74 (2H, m, 2-CCH_2), 3.81-3.84 (1H, d, *J* = 13.7 Hz, 17-CH), 6.55 (1H, s, ArH) and 6.88 (1H, s, ArH). ^{13}C NMR ($CDCl_3$, 101 MHz): δ 11.06 (18-CH_3), 23.11, 26.39, 27.26, 29.38, 30.62, 36.70 (CH_2), 38.85, 43.23 (CH), 43.87 (C), 50.03 (CH), 52.94 (2 × CH_2), 61.96 (2-C*C*H_2), 66.83 (2 × CH_2), 81.91 (17-CH), 115.90 (ArCH), 118.03 (ArC), 125.69 (ArCH), 131.22 , 137.55 (ArC) and 155.04 (ArC). LRMS (ESI) calcd for $C_{23}H_{34}NO_2$ $(M+H)^+$: *m/z* = 356.3, found *m/z* = 356.2. HRMS (ESI) calcd for $C_{23}H_{34}NO_2$ $(M+H)^+$: *m/z* = 356.2511, found *m/z* = 356.2578.

(8*R*,9*S*,13*S*,14*S*)-3-Methoxy-13-methyl-7,8,9,11,12,13,15,16-octahydro-6*H*-cyclopenta[a]-phenan-thren-17(14*H*)-one (Compound 133), $C_{19}H_{24}O_2$, MW 284.18,

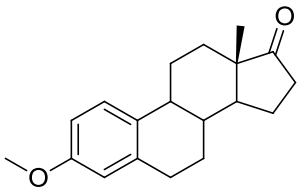

133

Potassium carbonate (41.46 g, 300 mmol) was added portion-wise to a magnetically stirred solution of estrone (20.00 g, 74 mmol) in anhydrous DMF (200 mL), the resulting mixture was stirred for 10 mins under an atmosphere of nitrogen. To the reaction mixture was added methyl iodide (9.96 mL, 160 mmol) drop-wise and the reaction mixture was stirred at room temperature for 2 d. Water was slowly added to the stirred solution and the product precipitated. The product was filtered from the solution and dried in an oven at 105 °C for 2 h to give the title compound **133** (21.03 g, 100%) as a white solid. m.p. 171-173 °C, ^{1}H NMR (400 MHz, $CDCl_3$): δ 0.91 (3H, s, 18-CH_3), 1.38-1.68 (6H, m), 1.92-2.20 (4H, m), 2.22-2.30 (1H, m), 2.36-2.44 (1H, m), 2.46-2.56 (1H, m), 2.86-2.94 (2H, m 6-CH_2), 3.78 (3H, s, 3-OCH_3), 6.65 (1H, d, *J* = 3 Hz, ArH), 6.72 (1H, dd, *J* = 9 and 3 Hz, ArH) and 7.20 (1H, d, *J* = 9 Hz, ArH). ^{13}C NMR (101 MHz, $CDCl_3$): δ 13.84 (18-CH_3), 21.57, 25.92, 26.54, 29.65, 31.57, 35.86 (CH_2), 38.37, 43.97 (CH), 48.00 (C), 50.40 (CH), 55.20 (3-OCH_3), 111.55 (ArCH), 113.87 (ArC), 126.33 (ArCH), 132.01, 137.74, 157.58 (ArC) and 220.97 (CO), LRMS (ESI) calcd for $C_{19}H_{25}O_2$ $(M+H)^+$: *m/z* = 285.2, found *m/z* = 285.2. Anal. Calcd. for $C_{19}H_{24}O_2$: C 80.24, H 8.51, N 0.00%, found C 80.50, H 8.33, N 0.10%. Data obtained for melting point identical to that in the literature. [143]

(13*S*)-2-Benzoyl-3-methoxy-13-methyl-7,8,9,11,12,13,15,16-octahydro-6*H*-cyclopenta[a]-phenan-thren-17(14*H*)-one (Compound 134), $C_{26}H_{28}O_3$, MW 388.50,

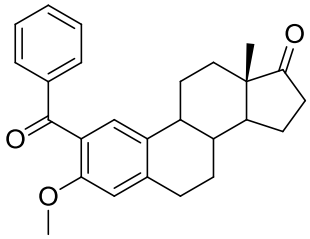

134

Benzoyl chloride (2.04 mL, 17.6 mmol) was added drop-wise to a cooled, 0 °C (ice bath), suspension of aluminium chloride (2.47 g, 18.5 mmol) in DCM (30 mL). A solution of (8*R*,9*S*,13*S*,14*S*)-3-methoxy-13-methyl-7,8,9,11,12,13,15,16-octahydro-6*H*-cyclopenta[a]-phenan-thren-17(14*H*)-one (2.5 g, 87.9 mmol) in DCM (10 mL) was added slowly and stirring continued for 15 min at this temperature. The reaction was quenched by pouring onto crushed ice. DCM (30 mL) and water (30 mL) were added and the resulting mixture was stirred vigorously for 10 min. The organic layer was separated and the organics extracted with DCM (2 × 10 mL), dried ($MgSO_4$), filtered and evaporated *in-vacuo* to give the title compound **134** (2.90 g, 82%) as a white amorphous solid. m.p. 221-226 ºC, HPLC: t_r 2.65 min (90% Acetonitrile in water) 98%, ^{1}H NMR (400 MHz, $CDCl_3$): δ 0.91 (3H, s, 18-CH_3), 1.43-1.69 (4H, m), 2.03-2.19 (5H, m), 2.24-2.37 (3H, m), 2.47-2.54 (1H, m), 2.96-2.99 (2H, m, 6-CH_2), 3.68 (3H, s, 3-OCH_3), 6.70 (1H, s, ArH), 7.30 (1H, s, ArH), 7.43 (2H, t, *J* = 8 Hz, ArH), 7.53 (1H, t, *J* = 8 Hz, ArH) and 7.80 (2H, d, *J* = 8 Hz, ArH). ^{13}C NMR ($CDCl_3$, 101 MHz): δ 13.81 (18-CH_3), 21.54, 25.75, 26.37, 29.92, 31.42, 35.81 (CH_2), 38.22, 43.77 (CH), 47.93 (CH_2), 50.60 (CH), 55.60 (3-OCH_3), 111.74, 127.06 (ArCH), 128.07 (2 × ArCH), 129.76 (2 × ArCH), 131.94 (ArC), 132.65 (ArCH), 138.16 , 140.98, 155.50 (ArC), 196.49 and 220.68 (CO), LRMS (ESI) calcd for $C_{26}H_{29}O_3$ $(M+H)^+$: *m/z* = 389.2, found *m/z* = 389.4. HRMS (ESI) calcd for $C_{26}H_{29}O_3$ $(M+H)^+$: *m/z* = 389.2038, found *m/z* = 389.2105.

(13*S*)-2-(Cyclohexanecarbonyl)-3-methoxy-13-methyl-7,8,9,11,12,13,15,16-octahydro-6*H*-cyclopenta[a]-phenan-thren-17(14*H*)-one (Compound 135), $C_{26}H_{34}O_3$, MW 394.55,

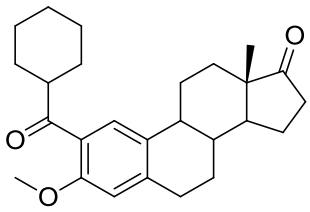

135

Cyclohexanecarbonyl chloride (4.17 mL, 35.2 mmol) was added drop-wise to a cooled, 0 °C (ice bath), suspension of aluminium chloride (4.93 g, 36.9 mmol) in DCM (60 mL). A solution of (8*R*,9*S*,13*S*,14*S*)-3-methoxy-13-methyl-7,8,9,11,12,13,15,16-octahydro-6*H*-cyclopenta[a]-phenan-thren-17(14*H*)-one (5.00 g, 17.6 mmol) in DCM (20 mL) was added slowly and stirring continued for 15 min at this temperature. The reaction mixture was quenched by pouring onto crushed ice. DCM (30 mL) and water (30 mL) were added and the resulting mixture was stirred vigorously for 10 min. The organic layer was separated and the organics extracted with DCM (2 × 10 mL), dried ($MgSO_4$), filtered and evaporated *in-vacuo* to give the title compound **135** (5.90 g, 85%) as a white amorphous solid. m.p. 158-160 ºC, HPLC: t_r 4.69 min (90% Acetonitrile in water) 97%, ^{1}H NMR (400 MHz, $CDCl_3$): δ 0.90 (3H, s, 18-CH_3), 1.24-1.67 (9H, m), 1.76-1.79 (4H, m), 1.87-1.97 (4H, m), 2.00-2.25 (4H, m), 2.43-2.53 (2H, m), 2.91-2.94 (2H, m, 6-CH_2), 3.17-3.22 (1H, m, 2-CCOCH), 3.84 (3H, s, 3-OCH_3), 6.65 (1H, s, ArH) and 7.47 (1H, s, ArH). ^{13}C NMR (101 MHz, $CDCl_3$): δ 13.78 (18-CH_3), 21.52, 25.75 (2 × CH_2), 25.93, 26.41, 30.02 (2 × CH_2), 31.52, 35.93 (CH_2), 37.97, 42.89 (CH), 47.98 (CH_2), 51.12 (CH), 55.48 (3-OCH_3), 111.65, 127.54 (ArCH), 131.87, 138.16, 156.31 (ArC), 196.75 and 221.24 (CO), LRMS (ESI) calcd for $C_{26}H_{35}O_3$ $(M+H)^+$: *m/z* = 395.3, found *m/z* = 395.5. HRMS (ESI) calcd for $C_{26}H_{35}O_3$ $(M+H)^+$: *m/z* = 395.2508, found *m/z* = 395.2587.

(13*S*)-2-(4-Chlorobenzoyl)-3-methoxy-13-methyl-7,8,9,11,12,13,15,16-octahydro-6*H*-cyclopenta[a]-phenan-thren-17(14*H*)-one (Compound 136), $C_{26}H_{27}ClO_3$, MW 422.94,

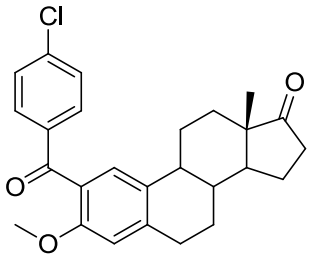

136

4-Chlorophenyl acid chloride (0.89 mL, 7.03 mmol) was added drop-wise to a cooled, 0 °C (ice bath), suspension of aluminium chloride (984 mg, 7.38 mmol) in DCM (60 mL). A solution of (8*R*,9*S*,13*S*,14*S*)-3-methoxy-13-methyl-7,8,9,11,12,13,15,16-octahydro-6*H*-cyclopenta[a]-phenan-thren-17(14*H*)-one (1.00 g, 3.52 mmol) in DCM (20 mL) was added slowly and stirring continued for 15 min at this temperature. The reaction mixture was quenched by pouring onto crushed ice. DCM (30 mL) and water (30 mL) were added and the resulting mixture was stirred vigorously for 10 min. The organic layer was separated and the crude products extracted with DCM (2 × 10 mL), dried ($MgSO_4$), filtered and evaporated *in-vacuo* to give the title compound **136** (1.27 g, 85%) as a white amorphous solid. m.p. 191-193 ºC, ^{1}H NMR (400 MHz, $CDCl_3$): δ 0.81 (3H, s, 18-CH_3), 1.32-1.57 (6H, m), 1.79-1.85 (1H, m), 1.93-2.06 (3H, m), 2.12-2.17 (1H, m), 2.22-2.27 (1H, m), 2.37-2.43 (1H, m), 2.88 (2H, m, 6-CH_2), 3.57 (3H, s, 3-OCH_3), 6.60 (1H, s, ArH), 7.20 (1H, s, ArH), 7.28 (2H, d, *J* = 9 Hz, 2 × ArH) and 7.62 (2H, d, *J* = 9 Hz, 2 × ArH). ^{13}C NMR (101 MHz, $CDCl_3$): δ 13.78 (18-CH_3), 21.50, 25.74, 26.31, 29.89, 31.42, 35.74 (CH_2), 38.19, 43.73 (CH), 47.85 (C), 50.32 (CH), 55.53 (3-OCH_3), 111.77 (ArCH), 125.91 (ArC), 127.06 (ArCH), 128.32 (2 × ArCH), 131.02 (2 × ArCH), 132.19, 136.69, 138.84, 141.44, 155.45, 195.12 (ArC) and 220.21 (CO). HRMS (ESI) calcd for $C_{26}H_{27}Cl^{35}O_3Na$ $(M+Na)^+$: *m/z* = 445.1541, found *m/z* = 445.1534, calcd for $C_{26}H_{27}Cl^{37}O_3Na$ $(M+Na)^+$: *m/z* = 447.1511, found *m/z* = 445.1534, Anal. Calcd. for $C_{26}H_{27}ClO_3$: C 73.83, H 6.43, N 0.00%, found C 73.40, H 6.42, N 0.00%.

(13*S*)-2-(2,4-Dichlorobenzoyl)-3-methoxy-13-methyl-7,8,9,11,12,13,15,16-octahydro-6*H*-cyclopenta[a]-phenan-thren-17(14*H*)-one (Compound 137), $C_{26}H_{26}Cl_2O_3$, MW 457.39,

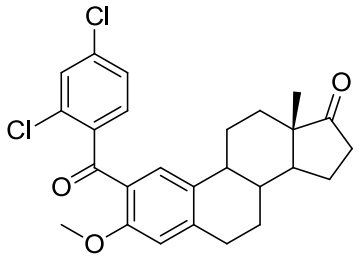

137

2,4-Dichlorobenzoyl chloride (0.98 mL, 7.03 mmol) was added drop-wise to a cooled, 0 °C (ice bath), suspension of aluminium chloride (984 mg, 7.38 mmol) in DCM (60 mL). A solution of (8*R*,9*S*,13*S*,14*S*)-3-methoxy-13-methyl-7,8,9,11,12,13,15,16-octahydro-6*H*-cyclopenta[a]-phenan-thren-17(14*H*)-one (1.00 g, 3.52 mmol) in DCM (20 mL) was added slowly and stirring continued for 15 min at this temperature. The reaction mixture was quenched by pouring onto crushed ice. DCM (30 mL) and water (30 mL) were added and the resulting mixture was stirred vigorously for 10 min. The organic layer was separated and the crude products extracted with DCM (2 × 10 mL), dried ($MgSO_4$), filtered and evaporated *in-vacuo* to give the title compound **137** (1.05 g, 65%) as a white amorphous solid. m.p. 217-220 ºC, ^{1}H NMR (400 MHz, $CDCl_3$): δ 0.92 (3H, s, 18-CH_3), 1.44-1.65 (7H, m), 1.95-2.10 (4H, m), 2.19-2.23 (1H, m), 2.40-2.54 (2H, m), 2.94 (2H, m, 6-CH_2), 3.59 (3H, s, 3-OCH_3), 7.25 (1H, s, ArH), 7.28 (1H, d, *J* = 2Hz, ArH), 7.31 (1H, s, ArH), 7.39 (1H, d, *J* = 2 Hz, ArH) and 7.64 (1H, s, ArH). ^{13}C NMR (101 MHz, $CDCl_3$): δ 13.78 (18-CH_3), 21.50, 25.72, 26.20, 30.00, 31.40, 35.74 (CH_2), 38.14, 43.70 (CH), 47.87 (C), 50.36 (CH), 55.67 (3-OCH_3), 112.04 (ArCH), 124.87 (ArC), 126.77, 128.43, 129.40, 129.99, 132.04 (ArCH), 132.53, 135.83, 139.76, 144.34, 157.32 (ArC), 193.05 (*C*O) and 220.31 (CO), HRMS (ESI) calcd for $C_{26}H_{27}Cl_2O_3$ $(M+H)^+$: *m/z* = 459.1302, found *m/z* = 459.1313, Anal. Calcd. for $C_{26}H_{27}Cl_2O_3$: C 68.27, H 5.73, N 0.00%, found C 67.70, H 5.71, N 0.00%.

(13*S*)-2-(2-(4-Chlorophenyl)acetyl)-3-methoxy-13-methyl-7,8,9,11,12,13,15,16-octahydro-6*H*-cyclopenta[a]-phenan-thren-17(14*H*)-one (Compound 138), $C_{27}H_{29}ClO_3$, MW 436.97,

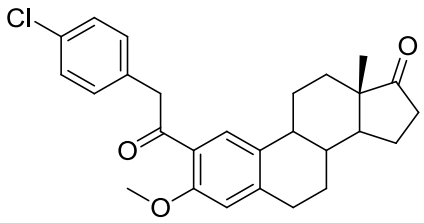

138

4-Chlorophenylacetyl chloride (1.03 mL, 7.03 mmol) was added drop-wise to a cooled, 0 °C (ice bath) suspension of aluminium chloride (984 mg, 7.38 mmol) in DCM (60 mL). A solution of (8*R*,9*S*,13*S*,14*S*)-3-methoxy-13-methyl-7,8,9,11,12,13,15,16-octahydro-6*H*-cyclopenta[a]-phenan-thren-17(14*H*)-one (1.00 g, 3.52 mmol) in DCM (20 mL) was added slowly and stirring continued for 15 min at this temperature. The reaction mixture was quenched by pouring onto crushed ice. DCM (30 mL) and water (30 mL) were added and the resulting mixture was stirred vigorously for 10 min. The organic layer was separated and the crude products extracted with DCM (2 × 10 mL), dried ($MgSO_4$), filtered and evaporated under reduced pressure to give the title compound **138** (1.11 g, 73%) as a white amorphous solid. m.p. 177-180 ºC, ^{1}H NMR (400 MHz, $CDCl_3$): δ 0.89 (3H, s, 18-CH_3), 1.41-1.66 (8H, m), 1.93-2.24 (5 H, m), 2.40-2.53 (2H, m), 2.93 (2H, m, 6-CH_2), 3.87 (3H, s, 3-OCH_3), 4.23 (2H, d, *J* = 4 Hz, 2-$CCOCH_2$), 6.66 (1H, s, ArH), 7.13 (2H, d, *J* = 8 Hz, 2 × ArH), 7.24 (2H, d, *J* = 8 Hz, 2 × ArH) and 7.64 (1H, s, ArH). ^{13}C NMR (101 MHz, $CDCl_3$): δ 13.75 (18-CH_3), 21.49, 25.69, 26.23, 29.84, 31.40, 35.73 (CH_2), 38.17, 43.69 (CH), 47.85 (2-CCO*C*H_2), 49.29 (C), 50.33 (CH), 55.39 (3-OCH_3), 111.73 (ArCH), 125.28 (ArC), 128.01 (ArCH), 128.33 (2 × ArCH), 130.92 (2 × ArCH), 132.31, 132.38, 133.95, 143.30, 156.62 (ArC), 198.76 (CO) and 220.24 (CO), HRMS (ESI) calcd for $C_{27}H_{30}ClO_3$ $(M+H)^+$: *m/z* = 437.1818, found *m/z* = 437.1866, Anal. Calcd. for $C_{27}H_{29}ClO_3$: C 74.21, H 6.69, N 0.00%, found C 73.40, H 6.67, N 0.00%

(13*S*)-2-Benzoyl-3-hydroxy-13-methyl-7,8,9,11,12,13,15,16-octahydro-6*H*-cyclopenta[a]-phenan-thren-17(14*H*)-one (Compound 139), $C_{25}H_{26}O_3$, MW 374.47,

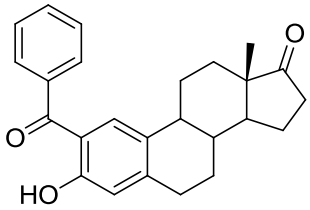

139

Trimethylamine hydrochloride (3.44 g, 36 mmol) was added to a suspension of aluminium chloride (13.51 g, 72 mmol) in DCM (20 mL) at 0 °C (ice bath). The resulting mixture was stirred for 30 min at room temperature before a solution of (13*S*)-2-benzoyl-3-methoxy-13-methyl-7,8,9,11,12,13,15,16-octahydro-6*H*-cyclopenta[a]-phenan-thren-17(14*H*)-one **134** (2.80 g, 7.2 mmol) in DCM (20 mL) was added drop-wise before the reaction mixture was brought to reflux for 2 h. After cooling to room temperature the reaction mixture was poured onto crushed ice and vigorously stirred for 10 min. The organics were extracted with DCM (2 × 20 mL), dried ($MgSO_4$), filtered and evaporated *in-vacuo* to give the title compound **139** (1.94 g, 74%) as a pale yellow solid. m.p. 199-203 ºC, HPLC: t_r 3.62 (90% Acetonitrile in water) 99%, ^{1}H NMR (400 MHz, $CDCl_3$): δ 0.90 (3H, s, 18-CH_3), 1.37-1.67 (6H, m), 1.87-1.90 (1H, m), 2.00-2.21 (5H, m), 2.46-2.54 (1H, quart, *J* = 9 Hz), 2.92-2.96 (2H, m, 6-CH_2), 6.81 (1H, s, ArH), 7.49 (1H, s, ArH), 7.52 (2H, t, *J* = 7 Hz, ArH), 7.60 (1H, t, *J* = 7 Hz, ArH), 7.66 (2H, d, *J* = 7 Hz, ArH) and 11.87 (1H, broad s, OH). ^{13}C NMR (101 MHz, $CDCl_3$): δ 13.79 (18-CH_3), 21.51, 25.65, 26.10, 29.85, 31.32, 35.79 (CH_2), 38.09, 43.55 (CH), 47.84 (C), 50.32 (CH), 117.20 (ArC), 117.71, 128.35 (2 × ArCH), 129.04 (2 × ArCH), 130.41 (ArCH), 130.64 (ArC), 131.82, 138.13 (ArCH), 146.84, 160.99 (ArC), 201.17 (CO) and 220.56 (CO). LRMS (ESI) calcd for $C_{25}H_{27}O_3$ $(M+H)^+$: *m/z* = 375.2, found *m/z* = 375.2.

(13*S*)-2-(Cyclohexanecarbonyl)-3-hydroxy-13-methyl-7,8,9,11,12,13,15,16-octahydro-6*H*-cyclopenta[a]-phenan-thren-17(14*H*)-one (Compound 140), $C_{25}H_{32}O_3$, MW 380.52,

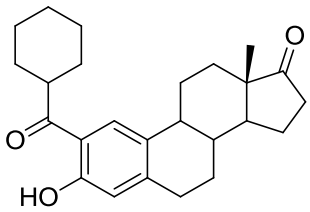

140

Trimethylamine hydrochloride (604 mg, 6.34 mmol) was added to a suspension of aluminium chloride (1.69 g, 12.7 mmol) in DCM (15 mL) at 0 °C (ice bath). The resulting mixture was stirred for 30 min at room temperature before a solution of (13*S*)-2-(cyclohexanecarbonyl)-3-methoxy-13-methyl-7,8,9,11,12,13,15,16-octahydro-6*H*-cyclopenta[a]-phenan-thren-17(14*H*)-one **135** (500 mg, 1.27 mmol) in DCM (10 mL) was added drop-wise before the reaction mixture was brought to reflux for 2 h. After cooling to room temperature the reaction mixture was poured onto crushed ice and vigorously stirred for 10 min. The organics were extracted with DCM (2 × 20 mL), dried ($MgSO_4$), filtered and evaporated *in-vacuo* to give the title compound **139** (1.94 g, 74%) as a pale yellow solid. HPLC: t_r 5.44 (90% Acetonitrile in water) 92%, ^{1}H NMR (400 MHz, $CDCl_3$): δ 0.92 (3H, s, 18-CH_3), 1.25-1.71 (9H, m), 1.76-1.82 (4H, m), 1.85-1.97 (4H, m), 2.00-2.31 (4H, m), 2.41-2.54 (2H, m), 2.90-2.93 (2H, m, 6-CH_2), 3.15-3.20 (1H, m, 2-CCOCH), 6.67 (1H, s, ArH) and 7.43 (1H, s, ArH). ^{13}C NMR (101 MHz, $CDCl_3$): δ 14.01 (18-CH_3), 21.61, 25.78 (2 × CH_2), 25.89, 26.44, 30.11 (2 × CH_2), 31.49, 35.97 (CH_2), 38.01, 42.92 (CH), 48.03 (CH_2), 51.23 (CH), 111.68, 127.57 (ArCH), 131.87, 138.16, 157.43 (ArC), 201.62 and 220.13 (CO) LRMS (ESI) calcd for $C_{25}H_{33}O_3$ $(M+H)^+$: *m/z* = 381.2, found *m/z* = 381.1.

(13*S*)-2-(4-Chlorobenzoyl)-3-hydroxy-13-methyl-7,8,9,11,12,13,15,16-octahydro-6*H*-cyclopenta[a]-phenan-thren-17(14*H*)-one (Compound 141), $C_{25}H_{25}ClO_3$, MW 408.92,

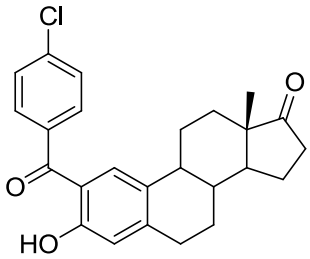

141

Trimethylamine hydrochloride (186 mg, 1.95 mmol) was added to a suspension of aluminium chloride (520 mg, 3.90 mmol) in DCM (10 mL) at 0 °C (ice bath). The resulting mixture was stirred for 30 min at room temperature before a solution of (13*S*)-2-(4-chlorobenzoyl)-3-methoxy-13-methyl-7,8,9,11,12,13,15,16-octahydro-6*H*-cyclopenta[a]-phenan-thren-17(14*H*)-one **136** (165 mg, 0.39 mmol) in DCM (10 mL) was added drop-wise. The reaction mixture was brought to reflux for 2 h. After cooling to room temperature the reaction mixture was quenched by pouring onto crushed ice and vigorously stirred for 10 min. The crude products were then extracted with DCM (2 × 10 mL), dried ($MgSO_4$), filtered and evaporated *in-vacuo* to give the title compound **141** (69 mg, 43%) as a pale yellow solid. HPLC: t_r 1.63 min (90% Acetonitrile in water) 93%, ^{1}H NMR (400 MHz, $CDCl_3$): δ 0.89 (3H, s, 18-CH_3), 1.39-1.66 (6H, m), 1.88-1.91 (1H, m), 1.99-2.17 (5H, m), 2.46-2.53 (1H, m), 2.93 (2H, m, 6-CH_2), 6.79 (1H, s, ArH), 7.42 (1H, s, ArH), 7.47 (2H, d, *J* = 9 Hz, 2 × ArH), 7.60 (2H, d, *J* = 9 Hz, 2 × ArH) and 11.71 (1H, s, OH). ^{13}C NMR (101 MHz, $CDCl_3$): δ 13.76 (18-CH_3), 21.49, 25.64, 26.04, 29.85, 31.25, 35.77 (CH_2), 38.00, 43.48 (CH), 47.81 (C), 50.26 (CH), 116.94 (ArC), 117.82 (ArCH), 128.70 (2 × ArCH), 129.40 (ArCH), 130.50 (2 × ArCH), 130.83, 136.37, 138.20, 147.18, 160.91 (ArC), 199.70 (CO) and 221.12 (C_{17}). LRMS (ESI) calcd for $C_{25}H_{26}ClO_3$ $(M+H)^+$: *m/z* = 409.2, found *m/z* = 409.1.

(13*S*)-2-(2,4-Dichlorobenzoyl)-3-hydroxy-13-methyl-7,8,9,11,12,13,15,16-octahydro-6*H*-cyclopenta[a]-phenan-thren-17(14*H*)-one (Compound 142), $C_{25}H_{24}Cl_2O_3$, MW 443.36,

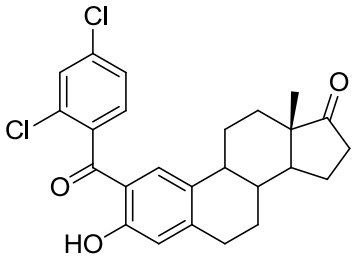

142

Trimethylamine hydrochloride (74 mg, 0.78 mmol) was added to a suspension of aluminium chloride (207 mg, 1.55 mmol) in DCM (10 mL) at 0 °C (ice bath). The resulting mixture was stirred for 30 min at room temperature before a solution of (13*S*)-2-(2,4-dichlorobenzoyl)-3-methoxy-13-methyl-7,8,9,11,12,13,15,16-octahydro-6*H*-cyclopenta[a]-phenan-thren-17(14*H*)-one **137** (71 mg, 0.16 mmol) in DCM (5 mL) was added drop-wise. The reaction mixture was brought to reflux for 2 h. After cooling to room temperature the reaction mixture was quenched by pouring onto crushed ice and vigorously stirred for 10 min. The crude products were then extracted with DCM (2 × 10 mL), dried ($MgSO_4$), filtered and evaporated under reduced pressure to give the title compound **142** (35 mg, 51%) as an amorphous pale yellow solid. HPLC: t_r 1.59 min (90% Acetonitrile in water) 95%, ^{1}H NMR (400 MHz, $CDCl_3$): δ 0.87 (3H, s, 18-CH_3), 1.24-1.63 (7H, m), 1.83-1.88 (1H, m), 1.96-2.14 (5H, m), 2.45-2.52 (1H, m), 2.93 (2H, m, 6-CH_2), 6.79 (1H, s, ArH), 7.09 (1H, s, ArH), 7.27 (1H, d, *J* = 8 Hz, ArH), 7.39 (1H, dd, *J* = 8 and 2 Hz, ArH), 7.52 (1H, d, *J* = 2 Hz, ArH) and 11.67 (1H, s, OH). ^{13}C NMR (101 MHz, $CDCl_3$): δ 13.74 (18-CH_3), 21.47, 25.51, 25.94, 29.98, 31.19, 35.76 (CH_2), 37.91, 43.34 (CH), 47.79 (C), 50.23 (CH), 117.26 (ArC), 117.80, 127.23, 129.55, 129.88, 130.06 (ArCH), 131.36, 131.83, 135.89, 136.63, 148.35, 160.97 (ArC), 198.82 (CO) and 220.84 (CO), LRMS (ESI) calcd for $C_{25}H_{25}Cl_2O_3$ $(M+H)^+$: *m/z* = 443.1, found *m/z* = 443.1.

(13*S*)-2-(2-(4-Chlorophenyl)acetyl)-3-hydroxy-13-methyl-7,8,9,11,12,13,15,16-octahydro-6*H*-cyclopenta[a]-phenan-thren-17(14*H*)-one (Compound 143), $C_{26}H_{27}ClO_3$, MW 422.94,

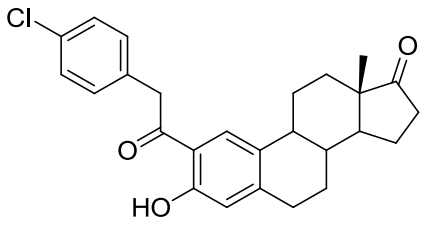

143

Trimethylamine hydrochloride (88 mg, 0.92 mmol) was added to a suspension of aluminium chloride (244 mg, 1.83 mmol) in DCM (10 mL) at 0 °C (ice bath). The resulting mixture was magnetically stirred for 30 min at room temperature before a solution of (13*S*)-2-(2-(4-chlorophenyl)acetyl)-3-methoxy-13-methyl-7,8,9,11,12,13,15,16-octahydro-6*H*-cyclopenta[a]-phenan-thren-17(14*H*)-one **138** (80 mg, 0.18 mmol) in DCM (5 mL) was added slowly. The reaction mixture was brought to reflux for 2 h. After cooling to room temperature the reaction mixture was poured onto crushed ice and vigorously stirred for 10 min. The crude products were then extracted with DCM (2 × 10 mL), dried ($MgSO_4$), filtered and evaporated under reduced pressure to give the title compound **143** (36 mg, 47%) as an amorphous white solid. HPLC: t_r 1.55 min (90% Acetonitrile in water) 95%, ^{1}H NMR (400 MHz, $CDCl_3$): δ 0.91 (3H, s, 18-CH_3), 1.39-1.67 (6H, m), 1.94-2.24 (5H, m), 2.35-2.38 (1H, m), 2.47-2.54 (1H, m), 2.90 (2H, m, 6-CH_2), 4.24 (2H, d, *J* = 3 Hz, 2-CCOCH_2), 6.70 (1H, s, ArH), 7.17 (2H, d, *J* = 9 Hz, 2 × ArH), 7.29 (2H, d, *J* = 9 Hz, 2 × ArH), 7.69 (1H, s, ArH) and 11.91 (1H, s, OH). ^{13}C NMR (101 MHz, $CDCl_3$): δ 13.75 (18-CH_3), 21.51, 25.85, 26.02, 29.72, 31.36, 35.78 (CH_2), 37.95, 43.44 (CH), 44.31 (2-CCO*C*H_2), 47.82 (C), 50.29 (CH), 116.95 (ArC), 117.89, 126.79 (ArCH), 128.84 (2 × ArCH), 130.77 (2 × ArCH), 131.09, 132.59, 133.05, 147.32, 160.57 (ArC), 202.73 (CO) and 220.03 (CO), LRMS (ESI) calcd for $C_{26}H_{28}ClO_3$ $(M+H)^+$: 423.2, found *m/z* = 423.1.

(13*S*)-2-Acetyl-3-methoxy-13-methyl-7,8,9,11,12,13,15,16-octahydro-6*H*-cyclopenta[a]-phenan-thren-17(14*H*)-one (Compound 144), $C_{21}H_{26}O_3$, MW 326.43,

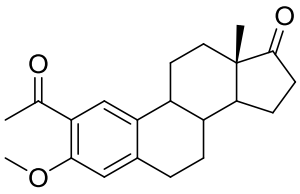

Acetyl chloride (14.5 mL, 204 mmol) was added to a suspension of aluminium trichloride (28.8g, 216 mmol) in DCM (200mL) at 0 ºC (ice bath). A solution of (8*R*,9*S*,13*S*,14*S*)-3-methoxy-13-methyl-7,8,9,11,12,13,15,16-octahydro-6*H*-cyclopenta[a]-phenan-thren-17(14*H*)-one **133** (24.6g, 86.5 mmol) in DCM (150 mL) and was added slowly over a period of 20 min. After addition, the reaction mixture was stirred for another 30 min at 0 ºC (ice bath). The reaction was quenched by pouring over ice and was left standing over-night. The organics were extracted with chloroform (200 mL), dried ($MgSO_4$), filtered and concentrated *in-vacuo* to give the title compound **144** as a white solid. (25.77g, 91%). m.p. 182-184 ºC, ^{1}H NMR (400 MHz, $CDCl_3$) δ: 0.89 (3H, s, 18-CH_3), 1.32-1.76 (6H, m), 1.88-2.27 (5H, m), 2.42-2.51 (2H, m), 2.55 (3H, s, 2-CCOCH_3), 2.87-2.92 (2H, m, 6-CH_2), 3.86 (3H, s, 3-OCH_3), 6.67 (1H, s, ArH) and 7.66 (1H, s, ArH). ^{13}C NMR (101 MHz, $CDCl_3$): δ 13.79 (18-CH_3), 21.54, 25.79, 26.28, 29.88, 31.42 (CH_2), 31.87 (2-CCO*C*H_3), 35.81, 35.81 (CH_2), 38.22, 43.74 (CH), 47.93 (C), 50.32 (CH), 55.47 (3-O*C*H_3), 111.79 (ArCH), 125.71 (ArC), 127.62 (ArCH), 132.07, 143.14, 157.11 (ArC), 199.36 (CO) and 220.60 (CO). Data obtained for melting point is identical to that in the literature.[144]

(13*S*)-2-Acetyl-3-hydroxy-13-methyl-7,8,9,11,12,13,15,16-octahydro-6*H*-cyclopenta[a]-phenan-thren-17(14*H*)-one (Compound 145), $C_{20}H_{24}O_3$, MW 312.40,

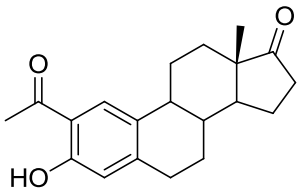

145

Trimethylamine HCl (41.5 g, 433 mmol) was added portion-wise over 30 min to a suspension of $AlCl_3$ (115.6 g, 867 mmol) in DCM (200 mL) at 0 °C (ice bath). The reaction is quite exothermic. After 10 min a solution of (13*S*)-2-acetyl-3-methoxy-13-methyl-7,8,9,11,12,13,15,16-octahydro-6*H*-cyclopenta[a]-phenan-thren-17(14*H*)-one **144** (25.74 g, 78.85 mmol) in DCM (70 mL) was added over 30 min. The reaction mixture was refluxed for 3 h until no more gas was evolved. The reaction mixture was cooled to room temperature and was quenched by slowly pouring onto crushed ice. After melting the phases were separated and the organics extracted with DCM (2 × 75 mL). The combined organics were washed with 2 M HCl (2 × 75 mL), water (2 × 75 mL) and brine (150 mL), dried ($MgSO_4$) and concentrated *in-vacuo* to ~ 100 mL and the product precipitated by the addition of hexane, collected by filtration and dried under high vacuum to give the title compound **145** as a beige solid (23.89 g, 97%). m.p. 136-138 ºC, ^{1}H NMR (400 MHz, $CDCl_3$): δ 0.89 (3H, s, 18-CH_3), 1.38-1.67 (6H, m), 1.92-2.08 (3H, m), 2.13-2.27 (2H, m), 2.33-2.51 (2H, m), 2.57 (3H, s, 2-CCOCH_3), 2.83-2.94 (2H, m, 6-CH_2), 6.63 (1H, s, ArH), 7.57 (1H, s, ArH) and 12.01 (1H, br. s, OH). ^{13}C NMR (101 MHz, $CDCl_3$): δ 13.74 (18-CH_3), 21.48, 25.83, 26.04 (CH_2), 26.42 (2-CCO*C*H_3), 29.69, 31.34, 35.75 (CH_2), 38.01, 43.46 (CH), 47.81 (C), 50.32 (CH), 117.56 (ArCH), 117.84 (ArC), 127.22 (ArCH), 130.85, 146.82, 160.05 (ArC), 203.96 (CO) and 220.47 (CO). LRMS (ESI) calcd for $C_{20}H_{25}O_3$ $(M+H)^+$: *m/z* = 313.2, found *m/z* = 312.9.

(13*S*)-2-Ethyl-3-hydroxy-13-methyl-7,8,9,11,12,13,15,16-octahydro-6*H*-cyclopenta[a]-phenan-thren-17(14*H*)-one (Compund 146), $C_{20}H_{26}O_2$, MW 298.42,

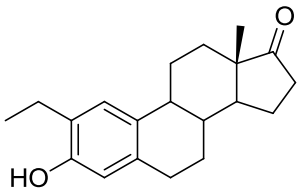

146

A solution of (13*S*)-2-acetyl-3-hydroxy-13-methyl-7,8,9,11,12,13,15,16-octahydro-6*H*-cyclopenta[a]-phenan-thren-17(14*H*)-one **145** (39.812 g, 0.128 mol) in MeOH / THF (3/2, 450 mL) was stirred with 10% palladium on charcoal (5 g, 0.037 eq. in Pd) under an atmosphere of hydrogen for 5 d. The reaction mixture was filtered through a pad of celite to remove the catalyst and the resulting yellow solution was evaporated *in-vacuo*. The resulting yellow solid was recrystallised from EtOAc / hexane (1/1) to give the title compound **146** (35.234 g, 93%) as colourless crystals. m.p. 201-205 ºC, ^{1}H NMR (400 MHz, $CDCl_3$): δ 0.91 (3H, s, 18-CH_3), 1.23 (3H, t, *J* = 8 Hz, 2-CCH_2CH_3), 1.32- 2.53 (13H, m), 2.62 (2H, quart, *J* = 8 Hz, 2-CCH_2), 2.82 (2H, m, 6-CH_2), 6.53 (ArH), 7.04 (ArH), LRMS (ESI) calcd for $C_{20}H_{27}O_2$ $(M+H)^+$: *m/z* = 298.2, found *m/z* = 298.2. Data obtained for melting point is identical to that in the literature.[107]

(13*S*)-4-((Dimethylamino)methyl)-2-ethyl-3-hydroxy-13-methyl-7,8,9,11,12,13,15,16-octahydro-6*H*-cyclopenta[a]-phenan-thren-17(14*H*)-one (Compound 147), $C_{23}H_{33}NO_2$, MW 355.51,

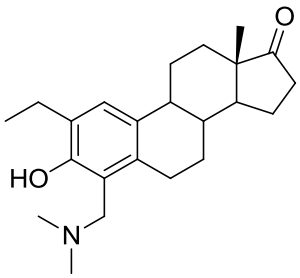

147

To a solution of (13*S*)-2-ethyl-3-hydroxy-13-methyl-7,8,9,11,12,13,15,16-octahydro-6*H*-cyclopenta[a]-phenan-thren-17(14*H*)-one **146** (2.98 g, 10.0 mmol) in EtOH /

toluene (1/1, 40 mL) was added *N*,*N*,*N'*,*N'*-tetramethyldiaminomethane (2.0 g, 20 mmol) and paraformaldehyde (300 mg). The mixture was heated to reflux for 5 h, cooled to room temperature and concentrated *in-vacuo*. Water (50 mL) was added to the residue and the organics were extracted with Et_2O (3 x 50 mL). The combined organic extracts were washed with brine (30 mL), dried ($MgSO_4$) and concentrated *in-vacuo* to give the title compound **147** (3.39 g, 95%) as a white foam. HPLC: t_r 1.12 min (90% Acetonitrile in water) 97%, ^{1}H NMR (400 MHz, $CDCl_3$) δ: 0.89 (3H, s, 18-CH_3), 1.20 (3H, t, *J* = 8 Hz, 2-CCH_2CH_3), 1.30-1.64 (6H, m), 1.90-1.96 (1H, m), 1.99-2.18 (3H, m), 2.20-2.28 (1H, m), 2.32 (6H, s, $N(CH_3)_2$), 2.39-2.68 (5H, m), 2.76-2.84 (1H, m), 3.60 (1H, d, *J* = 14 Hz, 4-CCH_{2A}), 3.68 (1H, d, *J* = 14 Hz, 4-CCH_{2B}), 7.00 (1H, s, ArH); ^{13}C NMR (101 MHz, $CDCl_3$) δ: 13.81 (18-CH_3), 14.43 (2-CCH_2CH_3), 21.33, 22.93, 26.04, 26.66, 26.74, 31.45, 35.62 (CH_2), 37.42, 44.12 (CH), 44.20 ($N(CH_3)_2$), 47.65 (C), 50.18 (CH), 58.00 (4-CCH_2), 118.32, 124.79 (ArCH), 128.19, 129.48, 131.48, 154.30 (ArC) and 221.1 (CO), LRMS (ESI) calcd for $C_{23}H_{34}NO_2$ $(M+H)^+$: *m/z* = 356.2, found *m/z* = 356.1, HRMS (FAB+) calcd for $C_{23}H_{34}NO_2$ $(M+H)^+$: *m/z* = 356.2584, found *m/z* = 356.2572.

(13*S*)-2-Ethyl-3-hydroxy-13-methyl-4-(pyrrolidin-1-ylmethyl)-7,8,9,11,12,13,15,16-octahydro-6*H*-cyclopenta[a]-phenan-thren-17(14*H*)-one (Compound 148), $C_{25}H_{35}NO_2$, MW 381.55,

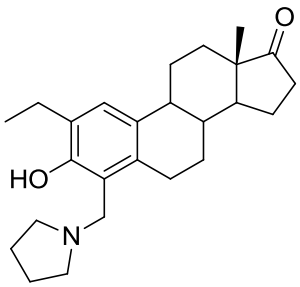

148

To a solution of (13*S*)-2-ethyl-3-hydroxy-13-methyl-7,8,9,11,12,13,15,16-octahydro-6*H*-cyclopenta[a]-phenan-thren-17(14*H*)-one **146** (300 mg, 1.0 mmol) in EtOH / toluene (1/1, 9 mL) was added pyrrolidine (0.166 mL, 2.0 mmol) and paraformaldehyde (60 mg). The mixture was heated to reflux for 5 h, cooled to room temperature and concentrated *in-vacuo*. Water (10 mL) was added to the residue and the organics were extracted with Et_2O (3 x 10 mL). The combined organic extracts were washed with brine (10 mL), dried ($MgSO_4$) and concentrated *in-vacuo* to give

the title compound **148** (199 mg, 52%) as white foam. HPLC: t_r 1.27 min (90% Acetonitrile in water) 95%, ^{1}H NMR (400 MHz, $CDCl_3$) δ: 0.90 (3H, s, 18-CH_3), 1.21 (3H, t, *J* = 8 Hz, 2-CCH_2CH_3), 1.33-1.66 (7H, m), 1.85 (4H, s, CH_2), 1.93-2.17 (4H, m), 2.24 (1H, m), 2.42-2.58 (2H, m), 2.60-2.70 (7H, m), 2.80 (1H, m), 3.78 (1H, d, *J* = 14 Hz, 4-CCH_{2A}), 3.88 (1H, d, *J* = 14 Hz, 4-CCH_{2B}) and 7.03 (1H, s, ArH). ^{13}C NMR (101 MHz, $CDCl_3$) δ: 13.69 (18-CH_3), 14.30 (2-CCH_2CH_3), 21.42, 23.07 (CH_2), 23.57 (2 × CH_2), 26.10, 26.75, 26.83, 31.52, 35.77 (CH_2), 37.51, 44.21 (CH), 47.76 (C), 50.28 (CH), 53.53 (4-CCH_2), 54.29 (2 × CH_2), 118.80 (ArC), 124.74 (ArCH), 128.29, 129.48, 131.21, 154.35 (ArC) and 220.84 (CO). LRMS (ESI) calcd for $C_{25}H_{36}NO_2$ $(M+H)^+$: *m/z* = 382.2, found *m/z* = 382.0. HRMS (ESI) calcd for $C_{25}H_{36}NO_2$ $(M+H)^+$: *m/z* = 382.2741, found *m/z* = 382.2749.

(13*S*)-2-Ethyl-3-hydroxy-13-methyl-4-(piperidin-1-ylmethyl)-7,8,9,11,12,13,15,16-octahydro-6*H*-cyclopenta[a]-phenan-thren-17(14*H*)-one (Compound 149), $C_{26}H_{37}NO_2$, MW 395.58,

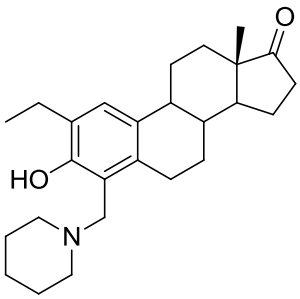

149

To a solution of (13*S*)-2-ethyl-3-hydroxy-13-methyl-7,8,9,11,12,13,15,16-octahydro-6*H*-cyclopenta[a]-phenan-thren-17(14*H*)-one **146** (300 mg, 1.0 mmol) in EtOH / toluene (1/1, 9 mL) was added piperidine (0.198 mL, 2.0 mmol) and paraformaldehyde (60 mg). The mixture was heated to reflux for 5 h, cooled to room temperature and concentrated *in-vacuo*. Water (10 mL) was added to the residue and the organics were extracted with Et_2O (3 x 10 mL). The combined organic extracts were washed with brine (10 mL), dried ($MgSO_4$) and concentrated *in-vacuo* to give the title compound **149** (190 mg, 48%) as white foam. HPLC: t_r 0.91 min (90% Acetonitrile in water) 97%, ^{1}H NMR (400 MHz, $CDCl_3$) δ: 0.90 (3H, s, 18-CH_3), 1.21 (3H, t, *J* = 8 Hz, 2-CCH_2CH_3), 1.32-1.53 (6H, m), 1.55-1.63 (6H, br. s), 1.91-2.17 (4H, m), 2.36 (1H, s, CH), 2.42-2.54 (2H, m), 2.61 (2H, quart, *J* = 8 Hz, 2-CCH_2), 2.68 (1H, m), 2.77 (1H, m), 3.60 (1H, d, *J* = 14 Hz, 4-CCH_{2A}), 3.68 (1H, d, *J*

= 14 Hz, 4-CCH_{2B}) and 7.03 (1H, s, ArH). ^{13}C NMR (101 MHz, $CDCl_3$) δ: 13.83 (18-CH_3), 14.43 (2-CCH_2CH_3), 21.56, 23.24, 23.98 (CH_2), 25.77 (2 × CH_2), 26.25, 26.89, 26.99, 31.65, 35.91 (CH_2), 37.66, 44.35 (CH), 47.90 (C), 50.41 (CH), 53.85 (2 ×CH_2), 57.54 (4-CCH_2), 118.27 (ArC), 124.90 (ArCH), 128.43, 129.69, 131.93, 154.53 (ArC), 221.00 (CO). LRMS (ESI) calcd for $C_{26}H_{38}NO_2$ $(M+H)^+$: *m/z* = 396.2, found *m/z* = 396.0. HRMS (ESI) calcd for $C_{26}H_{38}NO_2$ $(M+H)^+$: *m/z* = 396.2824, found *m/z* = 396.2888, Anal. Calcd. for $C_{26}H_{38}NO_2$: C 78.94, H 9.43, N 3.54%, found C 78.40, H 9.49, N 3.43%.

(13*S*)-2-Ethyl-3-hydroxy-13-methyl-4-(morpholinomethyl)-7,8,9,11,12,13,15,16-octahydro-6*H*-cyclopenta[a]-phenan-thren-17(14*H*)-one (Compound 150),
$C_{25}H_{35}NO_3$, MW 397.55,

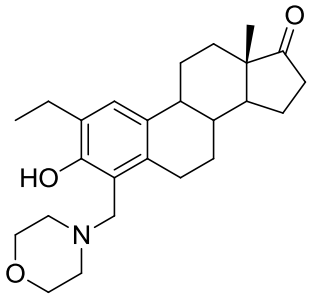

150

To a solution of (13*S*)-2-ethyl-3-hydroxy-13-methyl-7,8,9,11,12,13,15,16-octahydro-6*H*-cyclopenta[a]-phenan-thren-17(14*H*)-one **146** (300 mg, 1.0 mmol) in EtOH / toluene (1/1, 9 mL) was added morpholine (0.175 mL, 2.0 mmol) and paraformaldehyde (60 mg). The mixture was heated to reflux for 5 h, cooled to room temperature and concentrated *in-vacuo*. Water (10 mL) was added to the residue and the organics were extracted with Et_2O (3 x 10 mL). The combined organic extracts were washed with brine (10 mL), dried ($MgSO_4$) and concentrated *in-vacuo* to give the title compound **150** (164 mg, 41%) as a white foam. HPLC: t_r 2.74 min (90% Acetonitrile in water) 99%, ^{1}H NMR (400 MHz, $CDCl_3$) δ: 0.89 (3H, s, 18-CH_3), 1.20 (3H, t, *J* = 7 Hz, 2-CH_2CH_3), 1.33-1.63 (6H, m), 1.90-1.95 (1H, m), 2.02-2.17 (3H, m), 2.23-2.37 (1H, m), 2.41-2.71 (9H, m), 2.79-2.85 (1H, m), 3.46 (6H, m), 7.05 (1H, s, ArH) and 11.36 (1H, br. s, OH). ^{13}C NMR (101 MHz, $CDCl_3$) δ: 13.59 (18-CH_3), 14.20 (2-CCH_2CH_3), 21.32, 22.99, 26.04, 26.62, 26.87, 31.42, 35.65 (CH_2), 37.39, 44.10 (CH), 47.62 (C), 50.13 (CH), 52.62 (4-CCH_2), 56.85 (2 × CH_2), 66.50 (2 × CH_2), 117.23 (ArC), 125.51 (ArCH), 128.29, 130.00, 131.92, 153.70

(ArC) and 220.56 (CO). LRMS (ESI) calcd for $C_{25}H_{36}NO_3$ $(M+H)^+$: *m/z* = 398.2, found *m/z* = 398.2, HRMS (ESI) calcd for $C_{25}H_{36}NO_3$ $(M+H)^+$: *m/z* = 398.2690, found *m/z* = 398.2698.

(13*S*)-2-Ethyl-3-hydroxy-13-methyl-4-(thiomorpholinomethyl)-7,8,9,11,12,13,15,16-octahydro-6*H*-cyclopenta[a]-phenan-thren-17(14*H*)-one (Compound 151), $C_{25}H_{35}NO_2S$, MW 413.62,

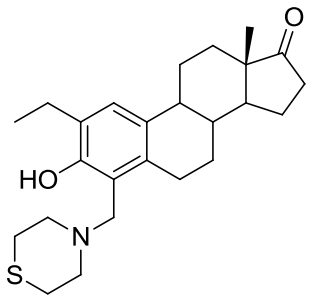

151

To a solution of (13*S*)-2-ethyl-3-hydroxy-13-methyl-7,8,9,11,12,13,15,16-octahydro-6*H*-cyclopenta[a]-phenan-thren-17(14*H*)-one **146** (300 mg, 1.0 mmol) in EtOH / toluene (1/1, 9 mL) was added thiomorpholine (0.190 mL, 2.0 mmol) and paraformaldehyde (60 mg). The mixture was heated to reflux for 5 h, cooled to room temperature and concentrated *in-vacuo*. Water (10 mL) was added to the residue and the organics were extracted with Et_2O (3 x 10 mL). The combined organic extracts were washed with brine (10 mL), dried ($MgSO_4$) and concentrated *in-vacuo* to give the title compound **151** (95 mg, 23%) as white foam. HPLC t_r 1.83 min (90% Acetonitrile in water) 100%, ^{1}H NMR (400 MHz, $CDCl_3$) δ: 0.89 (3H, s, 18-CH_3), 1.20 (3H, t, *J* = 8 Hz, 2-CCH_2CH_3), 1.34-1.66 (6H, m), 1.91-2.23 (6H, m), 2.41-2.81 (14H, m), 3.65 (1H, d, *J* = 14 Hz, 4-CCH_{2A}), 3.73 (1H, d, *J* = 14 Hz, 4-CH_{2B}) and 7.05 (1H, s, ArH). ^{13}C NMR (101 MHz, $CDCl_3$) δ: 13.78 (18-CH_3), 14.33 (2-CCH_2CH_3), 21.51, 23.15, 26.21, 26.80, 27.04 (CH_2), 27.87 (2 × CH_2), 31.59, 35.86 (CH_2), 37.58, 44.28 (CH), 47.85 (C), 50.34 (CH), 54.28 (4-CCH_2), 57.46 (2 × CH_2), 117.58 (ArC), 125.32 (ArCH), 128.62, 130.22, 132.16, 154.02 (ArC) and 220.93 (CO). LRMS (ESI) calcd for $C_{25}H_{36}NO_2S$ $(M+H)^+$: *m/z* = 414.2, found *m/z* = 414.0. HRMS (ESI) calcd for $C_{25}H_{36}NO_2S$ $(M+H)^+$: *m/z* = 414.2389, found *m/z* = 414.2449.

(13*S*)-4-(Azepan-1-ylmethyl)-2-ethyl-3-hydroxy-13-methyl-7,8,9,11,12,13,15,16-octahydro-6*H*-cyclopenta[a]-phenan-thren-17(14*H*)-one (Compound 152),
$C_{27}H_{39}NO_2$, MW 409.60,

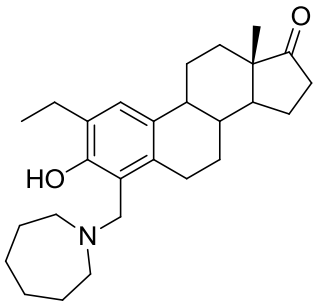

152

To a solution of (13*S*)-2-ethyl-3-hydroxy-13-methyl-7,8,9,11,12,13,15,16-octahydro-6*H*-cyclopenta[a]-phenan-thren-17(14*H*)-one **146** (300 mg, 1.0 mmol) in EtOH / toluene (1/1, 9 mL) was added azepane (0.226 mL, 2.0 mmol) and paraformaldehyde (60 mg). The mixture was heated to reflux for 5 h, cooled to room temperature and concentrated *in-vacuo*. Water (10 mL) was added to the residue and the organics were extracted with Et_2O (3 x 10 mL). The combined organic extracts were washed with brine (10 mL), dried ($MgSO_4$) and concentrated *in-vacuo* to give the title compound **152** (221 mg, 54%) as white foam. HPLC: t_r 1.16 min (90% Acetonitrile in water) 99%, ^{1}H NMR (400 MHz, $CDCl_3$) δ: 0.91 (3H, s, 18-CH_3), 1.22 (3H, t, *J* = 7 Hz, 2-CCH_2CH_3), 1.32-1.62 (6H, m), 1.65-1.70 (9H, m), 1.95-2.27 (5H, m), 2.43-2.58 (2H, m), 2.60-2.84 (8H, m), 3.73 (1H, d, *J* = 15 Hz, 4-CCH_{2A}), 3.81 (1H, d, *J* = 15 Hz, 4-CCH_{2B}) and 7.04 (1H, s, ArH), ^{13}C NMR (101 MHz, $CDCl_3$) δ: 13.71 (18-CH_3), 14.37 (2-CCH_2CH_3), 21.44, 23.13, 26.11 (CH_2), 26.53 (2 × CH_2), 26.79, 26.87 (CH_2), 27.56 (2 × CH_2), 31.55, 35.78 (CH_2), 37.53, 44.23 (CH), 47.78 (C), 50.29 (CH), 55.08 (2 × CH_2), 57.17 (4-CCH_2), 118.85 (ArC), 124.83 (ArCH), 128.40, 129.45, 131.63, 154.74 (ArC) and 220.85 (CO). LRMS (ESI) calcd for $C_{27}H_{40}NO_2$ $(M+H)^+$: *m/z* = 410.3, found *m/z* = 410.1.

(13*S*,17*S*)-4-((Dimethylamino)methyl)-2-ethyl-13-methyl-7,8,9,11,12,13,14,15,16,17-decahydro-6*H*-cyclopenta[a]-phenan-threne-3,17-diol (Compound 153), $C_{23}H_{35}NO_2$, MW 357.53,

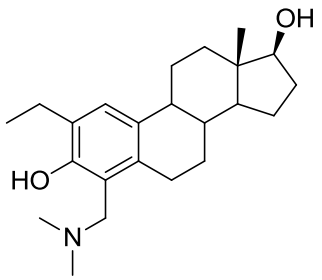

153

Prepared by modification to the literature procedure.[142]

Sodium borohydride (12 mg, 0.31 mmol) was added portion-wise to a solution of (13*S*)-4-((dimethylamino)methyl)-2-ethyl-3-hydroxy-13-methyl-7,8,9,11,12,13,15,16-octahydro-6*H*-cyclopenta[a]-phenan-thren-17(14*H*)-one **147** (100 mg, 0.28 mmol) dissolved in MeOH / THF (1/1, 4 mL) at 0 °C (ice bath). The resulting solution was stirred for 2 h and treated with water (5 mL). The crude products were extracted with ethyl acetate (2 × 5 mL), washed with brine (5 mL), dried ($MgSO_4$), filtered and evaporated *in-vacuo* to give the title compound **153** (82 mg, 82%) as a white foam. HPLC t_r = 2.73 min (90% Acetonitrile in water) 97%, ^{1}H NMR (400 MHz, $CDCl_3$) δ: 0.91 (3H, s, 18-CH_3), 1.23 (3H, t, *J* = 8 Hz, 2-CCH_2CH_3), 1.29-1.61 (6H, m), 1.87-1.92 (1H, m), 2.00-2.18 (3H, m), 2.21-2.32 (1H, m), 2.36 (6H, s, $N(CH_3)_2$), 2.39-2.70 (5H, m), 2.77-2.82 (2H, m), 3.59 (1H, d, *J* = 14 Hz, 4-CCH_{2A}), 3.72 (1H, d, *J* = 14 Hz, 4-CCH_{2B}), 7.02 (1H, s, ArH); ^{13}C NMR (101 MHz, $CDCl_3$) δ: 13.96 (18-CH_3), 14.53 (2-CCH_2CH_3), 21.30, 22.97, 26.12, 26.70, 26.77, 31.54, 35.64 (CH_2), 37.45, 44.14 (CH), 44.43 ($N(CH_3)_2$), 47.68 (C), 50.21 (CH), 58.06 (4-CCH_2), 81.73 (17-CH) 118.35, 124.83 (ArCH), 128.22, 129.53, 131.54 (ArC) and 154.35 (ArC), HRMS (ESI) calcd for $C_{23}H_{36}NO_2$ $(M+H)^+$: *m/z* = 358.2668, found *m/z* = 358.2754.

(13*S*,17*S*)-2-Ethyl-13-methyl-4-(morpholinomethyl)-7,8,9,11,12,13,14,15,16,17-decahydro-6*H*-cyclopenta[a]-phenan-threne-3,17-diol (Compound 154),
$C_{25}H_{37}NO_3$, MW 399.57,

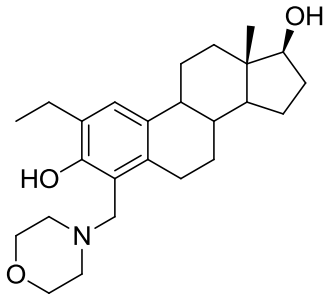

154

Prepared in accordance with the literature procedure. [142]

Sodium borohydride (8.0 mg, 0.29 mmol) was added portion-wise to a solution of (13*S*)-2-ethyl-3-hydroxy-13-methyl-4-(morpholinomethyl)-7,8,9,11,12,13,15,16-octahydro-6*H*-cyclopenta[a]-phenan-thren-17(14*H*)-one **150** (72.0 mg, 0.18 mmol) dissolved in MeOH / THF (1/1, 3 mL) at 0 °C (ice bath). The resulting solution was stirred for 2 h and treated with water (5 mL). The crude products were extracted with ethyl acetate (2 × 5 mL), washed with brine (5 mL), dried ($MgSO_4$), filtered and evaporated *in-vacuo* to give the title compound **154** (53 mg, 73%) as a white foam. HPLC: t_r 1.05 min (90% Acetonitrile in water) 97%, ^{1}H NMR (400 MHz, $CDCl_3$) δ: 0.76 (3H, s, 18-CH_3), 1.20 (3H, t, *J* = 8 Hz, 2-CCH_2CH_3), 1.24-1.51 (10H, m), 1.65-1.68 (1H, m), 1.92-1.96 (2H, m), 2.04-2.39 (2H, m), 2.62-2.73 (4H, m), 2.59 (2H, quart, *J* = 8 Hz, 2-CCH_2), 2.73-2.79 (3H, m), 3.69-3.74 (6H, m) and 7.05 (1H, s, ArH). ^{13}C NMR (101 MHz, $CDCl_3$) δ: 11.02 (18-CH_3), 14.46 (2-CCH_2CH_3), 24.51, 26.42, 27.03, 27.47, 29.24, 30.37, 36.64 (CH_2), 38.11, 43.17 (CH), 44.33 (C), 49.78 (CH), 50.42 (CH_2), 56.61 (2 × CH_2), 66.80 (2 × CH_2), 81.40 (17-CH), 117.48, 125.43 (ArC), 128.43 (ArCH), 130.93, 132.45 (ArC) and 153.77 (ArC). LRMS (ESI) calcd for $C_{25}H_{38}NO_3$ $(M+H)^+$: *m/z* = 400.3, found *m/z* = 400.1, HRMS (ESI) calcd for $C_{25}H_{38}NO_3$ $(M+H)^+$: *m/*z = 400.2773, found *m/z* = 400.2861.

(13*S*,17*S*)-4-(Azepan-1-ylmethyl)-2-ethyl-13-methyl-7,8,9,11,12,13,14,15,16,17-decahydro-6*H*-cyclopenta[a]-phenan-threne-3,17-diol (Compound 155), $C_{27}H_{41}NO_2$, MW 411.62,

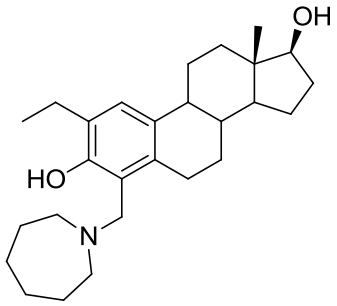

155

Prepared by modification to the literature procedure.[142]

Sodium borohydride (188 mg, 0.49 mmol) was added portion-wise to a solution of (13*S*)-4-(azepan-1-ylmethyl)-2-ethyl-3-hydroxy-13-methyl-7,8,9,11,12,13,15,16-octahydro-6*H*-cyclopenta[a]-phenan-thren-17(14*H*)-one **152** (185 mg, 0.45 mmol) dissolved in MeOH / THF (1/1, 10 mL) at 0 °C (ice bath). The resulting solution was stirred for 2 h and treated with water (5 mL). The crude products were extracted with ethyl acetate (2 × 5 mL), washed with brine (5 mL), dried ($MgSO_4$), filtered and evaporated *in-vacuo* to give the title compound **155** (146 mg, 79%) as a white foam. HPLC: t_r 3.21 min (90% Acetonitrile in water) 98%, ^{1}H NMR (400 MHz, $CDCl_3$) δ: 0.89 (3H, s, 18-CH_3), 1.27 (3H, t, *J* = 7 Hz, 2-CCH_2CH_3), 1.30-1.64 (6H, m), 1.67-1.73 (9H, m), 1.95-2.27 (5H, m), 2.38-2.42 (2H, m), 2.57-2.74 (8H, m), 3.74 (1H, d, *J* = 15 Hz, 4-CCH_{2A}), 3.77 (1H, t, *J* = 5 Hz, CH), 3.83 (1H, d, *J* = 15 Hz, 4-CCH_{2B}) and 7.09 (1H, s, ArH). ^{13}C NMR (101 MHz, $CDCl_3$) δ: 11.12 (18-CH_3), 14.52 (2-CCH_2CH_3), 23.27 (CH_2), 26.72 (2 × CH_2), 27.31 (CH_2), 27.73 (2 × CH_2), 29.81, 30.59, 36.91 (CH_2), 38.21, 43.20 (CH), 44.40 (C), 50.16 (CH), 55.24 (2 × CH_2), 57.33 (4-CCH_2), 81.87 (17-CH) 118.97, 125.02 (ArC), 128.39 (ArCH), 130.30, 131.99 (ArC) and 154.67 (ArC). LRMS (ESI) calcd for $C_{27}H_{42}NO_2$ $(M+H)^+$: *m/z* = 412.3, found *m/z* = 412.2, HRMS (ESI) calcd for $C_{27}H_{42}NO_2$ $(M+H)^+$: *m/z* = 412.3137, found *m/z* = 412.3218.

(13*S*)-3-(Benzyloxy)-13-methyl-7,8,9,11,12,13,15,16-octahydro-6*H*-cyclopenta[a]-phenan-thren-17(14*H*)-one (Compound 156), $C_{25}H_{28}O_2$, MW 360.49,

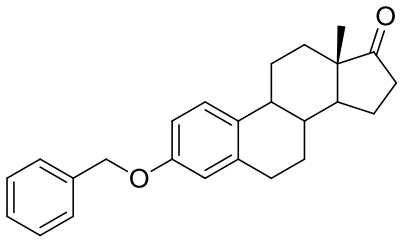

156

To a stirred solution of estrone (10.0 g, 37 mmol) and potassium carbonate (6.14 g, 44 mmol) in anhydrous DMF (300 mL) under an atmosphere of nitrogen, benzyl bromide (5.27 mL, 44 mmol) was added drop-wise. The resulting reaction mixture was stirred at room temperature for 30 h. To quench the reaction water (200 mL) was added and the resulting precipitate was filtered, re-dissolved in DCM (200 mL) and washed with brine (200 mL), dried ($MgSO_4$), filtered and the solvent evaporated *in-vacuo* to yield the title compound **156** (13.07 g, 98%) as a white solid. m.p. 128-130 ºC, ^{1}H NMR (400 MHz, $CDCl_3$) δ: 0.95 (3H, s, 18-CH_3), 1.43-1.69 (7H, m), 1.96-2.23 (5H, m), 2.26-2.34 (1H, m), 2.39-2.43 (1H, m), 2.48-2.57 (1H, m), 6.77(1H, d, *J* = 4 Hz, ArH), 6.84 (1H, dd, *J* = 8 and 4 Hz, ArH), 7.23 (1H, d, *J* = 8 Hz, 2 × ArH), 7.36 (1H, t, *J* = 8 Hz, ArH), 7.41 (2H, t, *J* = 8 Hz, 2 × ArH) and 7.46 (2H, d, *J* = 8 Hz, ArH), ^{13}C NMR (101 MHz, $CDCl_3$) δ: 13.90 (18-CH_3), 21.62, 25.96, 26.59, 29.69, 31.65, 35.90 (CH_2), 38.41, 44.04 (CH), 48.04 (C), 50.48 (CH), 70.01 (3-O*C*H_2), 112.45, 114.98, 126.37 (ArCH), 127.45 (2 × ArCH), 127.88 (ArCH), 128.57 (2 × ArCH), 132.38, 137.34, 137.82, 156.94 (ArC) and 220.14 (CO). LRMS (ESI) calcd for $C_{25}H_{29}O_2$ $(M+H)^+$: *m/z* = 361.2, found *m/z* = 361.2, HRMS (ESI) calcd for $C_{25}H_{29}O_2$ $(M+H)^+$: *m/z* = 361.2089, found *m/z* = 361.2154. Data obtained for melting point is identical to that in the literature.[145]

(13*S*,17*S*)-3-(Benzyloxy)-13-methyl-7,8,9,11,12,13,14,15,16,17-decahydro-6*H*-cyclopenta[a]-phenan-thren-17-amine (Compound 157), $C_{25}H_{31}NO$, MW 361.52,

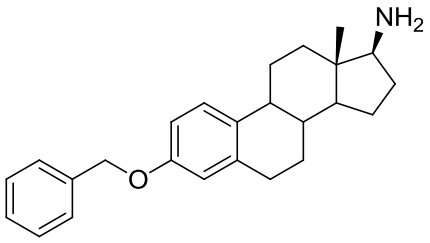

157

Sodium cyanoborohydride (2.85 g, 45.3 mmol) was added to a solution of (13*S*)-3-(benzyloxy)-13-methyl-7,8,9,11,12,13,15,16-octahydro-6*H*-cyclopenta[a]-phenan-thren-17(14*H*)-one **156** (13.62 g, 37.8 mmol) and ammonium acetate (29.14 g, 0.38 mol) in THF / MeOH (200/67) (267 mL) with stirring for 4 d. The reaction mixture was poured into chilled 5% sodium hydrogen carbonate (250 mL), at which point a precipitate formed. The precipitate was collected by filtration, re-dissolved in DCM (200 mL), dried ($MgSO_4$), filtered and the solvent evaporated *in-vacuo* to yield the title compound **157** (5.19 g, 38%) as a white solid. m.p. 88-91 ºC, IR (KBr): 561-1448, 1506, 1578, 1613, 2843, 2934, 3035 cm^{-1}, ^1H (400 MHz, $CDCl_3$) δ: 0.71 (3H, s, 18-CH_3), 1.21-1.57 (5H, m), 1.72-1.77 (1H, m), 1.87-1.91 (2H, m), 2.09 (3H, s), 2.18-2.24 (1H, m), 2.27-2.36 (1H, m), 2.80 (1H, t, *J* = 8 Hz, 17-CH), 2.85 (2H, quart, *J* = 4 Hz, CH_2), 5.03 (2H, s, 3-OCH_2), 6.72 (1H, d, *J* = 2 Hz, ArH), 6.78 (1H, dd, *J* = 8 and 2 Hz, ArH), 7.20 (1H, d, *J* = 8 Hz, ArH), 7.31 (1H, t, *J* = 8 Hz, ArH), 7.38 (2H, t, *J* = 8 Hz, 2 × ArH) and 7.44 (2H, d, *J* = 8 Hz, 2 × ArH), ^{13}C NMR (101 MHz, $CDCl_3$) δ: 11.22 (18-CH_3), 23.42, 26.38, 27.47, 29.84, 30.99, 36.78 (CH_2), 39.10 (CH), 42.86 (C), 44.03, 52.06 (CH), 62.84 (17-CH), 70.01 (3-O*C*H_2), 112.31, 114.91, 126.32 (ArCH), 127.45 (2 × ArCH), 127.84 (ArCH), 128.55 (2 ×ArCH), 133.03, 137.41, 138.08 (ArC) and 156.79 (ArC). LRMS (ESI) calcd for $C_{25}H_{32}NO$ $(M+H)^+$: *m/z* = 362.2, found *m/z* = 362.4, HRMS (ESI) calcd for $C_{25}H_{32}NO$ $(M+H)^+$: *m/z* = 362.2406, found *m/z* = 362.2481.

***N*-((13*S*,17*S*)-3-(Benzyloxy)-13-methyl-7,8,9,11,12,13,14,15,16,17-decahydro-6*H*-cyclopenta[a]-phenan-thren-17-yl)-2,4,5-trimethoxybenzamide (Compound 158),** $C_{35}H_{41}NO_5$, MW 555.70,

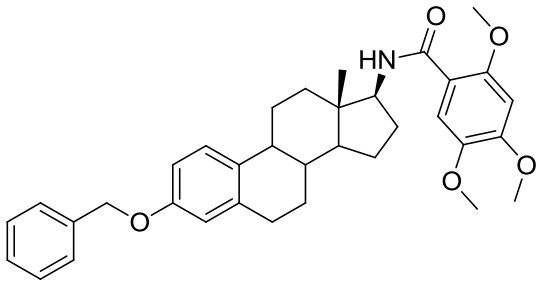

158

To a solution of 2,4,5-trimethoxybenzoic acid (236 mg, 1.11 mmol) in DCM (30 mL) EDCI.HCl (264 mg, 1.38 mmol) was added followed by addition of DMAP (169 mg, 1.38 mmol) and triethylamine (0.64 mL, 4.56 mmol) in a portionwise manner. The resulting reaction mixture was stirred for 15 min at room temperature. A solution (13*S*,17*S*)-3-(benzyloxy)-13-methyl-7,8,9,11,12,13,14,15,16,17-decahydro-6*H*-cyclopenta[a]-phenan-thren-17-amine **157** (500 mg, 1.38 mmol) in DCM (10 mL was added drop-wise to the reaction mixture and the mixture was stirred for 18 h at room temperature. The reaction was quenched with saturated ammonium chloride (30 mL). The crude products were extracted with DCM (2 × 15 mL), dried ($MgSO_4$), filtered and evaporated *in-vacuo* to give the crude product. The crude product was then purified by flash chromatography DCM / MeOH (0 – 20%) to yield the title compound **158** (560 mg, 73%) as a white solid. m.p. 197 – 200 °C, ^{1}H NMR (400 MHz, $CDCl_3$): δ 0.82 (3H, s, 18-CH_3), 1.38–1.44 (8H, m), 1.79-1.91 (4H, m), 2.25-2.31 (3H, m), 2.85-2.87 (2H, m, 6-CH_2), 3.89 (3H, s, OCH_3), 3.92 (3H, s, OCH_3), 3.95 (3H, s, OCH_3), 5.02 (2H, s, 3-OCH_2), 6.53 (1H, s, ArH), 6.72 (1H, d, *J* = 2 Hz, ArH), 6.76 (1H, dd, *J* = 8 and 2 Hz, ArH), 7.20 (1H, d, *J* = 8 Hz, ArH), 7.31 (1H, t, *J* = 8 Hz, ArH), 7.36 (2H, t, *J* = 8 Hz, 2 × ArH), 7.43 (2H, d, *J* = 8 Hz, 2 × ArH) and 7.78 (1H, s, ArH). ^{13}C NMR (101 MHz, $CDCl_3$) δ: 12.36 (18-CH_3), 23.60, 26.35, 27.44, 29.18, 29.84, 37.24 (CH_2), 39.11, 43.53 (CH), 43.94 (C), 51.71 (CH), 56.20, 56.30, 56.97 (OCH_3), 59.36 (17-CH), 70.00 (3-OCH_2), 97.12 (CH), 112.32 (ArCH), 113.81 (ArC), 114.24, 114.89, 126.38 (ArCH), 127.45 (2 × ArCH), 127.83 (ArCH), 128.53 (2 × ArCH), 133.04, 137.42, 138.00, 143.54, 152.16, 152.53, 156.79 (ArC) and 164.95 (CO), HRMS (ESI) $(M+H)^+$: calcd for $C_{35}H_{42}NO_5$ *m/z* = 556.2985, found *m/z* = 556.3057.

***N*-((13*S*,17*S*)-3-(Benzyloxy)-13-methyl-7,8,9,11,12,13,14,15,16,17-decahydro-6*H*-cyclopenta[a]-phenan-thren-17-yl)-4-methoxybenzamide (Compound 159),**
$C_{33}H_{37}NO_3$, MW 495.65,

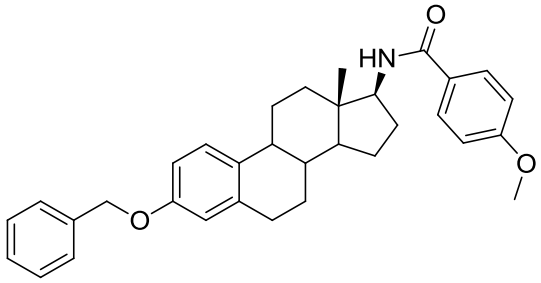

159

To a solution of 4-methoxybenzoic acid (169 mg, 1.11 mmol) in DCM (30 mL) EDCI.HCl (264 mg, 1.38 mmol) was added followed by addition of DMAP (169 mg, 1.38 mmol) and triethylamine (0.64 mL, 4.56 mmol) in a portionwise manner. The resulting reaction mixture was stirred for 15 min at room temperature. A solution of (13*S*,17*S*)-3-(benzyloxy)-13-methyl-7,8,9,11,12,13,14,15,16,17-decahydro-6*H*-cyclopenta[a]-phenan-thren-17-amine **157** (500 mg, 1.38 mmol) in DCM (10 mL) was added drop-wise to the reaction mixture and the mixture was stirred for 18 h at room temperature. The reaction was quenched with saturated ammonium chloride (30 mL). The crude products were then extracted with DCM (2 × 15 mL), dried ($MgSO_4$), filtered and evaporated *in-vacuo* to give the crude product. The crude product was then purified by flash chromatography DCM / MeOH (0 – 20%) to yield the title compound **159** (465 mg, 68%) as a white solid. m.p. 195 – 197 °C, ^{1}H NMR (400 MHz, $CDCl_3$) δ: 0.82 (3H, s, 18-CH_3), 1.41-1.54 (8H, m), 1.81-1.92 (3H, m), 2.24-2.37 (3H, m), 2.86 (2H, s, 6-CH_2), 3.85 (3H, s, OCH_3), 5.04 (2H, s, 3-OCH_2), 6.72 (1H, d, *J* = 2 Hz, ArH), 6.79 (1H, dd, *J* = 8 and 2 Hz, ArH), 6.93 (2H, d, *J* = 8 Hz, 2 × ArH), 7.21 (1H, d, *J* = 8 Hz, ArH), 7.31 (1H, t, *J* = 8 Hz, ArH), 7.38 (2H, t, *J* = 8 Hz, 2 × ArH), 7.43 (2H, d, *J* = 8 Hz, 2 × ArH) and 7.75 (2H, d, *J* = 8 Hz, 2 × ArH). ^{13}C NMR (101 MHz, $CDCl_3$) δ: 12.28 (18-CH_3), 23.47, 26.32, 27.41, 28.95, 29.83, 37.16 (CH_2), 39.08, 43.75 (CH), 43.91 (C), 51.73 (CH), 55.43 (OCH_3), 59.26 (17-CH), 70.02 (3-OCH_2), 112.33 (ArCH), 113.78 (2 × ArCH), 126.40 (ArCH), 127.39 (2 × ArCH), 127.84 (ArCH), 128.55 (2 × ArCH), 128.61 (2 × ArCH), 132.99, 137.42, 137.96, 156.81, 162.11 (ArC) and 166.94 (CO), HRMS (ESI) $(M+H)^+$: calcd for $C_{33}H_{38}NO_3$ *m/z* = 496.2773, found *m/z* = 496.2830.

***N*-((13*S*,17*S*)-3-(Benzyloxy)-13-methyl-7,8,9,11,12,13,14,15,16,17-decahydro-6*H*-cyclopenta[a]-phenan-thren-17-yl)-2,3-dimethoxybenzamide (Compound 160),**
$C_{34}H_{39}NO_4$, MW 525.68,

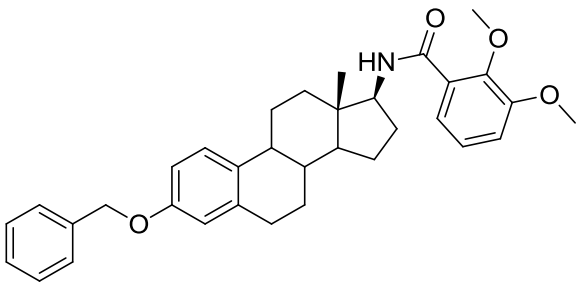

160

To a solution of 2,3-dimethoxybenzoic acid (169 mg, 1.11 mmol) in DCM (30 mL) EDCI.HCl (264 mg, 1.38 mmol) was added followed by addition of DMAP (169 mg, 1.38 mmol) and triethylamine (0.64 mL, 4.56 mmol) in a portionwise manner. The resulting reaction mixture was stirred for 15 min at room temperature. A solution of (13*S*,17*S*)-3-(benzyloxy)-13-methyl-7,8,9,11,12,13,14,15,16,17-decahydro-6*H*-cyclopenta[a]-phenan-thren-17-amine **157** (500 mg, 1.38 mmol) in DCM (10 mL) was added drop-wise to the reaction mixture and the mixture was stirred for 18 h at room temperature. The reaction was quenched with saturated ammonium chloride (30 mL). The crude products were extracted with DCM (2 × 15 mL), dried ($MgSO_4$), filtered and evaporated *in-vacuo* to give the crude product. The crude product was then purified by flash chromatography DCM / MeOH (0 – 20%) to yield the title compound **160** (551 mg, 76%) as a white solid. m.p. 135 – 139 °C, ^{1}H NMR (400 MHz, $CDCl_3$) δ: 0.85 (3H, s, 18-CH_3), 1.42-1.51 (8H, m), 1.93 (3H, m), 2.31 (3H, m), 2.87 (2H, s, 6-CH_2), 3.90 (3H, s, OCH_3), 3.94 (3H, s, OCH_3), 5.04 (2H, s, 3-OCH_2), 6.74 (1H, d, *J* = 4 Hz, ArH), 6.79 (1H, dd, *J* = 8 and 4 Hz, ArH), 7.05 (1H, dd, *J* = 8 and 4 Hz, ArH), 7.17 (1H, t, *J* = 8 Hz, ArH), 7.22 (1H, d, *J* = 8 Hz, ArH), 7.33 (1H, t, *J* = 8 Hz ArH), 7.38 (2H, t, *J* = 8 Hz, 2 × ArH), 7.45 (2H, d, *J* = 8 Hz, 2 × ArH), 7.75 (1H, dd, *J* = 8Hz, ArH) and 8.10 (1H, d, *J* = 8 Hz, NH). ^{13}C NMR (101 MHz, $CDCl_3$) δ: 12.45 (18-CH_3), 23.59, 26.36, 27.46, 29.06, 29.85, 37.28 (CH_2), 39.09, 43.95, 51.79 (CH), 56.14 (OCH_3), 59.37 (17-CH), 61.38 (OCH_3), 70.01 (3-OCH_2), 112.35, 114.93, 115.27, 122.98, 124.51, 126.39 (ArCH), 127.14 (ArC), 127.46 (2 × ArCH), 127.84 (ArCH), 128.55 (2 × ArCH), 133.02, 137.46, 137.99,

147.46, 152.64, 156.83 (ArC) and 164.99 (CO), HRMS (ESI) $(M+H)^+$: calcd for $C_{34}H_{40}NO_4$ *m/z* = 526.2879, found *m/z* = 526.2935.

***N*-((13*S*,17*S*)-3-Benzyloxy)-13-methyl-7,8,9,11,12,13,14,15,16,17-decahydro-6*H*-cyclopenta[a]-phenan-thren-17-yl)-2,4-dimethoxybenzamide (Compound 161),** $C_{34}H_{39}NO_4$, MW 525.68,

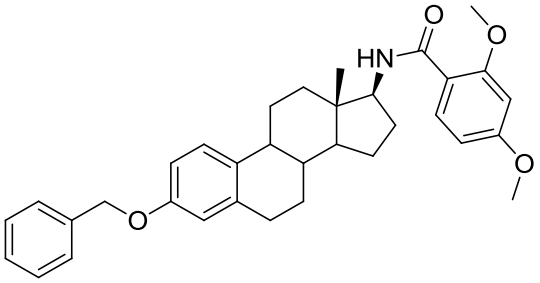

161

To a solution of 2,4-dimethoxybenzoic acid (169 mg, 1.11 mmol) in DCM (30 mL) EDCI.HCl (264 mg, 1.38 mmol) was added followed by addition of DMAP (169 mg, 1.38 mmol) and triethylamine (0.64 mL, 4.56 mmol) in a portionwise manner. The resulting reaction mixture was stirred for 15 min at room temperature. A solution of (13*S*,17*S*)-3-(benzyloxy)-13-methyl-7,8,9,11,12,13,14,15,16,17-decahydro-6*H*-cyclopenta[a]-phenan-thren-17-amine **157** (500 mg, 1.38 mmol) in DCM (10 mL) was added drop-wise to the reaction mixture and the mixture was stirred for 18 h at room temperature. The reaction was quenched with saturated ammonium chloride (30 mL). The crude products were extracted with DCM (2 × 15 mL), dried ($MgSO_4$), filtered and evaporated *in-vacuo* to give the crude product. The crude product was then purified by flash chromatography DCM / MeOH (0 – 20%) to yield the title compound **161** (515 mg, 71%) as a white solid. m.p. 159 – 162 °C, ^{1}H NMR (400 MHz, $CDCl_3$) δ: 0.85 (3H, s, 18-CH_3), 1.42-1.46 (8H, m), 1.91-1.94 (3H, m), 2.30-2.34 (3H, m), 2.88 (2H, s, 6-CH_2), 3.84 (3H, s, OCH_3), 3.94 (3H, s, OCH_3), 5.04 (3-OCH_2), 6.50 (1H, d, *J* = 4 Hz, ArH), 6.62 (1H, dd, *J* = 8 and 4 Hz, ArH), 6.75 (1H, d, *J* = 4 Hz, ArH), 6.80 (1H, dd, *J* = 8 and 4 Hz, ArH), 7.21 (1H, d, *J* = 8 Hz, ArH), 7.33 (1H, t, *J* = 8 Hz, ArH), 7.38 (2H, t, *J* = 8 Hz, 2 × ArH), 7.44 (2H, d, *J* = 8 Hz, 2 × ArH) and 7.88 (1H, d, *J* = 8 Hz, ArH). ^{13}C NMR (101 MHz, $CDCl_3$) δ: 12.39 (18-CH_3), 23.64, 26.40, 27.49, 29.24, 29.88, 37.23 (CH_2), 39.15, 43.51 (CH), 43.98 (C), 51.76 (CH), 55.54, 56.07 (OCH_3), 59.26 (17-CH), 70.01 (3-OCH_2),

98.76, 105.47, 112.35, 114.94, (ArCH) 115.01 (ArC), 126.42, 127.48 (2 × ArCH), 127.85 (ArCH), 128.56 (2 × ArCH), 133.10 (ArCH), 133.91, 137.48, 138.02, 156.83, 158.82, 163.27 (ArC), and 164.97 (CO), HRMS (ESI) $(M+H)^+$: calcd for $C_{34}H_{40}NO_4$ *m/z* = 526.2879, found *m/z* = 526.2945.

***N*-((13*S*,17*S*)-3-(Benzyloxy)-13-methyl-7,8,9,11,12,13,14,15,16,17-decahydro-6*H*-cyclopenta[a]-phenan-thren-17-yl)-2,5-dimethoxybenzamide (Compound 162),** $C_{34}H_{39}NO_4$, MW 525.68,

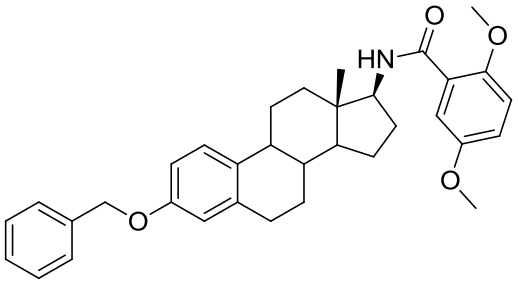

162

To a solution of 2,5-dimethoxybenzoic acid (169 mg, 1.11 mmol) in DCM (30 mL) EDCI.HCl (264 mg, 1.38 mmol) was added followed by addition of DMAP (169 mg, 1.38 mmol) and triethylamine (0.64 mL, 4.56 mmol) in a portionwise manner. The resulting reaction mixture was stirred for 15 min at room temperature. A solution of (13*S*,17*S*)-3-(benzyloxy)-13-methyl-7,8,9,11,12,13,14,15,16,17-decahydro-6*H*-cyclopenta[a]-phenan-thren-17-amine **157** (500 mg, 1.38 mmol) in DCM (10 mL) was added portion-wise to the reaction mixture and the mixture was stirred for 18 h at room temperature. The reaction was quenched with saturated ammonium chloride (30 mL). The crude products were extracted with DCM (2 × 15 mL), dried ($MgSO_4$), filtered and evaporated *in-vacuo* to give the crude product. The crude product was then purified by flash chromatography DCM / MeOH (0 – 20%) to yield the title compound **162** (464 mg, 64%) as a white solid. m.p. 152 – 156 °C, ^{1}H NMR (400 MHz, $CDCl_3$) δ: 0.85 (3H, s, 18-CH_3), 1.42-1.57 (8H, m), 1.83-1.94 (3H, m), 2.23-2.34 (3H, m), 2.88 (2H, s, 6-CH_2), 3.84 (3H, s, OCH_3), 3.94 (3H, s, OCH_3), 5.04 (2H, s, 3-OCH_2), 6.50 (1H, d, *J* = 4 Hz, ArH), 6.62 (1H, dd, *J* = 8 and 2 Hz, ArH), 6.75 (1H, d, *J* = 2 Hz, ArH), 6.80 (1H, dd, *J* = 8 and 2 Hz, ArH), 7.21 (1H, d, *J* = 8 Hz, ArH), 7.33 (1H, t, *J* = 8 Hz, ArH), 7.38 (2H, t, *J* = 8 Hz, 2 × ArH), 7.45 (2H, d, *J* = 8 Hz, 2 × ArH) and 7.88 (1H, d, *J* = 8 Hz, ArH), ^{13}C NMR (101 MHz, $CDCl_3$) δ: 12.39 (18-CH_3), 23.64, 26.40, 27.49, 29.24, 29.88, 37.23 (CH_2), 39.15,

43.51 (CH), 43.98 (C), 51.76 (CH), 55.54, 56.07 (OCH_3), 59.26 (17-CH), 70.01 (3-OCH_2), 98.76, 105.47 (CH), 112.35, 114.94 (ArCH), 115.02 (ArC), 126.42 (ArCH), 127.48 (2 × ArCH), 127.85 (ArCH), 128.56 (2 × ArCH), 133.10 (ArCH), 133.91, 137.48, 138.02, 156.83, 158.82, 163.27 (ArC) and 164.97 (CO), HRMS (ESI) $(M+H)^+$: calcd for $C_{34}H_{40}NO_4$ *m/z* = 526.2879, found *m/z* = 526.2955.

***N*-((13*S*,17*S*)-3-Hydroxy-13-methyl-7,8,9,11,12,13,14,15,16,17-decahydro-6*H*-cyclopenta[a]phenan-thren-17-yl)-4-methoxybenzamide (Compound 163),**
$C_{26}H_{31}NO_3$, MW 405.53,

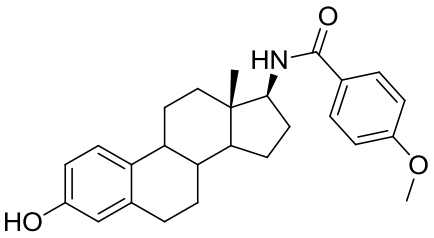

163

N-((13*S*,17*S*)-3-(Benzyloxy)-13-methyl-7,8,9,11,12,13,14,15,16,17-decahydro-6*H*-cyclopenta[a]-phenan-thren-17-yl)-4-methoxybenzamide **159** (100 mg, 0.20 mmol) was dissolved in a mixture of THF / EtOH (3/2, 50 mL) and pumped through an H Cube at 0.8 mL/min, 40 °C, full hydrogen 10% Pd/C. The reaction mixture was collected, dried ($MgSO_4$), filtered and concentrated *in-vacuo* to give the crude product as a white amorphous solid. Re-crystallisation from methanol gave the title compound **163** (70 mg, 86%) as white crystalline needles. ^{1}H NMR (400 MHz, $CDCl_3$) δ: 0.79 (3H, s, 18-CH_3), 1.25-1.43 (7H, m), 1.65-1.86 (3H, m), 2.12-2.26 (3H, m), 2.78 (2H, s, 6-CH_2), 3.84 (3H, s, OMe), 6.61 (1H, d, *J* = 2 Hz, ArH), 6.67 (1H, dd, *J* = 8 and 2 Hz, ArH), 6.74 (1H, s, NH), 6.69 (2H, d, *J* = 8 Hz, 2 × ArH), 7.09 (2H, d, *J* = 8 Hz, ArH) and 7.73 (2H, d, *J* = 8 Hz, 2 × ArH). ^{13}C NMR (101 MHz, $CDCl_3$) δ: 12.26 (18-CH_3), 23.44, 26.30, 27.39, 28.88, 29.66, 37.09 (CH_2), 39.06 (CH), 43.75 (C), 43.81, 51.65 (CH), 55.44 (OMe), 59.39 (17-CH), 112.98 (ArCH), 113.869 (2 × ArCH), 115.48 (ArCH), 126.37 (2 ×ArCH), 127.08 (ArC), 128.68 (ArCH), 132.00, 137.91, 154.15, 162.23 (ArC) and 167.40 (CO). HRMS (ESI) calcd for $C_{26}H_{32}NO_3$ $(M+H)^+$: *m/z* = 406.2377, found *m/z* = 406.2363.

***N*-((13*S*,17*S*)-3-Hydroxy-13-methyl-7,8,9,11,12,13,14,15,16,17-decahydro-6*H*-cyclopenta[a]phenan-thren-17-yl)-2,4-dimethoxybenzamide (Compound 164),** $C_{27}H_{33}NO_4$, MW 435.56,

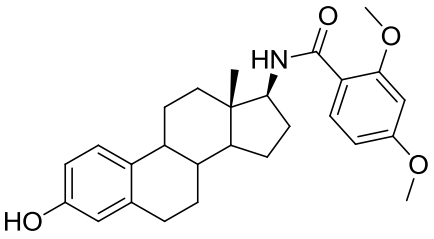

164

N-((13*S*,17*S*)-3-(Benzyloxy)-13-methyl-7,8,9,11,12,13,14,15,16,17-decahydro-6*H*-cyclopenta[a]phenan-thren-17-yl)-2,4-dimethoxybenzamide **161** (110 mg, 0.21 mmol) was dissolved in a mixture of THF / EtOH (3/2, 50 mL) and pumped through an H Cube at 0.8 mL/min, 40 °C, full hydrogen 10% Pd/C. The reaction mixture was collected, dried ($MgSO_4$), filtered and concentrated *in-vacuo* to give the crude product. Re-crystallisation from MeOH gave the title compound **164** (72 mg, 79%) as white crystalline cubes. m.p. 230-233 ºC, ^{1}H NMR (400 MHz, $CDCl_3$) δ: 0.81 (3H, s, 18-CH_3), 1.36-1.44 (8 H, m), 1.82-1.88 (4H, m), 2.17-2.25 (4H, m), 2.84 (2H, m, 6-CH_2), 3.89 (3H, s, OCH_3), 3.94 (3H, s, OCH_3), 6.57 (1H, s, ArH), 6.62 (1H, d, *J* = 2 Hz, ArH), 6.65 (1H, dd, *J* = 8 and 2 Hz, ArH), 7.13 (1H, d, *J* = 8 Hz, ArH) and 7.75 (1H, s, ArH). ^{13}C NMR (101 MHz, $CDCl_3$) δ: 12.36 (18-CH_3), 23.61, 26.35, 27.44, 29.18, 29.70, 37.16 (CH_2), 39.14 (CH), 43.51 (C), 43.88, 51.65 (CH), 56.19, 5583., 56.94 (OCH_3), 59.45 (17-CH), 97.08, 112.92 (ArCH), 113.57 (ArC), 114.22, 115.48, 126.36 (ArCH), 132.15, 137.91, 143.56, 152.24, 152.55, 154.16 (ArC) and 165.23 (CO). HRMS (ESI) calcd for $C_{27}H_{34}NO_4$ $(M+H)^+$: *m/z* = 436.2482, found *m/z* = 436.2480.

***N*-((13*S*,17*S*)-3-Hydroxy-13-methyl-7,8,9,11,12,13,14,15,16,17-decahydro-6*H*-cyclopenta[a]phenan-thren-17-yl)-2,3-dimethoxybenzamide (Compound 165),** $C_{27}H_{33}NO_4$, MW 435.56,

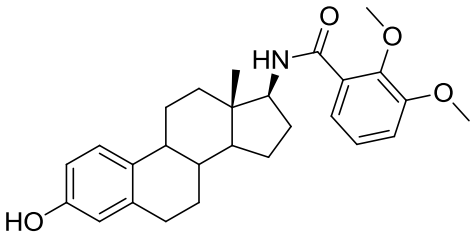

165

N-((13*S*,17*S*)-3-(Benzyloxy)-13-methyl-7,8,9,11,12,13,14,15,16,17-decahydro-6*H*-cyclopenta[a]phenan-thren-17-yl)-2,3-dimethoxybenzamide **160** (92 mg, 0.17 mmol) was dissolved in anhydrous methanol (10 mL) at room temperature and 10% Pd/C (8 mg, 5% mol eq.), was added and the reaction vessel was then charged with hydrogen with the use of a hydrogen balloon and the mixture was stirred overnight. The reaction mixture was filtered through celite and, the filtrate washed with methanol (3 × 15 mL). The organic filtrate was dried ($MgSO_4$) and concentrated *in-vacuo* to give the title compound **165** as a white solid (65 mg, 88%). m.p. 267-269 ºC ^{1}H NMR (400 MHz, $CDCl_3$) δ: 0.82 (3H, s, 18CH_3), 1.36-1.58 (7H, m), 1.73-1.86 (3H, m), 2.14-2.28 (3H, m), 2.81 (2H, s, 6-CH_2), 3.90 (3H, s, OCH_3), 3.92 (3H, s, OCH_3), 6.04 (1H, broad s, OH), 6.60 (1H, d, *J* = 4 Hz, ArH), 6.66 (1H, dd, *J* = 8 and 4 Hz, ArH), 7.03 (1H, dd, *J* = 8 and 4 Hz, ArH), 7.13 (1H, t, *J* = 8 Hz, ArH), 7.16 (1H, d, *J* = 8 Hz, ArH), 7.71 (1H, dd, *J* = 8 and 4 Hz, ArH) and 8.12 (1H, d, *J* = 8 Hz, NH). ^{13}C NMR (101 MHz, $CDCl_3$) δ: 12.41 (18-CH_3), 23.54, 26.33, 27.40, 29.00, 29.65, 37.18 (CH_2), 39.07, 43.54 (CH), 43.87 (C), 51.70 (CH), 56.13 (OCH_3), 59.41 (17-CH), 61.40 (OCH_3), 112.88, 115.31, 115.41, 122.97, 124.56, 126.98 (ArCH), 128.53, 132.24, 138.03, 147.43, 152.59, 153.94 (ArC) and 165.19 (CO), HRMS (ESI) calcd for $C_{27}H_{33}NO_4Na$ $(M+Na)^+$: *m/z* = 458.2307, found *m/z* = 458.2270.

***N*-((13*S*,17*S*)-3-Hydroxy-13-methyl-7,8,9,11,12,13,14,15,16,17-decahydro-6*H*-cyclopenta[a]phenan-thren-17-yl)-2,5-dimethoxybenzamide (Compound 166),** $C_{27}H_{33}NO_4$, MW 435.56,

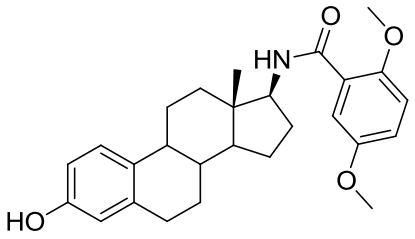

166

N-((13*S*,17*S*)-3-(Benzyloxy)-13-methyl-7,8,9,11,12,13,14,15,16,17-decahydro-6*H*-cyclopenta[a]phenan-thren-17-yl)-2,5-dimethoxybenzamide **161** (125 mg, 0.24 mmol) was dissolved in a mixture of THF / EtOH (3/2, 50 mL) and pumped through an H Cube at 0.8 mL/min, 40 °C, full hydrogen 10% Pd/C. The reaction mixture was collected, dried ($MgSO_4$), filtered and concentrated *in-vacuo* to give the crude product. Re-crystallisation from methanol gave the title compound **166** (71 mg, 68%) as white crystalline needles. ^{1}H NMR (400 MHz, $CDCl_3$) δ: 0.82 (3H, s, 18-CH_3), 1.43 (8H, m), 1.88-1.91 (3H, m), 2.17-2.30 (3H, m), 2.83 (2H, m, 6-CH_2), 3.82 (3H, s, OCH_3), 3.93 (3H, s, OCH_3), 4.74 (1H, s, OH), 6.57 (1H, d, *J* = 2 Hz, ArH), 6.63 (1H, dd, *J* = 8 and 2 Hz, ArH), 6.97 (1H, d, *J* = 2 Hz, ArH), 7.15 (1H, d, *J* = 8 Hz, ArH), 7.78 (1H, d, *J* = 2 Hz, ArH) and 8.08 (1H, d, *J* = 4 Hz, NH). ^{13}C NMR (101 MHz, $CDCl_3$) δ: 12.31 (18-CH_3), 23.58, 26.54, 27.42, 29.08, 29.64, 37.16 (CH_2), 39.09, 43.56 (CH), 43.63 (C), 51.69 (CH), 55.45, 55.84 (OCH_3), 59.41 (17-CH), 112.70, 113.24, 115.27, 115.54, 126.55 (ArCH), 132.56, 137.73, 143.35, 152.14, 153.42, 153.89 (ArC) and 164.86 (CO), HRMS (ESI) calcd for $C_{27}H_{34}NO_4$ $(M+H)^+$: *m/z* = 436.2482, found *m/z* = 436.2465.

***N*-((13*S*,17*S*)-3-Hydroxy-13-methyl-7,8,9,11,12,13,14,15,16,17-decahydro-6*H*-cyclopenta[a]phenan-thren-17-yl)-2,4,5-trimethoxybenzamide (Compound 167),** $C_{28}H_{35}NO_5$, MW 465.58,

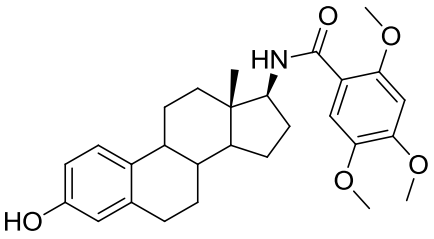

167

N-((13*S*,17*S*)-3-(Benzyloxy)-13-methyl-7,8,9,11,12,13,14,15,16,17-decahydro-6*H*-cyclopenta[a]phenan-thren-17-yl)-2,4,5-trimethoxybenzamide **158** (85 mg, 0.15 mmol) was dissolved in a mixture of THF / EtOH (3/2, 50 mL) and pumped through an H Cube at 0.8 mL/min, 40 °C, full hydrogen 10% Pd/C. The reaction mixture was collected, dried ($MgSO_4$), filtered and concentrated *in-vacuo* to give the crude product. Re-crystallisation from MeOH gave the title compound **167** (61 mg, 87%) as white crystalline needles. ^{1}H NMR (400 MHz, $CDCl_3$) δ: 0.80 (3H, s, 18-CH_3), 1.38-1.46 (8 H, m), 1.82-1.88 (4H, m), 2.19-2.27 (4H, m), 2.80 (2H, m, 6-CH_2), 3.87 (3H, s, OCH_3), 3.92 (3H, s, OCH_3), 3.95 (3H, s, OCH_3), 6.53 (1H, s, ArH), 6.60 (1H, d, *J* = 2 Hz, ArH), 6.67 (1H, dd, *J* = 8 and 2 Hz, ArH), 7.10 (1H, d, *J* = 8 Hz, ArH), 7.77 (1H, s, ArH) and 8.03 (1H, d, *J* = 8 Hz, NH). ^{13}C NMR (101 MHz, $CDCl_3$) δ: 12.34 (18-CH_3), 23.58, 26.34, 27.42, 29.15, 29.67, 37.13 (CH_2), 39.11 (CH), 43.49 (C), 43.86, 51.62 (CH), 56.19, 56.26, 56.96 (OCH_3), 59.42 (17-CH), 97.05, 112.94 (ArCH), 113.59 (ArC), 114.20, 115.46, 126.38 (ArCH), 132.13, 137.99, 143.55, 152.22, 152.57, 154.12 (ArC) and 165.20 (CO). HRMS (ESI) calcd for $C_{28}H_{36}NO_5$ $(M+H)^+$: *m/z* = 466.2588, found *m/z* = 466.2578.

(13*S*,*Z*)-3-(Benzyloxy)-16-(hydroxymethylene)-13-methyl-7,8,9,11,12,13,15,16-octahydro-6*H*-cyclopenta[a]-phenan-thren-17(14*H*)-one (Compound 170),
$C_{26}H_{28}O_3$, MW 388.50,

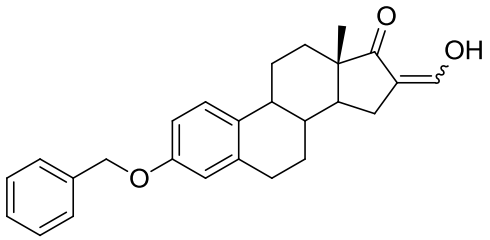

170

Potassium *tert*-butoxide (4.7g, 41 mmol) was added portion-wise to a stirred solution of (13*S*)-3-(benzyloxy)-13-methyl-7,8,9,11,12,13,15,16-octahydro-6*H*-cyclopenta[a]-phenan-thren-17(14*H*)-one **156** (5.0 g, 14 mmol) in toluene (125 mL) at room temperature under an atmosphere of nitrogen. After 20 min ethyl formate (7.4 mL, 97 mmol) was added over 5 min and the resulting suspension was stirred for 2.5 h. The reaction mixture was poured onto water (150 mL) and acidified with 5 M HCl. The organics were extracted with ethyl acetate (3 × 75 mL), washed with brine (100 mL), dried ($MgSO_4$), filtered and concentrated *in-vacuo* to give the crude product. The crude product was purified on silica by flash chromatography DCM / MeOH (0 – 5%) to give the title compound **170** (2.99 g, 55%) as white solid. m.p. 147-149 ºC, IR (KBr): 542-1499, 1606, 1699, 2925, 3230 cm^{-1}, ^{1}H NMR (400 MHz, $CDCl_3$) δ: 0.98 (3H, s, 18-CH_3), 1.41-1.52 (2H, m), 1.53-1.61 (6H, m), 1.93-2.07 (2H, m), 2.16-2.21 (1H, m), 2.27-2.32 (1H, m), 2.38-2.42 (1H, m), 2.46-2.49 (1H, m), 2.88-2.90 (2H, m, 6-CH_2), 5.04 (2H, s, 3-OCH_2), 6.74 (1H, s, ArH), 6.79 (1H, d, *J* = 8 Hz, ArH), 7.09 (1H, s, 16-CC*H*OH), 7.20 (1H, d, *J* = 8 Hz, ArH), 7.32 (1H, t, *J* = 8 Hz, ArH), 7.36 (2H, t, *J* = 8 Hz, 2 × ArH) and 7.43 (2H, d, *J* = 8 Hz, 2 × ArH), ^{13}C NMR (101 MHz, $CDCl_3$) δ: 14.62 (18-CH_3), 24.78, 25.87, 26.82, 29.60, 31.57 (CH_2), 38.02, 44.03 (CH), 48.93 (C), 51.04 (CH), 70.03 (3-O*C*H_2), 112.56, 115.00, 126.23 (ArCH), 127.43 (2 × ArCH), 127.87 (ArCH), 128.55 (2 × ArCH), 132.35 (16-C), 137.32, 137.75, 156.96 (ArC), 197.76 (16-C*C*HOH) and 214.88 (CO), LRMS (ESI) calcd for $C_{26}H_{29}O_3$ $(M+H)^+$: *m/z* = 388.2, found *m/z* = 388.1. Data obtained for melting point is identical to that in the literature.[78]

(*Z*)-Methyl 3-((13*S*)-3-(benzyloxy)-13-methyl-17-oxo-7,8,11,12,13,14,15,17-octahydro-6*H*-cyclopenta[a]-phenan-thren-16(9*H*)-ylidene)propanoate (Compound 171), $C_{29}H_{32}O_4$, MW 444.56,

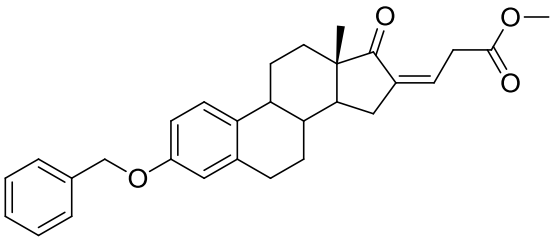

171

To a solution of (13*S*,*Z*)-3-(benzyloxy)-16-(hydroxymethylene)-13-methyl-7,8,9,11,12,13,15,16-octahydro-6*H*-cyclopenta[a]-phenan-thren-17(14*H*)-one **170** (2.82 g, 7.26 mmol) in chloroform (50 mL) was added (triphenylphosphoranylidene)acetate (2.42 g, 7.26 mmol). The mixture was stirred at room temperature overnight. The reaction mixture was concentrated *in-vacuo* and the residue was purified by flash chromatography $CHCl_3$ / acetone (100/1) followed by re-crystallization from MeOH to give the title compound **171** (2.78 g, 86%) as colorless needles. m.p. 179-181 °C, ^{1}H NMR (400 MHz, $CDCl_3$) δ: 0.93 (3H, s, 18-CH_3), 1.42-1.69 (5H, m), 1.94-2.06 (2H, m), 2.13 (1H, t, *J* = 8 Hz), 2.20-2.28 (1H, m), 2.36-2.42 (1H, m), 2.66 (1H, dd, *J* = 8 and 4 Hz), 2.87-2.94 (2H, m, 6-CH_2), 3.23 (2H, d, *J* = 8 Hz, 16-CCHC*H*$_2$), 3.73 (3H, s, OCH_3), 5.02 (2H, s, 3-OCH_2), 6.75 (1H, d, *J* = 4 Hz, ArH), 6.77 (1H, t, *J* = 8 Hz, 16-CCH), 6.81 (1H, dd, *J* = 8 and 4 Hz, ArH), 7.21 (1H, d, *J* = 8 Hz, ArH), 7.31 (1H, t, *J* = 8 Hz, ArH), 7.38 (2H, t, *J* = 8 Hz, 2 × ArH) and 7.43 (2H, d, *J* = 8 Hz, 2 × ArH). ^{13}C NMR (101 MHz, $CDCl_3$) δ: 14.44 (18-CH_3), 25.97, 26.40, 26.80, 29.66, 31.62, 35.01 (CH_2), 37.93, 44.03 (CH), 47.72 (C), 48.46 (CH), 52.15 (OCH_3), 69.98 (3-OCH_2), 112.49, 115.03, 126.32 (ArCH), 127.45 (2 × ArCH), 127.88 (ArCH), 128.58 (2 × ArCH), 132.35 (16-C), 137.39, 137.72 (ArC), 139.90 (16-C*C*H), 156.99 (ArC), 170.53 (*C*OOCH$_3$) and 207.70 (CO), LRMS (ESI) calcd for $C_{29}H_{33}O_4$ $(M+H)^+$: *m/z* = 445.2, found *m/z* = 445.3, HRMS (FAB^+) calcd for $C_{29}H_{33}O_4$ $(M+H)^+$: 445.2373, found 445.2368.

Methyl 3-((13*S*)-3-hydroxy-13-methyl-17-oxo-7,8,9,11,12,13,14,15,16,17-decahydro-6*H*-cyclopenta[a]-phenan-thren-16-yl)propanoate (Compound 172), $C_{22}H_{22}O_4$, MW 356.46,

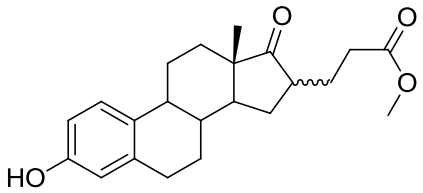

172

(*Z*)-Methyl-3-((13*S*)-3-(benzyloxy)-13-methyl-17-oxo-7,8,11,12,13,14,15,17-octahydro-6*H*-cyclopenta[a]-phenan-thren-16(9*H*)-ylidene)propanoate **171** (2.66 g, 5.98 mmol) was dissolved in anhydrous MeOH / THF (1/1, 120 mL). 10% Pd/C (160 mg, 0.60 mmol) was added to the reaction mixture and placed under an atmosphere of hydrogen. The reaction mixture was stirred for 18 h, and filtered over celite. The reaction filtrate was concentrated *in-vacuo* to give the crude product (1.77 g, 83%). The residue was purified by flash chromatography $CHCl_3$ / acetone (10:1) followed by crystallization from MeOH to give the title compound **172** as colourless crystalline needles (2.08 g, 98%). m.p. 178-180 ºC, ^{1}H NMR (400 MHz, $CDCl_3$) δ: 0.84 (3H, s, 18-CH_3), 1.12-1.55 (6H, m), 1.67-1.79 (1H, m), 1.94-2.03 (2H, m), 2.14-2.27 (4H, m), 2.31-2.38 (1H, m), 2.47 (2H, t, *J* = 8 Hz, 16-$CHCH_2CH_2$), 2.84 (2H, m, 6-CH_2), 3.69 (3H, s, OCH_3), 5.89 (1H, broad s, OH), 6.58 (1H, d, *J* = 4 Hz, ArH), 6.65 (1H, dd, *J* = 8 and 4 Hz, ArH) and 7.11 (1H, d, *J* = 8 Hz, ArH). ^{13}C NMR (101 MHz, $CDCl_3$) δ: 14.05 (18-CH_3), 25.84, 26.71, 27.64, 28.48, 29.46, 31.89, 32.59 (CH_2), 37.95, 44.07 (CH), 48.41 (C), 48.60, 48.87 (CH), 51.75 (OCH_3), 112.97, 115.38, 126.38 (ArCH), 131.75, 137.87, 153.93 (ArC) and 173.90 (CO), LRMS (ESI) calcd for $C_{22}H_{23}O_4$ $(M+H)^+$: *m/z* = 357.2, found *m/z* = 357.2.

3-((13*S*)-3-Hydroxy-13-methyl-17-oxo-7,8,9,11,12,13,14,15,16,17-decahydro-6*H*-cyclopenta[a]-phenan-thren-16-yl)propanoic acid (Compound 173), $C_{21}H_{26}O_4$, MW 342.43,

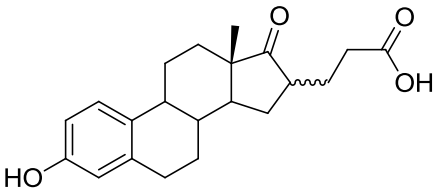

173

Methyl-3-((13*S*)-3-hydroxy-13-methyl-17-oxo-7,8,9,11,12,13,14,15,16,17-decahydro-6*H*-cyclopenta[a]-phenan-thren-16-yl)propanoate **172** (2.00 g, 5.61 mmol) was dissolved in 3 M NaOH (150 mL) and heated to reflux for 2 h. The reaction mixture was neutralised with 6 M HCl and the organics extracted with DCM (3 × 50 mL), dried ($MgSO_4$), filtered and concentrated *in-vacuo* to give the crude product (1.40 g, 73%). The residue was purified by flash chromatography DCM / MeOH (0–10%) followed by crystallization from MeOH to give the title compound **173** as colourless crystalline needles (1.84 g, 96%). ^{1}H NMR (400 MHz, $CDCl_3$) δ: 0.88 (1.5H, s, 18-CH_{3A}), 0.95 (1.5H, s, 18-CH_{3B}), 1.37-1.52 (6H, m), 1.98-2.36 (9H, m), 2.86 (2H, m, 6-CH_2), 6.57 (1H, d, *J* = 4 Hz, ArH), 6.65 (1H, dd, *J* = 8 and 4 Hz, ArH) and 7.14 (1H, d, *J* = 8 Hz, ArH). ^{13}C NMR (101 MHz, $CDCl_3$) δ: 14.02 (18-CH_3), 25.81, 26.46, 26.71, 27.45, 27.60, 28.38, 29.44, 31.91, 32.53 (CH_2), 37.96 (CH), 38.33 (C), 43.97, 48.37, 48.84 (CH), 113.05, 115.39, 126.07 (ArCH), 130.61, 137.53, 154.99 (ArC), 175.10 (CO) and 220.13 (CO), LRMS (ESI) calcd for $C_{21}H_{27}O_4$ $(M+H)^+$: *m/z* = 343.2, found *m/z* = 343.2.

3-((13*S*)-3-Hydroxy-13-methyl-17-oxo-7,8,9,11,12,13,14,15,16,17-decahydro-6*H*-cyclopenta[a]-phenan-thren-16-yl)-*N*-(pyridin-2-ylmethyl)propanamide (Compound 174), $C_{27}H_{32}N_2O_2$, MW 432.55,

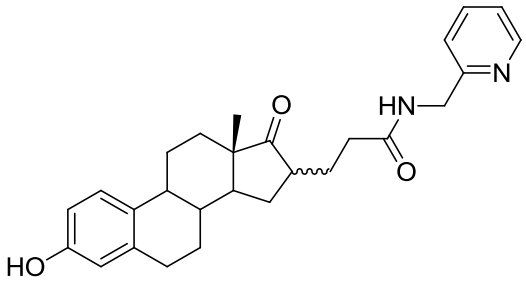

174

To a solution of 2-picoylamine (0.07 ml, 0.70 mmol) in DCM (15 mL) EDCI.HCl (112 mg, 0.58 mmol) was added portion-wise followed by addition of DMAP (71 mg, 0.58 mmol) and triethylamine (0.27 mL, 1.93 mmol). The resulting reaction mixture was stirred for 15 min at room temperature. A solution of 3-((13*S*)-3-hydroxy-13-methyl-17-oxo-7,8,9,11,12,13,14,15,16,17-decahydro-6*H*-cyclopenta[a]-phenan-thren-16-yl)propanoic acid **173** (200 mg, 0.58 mmol) in DCM (5 mL) was added portion-wise to the reaction mixture and the mixture stirred for 18 h at room temperature. The reaction was quenched with saturated ammonium chloride (15 mL). The crude products were extracted with DCM (2 × 15 mL), dried ($MgSO_4$), filtered and evaporated *in-vacuo* to give the crude product. The crude product was then purified by flash chromatography DCM / MeOH (0 – 5%) to yield the title compound **174** (115 mg, 46%) as an amorphous pale yellow solid. m.p. 179-183 ºC, ^{1}H NMR (400 MHz, $CDCl_3$) δ: 0.72 (18-CH_3), 1.36-1.47 (7H, m), 2.10-2.31 (4H, m), 2.39-2.44 (3H, m), 2.83 (2H, m, 6-CH_2), 4.57 (2H, d, *J* = 4 Hz, NHCH_2), 6.59 (1H, s, ArH), 6.61 (1H, dd, *J* = 9 Hz, ArH), 7.00 (1H, d, *J* = 9 Hz, ArH), 7.21 (1H, t, *J* = 5 Hz, ArH), 7.30 (1H, d, *J* = 5 Hz, ArH), 7.68 (1H, t, *J* = 5 Hz, ArH) and 8.54 (1H, d, *J* = 5 Hz, ArH). ^{13}C NMR (101 MHz, $CDCl_3$) δ: 13.87 (18-CH_{3A}), 13.98 (18-CH_{3B}), 25.75, 26.68, 27.49, 27.71, 28.44, 28.62, 31.67, 31.78, 34.85, 35.03, 37.93, 38.19 (CH_2), 43.90, 44.39, 48.25 (CH), 48.46 (C), 48.82 (CH), 113.05, 115.46, 122.40, 122.52, 126.30 (ArCH), 131.30 (ArC), 137.05 (ArCH), 137.66 (ArC), 148.81 (ArCH), 154.41, 156.32 (ArC), 172.99 (CONH) and 222.18 (CO), HRMS (ESI) calcd for $C_{27}H_{33}N_2O_2$ $(M+H)^+$: *m/z* = 433.2486, found *m/z* = 433.2470.

3-((13*S*)-3-Hydroxy-13-methyl-17-oxo-7,8,9,11,12,13,14,15,16,17-decahydro-6*H*-cyclopenta[a]phenan-thren-16-yl)-*N*-(pyridin-3-ylmethyl)propanamide (Compound 175), $C_{27}H_{32}N_2O_2$, MW 432.55,

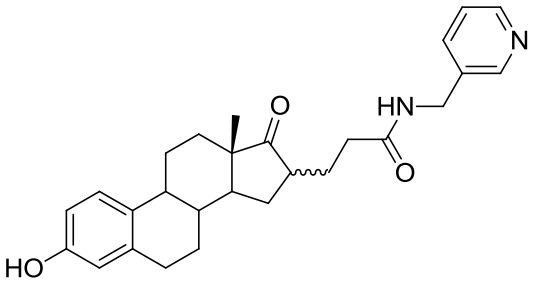

175

To a solution of 3-picoylamine (0.07 ml, 0.70 mmol) in DCM (15 mL) EDCI.HCl (112 mg, 0.58 mmol) was added portion-wise followed by addition of DMAP (71 mg, 0.58 mmol) and triethylamine (0.27 mL, 1.93 mmol). The resulting reaction mixture was then stirred for 15 min at room temperature. A solution of 3-((13*S*)-3-hydroxy-13-methyl-17-oxo-7,8,9,11,12,13,14,15,16,17-decahydro-6*H*-cyclopenta[a]-phenan-thren-16-yl)propanoic acid **173** (200 mg, 0.58 mmol) in DCM (5 mL) was added portion-wise to the reaction mixture and the mixture stirred for 18 h at room temperature. The reaction was quenched with saturated ammonium chloride (15 mL). The crude products were extracted with DCM (2 × 15 mL), dried ($MgSO_4$), filtered and evaporated *in-vacuo* to give the crude product. The crude product was purified by flash chromatography DCM / MeOH (0 – 5%) to yield the title compound **175** (130 mg, 52%) as an amorphous pale yellow solid. m.p. 178-182 ºC, ^{1}H NMR (400 MHz, $CDCl_3$) δ: 0.85 (3H, s, 18-CH_3), 1.15-1.53 (7H, m), 1.76-2.01 (4H, m), 2.09-2.43 (3H, m), 2.78 (2H, m, 6-CH_2), 4.45 (2H, s, NHC*H*$_2$), 6.53 (1H, s, ArH), 6.64 (1H, t, *J* = 6 Hz, ArH), 6.83 (1H, d, *J* = 5 Hz, ArH), 7.01 (1H, d, *J* = 5 Hz, ArH), 7.29 (1H, d, *J* = 6 Hz, ArH), 7.67 (1H, d, *J* = 6 Hz, ArH) and 8.50 (1H, s, ArH), ^{13}C NMR (101 MHz, $CDCl_3$) δ: 13.94 (18-CH_{3A}), 14.06 (18-CH_{3B}), 25.70, 26.62, 28.50, 29.44, 31.76, 34.64 (CH_2), 37.90 (CH), 40.97 (NH*C*H$_2$), 43.85, 47.66 (CH), 48.53 (C), 48.67 (CH), 113.04, 115.44, 123.75, 126.24 (ArCH), 131.04 (ArC), 134.33 (ArCH), 136.04, 137.71 (ArC), 148.32, 148.65 (ArCH), 154.53 (ArC), 172.99 (CONH) and 222.88 (CO), HRMS (ESI) calcd for $C_{27}H_{33}N_2O_2$ $(M+H)^+$: *m/z* = 433.2486, found *m/z* = 433.2473.

3-((13*S*)-3-Hydroxy-13-methyl-17-oxo-7,8,9,11,12,13,14,15,16,17-decahydro-6*H*-cyclopenta[a]-phenan-thren-16-yl)-*N*-(pyridin-4-ylmethyl)propanamide (Compound 176), $C_{27}H_{32}N_2O_2$, MW 432.55,

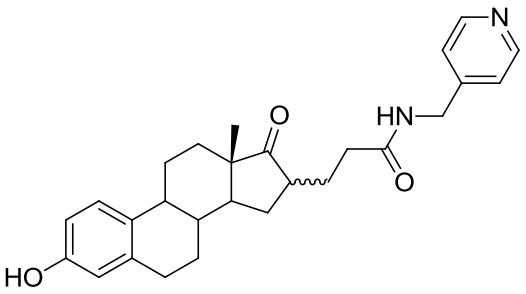

176

To a solution of 4-picoylamine (0.07 ml, 0.70 mmol) in DCM (15 mL) EDCI.HCl (112 mg, 0.58 mmol) was added portion-wise followed by addition of DMAP (71 mg, 0.58 mmol) and triethylamine (0.27 mL, 1.93 mmol). The resulting reaction mixture was stirred for 15 min at room temperature. 3-((13*S*)-3-hydroxy-13-methyl-17-oxo-7,8,9,11,12,13,14,15,16,17-decahydro-6*H*-cyclopenta[a]-phenan-thren-16-yl)propanoic acid **173** (200 mg, 0.58 mmol) in DCM (5 mL) was added drop-wise to the reaction mixture and stirred the mixture for 18 h at room temperature. The reaction was quenched with saturated ammonium chloride (15 mL). The crude products were extracted with DCM (2 × 15 mL), dried ($MgSO_4$), filtered and evaporated *in-vacuo* to give the crude product. The crude product was then purified by flash chromatography DCM / MeOH (0 – 5%) to yield the title compound **176** (128 mg, 51%) as an amorphous yellow solid. m.p. 163-165 ºC, ^{1}H NMR (400 MHz, $CDCl_3$) δ: 0.87 (3H, s, 18-CH_3), 1.39-1.54 (7H, m), 1.92-2.24 (4H, m), 2.27-2.51 (3H, m), 2.90 (2H, m, 6-CH_2), 4.46 (2H, d, *J* = 3 Hz, NHC*H*$_2$), 6.59 (1H, s, ArH), 6.64 (1H, dd, *J* = 7 and 2 Hz, ArH), 6.84 (1H, d, *J* = 7 Hz, ArH), 7.22 (2H, d, *J* = 6 Hz, 2 × ArH) and 8.54 (2H, d, *J* = 6 Hz, 2 × ArH). ^{13}C NMR (101 MHz, $CDCl_3$) δ: 14.00 (18-CH_{3A}), 14.08 (18CH_{3B}), 25.80, 26.50, 28.79, 28.87, 31.70, 32.90, 34.57 (CH_2), 37.94 (CH), 42.16 ($NHCH_2$), 44.01, 47.67 (CH), 48.36 (C), 48.87 (CH), 112.99, 115.40 (ArCH), 122.46 (2 × ArCH), 131.35, 137.77, 147.83 (ArC), 149.64 (2 × ArCH), 154.23 (ArC), 172.99 (CONH) and 222.88 (CO), HRMS (ESI) calcd for $C_{27}H_{33}N_2O_2$ $(M+H)^+$: *m/z* = 433.2486, found *m/z* = 433.2470.

(13*S*)-2-Ethyl-3-methoxy-13-methyl-7,8,9,11,12,13,15,16-octahydro-6*H*-cyclopenta[a]-phenan-thren-17(14*H*)-one (Compound 177), $C_{21}H_{28}O_2$, MW 312.45,

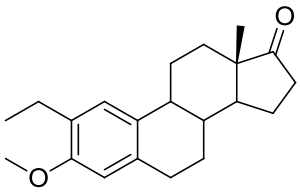

177

Potassium carbonate (9.26 g, 67 mmol) was added portion-wise to a solution of (13*S*)-2-ethyl-3-hydroxy-13-methyl-7,8,9,11,12,13,15,16-octahydro-6*H*-cyclopenta[a]-phenan-thren-17(14*H*)-one (4.968 g, 17 mmol) in anhydrous DMF (50 mL). The resulting mixture was stirred for 10 mins under an atmosphere of nitrogen. To the reaction mixture was added methyl iodide (2.30 mL, 37 mmol) drop-wise and the reaction mixture was stirred at room temperature for 2 d. Water was slowly added to the stirred solution and the product precipitated. The product was filtered from the solution and dried in an oven at 105 °C for 2 h to give the title compound **177** (5.31 g, 100%) as a white solid. m.p. 105-108 °C, ^{1}H NMR (400 MHz, $CDCl_3$): δ 0.84 (3H, s, 18-CH_3), 1.10 (3H, t, *J* = 8 Hz, 2-$CCH_2C\mathit{H}_3$), 1.34-1.59 (7H, m), 1.91-2.09 (5H, m), 2.12-2.23 (1H, m), 2.35-2.46 (2H, m), 2.54 (2H, quart, *J* = 8 Hz, 2-$CC\mathit{H}_2$), 2.82 (2H, m, 6-CH_2), 3.73 (3H, s, OCH_3), 6.51 (1H, s, ArH) and 7.01 (1H, s, ArH). ^{13}C NMR (101 MHz, $CDCl_3$): δ 13.83 (18-CH_3), 14.49 (2-$CCH_2\mathit{C}H_3$), 21.55 (CH_2), 23.20 (2-$C\mathit{C}H_2$), 25.99, 26.65, 29.53, 31.64, 35.82 (CH_2), 38.49, 44.03 (CH), 47.98 (C), 50.41 (CH), 55.29 (OCH_3), 110.67, 126.04 (ArCH), 130.07, 131.33, 134.65, 155.43 (ArC) and 220.31 (CO).

(13*S*,*Z*)-2-Ethyl-16-(hydroxymethylene)-3-methoxy-13-methyl-7,8,9,11,12,13,15,16-octahydro-6*H*-cyclopenta[a]-phenan-thren-17(14*H*)-one (Compound 178), $C_{22}H_{28}O_3$, MW 340.46,

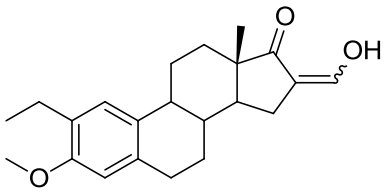

178

Potassium *tert*-butoxide (8.08g, 72 mmol) was added portion-wise to a stirred solution of (13*S*)-2-ethyl-3-methoxy-13-methyl-7,8,9,11,12,13,15,16-octahydro-6*H*-cyclopenta[a]-phenan-thren-17(14*H*)-one **177** (7.5 g, 24 mmol) in toluene (175 mL) at room temperature under an atmosphere of nitrogen. After 20 min ethyl formate (12.97 mL, 170 mmol) was added over 5 min and the resulting suspension was stirred for 2.5 h. The reaction mixture was poured onto water (200 mL) and acidified with 5 M HCl. The organics were extracted with ethyl acetate (3 × 100 mL), washed with brine (200 mL), dried ($MgSO_4$), filtered and concentrated *in-vacuo* to give the crude product. The crude product was purified on silica by flash chromatography DCM / MeOH (0 – 5%) to give the title compound **178** as an amorphous white solid (3.51 g, 43%). IR (KBr): 542-1409, 1464, 1505, 1612, 1718, 2866, 2933, 3421 cm^{-1}, ^1H NMR (400 MHz, $CDCl_3$): δ 1.02 (3H, s, 18-CH_3), 1.25 (3H, t, *J* = 8 Hz, 2-CCH_2CH_3), 1.39-1.67 (5H, m), 2.03-2.34 (4H, m), 2.46-2.49 (2H, m), 2.64 (2H, quart, *J* = 8 Hz, 2-CCH_2), 2.94 (2H, m, 6-CH_2), 3.84 (3H, s, OCH_3), 6.62 (1H, s, ArH) and 7.12 (1H, s, ArH). ^{13}C NMR (101 MHz, $CDCl_3$): δ 14.64 (18-CH_3), 15.34 (2-CCH_2CH_3), 23.35, 24.82, 25.71, 26.73, 29.56, 31.24 (CH_2), 37.95, 44.06 (CH), 47.69 (C), 48.98 (CH), 55.36 (OCH_3), 110.78 (ArCH), 112.58 (ArC), 126.00 (ArCH), 130.20 (16-C), 131.40, 134.70, 155.56 (ArC), 196.78 (16-C*C*HOH) and 211.98 (CO), LRMS (ESI) calcd for $C_{22}H_{29}O_3$ $(M+H)^+$: *m/z* = 341.2, found *m/z* = 341.1.

(13*S*,16*R*)-2-Ethyl-3-methoxy-13-methyl-17-oxo-7,8,9,11,12,13,14,15,16,17-decahydro-6*H*-cyclopenta[a]-phenan-threne-16-carbonitrile (Compound 180), $C_{22}H_{27}NO_2$, MW 337.46,

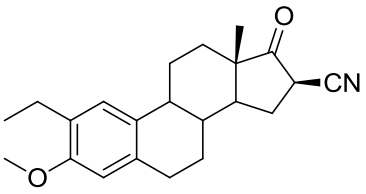

180

(13*S*,*Z*)-2-Ethyl-16-(hydroxymethylene)-3-methoxy-13-methyl-7,8,9,11,12,13,15,16-octahydro-6*H*-cyclopenta[a]-phenan-thren-17(14*H*)-one **178** (1.93 g, 5.68 mmol) was added portionwise to a solution of pyridine in anhydrous toluene (75 mL) and 2,2,2-trifluoro-*N*-(2,2,2-trifluoroacetoxy)acetamide which was prepared in accordance with the literature procedure[126] **179** (3.83 g, 17.04 mmol) by reacting hydroxylamine hydrochloride (5.63 g, 81 mmol) and trifluoroacetic anhydride (28.15 mL, 0.20 mol) at reflux for 1.5 h under atmosphere of nitrogen. The resulting mixture was heated to reflux for 3 h. The reaction mixture was cooled and the reaction was quenched with water (40 mL). The organics were extracted with DCM (2 × 75 mL), washed with brine (40 mL), dried ($MgSO_4$), filtered and concentrated *in-vacuo* to give the crude product. The crude product was re-crystallised from DCM to give the title compound **180** as pale yellow cubic crystals (2.35 g, 41%). IR (KBr): 532-1456, 1499, 1574, 1611, 1745, 2245, 2858, 2904 cm^{-1}, ^1H NMR (400 MHz, $CDCl_3$): δ 1.00 (3H, s, 18-CH_3), 1.13 (3H, t, *J* = 8 Hz, 2-CCH_2CH_3), 1.38-1.47 (4H, m), 1.54-1.62 (1H, m), 1.87-2.02 (3H, m), 2.17-2.26 (1H, m), 2.36-2.43 (1H, m), 2.45-2.53 (1H, m), 2.56 (2H, quart, *J* = 8 Hz, 2-CCH_2), 2.85 (2H, m, 6-CH_2), 3.03 (1H, t, *J* = 5 Hz, 16-CH), 3.72 (3H, s, OCH_3), 6.65 (1H, s, ArH) and 7.01 (1H, s, ArH), ^{13}C NMR (101 MHz, $CDCl_3$): δ 14.15 (18-CH_3), 14.52 (2-CCH_2CH_3), 23.34, 25.66, 26.34, 28.04, 29.29, 32.70 (CH_2), 36.64, 37.93 (CH), 43.87 (16-CH), 48.36 (C), 48.26 (CH), 55.34 (OCH_3), 110.72 (ArCH), 117.40 (16-CHC), 125.99 (ArCH), 130.25, 130.52, 134.42 (C), 155.63 (ArC) and 207.84 (CO), LRMS (ESI) calcd for $C_{22}H_{28}NO_2$ $(M+H)^+$: *m/z* = 337.2, found *m/z* = 337.2.

(13*S*,16*R*,17*S*)-16-(Aminomethyl)-2-ethyl-3-methoxy-13-methyl-7,8,9,11,12,13,14,15,16,17-decahydro-6*H*-cyclopenta[a]-phenan-thren-17-ol (Compound 181), $C_{22}H_{33}NO_2$, MW 343.50,

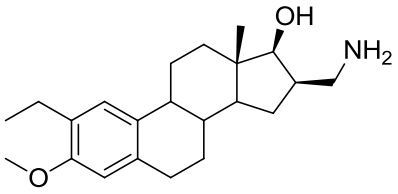

181

Prepared by modification to the literature procedure.[127]

A solution of (13*S*,16*R*)-2-ethyl-3-methoxy-13-methyl-17-oxo-7,8,9,11,12,13,14,15,16,17-decahydro-6*H*-cyclopenta[a]-phenan-threne-16-carbonitrile **180** (1.26 g, 3.73 mmol) in anhydrous THF (75 mL) was added drop-wise to a suspension of $LiAlH_4$ (424 mg, 11.20 mmol) in THF (50 mL) at 4 ºC under at atmosphere of nitrogen, and stirred overnight at 22 ºC. The excess of $LiAlH_4$ was destroyed by the successive drop-wise additions of water (25 mL), 15% aqueous NaOH (15 mL) and water (25 mL). The reaction mixture was filtered and the solid fraction was washed with THF (4 × 50 mL) after evaporation of the solvent the crude residue was purified by flash chromatography DCM / MeOH (0-10%) to give the title compound **181** as an amorphous white solid (973 mg, 76%). m.p. 160-163 ºC, IR (KBr): 556-1464, 1506, 1543, 1613, 2924, 3146, 3677 cm^{-1}, ^1H NMR (400 MHz, MeOD): δ 0.78 (3H, s, 18-CH_3), 1.11 (3H, t, *J* = 8 Hz, 2-CCH_2CH_3), 1.27-1.44 (5H, m), 1.84-1.98 (3H, m), 2.13-2.17 (1H, m), 2.21-2.31 (2H, m), 2.54 (2H, quart, *J* =8 Hz, 2-CCH_2), 2.80 (2H, m, 6-CH_2), 3.76 (3H, s, OCH_3), 6.55 (1H, s, ArH) and 6.99 (1H, s, ArH). ^{13}C NMR (101 MHz, MeOD): δ 13.12 (18-CH_3), 15.17 (2-CCH_2CH_3), 24.32, 27.65, 28.87, 30.69, 30.94, 31.38 (CH_2), 38.96 (16-CH), 39.95, 43.55 (CH), 45.41 (C), 50.15 (CH), 55.69 (OCH_3), 83.21 (17-CH), 111.70, 126.96 (ArCH), 130.79, 133.18, 136.00 (ArC) and 156.65 (ArC), LRMS (ESI) calcd for $C_{22}H_{34}NO_2$ $(M+H)^+$: *m/z* = 344.2, found *m/z* = 344.2, HRMS (ESI) calcd for $C_{22}H_{34}NO_2$ $(M+H)^+$: *m/z* = 344.2584, found *m/z* = 344.2575.

***N*-(((13*S*,16*R*,17*S*)-2-Ethyl-17-hydroxy-3-methoxy-13-methyl-7,8,9,11,12,13,14,15,16,17-decahydro-6*H*-cyclopenta[a]-phenan-thren-16-yl)methyl)-2-(pyridin-2-yl)acetamide (Compound 182),** $C_{29}H_{38}N_2O_3$, MW 462.62,

Fischer J med chem 2005 48 18 5749

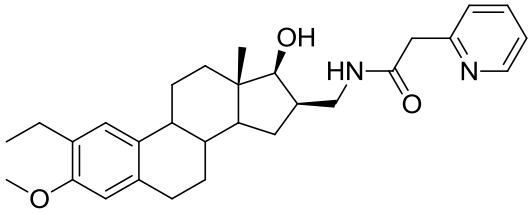

182

To a solution of 4-pyridylacetic acid hydrochloride (189 mg, 1.09 mmol) in DCM (12 mL), EDCI.HCl (238 mg, 1.24 mmol) was added portion-wise, followed by addition of DMAP (catalytic) and triethylamine (0.36 mL, 2.55 mmol). The resulting reaction mixture was stirred for 15 min at room temperature. A solution of (13*S*,16*R*,17*S*)-16-(aminomethyl)-2-ethyl-3-methoxy-13-methyl-7,8,9,11,12,13,14,15,16,17-decahydro-6*H*-cyclopenta[a]-phenan-thren-17-ol **181** (250 mg, 0.73 mmol) in DCM (5 mL) was added drop-wise to the reaction mixture, which was stirred for 18 h at room temperature. The reaction was quenched with saturated ammonium chloride (20 mL). The crude products were extracted with DCM (2 × 20 mL), dried ($MgSO_4$), filtered and evaporated *in-vacuo* to give the crude product. The crude product was then purified by flash chromatography DCM / MeOH (0 – 5%) to yield the title compound **182** (159 mg, 47%) as an amorphous yellow solid. ^{1}H NMR (400 MHz, $CDCl_3$): δ 0.73 (3H, s, 18-CH_3), 1.03-1.13 (2H, m), 1.16 (3H, t, *J* = 7 Hz, 2-CCH_2CH_3), 1.25-1.44 (3H, m), 1.81-1.94 (3H, m), 2.13-2.18 (1H, m), 2.26-2.32 (2H, m, CH_2), 2.56 (2H, quart, *J* = 7 Hz, 2-CH_2), 2.81(2H, m, 6-CH_2), 3.15 (1H, td, *J* = 7 and 3 Hz, CH), 3.56 (OCH_3), 3.77 (2H, s, CH_2), 6.54 (1H, s, ArH), 7.01 (1H, s, ArH), 7.16 (1H, d, *J* = 6 Hz, ArH), 7.29 (1H, t, *J* = 6 Hz, ArH), 7.64 (2H, t, *J* = 6 Hz, ArH) and 8.54 (2H, d, *J* = 6 Hz, ArH). ^{13}C NMR (101 MHz, $CDCl_3$): δ 12.74 (18-CH_3), 14.50 (2-CCH_2CH_3), 23.18, 26.34, 27.43, 29.53, 29.83, 37,64 (CH_2), 38.25, 40.59 (CH), 41.17 (C), 43.66 (CH_2), 44.03 (CH), 44.19 (CH_2), 48.71 (CH), 55.26 (OCH_3), 81.70 (CH), 110.65, 121.88, 123.94, 125.97 (ArCH), 129.82, 134.85 (ArC) 136.85, 149.04 (ArCH), 154.48, 155.88 (ArC) and 168.54 (CO), HRMS (ESI) calcd for $C_{29}H_{39}N_2O_3$ $(M+H)^+$: *m/z* = 463.2955, found *m/z* = 463.2943.

***N*-(((13*S*,17*S*)-2-Ethyl-17-hydroxy-3-methoxy-13-methyl-7,8,9,11,12,13,14,15,16,17-decahydro-6*H*-cyclopenta[a]-phenan-thren-16-yl)methyl)-2-(pyridin-3-yl)acetamide (Compound 183),** $C_{29}H_{38}N_2O_3$, MW 462.62,

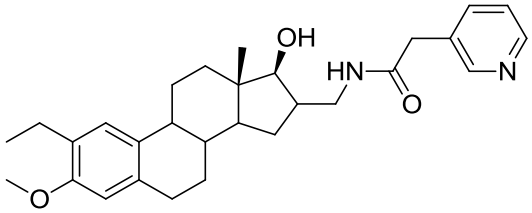

183

To a solution of 3-pyridylacetic acid hydrochloride (198 mg, 1.14 mmol) in DCM (15 mL) EDCI.HCl (252 mg, 1.32 mmol) was added portion-wise followed by addition of DMAP (catalytic) and triethylamine (0.39 mL, 2.88 mmol). The resulting reaction mixture was stirred for 15 min at room temperature. A solution of (13*S*,16*R*,17*S*)-16-(aminomethyl)-2-ethyl-3-methoxy-13-methyl-7,8,9,11,12,13,14,15,16,17-decahydro-6*H*-cyclopenta[a]-phenan-thren-17-ol **181** (300 mg, 0.87 mmol) in DCM (15 mL) was added drop-wise to the reaction mixture, which was stirred for 18 h at room temperature. The reaction was quenched with saturated ammonium chloride (20 mL). The crude products were extracted with DCM (2 × 20 mL), dried ($MgSO_4$), filtered and evaporated *in-vacuo* to give the crude product. The crude product was then purified by flash chromatography DCM / MeOH (0 – 5%) to yield the title compound **183** (213 mg, 53%) as an amorphous pale yellow solid. ^{1}H NMR (400 MHz, $CDCl_3$): δ 0.74 (3H, s, 18-CH_3), 1.03-1.13 (6H, m), 1.15 (3H, t, *J* = 8 Hz, 2-CCH_2CH_3), 1.41-1.48 (2H, m), 1.85-1.90 (3H, m), 2.13-2.19 (1H, m), 2.27-2.31 (2H, m), 2.57 (2H, quart, *J* = 8 Hz, 2-CCH_2), 2.81 (2H, m, 6-CH_2), 3.18 (1H, td, *J* = 10 and 4 Hz, 17-CH), 3.56-3.64 (2H, m 16-$CHCH_2$), 3.77 (3H, s, OCH_3), 6.54 (1H, s, ArH), 7.03 (1H, s, ArH), 7.27 (1H, t, *J* = 7 Hz, ArH), 7.70 (1H, dt, *J* = 7 Hz and 2 Hz, ArH), 8.43 (1H, dd, *J* = 8 and 2 Hz, ArH) and 8.47 (1H, d, *J* = 2 Hz, ArH). ^{13}C NMR (101 MHz, $CDCl_3$): δ 12.43 (18-CH_3), 14.55 (2-CCH_2CH_3), 23.24, 26.28, 27.51, 29.56, 29.61, 37.58 (CH_2), 38.21 (16-CH), 40.32, 40.85 (CH), 41.55 (CH_2), 43.85 (CH), 44.33 (CH_2), 46.19 (C), 48.81 (CH), 55.27 (OCH_3), 81.89 (17-CH), 110.60, 123.72, 125.99 (ArCH), 129.80, 131.33, 131.69, 134.84 (ArC), 137.25, 148.08, 149.95 (ArCH), 155.23 (ArC) and 169.50 (CO), HRMS (ESI) calcd for $C_{29}H_{39}N_2O_3$ $(M+H)^+$: *m/z* = 463.2955, found *m/z* = 463.2942.

***N*-(((13*S*,17*S*)-2-Ethyl-17-hydroxy-3-methoxy-13-methyl-7,8,9,11,12,13,14,15,16,17-decahydro-6*H*-cyclopenta[a]-phenan-thren-16-yl)methyl)-2-(pyridin-4-yl)acetamide (Compound 184),** $C_{29}H_{38}N_2O_3$, MW 462.62,

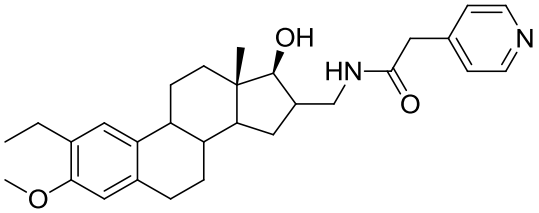

184

To a solution of 4-pyridylacetic acid hydrochloride (189 mg, 1.09 mmol) in DCM (10 mL) EDCI.HCl (238 mg, 1.24 mmol) was added portion-wise followed by addition of DMAP (catalytic) and triethylamine (0.36 mL, 2.55 mmol). The resulting reaction mixture was stirred for 15 min at room temperature. A solution of (13*S*,16*R*,17*S*)-16-(aminomethyl)-2-ethyl-3-methoxy-13-methyl-7,8,9,11,12,13,14,15,16,17-decahydro-6*H*-cyclopenta[a]-phenan-thren-17-ol **181** (250 mg, 0.73 mmol) in DCM (15 mL) was added drop-wise to the reaction mixture, which was stirred for 18 h at room temperature. The reaction was quenched with saturated ammonium chloride (20 mL). The crude products were then extracted with DCM (2 × 20 mL), dried ($MgSO_4$), filtered and evaporated *in-vacuo* to give the crude product. The crude product was then purified by flash chromatography DCM / MeOH (0 – 5%) to yield the title compound **184** (162 mg, 48%) as an amorphous pale yellow solid. ^{1}H NMR (400 MHz, $CDCl_3$): δ 0.75 (3H, s, 18-CH_3), 1.03-1.08 (2H, m), 1.16 (3H, t, *J* = 8 Hz, 2-CCH_2CH_3), 1.27-1.33 (1H, m), 1.42-1.47 (2H, m), 1.81-1.94 (3H, m), 2.13-2.18 (1H, m), 2.26-2.32 (2H, m, CH_2), 2.56 (2H, quart, *J* = 8 Hz, 2-CCH_2), 2.81(2H, m, 6-CH_2), 3.15 (1H, td, *J* = 7 and 3 Hz, CH), 3.56 (OCH_3), 3.77 (2H, s, CH_2), 6.54 (1H, s, ArH), 7.03 (1H, s, ArH), 7.26 (2H, d, *J* = 6 Hz, 2 × ArH) and 8.44 (2H, d, *J* = 6 Hz, 2 × ArH). ^{13}C NMR (101 MHz, $CDCl_3$): δ 12.52, 14.54 (CH_3), 23.23, 26.28, 27.52, 29.46, 29.62, 37,62 (CH_2), 38.23, 40.19 (CH), 41.67 (C), 43.19 (CH_2), 43.85 (CH), 44.42 (CH_2), 48.87 (CH), 55.27 (OCH_3), 81.89 (CH), 110.60 (ArCH), 124.92 (2 × ArCH), 125.97 (ArCH), 129.78, 131.68, 134.85, 144.67 (ArC), 149.54 (2 × ArCH), 155.23 (ArC) and 168.54 (CO). HRMS (ESI) calcd for $C_{29}H_{39}N_2O_3$ $(M+H)^+$: *m/z* = 463.2955, found *m/z* = 463.2947.

***N*-(((13*S*,16*R*,17*S*)-2-Ethyl-3,17-dihydroxy-13-methyl-7,8,9,11,12,13,14,15,16,17-decahydro-6*H*-cyclopenta[a]-phenan-thren-16-yl)methyl)-2-(pyridin-2-yl)acetamide (Compound 185),** $C_{28}H_{36}N_2O_3$, MW 448.60,

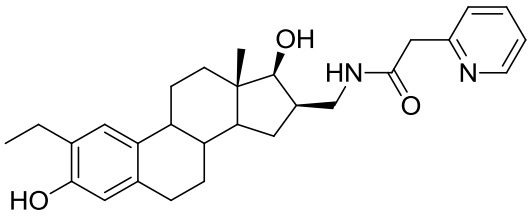

185

To a solution of *N*-(((13*S*,17*S*)-2-ethyl-17-hydroxy-3-methoxy-13-methyl-7,8,9,11,12,13,14,15,16,17-decahydro-6*H*-cyclopenta[a]-phenan-thren-16-yl)methyl)-2-(pyridin-4-yl)acetamide **182** (150 mg, 0.32 mmol) in DCM (7 mL) at -78 ºC (dry ice/acetone bath) under an atmosphere of nitrogen, boron tribromide (0.09 mL, 0.97 mmol) was added drop-wise. The resulting solution was stirred for 20 h at room temperature. The reaction was quenched with H_2O (10 mL). The crude products were extracted with DCM (2 × 10 mL), dried ($MgSO_4$), filtered and evaporated *in-vacuo* to give the crude product. The crude product was then purified by flash chromatography DCM / MeOH (0 – 10%) to yield the title compound **185** (59 mg, 41%) as an amorphous yellow solid. HPLC: t_r 1.36 min (90% Acetonitrile in water) 95%, ^{1}H NMR (400 MHz, MeOD): δ 0.81 (3H, s, 18-CH_3), 1.12-1.15 (2H, m), 1.20 (3H, t, *J* = 7 Hz, 2-CCH_2CH_3), 1.28-1.54 (5H, m), 1.80-2.02 (2H, m), 2.11-2.17 (1H, m), 2.27-2.46 (2H, m), 2.59 (2H, quart, *J* = 7 Hz, 2-CCH_2), 2.75 (2H, m, 6-CH_2), 3.26 (1H, m), 3.76 (2H, s, CH_2), 3.80 (1H, d, *J* = 10 Hz, CH), 6.50 (1H, s, ArH), 7.00 (1H, s, ArH), 7.35 (1H, t, *J* = 6 Hz, ArH), 7.46 (1H, d, *J* = 6 Hz, ArH), 7.83 (1H, t, *J* = 6 Hz, ArH) and 8.54 (1H, d, *J* = 6 Hz, ArH). ^{13}C NMR (101 MHz, MeOD): δ 13.00 (18-CH_3), 15.10 (2-CCH_2CH_3), 24.27, 27.40, 28.65, 30.31, 31.23, 38.84 (CH_2), 39.61, 41.43 (CH), 42.28, 45.00 (CH_2), 45.21 (C), 45.31, 49.99, 82.47 (CH), 115.85, 123.57, 125.92, 126.98 (ArCH), 128.97 (ArC), 132.31, 135.73 (ArC), 138.76, 149.88 (ArCH), 153.62 156.86 (ArC) and 171.80 (CO), LRMS (ESI) calcd for $C_{28}H_{37}N_2O_3$ $(M+H)^+$: *m/z* = 449.2, found 449.1, HRMS (ESI) calcd for $C_{28}H_{37}N_2O_3$ $(M+H)^+$: *m/z* = 449.2799, found *m/z* = 449.2823.

***N*-(((13*S*,16*R*,17*S*)-2-Ethyl-3,17-dihydroxy-13-methyl-7,8,9,11,12,13,14,15,16,17-decahydro-6*H*-cyclopenta[a]-phenan-thren-16-yl)methyl)-2-(pyridin-3-yl)acetamide (Compound 186),** $C_{28}H_{36}N_2O_3$, MW 448.60,

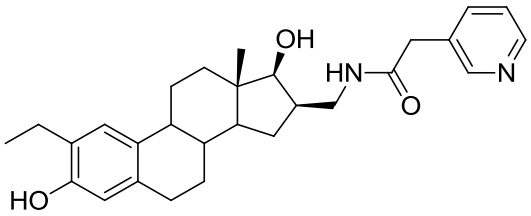

186

To a solution of *N*-(((13*S*,17*S*)-2-ethyl-17-hydroxy-3-methoxy-13-methyl-7,8,9,11,12,13,14,15,16,17-decahydro-6*H*-cyclopenta[a]-phenan-thren-16-yl)methyl)-2-(pyridin-3-yl)acetamide **183** (150 mg, 0.32 mmol) in anhydrous DCM (7 mL) at -78 ºC (dry ice/acetone bath), boron tribromide in DCM (0.09 mL, 1.0 M in DCM) was added drop-wise. The reaction mixture was stirred for 20 h at room temperature under an atmosphere of nitrogen. The reaction was quenched with H_2O (10 mL). The crude products were extracted with DCM (2 × 10 mL), dried ($MgSO_4$), filtered and evaporated *in-vacuo* to give the crude product. The crude product was then purified by flash chromatography DCM / MeOH (0 – 10%) to yield the title compound **186** (54 mg, 38%) as an amorphous yellow solid. HPLC: t_r 1.30 min (90% Acetonitrile in water) 94%, ^{1}H NMR (400 MHz, MeOD): δ 0.84 (3H, s, 18-CH_3), 1.10-1.16 (2H, m), 1.21 (3H, t, *J* = 8 Hz, 2-CCH_2CH_3), 1.32-1.52 (6H, m), 1.84-1.94 (2H, m), 2.01-2.04 (1H, m), 2.17-2.23 (1H, m), 2.34-2.44 (2H, m), 2.60 (2H, quart, *J* = 8 Hz, 2-CCH_2), 2.78 (2H, m, 6-CH_2), 3.44 (1H, m), 3.63 (2H, s, CH_2), 3.82 (1H, d, *J* = 10 Hz, CH), 6.50 (1H, s, ArH), 7.01 (1H, s, ArH), 7.46 (1H, t, *J* = 5 Hz, ArH), 7.87 (1H, d, *J* = 5 Hz, ArH), 8.50 (1H, d, *J* = 5 Hz, ArH) and 8.55 (1H, s, ArH). ^{13}C NMR (101 MHz, MeOD): δ 12.99 (18-CH_3), 15.09 (2-CCH_2CH_3), 24.28, 27.66, 30.34, 31.32, 38.85 (CH_2), 40.02 (CH_2), 40.87 (CH), 41.44 (CH_2), 45.44, 49.19, 85.55 (CH), 115.85, 125.27 (ArCH), 127.00 (ArC), 129.00, (ArCH), 132.32, 133.45, 135.76 (ArC), 138.98, 148.47, 150.53 (ArCH), 153.65 (ArC) and 171.65 (CO), LRMS (ESI) calcd for $C_{28}H_{37}N_2O_3$ $(M+H)^+$: *m/z* = 449.2, found 449.2. HRMS (ESI) calcd for $C_{28}H_{37}N_2O_3$ $(M+H)^+$: *m/z* = 449.2799, found *m/z* = 449.2784.

***N*-(((13*S*,16*R*,17*S*)-2-Ethyl-3,17-dihydroxy-13-methyl-7,8,9,11,12,13,14,15,16,17-decahydro-6*H*-cyclopenta[a]-phenan-thren-16-yl)methyl)-2-(pyridin-4-yl)acetamide (Compound 187),** $C_{28}H_{36}N_2O_3$, MW 448.60,

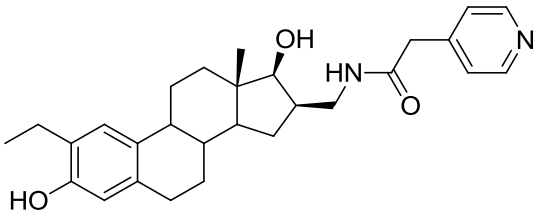

187

To a solution of *N*-(((13*S*,17*S*)-2-ethyl-17-hydroxy-3-methoxy-13-methyl-7,8,9,11,12,13,14,15,16,17-decahydro-6*H*-cyclopenta[a]-phenan-thren-16-yl)methyl)-2-(pyridin-4-yl)acetamide **184** (131 mg, 0.28 mmol) in DCM (7 mL) at -78 ºC (dry ice/acetone bath) under an atmosphere of nitrogen, boron tribromide (0.08 mL, 0.85 mmol) was added drop-wise. The resulting solution was stirred for 20 h at room temperature. The reaction was quenched with H_2O (10 mL). The crude products were extracted with DCM (2 × 10 mL), dried ($MgSO_4$), filtered and evaporated *in-vacuo* to give the crude product. The crude product was then purified by flash chromatography DCM / MeOH (0 – 10%) to yield the title compound **187** (54 mg, 43%) as an amorphous yellow solid. HPLC: t_r 1.24 min (90% Acetonitrile in water) 93%, ^{1}H NMR (400 MHz, MeOD): δ 0.84 (3H, s, 18-CH_3), 1.12-1.15 (2H, m), 1.21 (3H, t, *J* = 8 Hz, 2-CCH_2CH_3), 1.31-1.54 (5H, m), 1.82-1.93(2H, m), 1.96-2.04 (1H, m), 2.14-2.23 (1H, m), 2.33-2.46 (2H, m), 2.60 (2H, quart, *J* = 8 Hz, 2-CCH_2), 2.77 (2H, m, 6-CH_2), 3.44 (1H, m), 3.65 (2H, s, CH_2), 3.80 (1H, d, *J* = 10 Hz, CH), 6.50 (1H, s, ArH), 7.01 (1H, s, ArH), 7.45 (2H, d, *J* = 5 Hz, 2 × ArH) and 8.52 (2H, d, *J* = 5 Hz, 2 × ArH). ^{13}C NMR (101 MHz, MeOD): δ 13.01 (18-CH_3), 15.10 (2-CCH_2CH_3), 24.27, 27.63, 28.83, 30.32, 31.32, 38.82 (CH_2), 39.99, 41.42 (CH), 42.87, 43.18 (CH_2), 45.33 (C), 45.39, 49.99, 82.51 (CH), 115.84, 126.19 (ArCH), 127.00 (2 ×ArCH), 128.98, 132.32, 135.75, 147.72 (ArC), 150.05 (2 × ArCH), 153.65 (ArC) and 171.77 (CO), LRMS (ESI) calcd for $C_{28}H_{37}N_2O_3$ $(M+H)^+$: *m/z* = 449.2, found 449.1, HRMS (ESI) calcd for $C_{28}H_{37}N_2O_3$ $(M+H)^+$: *m/z* = 449.2799, found *m/z* = 449.2834.

Experimental Details: Computational Chemistry

For the docking studies of inhibitors in 1FDT[76] the starting conformations used for receptor docking were generated from an energy minimization performed using the MMFF94s force field, with MMFF94 charges applied, as implemented in Sybyl 7.0. The resulting lowest energy conformer was then used for docking studies using Gold version 2.2 with default parameters. The active site was defined as a 12 Å radius around the C alpha atom of Serine 142 and 30 attempts were computed and scored using Gold score. To develop a QSAR using CoMSIA, the ligands were initially minimized using the MMFF94s force field as implemented within the Sybyl 7.0 package. The molecules were aigned using FlexS, with a common core elucidated by DISTILL which correspond to the steroid backbone. Gastegier-Huckel charges were used for the charge descriptors in FlexS and CoMSIA was performed using the aligned compounds and the standard Sybyl 7.0 CoMSIA fields. Alignment and shape similarity studies were carried out using The PyMOL Molecular Graphics System (2002), http://www.pymol.org.

Experimental Details: Biochemistry

All chemicals were purchased from Aldrich Chemical Co. (Gillingham, UK), or Fischer Scientific (Loughborough, UK). pET-24a bacterial expression vector, Rosetta 2 competent cells and the BugBuster master mix were purchased from Novagen. The 17β-HSD1 gene was supplied in the pCEP4 vctor by colleagues at Imperial College London. The Quick ligation kit, restriction enzymes, NheI and XhoI and calf intestinal alkaline phosphatase, were purchased from New England Biolabs. XL10-Gold Ultracompetent cells were purchased from Stratagene. For purification of the H_6-17β-HSD1 protein Wizard mini-prep kits were purchased from Promega (Southampton, UK) an AKTA FPLC from Amersham Biosciences (GE Healthcare), HiTrap chelating HP column from Pharmacia (GE Healthcare) loaded with Ni^{2+}, and a Q-sepharose column Amersham Biosciences (GE Healthcare) were used. For enzyme and inhibitor assays Cell Titer 96® AQ_{ueous} One solution was purchased from Promega (Southampton, UK).

Experimental Details: Chapter 6

Protein Expression

Miniprep plasmid purification

Splinters of 'ice' were scraped off from frozen cells using a sterile loop, and streaked onto a LB plate containing the appropriate antibiotic. The plate was incubated overnight at 37 °C. A single colony was inoculated into 5 mL of LB medium containing the antibiotic in a 50 mL Falcon tube, and the culture grown overnight at 37 °C and 250 r.p.m. The pellet was collected from the overnight culture by centrifugation at 13,000 r.p.m. for one minute DNA was prepared by either of the following miniprep methods:

Standard miniprep procedures

The cell pellet was completely resuspended in solution I (250 μL, 50 mM Tris-HCl, pH 8.0, 10 mM EDTA, 50 mM glucose, 100 μg/mL RNase A). Solution II (250 μL, 200 mM NaOH, 1% SDS) was added and the tube was inverted five times to give a clear solution and left at room temperature for 5 min. Solution III (250 μL, 2.55 M potassium acetate, pH 5.4) was added and the tube inverted again five times and the kept in ice for 15 min. The resulting solution was centrifuged at 13,000 r.p.m. for 15-20 min. The supernatant was transferred into a fresh tube and 0.7 volumes, relative to the supernatant of isopropanol was added. After keeping the tubes at room temperature for 5 min the solution was centrifuged at 13,000 r.p.m. for 15-20 min. The DNA pellet was washed twice by centrifugation with 70% (v/v) cold ethanol in water and bench dried. The DNA was redissolved in 40 μL of sterile Milli-Q water or TE buffer and stored at –20 °C.

Wizard Minipreps DNA purification system

The cell pellet was completely resuspended in cell resuspension solution (200 μL, containing 50 mM Tris-HCl, 10 mM EDTA, pH 7.5 and 100 μg/mL of RNase A). Cell lysis solution (200 μL, containing 0.2 M NaOH and 1% SDS) was added and the suspension mixed by inverting the tube five times until the suspension became clear. Neutralisation solution (200 μL, containing 1.32 M potassium acetate, pH 4.8) was added and mixed as before. After cooling on ice for 5 min, the solution was centrifuged at 13,000 r.p.m. for 12 min and the supernatant was carefully transferred to a new tube. After mixing with Wizard^{TM} Plus minipreps resin (1 mL), the solution

was poured to a Wizard™ minicolumn. The solution was slowly expelled using the syringe plunger. DNA adhering to the resin was washed twice with 2 mL of the wash solution (80 mM potassium acetate, 8.3 mM Tris-HCl, pH 7.5, 40 μM EDTA and 55% ethanol in water), and the minicolumn was dried by centrifugation for 2 min. Plasmid DNA was eluted by adding sterile water or TE buffer (20 μL), waiting for 1 min followed by centrifugation at 13,000 r.p.m. for 1 min, and stored at –20 °C until required.

Restriction enzyme digestion

Plasmid DNA was digested with various restriction enzymes for cloning. Enzyme digestions were usually performed in a 0.5 mL Eppendorf tube containing the following: plasmid (3-30 μL, *ca.* 1-10 μg), BSA if needed (1 μL), recommended buffer (1-5 μL, 10X), sterile Milli-Q water (to final volume of 10-50 μL) and restriction enzymes (1-4 μL, *ca.* 10-400 U) were mixed and incubated at 37 °C for 1-4 h. A sample of 5 μL was used for the subsequent agarose electrophoresis analyses. When large scale restricted DNA was needed for cloning, the whole 50 μL sample was loaded on gel and the required DNA fragments were gel purified.

Alkaline Phosphatase Treatment

Suspend DNA in 1X NEBuffer (0.5 μg/10 μl). Add 0.5 units/μg vector DNA. Incubate for 60 minutes at 37 °C. Purify DNA by gel purification, spin-column purification or phenol extraction. 10 mM sodium orthovanadate inhibits CIP activity (10 units) by 90% and 50 mM EDTA inactivates CIP (10 units) by 100%.

Agarose Gel Electrophoresis

DNA samples were analysed by electrophoresis using a submarine gel electrophoresis system (Bio-Rad) with a horizontal agarose minigel. In general, 1X TBE or 1X TAE was used as running buffer. The concentration of agarose used was 0.8-2.0%, (w/v) depending on the size of DNA to be analysed and the resolution required. Samples were mixed with 0.2 volumes of 6X loading solution before applying to individual wells in the minigel. A DNA ladder (1 kb marker) was run alongside as a standard marker. Gels were run at 80 V and stained in 1X TAE containing 3.0 μg/mL ethidium bromide for 15 min. After destaining in 1X TAE for 10 min, gels were viewed on a UV transluminator at 312 nm.

Preparation of agarose gels: Ultrapure agarose (0.8 g for 0.8% gel or 2 g for 2% gel) was added to TAE buffer (100 mL, 1X) and dissolved in microwave for 2 min. After cooling to ~50 ºC the mixture was poured into the gel tank to a depth of 3-7 mm thick. The comb was then inserted and the gel was left to solidify at room temperature.

Sample loading buffer (6x): Bromophenol blue [0.2% (w/v)], xylene cyanol [0.25% (w/v)] and Ficoll 400 [15% (w/v)].

Purification of DNA from agarose gels

The DNA fragment on the agarose gel was excised using a clean scalpel. The slice was weighed and transferred into a sterile 1.5 mL Eppendorf tube. Add 3 volumes Buffer QG to 1 volume gel (100 mg ~ 100 µl). After incubate at 50 °C for 10 min (or until the gel slice has completely dissolved), and mixing the solution every 2–3 min to help dissolve the gel slice. After the gel slice has dissolved completely, check that the colour of the mixture is yellow, if the colour of the mixture is orange or violet; add 10 µl of 3 M sodium acetate, pH 5.0, and mix. The colour of the mixture will turn yellow. Add 1 gel volume of isopropanol to the sample and mix. A QIAquick spin column was placed into a provided 2 ml collection tube. To bind the DNA, the sample was applied to the QIAquick column and centrifuged at 13,000 r.p.m. for 1 min through the column. Discard the flow-through and place the QIAquick column back into the same collection tube. For sample volumes of >800 µl, the sample was loaded and spun again, 0.5 ml of Buffer QG was added to the QIAquick column and centrifuged at 13,000 r.p.m.for 1 min. The flow-through was discarded and the QIAquick column placed back into the same collection tube. To wash the DNA, add 0.75 ml Buffer PE to QIAquick column and was centrifuged at 13,000 r.p.m. for 1 min. The flow-through was discarded and the QIAquick column placed back into the same collection tube. The QIAquick column was centrifuged at 13,000 r.p.m. for 1 min to remove residual wash buffer. The QIAquick column was placed into a clean 1.5 ml microcentrifuge tube.The DNA was eluted by, adding 50 µl Buffer EB (10 mM Tris·Cl, pH 8.5) to the center of the QIAquick membrane and the QIAquick column was centrifuged at 13,000 r.p.m. for 1 min. For increased DNA concentration, 30 µl Buffer EB was added to the center of the QIAquick membrane,

and the column was left to stand for 1 min, and then centrifuged at 13,000 r.p.m. for 1 min.

Ligation into expression vectors

The plasmids were purified from an overnight culture and digested with appropriate restriction enzyme at 37 °C for 4 h. Upon completion of the reaction the samples and the 1 kb DNA ladder were loaded onto a 0.8%-2% (w/v) agarose gel. The vector and the insert bands were excised from the agarose gel and the DNA was purified from the gel. In the ligation solution, the vector DNA fragment (2.5 μL, 100 ng, pET-24a) and the insert DNA fragment (2.5 μL, 100 ng) were mixed and incubated at 48 °C for 5 min followed by keeping on ice for 5 min. T4 DNA ligase buffer (1 μL, 10X), rATP (1 μL, 10 mM), autoclaved Milli-Q water (2 μL) and T4 DNA ligase (1.0 μL) were then added into the solution to make the final volume of 10 μL and incubated at 16 °C overnight (> 20 h). The ligated DNA (10 μL) was transformed into *E. coli* XL10-Gold competent cells (100 μL) and plated onto a LB agar containing the appropriate antibiotics, and incubated at 37 °C overnight. To identify the new recombinant plasmid, the DNA was purified and double digested with the appropriate restriction enzymes. Only those plasmids with the correct gene inserted gave a fragment of the appropriate length.

Preparation of competent cells

Splinters of 'ice' were scraped from frozen cells using a sterile loop and streaked onto an LB plate [15 μg/mL of tetracycline for *E. coli* XL cell; no antibiotic was required for BL21(DE3)pLysS cells]. One colony was inoculated into 10 mL of LB medium containing antibiotic, if required in a 50 mL Falcon tube, and grown overnight at 37 °C and 250 r.p.m. The overnight culture (0.5 mL) was aseptically transferred to a 20 mL Erlenmeyer flask containing 10 mL of LB medium with antibiotic if required and incubated at 37 °C and 250 r.p.m. until the OD_{600} was reached 0.25 ~ 0.5. The cells were then harvested re-suspended in 1 mL of sterile, ice cold 50 mM $CaCl_2$. After centrifugation at 4,000 r.p.m. the supernatant was discarded, the pellet was resuspended gently in 0.5 mL of sterile, ice cold 50 mM $CaCl_2$ and incubated on ice for 30 min ready for transformation

Transformation

DNA (10 μL ligation mixture or 1 μL of miniprep plasmid DNA) solution was mixed with *E. coli* competent cells (200 μL) in a pre-chilled 50 mL Falcon tube, and the mixture was placed on ice for 30 mins. The sample was heat shocked in a 42 °C water bath for exactly 45 s and chilled on ice for 2 min. SOC medium (1 mL) was added and the mixture was incubated at 37 °C and 250 r.p.m. for 1 h. When the ligation mixture was transformed the cells were precipitated by centifugation at 4,000 r.p.m. for 10 min. The pellet was redissolved in 100 μL of residual SOC medium and plated onto a LB agar plate supplemented with the appropriated antibiotics. When miniprep DNA was transformed then cultured cells (100 μL) were spread evenly onto a LB agar plate supplemented with the appropriate antibiotic and incubated overnight at 37 °C.

Quick 5 minTransformation

Pre-warm the agar plates to 37–42 °C. 1–3 μL of miniprep DNA was added to 100 μL of ice cold competent cells. Incubate the competent cells on ice for 5 mins. The competent cells were spread onto the pre-warmed agar plates and incubated at 37 °C overnight.

Glycerol stock

A single colony from an overnight plate was inoculated into 5 mL of LB broth with the appropriate antibiotic. The cells were grown to late log phase (OD_{600} *ca.* 0.8), and 1 mL of cell culture was mixed with 0.2 mL of sterile glycerol, and stored at –80 °C.

Time-dependent expression

A single colony was inoculated into 5 mL of LB medium with the appropriate antibiotic and incubated overnight at 37 °C and 250 r.p.m. The overnight culture (1 mL) was used to inoculate LB medium (100 mL) with antibiotic in a 500 mL flask and incubated at 30 °C and 250 r.p.m. until the OD_{600} reached 0.7~0.8, IPTG was added to a final concentration of 0.5 mM. Growth media (5 mL) was transferred into a 50 mL Falcon tube and centrifuged at 4,000 r.p.m. for 10 min and the pellet was stored at –80 °C until analyses. Further samples were taken after 1, 2, 3 and 4 h. Pellets were thawed and resuspended in 50 mM Tris-HCl, pH 7.5, 100 mM NaCl (4

mL/100 mL culture). The suspension was treated with the BugBuster™ kit from Novagen. Cell lysate (200 µL) was aliquoted in a 1.5 mL Eppendorf tube and centrifuged at 13,000 r.p.m. for 10 min. Supernatant was separated in a separate tube and mixed with 50 µL of 5X SDS sample loading buffer. To check for insoluble expression of protein, the pellet was dissolved in 200 µL of 1X loading buffer. Both soluble and insoluble fraction tubes were incubated in heat block at 90 °C for 10 min. Insoluble fractions (mostly cell wall lipids) were precipitated by centrifugation at 13,000 r.p.m. for 5 min, and samples were analysed by loading 15 µL of each onto 10-15% SDS-PAGE.

Large Scale expression

Large scale overnight expression required a single colony to be inoculated into 5mL of LB medium with the appropriate antibiotic and incubated for 6 h at 37 ^{o}C. Transfer the 5mL culture to 100mL of fresh LB medium with antibiotic and incubate overnight at 37 ^{o}C and 250 r.p.m. Transfer 25mL of the overnight culture to 1 L fresh LB medium and incubate at 37 ^{o}C and 250 r.p.m until an OD_{600} = 0.6 Abs is measured. Cool the culture to room temperature and add 12.5µM IPTG. Incubate overnight. Growth media (1 L) was transferred into a 50 mL Falcon tubes and centrifuged at 4,000 r.p.m. for 10 min and the pellet was stored at –80 °C.

Protein Purification

Batch purification

Pellets were re-suspended in approximately 30 mL of Buffer A containing 40 mM Tris HCl pH 7.5, 20% Glycerol, 100 mM NaCl, 20 mM imidazole, 0.2 mM DTT, 0.4 mM PMSF and Benzonase. The re-suspended pellet was put through a One Shot Constant Cell Disruption System and then centrifuged at 10000 r.p.m. for 30 min at 4 ^{o}C. The supernatant was collected and steri-filtered prior to manually passing through a HiTrap chelating HP column pre-loaded with Nickel ions. The protein was eluted with 40 mL of Buffer A, followed by 40 mL of Buffer B containing 40 mM Tris HCl pH 7.5, 20% Glycerol, 500 mM imidazole, 0.2 mM DTT and 0.4 mM PMSF. The eluted protein was concentrated to approximately 1 mL using a size filter falcon tube centrifuging at 5,500 r.p.m. for 15 min. The protein was dialysed at 5 ^{o}C using a dialysis buffer containing 40 mM Tris HCl, pH 7.5, 20% Glycerol, 0.2 mM DTT and 1 mM EDTA and a Slide-a-lyzer® Dialysis cassette 10000 MCUCO cartridge for 3-4

h before leaving the dialysis cell in fresh dialysis buffer overnight. For storage the protein was removed from the dialysis cell and stored at 5 ºC.

HiTrap column purification

Pellets were re-suspended in approximately 30 mL of Buffer A. The re-suspended pellet was put through a One Shot Constant Cell Disruption System and then centrifuged at 10000 r.p.m. for 30 min at 4 ºC. The supernatant was collected and steri-filtered prior to injection onto an AKTA FPLC using a HiTrap chelating HP column pre-loaded with Nickel ions. After the supernatant was injected the protein was eluted with 40 mL of Buffer A, followed by 20 mL of Buffer B, followed by a gradient of 10% Buffer B to 100% Buffer B at 3.0 mL/min for 30 min. The fractions containing the purified protein were identified by using SDS-PAGE gel electrophoresis. Prior to concentration of the eluted protein 0.06% of N-Octyl-β-D-glucopyranoside was added. The eluted protein was concentrated to approximately 1 mL using a size filter falcon tube centrifuging at 5,500 r.p.m. for 15 min. The protein was dialysed at 5 ºC using a dialysis buffer containing 40 mM Tris HCl, pH 7.5, 20% Glycerol, 0.2 mM DTT and 1 mM EDTA and a Slide-a-lyzer® Dialysis cassette 10000 MCUCO cartridge for 3-4 h before leaving the dialysis cell in fresh dialysis buffer overnight. For storage the protein was removed from the dialysis cell and stored at 5 ºC.

Q-Sepharose column purification

The concentrated protein was diluted to approximately 30 mL using Buffer C containing 40 mM Tris HCl pH 7.5, 20% Glycerol, 20 mM NaCl, 0.2 mM DTT and 0.4 mM PMSF. The diluted protein was steri-filtered prior to injection onto an AKTA FPLC using a Q-sepharose column. After the diluted protein was injected the protein was eluted with 40 mL of Buffer C, followed by 20 mL of Buffer D containing 40 mM Tris HCl pH 7.5, 20% Glycerol, 500 mM NaCl, 0.2 mM DTT and 0.4 mM PMSF, followed by a gradient of 10% Buffer D to 100% Buffer D at 3.0 mL/min for 30 min. The fractions containing the purified protein were identified by using SDS-PAGE gel electrophoresis. Prior to concentration of the eluted protein 0.06% of N-Octyl-β-D-glucopyranoside was added. The eluted protein was concentrated to approximately 1 mL using a size filter falcon tube centrifuging at 5,500 r.p.m. for 15 min. The protein was dialysed at 5 ºC using a dialysis buffer

containing 40 mM Tris HCl, pH 7.5, 20% Glycerol, 0.2 mM DTT and 1 mM EDTA and a Slide-a-lyzer® Dialysis cassette 10000 MCUCO cartridge for 3-4 h before leaving the dialysis cell in fresh dialysis buffer overnight. For storage the protein was removed from the dialysis cell and stored at 5 ºC.

SDS polyacrylamide gel electrophoresis (SDS-PAGE)

SDS-PAGE was carried out using a Mini Protean II™ apparatus (Bio-Rad). A 3% stacking gel and 10%, 12.5% or 15% running gel were used along with gel running buffer containing 25 mM Tris, 0.2 M glycine and 0.5% (w/v) SDS.

Stacking gel: 30% (w/v) acrylamide and 0.8% (w/v) bisacrylamide solution (320 µL), Tris-HCl (1 M, pH 6.8, 400 µL), 10% (w/v) SDS (32 µL), 1% (w/v) ammonium persulphate (160 µL), H_2O (2.32 mL), TEMED (5 µL).

Running gel: 30% (w/v) acrylamide and 0.8% (w/v) bisacrylamide solution (2 mL for 10%, 2.5 mL for 12.5%, 3 mL for 15%), Tris-HCl (0.75 M, pH 8.8, 3 mL), 10% Pr(w/v) SDS (60 µL), 1% (w/v) ammonium persulphate (300 µL), H_2O (750 µL for 10%, 200 µL for 12.5% and no water in 15%), TEMED (5 µL).

Sample loading buffer (2x): Tris-HCl (0.625 M, pH 6.8, 2.5 mL), glycerol (2.0 mL), 10% (w/v) SDS solution (5.0 mL), β-mercaptoethanol (1.0 mL), H_2O (9.5 mL), 0.01% (w/v) bromophenol blue.

Gel staining solution: Coomassie Brilliant Blue R-250 [0.25% (w/v)] with water in methanol [30% (v/v)] in water and acetic acid [10% (v/v)] in water.

Gel destaining solution: methanol [30% (v/v)] in water, acetic acid [10% (v/v)] in water.

Gel storing solution: methanol [30% (v/v)] in water, glycerol [3% (v/v)] in water.

The protein sample (10 µL, ~10 µg) and 5X SDS sample loading buffer (2 µL) were transferred into an Eppendorf tube. The tube was boiled for 5 min and the sample loaded onto a SDS-PAGE with a 3% stacking gel. The power supply was set at 40 mA per gel, 250 V for gel electrophoresis. Gels were stained and destained after electrophoresis using the above solutions. Standard molecular weight markers were used to calibrate the SDS-PAGE containing: 250 kDa, 148 kDa, 98 kDa, 64 kDa, 50 kDa, 36 kDa, 22 kDa, 16 kDa and 4 kDa marker proteins.

Protein concentration determination

Protein concentrations were determined by the method of Bradford. The Bradford reagent was gently mixed and brough to room temperature. Protein standards in buffer ranging from 0.1-1.4 mg/ml were prepared using a BSA standard. 5 µL of the protein standard were added to separate wells in a 96 well plate. For the blank wells 5 µL of buffer were added. The unknown protein sample was prepared with approximate concentrations between 0.1-1.4 mg/ml. To each well, 250 µL of the Bradford reagent was added and mixed on a shaker for approximately 30 s. The samples were left to incubate at room temperature for 5 to 45 min to construct a standard curve at 595 nm. The protein concentration was determined by comparing the absorbance vaues of the sample protein against the standard curve at 595 nm.

Enzyme Assay

Enzyme Kinetic Absorbance Assay

The enzyme was assayed by spectrophotometric measurement of the concentration changes of NADPH at 340 nm. Reactions were run in 1 mL solutions made up of 50 nM Sodium Pyrophosphate buffer, pH 9.2, and 10% THF, containing 0-400 µM steroid (E2), 0.1 mM NADP solution and Milli-Q water. Reactions were initiated by the addition of 1.9 µM of H_6-17β-HSD1, and the absorbance variations were measured against a blank containing all components except the steroid (E2). Reactions were followed from 30 s to 5 min after addition of NADP on a Perkin Elmer λ40 UV-vis spectrophotometer.

Inhibitor Enzyme Kinetic Absorbance Assay

The enzyme was assayed by spectrophotometric measurement of the concentration changes of NADPH at 340 nm. Reactions were run in 1 mL solutions made up of 50 nM Sodium Pyrophosphate buffer, pH 9.2, and 10% THF, containing 30 µM steroid (E2), 0.1 mM NADP solution and Milli-Q water. Reactions were initiated by the addition of 1.9 µM of H_6-17β--HSD1 which was incubated with 20-400 µM of inhibitor dissolved in DMSO before addition. The absorbance variations were measured against a blank containing all components except the steroid. Reactions were followed from 30 s to 5 min after addition of NADP on a Perkin Elmer λ40 UV-vis spectrophotometer.

Enzyme Kinetic Absorbance Assay – Plate Reader

The enzyme was assayed by spectrophotometric measurement of the concentration changes of NADPH at 340 nm. Reactions were run in 200 μL solutions made up of 10 mM Sodium Pyrophosphate buffer, pH 9.2, and 10% DMSO, containing 0–400 μM steroid (E2), 0.1 mM NADP solution and Milli-Q Water. Reactions were initiated by the addition of 1.9 μM of H_6-17β-HSD1, and the absorbance variations were measured against a blank containing all components except the steroid (E2). Reactions were followed from 30 s to 5 min after addition of NADP on a Molecular Devices Versamax tunable microplate reader.

Inhibitor Enzyme Kinetic Absorbance Assay – Plate Reader

The enzyme was assayed by spectrophotometric measurement of the concentration changes of NADPH at 340 nm. Reactions were run in 200 μL solutions made up of 10 mM Sodium Pyrophosphate buffer, pH 9.2, and 10% DMSO, containing 10 μM steroid (E2), 0.1 mM NADP solution and Milli-Q Water. Reactions were initiated by the addition of 1.9 μM of H_6-17β--HSD1 which was incubated with 75-300 μM of inhibitor dissolved in DMSO before addition. The absorbance variations were measured against a blank containing all components except the steroid (E2). Reactions were followed from 30 s to 5 min after addition of NADP on a Molecular Devices Versamax tunable microplate reader.

Enzyme Kinetic Absorbance Assay – MTS Assay Plate Reader Temperature Investigation

The enzyme was assayed by spectrophotometric measurement of the concentration changes of NADPH at 459 nm at 22ºC or 37 ºC. Reactions were run in 100 μL solutions made up of 10 mM Tris HCl buffer, pH 7.5, and 10% DMSO, containing 0–200 μM steroid (E2), 0.1 mM NADP solution, 10 μL MTS/PES and Milli-Q Water. Reactions were initiated by the addition of H_6-17β-HSD1 giving a final concentration of 0.069 μM, and the absorbance variations were measured against a blank containing all components except the steroid (E2). Reactions were followed from 0 s to 60 s after addition of NADP on a Molecular Devices Versamax tunable microplate reader.

Enzyme Kinetic Absorbance Assay – MTS Assay Plate Reader Buffer Investigation

The enzyme was assayed by spectrophotometric measurement of the concentration changes of NADPH at 459 nm at 37 ºC. Reactions were run in 100 µL solutions made up of 10 mM Tris HCl buffer, pH 7.5 or 5 mM Potassium pyrophosphate buffer, pH 9.2, and 10% DMSO, containing 0–200 µM steroid (E2), 0.1 mM NADP solution, 10 µL MTS/PES and Milli-Q Water. Reactions were initiated by the addition of H_6-17β-HSD1 giving a final concentration of 0.069 µM, and the absorbance variations were measured against a blank containing all components except the steroid (E2). Reactions were followed from 0 s to 60 s after addition of NADP on a Molecular Devices Versamax tunable microplate reader.

Enzyme Kinetic Absorbance Assay – MTS Assay Plate Reader (E2)

The enzyme was assayed by spectrophotometric measurement of the concentration changes of NADPH at 459 nm at 37 ºC. Reactions were run in 100 µL solutions made up of 10 mM Tris HCl buffer, pH 7.5, and 10% DMSO, containing 0–200 µM steroid (E2), 0.1 mM NADP solution, 10 µL MTS/PES and Milli-Q Water. Reactions were initiated by the addition of H_6-17β-HSD1 giving a final concentration of 0.069 µM, and the absorbance variations were measured against a blank containing all components except the steroid (E2). Reactions were followed from 0 s to 60 s after addition of NADP on a Molecular Devices Versamax tunable microplate reader.

Enzyme Kinetic Absorbance Assay – MTS Assay Plate Reader (NADP)

The enzyme was assayed by spectrophotometric measurement of the concentration changes of NADPH at 459 nm at 37 ºC. Reactions were run in 100 µL solutions made up of 10 mM Tris HCl buffer, pH 7.5, and 10% DMSO, containing 0–1000 µM NADP, 0.3 mM steroid (E2) solution, 10 µL MTS/PES and Milli-Q Water. Reactions were initiated by the addition of H_6-17β-HSD1 giving a final concentration of 0.069 µM, and the absorbance variations were measured against a blank containing all components except the steroid (E2). Reactions were followed from 0 s to 60 s after addition of NADP on a Molecular Devices Versamax tunable microplate reader.

Inhibitor Enzyme Kinetic Absorbance Assay – MTS Assay Plate Reader

The enzyme was assayed by spectrophotometric measurement of the concentration changes of NADPH at 459 nm at 37 ºC. Reactions were run in 100 µL solutions made up of 10 mM Tris HCl buffer, pH 7.5, and 10% DMSO, containing 0–200 µM steroid (E2), 0.1 mM NADP solution, 10 µL MTS/PES and Milli-Q Water. Reactions were initiated by the addition of H_6-17β--HSD1 giving a final concentration of 0.069 µM which was incubated with 0-200 µM of inhibitor dissolved in DMSO before addition. The absorbance variations were measured against a blank containing all components except the steroid (E2). Reactions were followed from 0 s to 60 s after addition of NADP on a Molecular Devices Versamax tunable microplate reader.

Experimental Details: Cell Based Assay

Measurement of inhibition of 17β-HSD1

T-47D human breast cancer cells were incubated with ^{3}H-E1 at a concentration of 2 nM per well, in a 24 well tissue culture plate, in the absence or presence of the inhibitor (0.1 nM – 10 µM). After incubation of the substrate ± inhibitor for 30 min at 37 ºC, the products were isolated from the mixture by extraction with diethyl ether (4 ml), using ^{14}C-E2 (5000 dpm) to monitor procedural losses. Separation of ^{3}H-E2 from the mixture was achieved using TLC (DCM/EtOAc, 4:1 v/v) and the mass of ^{3}H-E2 produced was calculated from the ^{3}H counts detected and recovery of ^{14}C-E2.

References

1. UK, C. R. Cancer stats, Key facts all cancers. http://info.cancerresearchuk.org/cancerstats/incidence/?a=5441 (29-07-08).

2. Breakthrough Breast Cancer, The Best Treatment Your guide to breast cancer treatment in England and Wales. www.breakthrough.org.uk/document.rm?id=1146 (07-05-2011).

3. National Institute for Health and Clinical Excellence. Hormonal therapies for the adjuvant treatment of early oestrogen -receptor-positive breast cancer. NICE technology appraisal 112 2006.

4. Poirier, D. Inhibitors of 17 beta-hydroxysteroid dehydrogenases. *Current Medicinal Chemistry* **2003,** 10, 453-477.

5. Payne, A. H.; Abbaszade, I. G.; Clarke, T. R.; Bain, P. A.; Park, C. H. J. The multiple murine 3 beta-hydroxysteroid dehydrogenase isoforms: Structure, function, and tissue- and developmentally specific expression. *Steroids* **1997,** 62, 169-175.

6. Smith, H. N., P.; Simons, C.; LeLain, R. Inhibitors of Steriodogenesis as agents for the treatment of hormone dependant cancers. *Expert Opinions in Therapeutic Patents* **2001,** 11, 789-824.

7. Day, J. M.; Tutill, H. J.; Foster, P. A.; Bailey, H. V.; Heaton, W. B.; Sharland, C. M.; Vicker, N.; Potter, B. V. L.; Purohit, A.; Reed, M. J. Development of hormone-dependent prostate cancer models for the evaluation of inhibitors of 17β-hydroxysteroid dehydrogenase Type 3. *Molecular and Cellular Endocrinology* **2009,** 301, 251-258.

8. Penning, T.M. Hydroxysteroid dehydrogenases and pre-receptor regulation of steroid hormone action. *Human Reproduction Update*, **2003,** 9, 193-205.

9. Reed, M. J.; Purohit, A.; Woo, L. W. L.; Potter, B. V. L. The development of steroid sulphatase inhibitors. *Endocrine Related Cancer* **1996,** 3, 9-23.

10. Katzenellenbogen, B. S.; Frasor, J. Therapeutic targeting in the estrogen receptor hormonal pathway. *Seminars in Oncology* **2004,** 31, 28-38.

11. Nilsson, S.; Koehler, K. F. Oestrogen receptors and selective oestrogen receptor modulators: Molecular and cellular pharmacology. *Basic & Clinical Pharmacology & Toxicology* **2005,** 96, 15-25.

12. Purohit, A.; Tutill, H. J.; Day, J. M.; Chander, S. K.; Lawrence, H. R.; Allan, G. M.; Fischer, D. S.; Vicker, N.; Newman, S. P.; Potter, B. V. L.; Reed, M. J. The regulation and inhibition of 17 beta-hydroxysteroid dehydrogenase in breast cancer. *Molecular and Cellular Endocrinology* **2006,** 248, 199-203.

13. Luu-The, V.; Belanger, A.; Labrie, F. Androgen biosynthetic pathways in the human prostate. *Best Practice & Research Clinical Endocrinology & Metabolism* **2008,** 22, 207-221.

14. Peltoketo, H.; Isomaa, V.; Maentausta, O.; Vihko, R. Complete amino-acid sequence of human placental 17-beta-hydroxysteroid dehydrogenase deduced from cDNA. *Febs Letters* **1988,** 239, 73-77.

15. The, V. L.; Labrie, C.; Zhao, H. F.; Couet, J.; Lachance, Y.; Simard, J.; Leblanc, G.; Cote, J.; Berube, D.; Gagne, R.; Labrie, F. Characterizaion of cDNAS for human estradiol 17-beta-dehydrogenase and assignment of the gene to chromosone-17 - evidence of 2 messenger-RNA species with distinct 5'-Termini in human-placenta. *Molecular Endocrinology* **1989,** 3, 1301-1309.

16. Geissler, W. M.; Davis, D. L.; Wu, L.; Bradshaw, K. D.; Patel, S.; Mendonca, B. B.; Elliston, K. O.; Wilson, J. D.; Russell, D. W.; Andersson, S. Male pseudohermaphroditism caused by mutations of testicular 17-beta-hydroxysteroid dehydrogenase-3. *Nature Genetics* **1994,** 7, 34-39.

17. Wu, L.; Einstein, M.; Geissler, W. M.; Chan, H. K.; Elliston, K. O.; Andersson, S. Expression cloning and characterization of human 17-beta-hydroxysteroid dehydrogenase type-2, a microsomal-enzyme possessing 20-alpha-hydroxysteroid dehydrogenase-activity. *Journal of Biological Chemistry* **1993,** 268, 12964-12969.

18. Adamski, J.; Normand, T.; Leenders, F.; Monte, D.; Begue, A.; Stehelin, D.; Jungblut, P. W.; Delaunoit, Y. Molecular-cloning of a novel widely expressed human 80 kDA 17-beta-hydroxysteroid dehydrogenase-IV. *Biochemical Journal* **1995,** 311, 437-443.

19. Dufort, I.; Rheault, P.; Huang, X. F.; Soucy, P.; Luu-The, V. Characteristics of a highly labile human type 5 17 beta-hydroxysteroid dehydrogenase. *Endocrinology* **1999,** 140, 568-574.

20. Nokelainen, P.; Peltoketo, H.; Vihko, R.; Vihko, P. Expression cloning of a novel estrogenic mouse 17 beta-hydroxysteroid dehydrogenase 17-ketosteroid reductase (m17-HSD7), previously described as a prolactin receptor-associated protein (PRAP) in rat. *Molecular Endocrinology* **1998,** 12, 1048-1059.

21. Krazeisen, A.; Breitling, R.; Imai, K.; Fritz, S.; Moller, G.; Adamski, J. Determination of cDNA, gene structure and chromosomal localization of the novel human 17 beta-hydroxysteroid dehydrogenase type 7. *Febs Letters* **1999,** 460, 373-379.

22. Fomitcheva, J.; Baker, M. E.; Anderson, E.; Lee, G. Y.; Aziz, N. Characterization of Ke 6, a new 17 beta-hydroxysteroid dehydrogenase, and its expression in gonadal tissues. *Journal of Biological Chemistry* **1998,** 273, 22664-22671.

23. Biswas, M. G.; Russell, D. W. Expression cloning and characterization of oxidative 17 beta- and 3 alpha-hydroxysteroid dehydrogenases from rat and human prostate. *Journal of Biological Chemistry* **1997,** 272, 15959-15966.

24. Napoli, J. L. 17 beta-Hydroxysteroid dehydrogenase type 9 and other short-chain dehydrogenases/reductases that catalyze retinoid, 17 beta- and 3 alpha-hydroxysteroid metabolism. *Molecular and Cellular Endocrinology* **2001,** 171, 103-109.

25. He, X. Y.; Merz, G.; Mehta, P.; Schulz, H.; Yang, S. Y. Human brain short chain L-3-hydroxyacyl coenzyme A dehydrogenase is a single-domain multifunctional enzyme - Characterization of a novel 17 beta-hydroxysteroid dehydrogenase. *Journal of Biological Chemistry* **1999,** 274, 15014-15019.

26. Li, K. X. Z.; Smith, R. E.; Krozowski, Z. S. Cloning and expression of a novel tissue specific 17 beta-hydroxysteroid dehydrogenase. *Endocrine Research* **1998,** 24, 663-667.

27. Luu-The, V.; Tremblay, P.; Labrie, F. Characterization of type 12 17 beta-hydroxysteroid dehydrogenase, an isoform of type 3 17 beta-hydroxysteroid dehydrogenase responsible for estradiol formation in women. *Molecular Endocrinology* **2006,** 20, 437-443.

28. Lukacik, P.; Keller, B.; Bunkoczi, G.; Kavanagh, K. L.; Lee, W. H.; Adamski, J.; Oppermann, U. Structural and biochemical characterization of human orphan DHRS10 reveals a novel cytosolic enzyme with steroid dehydrogenase activity (vol 402, pg 419, 2007). *Biochemical Journal* **2007,** 403, 615-615.

29. Lukacik, P.; Kavanagh, K. L.; Oppermann, U. Structure and function of human 17 beta-hydroxysteroid dehydrogenases. *Molecular and Cellular Endocrinology* **2006,** 248, 61-71.

30. Moghrabi, N.; Andersson, S. 17 beta-hydroxysteroid dehydrogenases: Physiological roles in health and disease. *Trends in Endocrinology and Metabolism* **1998,** 9, 265-270.

31. Mindnich, R.; Moller, G.; Adamski, J. The role of 17 beta-hydroxy steroid dehydrogenases. *Molecular and Cellular Endocrinology* **2004,** 218, 7-20.

32. Duax, W. L.; Ghosh, D.; Pletnev, V. Steroid dehydrogenase structures, mechanism of action, and disease. In *Vitamins and Hormones - Advances in Research and Applications* **2000,** 58, 121-+.

33. Ghosh, D.; Pletnev, V. Z.; Zhu, D. W.; Wawrzak, Z.; Duax, W. L.; Pangborn, W.; Labrie, F.; Lin, S. X. Structure of human estrogenic 17-beta-hydroxysteroid dehydrogenase at 2.20 angstrom resolution. *Structure* **1995,** 3, 503-513.

34. Labrie, F.; Luu-The, V.; Lin, S. X.; Simard, J.; Labrie, C. Role of 17 beta-hydroxysteroid dehydrogenases in sex steroid formation in peripheral intracrine tissues. *Trends in Endocrinology and Metabolism* **2000,** 11, 421-427.

35. Azzi, A.; Rehse, P. H.; Zhu, D. W.; Campbell, R. L.; Labrie, F.; Lin, S. X. Crystal structure of human estrogenic 17 beta-hydroxysteroid dehydrogenase complexed with 17 beta-estradiol. *Nature Structural Biology* **1996,** 3, 665-668.

36. Lin, S. X.; Han, Q.; Azzi, A.; Zhu, D. W.; Gongloff, A.; Campbell, R. L. 3D-structure of human estrogenic 17 beta-HSD1: binding with various steroids. *Journal of Steroid Biochemistry and Molecular Biology* **1999,** 69, 425-429.

37. Negri, M.; Recanatini, M.; Hartmann, R. W. Insights in 17β-HSD1 enzyme kinetics and ligand binding by dynamic motion investigation. *Plos One* **2010,** 5, article number e12026.

38. Suzuki, T.; Moriya, T.; Ariga, N.; Kaneko, C.; Kanazawa, M.; Sasano, H. 17β-Hydroxysteroid dehydrogenase type 1 and type 2 in human breast carcinoma: a correlation to clinicopathological parameters. *British Journal of Cancer,* **2000,** 82, 518-523.

39. Miyoshi, Y.; Ando, A.; Shiba, E.; Taguchi, T.; Tamaki, Y.; Noguchi, S. Involvement of up-regulation of 17 beta-hydroxysteroid dehydrogenase type 1 in maintenance of intratumoral high estradiol levels in postmenopausal breast cancers *International Journal of Cancer* **2001,** 94, 685-689.

40. Salhab, M.; Reed, M. J.; Al Sarakbi, W.; Jiang, W. G.; Mokbel, K. The role of aromatase and 17-beta-hydroxysteroid dehydrogenase type 1 mRNA expression in predicting the clinical outcome of human breast cancer. *Breast Cancer Research and Treatment* **2006,** 99, 155-162.

41. Vikho, P.; Herrala, A.; Harkonen, P,; Ismoaa, V.; Kaija, H.; Kurkela, R.; Pullka, A. Control of cell proliferation by steroids: The role of 17-HSDs. *Molecular and Cellular Endocrinology* **2006,** 248, 141-148.

42. Gunnarsson, C.; Helqvist, E.; Stål, O.; the Southeast Sweden Breast Cancer Group. 17β-Hydroxysteroid dehydrogenases involved in local oestrogen synthesis have prognostic significance in breast cancer. *British Journal of Cancer,* **2005,** 92, 547-552.

43. Allan, G. M.; Vicker, N.; Lawrence, H. R.; Tutill, H. J.; Day, J. M.; Huchet, M.; Ferrandis, E.; Reed, M. J.; Purohit, A.; Potter, B. V. L. Novel inhibitors of 17 beta-hydroxysteroid dehydrogenase type 1: Templates for design. *Bioorganic & Medicinal Chemistry* **2008,** 16, 4438-4456.

44. Frotscher, M. T.; Ziegler, E.; Marchais-Oberwinkler, S.; Kruchten, P.; Neugebauer, A.; Fetzer, L.; Scherer, C.; Mueller-Vieira, U.; Messinger, J.; Thole, H.; Hartmann, R. W. Design, synthesis, and biological evaluation of (hydroxyphenyl)naphthalene and -quinoline derivatives: Potent and selective nonsteroidal inhibitors of 17 beta-hydroxysteroid dehydrogenase type 1 (17 beta-HSD1) for the treatment of estrogen-dependent diseases. *Journal of Medicinal Chemistry* **2008,** 51, 2158-2169.

45. Bey, E.; Marchais-Oberwinkler, S.; Kruchten, P.; Frotscher, M.; Werth, R.; Oster, A.; Algul, O.; Neugebauer, A.; Hartmann, R. W. Design, synthesis and biological evaluation of bis(hydroxyphenyl) azoles as potent and selective non-steroidal inhibitors of 17 beta-hydroxysteroid dehydrogenase type 1 (17 beta-HSD1) for the treatment of estrogen-dependent diseases. *Bioorganic & Medicinal Chemistry* **2008,** 16, 6423-6435.

46. Vicker, N.; Lawrence, H. R.; Allan, G. M.; Bubert, C.; Smith, A.; Tutill, H. J.; Purohit, A.; Day, J. M.; Mahon, M. F.; Reed, M. J.; Potter, B. V. L. Focused libraries of 16-substituted estrone derivatives and modified E-ring steroids: Inhibitors of 17 beta-hydroxysteroid dehydrogenase type 1. *Chemmedchem* **2006,** 1, 464-481.

47. Allan, G. M.; Bubert, C.; Vicker, N.; Smith, A.; Tutill, H. J.; Purohit, A.; Reed, M. J.; Potter, B. V. L. Novel, potent inhibitors of 17 beta-hydroxy steroid dehydrogenase type 1. *Molecular and Cellular Endocrinology* **2006,** 248, 204-207.

48. Day, J. M.; Foster, P. A.; Tutill, H. J.; Parsons, M. F. C.; Newman, S. P.; Chander, S. K.; Allan, G. M.; Lawrence, H. R.; Vicker, N.; Potter, B. V. L.; Reed, M. J.; Purohit, A. 17 beta-hydroxysteroid dehydrogenase Type 1, and not Type 12, is a target for endocrine therapy of hormone-dependent breast cancer. *International Journal of Cancer* **2008,** 122, 1931-1940.

49. Laplante, Y.; Rancourt, C.; Poirier, D. Relative involvement of three 17 beta-hydroxysteroid dehydrogenases (types 1, 7 and 12) in the formation of estradiol in various breast cancer cell lines using selective inhibitors. *Molecular and Cellular Endocrinology* **2009,** 301, 146-153.

50. Luu-The, V. Analysis and characteristics of multiple types of human 17 beta-hydroxysteroid dehydrogenase. *Journal of Steroid Biochemistry and Molecular Biology* **2001,** 76, 143-151.

51. Casey, M. L.; Macdonald, P, C.; Andersson, S. 17-Beta-hydroxysteroid dehydrogenase type-2 - chromosonal assignment and progestin regulation of gene-expression in human endometrium. *Journal of Clinical Investigation* **1994,** 94, 2135-2144.

52. Moghrabi, N.; Head, J. R.; Andersson, S. Cell type-specific expression of 17 beta-hydroxysteroid dehydrogenase type 2 in human placenta and fetal liver. *Journal of Clinical Endocrinology and Metabolism* **1997,** 82, 3872-2878.

53. Mustonen, M.; Poutanen, M.; ChotteauLelievre, A.; deLaunoit, Y.; Isomaa, V.; Vainio, S.; Vihko, R.; Vihko, P. Ontogeny of 17 beta-hydroxysteroid dehydrogenase type 2 mRNA expression in the developing mouse placenta and fetus. *Molecular and Cellular Endocrinology* **1997,** 134, 33-40.

54. Mustonen, M. V. J.; Poutanen, M. H.; Kellokumpu, S.; de Launoit, Y.; Isomaa, V. V.; Vihko, R. K.; Vihko, P. T. Mouse 17 beta-hydroxysteroid dehydrogenase type 2 mRNA is predominantly expressed in hepatocytes and in surface epithelial cells of the gastrointestinal and urinary tracts. *Journal of Molecular Endocrinology* **1998,** 20, 67-74.

55. Peltoketo, H.; Luu-The, V.; Simard, J.; Adamski, J. 17 beta-Hydroxysteroid dehydrogenase (HSD)/17-ketosteroid reductase (KSR) family; nomenclature and main characteristics of the 17-HSD/KSR enzymes. *Journal of Molecular Endocrinology* **1999,** 23, 1-11.

56. Soronen, P.; Laiti, A.; Torn, S.; Harkonen, P.; Patrikainen, L.; Li, Y.; Pulkka, A.; Kurkela, R.; Herrala, A.; Kaija, H.; Isomaa, V.; Vihko, P. Sex steroid hormone metabolism and prostate cancer *Journal of Steroid Biochemistry and Molecular Biology* **2004,** 94, 281-286.

57. Vicker, N.; Sharland, C. M.; Heaton, W. B.; Ramos Gonzalez, A. M.; Bailey, H. V.; Smith, A.; Springall, J. S.; Day, J. M.; Tutill, H. J.; Reed, M. J.; Purohit, A.; Potter, B. V. L. The Design of Novel 17β-Hydroxysteroid Dehydrogenase Type 3 Inhibitors. *Molecular and Cellular Endocrinology* **2009,** 301 259-265.

58. Lin, H. K.; Jez, J. M.; Schlegel, B. P.; Peehl, D. M.; Pachter, J. A.; Penning, T. M. Expression and characterization of recombinant type 2 3 alpha hydroxysteroid dehydrogenase (HSD) from human prostate: Demonstration of bifunctional 3 alpha/17 beta-HSD activity and cellular distribution. *Molecular Endocrinology* **1997,** 11, 1971-1984.

59. Matsuura, K.; Shiraishi, H.; Haro, A.; Sato, K.; Deyashiki, Y.; Ninomiya, M.; Sakai, S. Identification of a principal mRNA species for human 3 alpha-hydroxysteroid dehydrogenase isoform (AKR1C3) that exhibits high prostaglandin D-2 11-ketoreductase activity. *Journal of Biochemistry* **1998,** 124, 940-946.

60. Penning, T. M.; Burczynski, M. E.; Jez, J. M.; Lin, H.K.; Ma, H. C.; Moore, M.; Ratnam, K.; Palackal, N. Structure-function aspects and inhibitor design of type 5 17 beta-hydroxysteroid dehydrogenase (AKR1C3). *Molecular and Cellular Endocrinology **2001,*** 171, 137-149.

61. Dufort, I.; Rheault, P.; Huang, X. F.; Soucy, P.; Luu-The, V. Characteristics of a highly labile human type 5 17 beta-hydroxysteroid dehydrogenase. *Endocrinology* **1999,** 140, 568-574.

62. Luu-The, V.; Dufort, I.; Pelletier, G.; Labrie, F. Type 5 17 beta-hydroxysteroid dehydrogenase: its role in the formation of androgens in women. *Molecular and Cellular Endocrinology* **2001,** 171, 77-82.

63. Song, D.; Liu, G.; Luu-The, V.; Zhao, D.; Wang, L.; Zhang, H.; Xueling, G.; Li, S.; Desi, L.; Labrie, F.; Pelletier, G. Expression of aromatase and 17 beta-hydroxysteroid dehydrogenase types 1, 7 and 12 in breast cancer - An immunocytochemical study. *Journal of Steroid Biochemistry and Molecular Biology* **2006,** 101, 136-144.

64. Torn, S.; Nokelainen, P.; Kurkela, R.; Pulkka, A.; Menjivar, M.; Ghosh, S.; Coca-Prados, M.; Peltoketo, H.; Isomaa, V.; Vihko, P. Production, purification, and functional analysis of recombinant human and mouse 17 beta-hydroxysteroid dehydrogenase type 7. *Biochemical and Biophysical Research Communications* **2003,** 305, 37-45.

65. Krusche, C. A.; Moller, G.; Beier, H. M.; Adamski, J. Expression and regulation of 17 beta-hydroxysteroid dehydrogenase 7 in the rabbit. *Molecular and Cellular Endocrinology* **2001,** 171, 169-177.

66. Husen, B.; Adamski, J.; Bruns, A.; Deluca, D.; Fuhrmann, K.; Moller, G.; Schwabe, I.; Einspanier, A. Characterization of 17 beta-hydroxysteroid dehydrogenase type 7 in reproductive tissues of the marmoset monkey. *Biology of Reproduction* **2003,** 68, 2092-2099.

67. Bellavance, E.; Luu-The, V.; Poirier, D. Potent and Selective Steroidal Inhibitors of 17 beta-Hydroxysteroid Dehydrogenase Type 7, an Enzyme That Catalyzes the Reduction of the Key Hormones Estrone and Dihydrotestosterone. *Journal of Medicinal Chemistry* **2009,** 52, 7488-7502.

68. Ohnesorg, T.; Keller, B.; Hrabe de Angelis, M.; Adamski, J. Transcriptional regulation of human and murine 17 beta-hydroxysteroid dehydrogenase type-7 confers its participation in cholesterol biosynthesis. *Journal of Molecular Endocrinology* **2006,** 37, 185-197.

69. Moon, Y. A.; Horton, J. D. Identification of two mammalian reductases involved in the two-carbon fatty acyl elongation cascade. *Journal of Biological Chemistry* **2003,** 278, 7335-7343.

70. Sakurai, N.; Miki, Y.; Suzuki, T.; Watanabe, K.; Narita, T.; Ando, K.; Yung, T. M. C. Systemic distribution and tissue localizations of human 17beta-hydroxysteroid dehydrogenase type 12. *Journal of Steroid Biochemistry and Molecular Biology* **2006,** 99, 174-181.

71. Lipinski, C. A.; Lombardo, F.; Dominy, B. W.; Feeney, P. J. Experimental and computational approaches to estimate solubility and permeability in drug discovery and development settings. *Advanced Drug Delivery Reviews,* **1997,** 23, 3-25.

72. Hillisch, A.; Gege, C.; Regenhardt, W.; Rosinius, A.; Adamski, J.; Moeller, G. Novel 2-substituted estra-1,3,5(10)-trien-17-ones used in a form of inhibitors of 17β-hydroxysteroid dehydrogenase of type 1. PCT Int. Appl. WO2006/003013A2, Jan 12, 2006 (Also US2006/0009434A1).

73. Gege, C.; Regenhardt, W.; Peters, O.; Hillisch, A.; Adamski, J.; Möller, G.; Deluca, D.; Elger, W.; Schneider, B. Novel 2-substituted D-homo-estra-1,3,5(10)-trienes as inhibitors of 17β-hydroxysteroid dehydrogenase type 1. PCT Int. Appl. WO2006/003012A1, Jan 12, 2006.

74. Zhu, B. T.; Lee, A. J. NADPH-dependent metabolism of 17 beta-estradiol and estrone to polar and nonpolar metabolites by human tissues and cytochrome P450 isoforms. *Steroids* **2005,** 70, 225-244.

75. Allan, G. M.; Lawrence, H. R.; Cornet, J.; Bubert, C.; Fischer, D. S.; Vicker, N.; Smith, A.; Tutill, H. J.; Purohit, A.; Day, J. M.; Mahon, M. F.; Reed, M. J.; Potter, B. V. L. Modification of estrone at the 6, 16, and 17 positions: Novel potent

inhibitors of 17 beta-hydroxysteroid dehydrogenase type 1. *Journal of Medicinal Chemistry* **2006,** 49, 1325-1345.

76. Breton, R.; Housset, D.; Mazza, C.; FontecillaCamps, J. C. The structure of a complex of human 17 beta-hydroxysteroid dehydrogenase with estradiol and NADP(+) identifies two principal targets for the design of inhibitors. *Structure* **1996,** 4, 905-915.

77. Berman, H. M.; Westbrook, J.; Feng, Z.; Gilliland, G.; Bhat, T. N.; Weissig, H.; Shindyalov, I. N.; Bourne, P. E. The Protein Data Bank. *Nucleic Acids Research* **2000,** 28, 235-242.

78. Fischer, D. S.; Allan, G. M.; Bubert, C.; Vicker, N.; Smith, A.; Tutill, H. J.; Purohit, A.; Wood, L.; Packham, G.; Mahon, M. F.; Reed, M. J.; Potter, B. V. L. E-ring modified steroids as novel potent inhibitors of 17β-hydroxysteroid dehydrogenase type 1. *Journal of Medicinal Chemistry* **2005,** 48, 5749-5770.

79. Poirier, D.; Dionne, P.; Auger, S. A. 6β-(Thiaheptanamide) derivative of estradiol as inhibitor of 17β-hydroxysteroid dehydrogenase type 1. *Journal of Steroid Biochemistry and Molecular Biology* **1998,** 64, 83-90.

80. Tremblay, M.R.; Boivin, R.P.; Luu-The, V.; Poirier, D. Inhibitors of type 1 17 beta-hydroxysteroid dehydrogenase with reduced estrogenic activity: Modifications of the positions 3 and 6 of estradiol. *Journal of enzyme inhibition and medicinal chemistry* **2005,** 20, 153-163.

81. Cadot, C.; Laplante, Y.; Kamal, F.; Luu-The, V.; Poirier, D. C6-(N,N-butyl-methyl-heptanamide) derivatives of estrone and estradiol as inhibitors of type 1 17 beta-hydroxysteroid dehydrogenase: Chemical synthesis and biological evaluation. *Bioorganic and medicinal chemistry* **2007,** 15 714-726.

82. Auger, S.; Merand, Y.; Pelletier, J. D.; Poirier, D.; Labrie, F. Synthesis and biological-activities of thioether derivatives related to the antiestrogens tamoxifen and ICI-164384. *Journal of Steroid Biochemistry and Molecular Biology* **1995,** 52, 547-565.

83. Messinger, J.; Thole, H.-H.; Husen, B.; Van Steen, B. J.; Schneider, G.; Hulshof, J. B. E.; Koskimies, P.; Johansson, N.; Adamski, J. Novel 17β-hydroxysteroid dehydrogenase type 1 inhibitors. PCT Int. Appl. WO 2005/047303 A2, May 26, 2005.

84. Messinger, J,; Husen, B.; Schoen, U.; Thole, H. H.; Koskimies, P.; Unkila, M.; Substituted estratrien derivatives As 17 beta -HSD inhibitors. PCT INT. Appl. WO2008/065100, June 05, 2008.

85. Messinger, J.; Husen, B.; Koskimies, P.; Hirvela, L.; Kallio, L.; Saarenketo,P.; Thole, H. Estrone C15 derivatives-A new class of 17 beta-hydroxysteroid dehydrogenase type 1 inhibitors. *Journal of Molecular and Cellular Endocrinology* **2009,** 301, 216-234.

86. Husen, B.; Huhtinen, K.; Poutanen, M.; Kangas, L.; Messinger, J.; Thole, H. Evaluation of inhibitors for 17 beta-hydroxysteroid dehydrogenase type 1 in vivo in immunodeficient mice inoculated with MCF-7 cells stably expressing the recombinant human enzyme. *Molecular and Cellular Endocrinology* **2006,** 248, 109-113.

87. Sweet, F.; Warren, J. C.; Arias, F. Affinity labeling of steroid binding-sites - synthesis of 16 alpha-bromoacetoxyprogesterone and its use for affinity labeling of 20 beta-hydroxysteroid dehydrogenase. *Journal of Biological Chemistry* **1972,** 247, 3424-3433.

88. Strickler, R. C.; Sweet, F.; Warren, J. C. Affinity labeling of steroid binding-sites - study of active-site of 20-beta hydroxysteroid dehydrogenase with 2-alpha-bromoacetoxyprogesterone and 11-alpha-bromoacetoxyprogesterone. *Journal of Biological Chemistry* **1975,** 250, 7656-7662.

89. Arias, F.; Sweet, F.; Warren, J. C. Affinity labeling of steroid binding-sites - study of active-site of 20-beta-hydroxysteroid dehydrogenase with 6-beta and 11-alpha-bromoacetoxyprogesterone. *Journal of Biological Chemistry* **1973,** 248, 5641-5647.

90. Chin, C.-C.; Warren, J. C. Synnthesis of 16α-bromoacetoxyestradiol 3-methyl ether and the study of the steroid binding site of human placental estradiol 17β-dehydrogenase. *Journal of Biological Chemistry*, **1975,** 250, 7682-7686.

91. Pelletier, J. D.; Poirier, D. Synthesis and evaluation of estradiol derivatives with 16α-(bromoalkylamide), 16α-(bromoalkyl) or 16α-(bromoalkynyl) side chains as inhibitors of 17β-hydroxysteroid dehydrogenase type 1 without estrogenic activity. *Bioorganic and Medicinal Chemistry*, **1996,** 4, 1617-1628.

92. Pelletier, J. D.; Labrier, F.; Poirier, D. *N*-Butyl, *N*-methyl, 11-[3′,17′β-(dihydroxy)-1,3,5,(10H)-estratrien-16Hα-yl]-bromo undecanamide: synthesis and 17β--HSD inhibiting, estrogenic and antiestrogenic activities, *Steroids*, **1994,** 59, 536-547.

93. Qiu, W.; Campbell, R. L.; Gangloff, A.; Dupuis, P.; Boivin, R. P.; Tremblay, M. R.; Poirier, D.; Lin, S. X. A concerted, rational design of type 1 17 beta-hydroxysteroid dehydrogenase inhibitors: estradiol-adenosine hybrids with high affinity. *Faseb Journal* **2002,** 16, 1829-+.

94. Poirier, D.; Boivin, R. P.; Berube, M.; Lin, S.-X. Syntheis of the first estradiol-adenosine hybrid compound. *Synthetic Communications* **2003,** 18, 3183-3192.

95. Berube, M.; Poirier, D. Synthesis of simplified hybrid inhibitors of type 1 17β-hydroxysteroid dehydrogenase via cross-metathesis and Sonogashira coupling reactions. *Organic Letters* **2004,** 6, 3127-3130.

96. Poirier, D.; Boivin, R. P.; Tremblay, M.; Berube, M.; Qiu, W.; Lin, S.-X. Estradiol-adenosine hybrid compounds designed to inhibit 17β-hydroxysteroid dehydrogenase. *Journal of Medicinal Chemistry* **2005,** 48, 8134-8147.

97. Fournier, D.; Poirier, D.; Mazumdar, M.; Lin, S. X. Design and synthesis of bisubstrate inhibitors of type 1 17 beta-hydroxysteroid dehydrogenase: Overview and perspectives. *European Journal of Medicinal Chemistry* **2008,** 43, 2298-2306.

98. Jin, J. Z.; Lin, S. X. Human estrogenic 17 beta-hydroxysteroid dehydrogenase: Predominance of estrone reduction and its induction by NADPH. *Biochemical and Biophysical Research Communications* **1999,** 259, 489-493.

99. Bérubé, M.; Poirier, D. Improved synthesis of EM-1745, preparation of its C17-ketone analogue and comparison of their inhibitory potency on 17β-hydroxysteroid dehydrogenase type 1. *Journal of Enzyme Inhibition and Medicinal Chemistry* **2009,** 24, 832-843.

100. Poirier, D.; Chang, H.; Azzi, A.; Boivin, R. P.; Lin, S. X. Estrone and estradiol C-16 derivatives as inhibitors of type 1 17 beta-hydroxysteroid dehydrogenase. *Molecular and Cellular Endocrinology* **2006,** 248, 236-238.

101. Laplante, Y.; Cadot, C.; Fournier, M.; Poirier, D. Estradiol and estrone C-16 derivatives as inhibitors of type 1 17 beta-hydroxysteroid dehydrogenase: Blocking of ER+ breast cancer cell proliferation induced by estrone. *Bioorganic and Medicinal Chemistry* **2008,** 16, 1849-1860.

102. Cushman, M.; He, H. M.; Katzenellenbogen, J. A.; Varma, R. K.; Hamel, E.; Lin, C. M.; Ram, S.; Sachdeva, Y. P. Synthesis of analogs of 2-methoxyestradiol with enhanced inhibitory effects on tubulin polymerization and cancer cell growth. *Journal of Medicinal Chemistry* **1997,** 40, 2323-2334.

103. Merriam, G. R.; Maclusky, N. J.; Johnson, L. A.; Naftolin, F. 2-Hydroxyestradiol-17-alpha and 4-hydroxyestradiol-17-alpha, catechol estrogen analogs with reduced estrogen-receptor affinity. *Steroids* **1980,** 36, 13-20.

104. Lawrence, H. R.; Vicker, N.; Allan, G. M.; Smith, A.; Mahon, M. F.; Tutill, H. J.; Purohit, A.; Reed, M. J.; Potter, B. V. L. Novel and potent 17 beta-hydroxysteroid dehydrogenase type 1 inhibitors. *Journal of Medicinal Chemistry* **2005,** 48, 2759-2762.

105. Wakeling, A. E.; Bowler, J. Steroidal pure antiestrogens. *Journal of Endocrinology* **1987,** 112, R7-R10.

106. Thomas, J. L.; LaRochelle, M. C.; Covey, D. F.; Strickler, R. C. Inactivation of human placental 17β,20α-hydroxysteroid dehydrogenase by 16-methylene estrone, an affinity alkylator enzymatically generated from 16-methylene estradiol-17β. *Journal of Biological Chemistry,* **1983,** 258, 11500-11504.

107. Leese, M. P.; Hejaz, H. A. M.; Mahon, M. F.; Newman, S. P.; Purohit, A.; Reed, M. J.; Potter, B. V. L. A-ring-substituted estrogen-3-O-sulfamates: Potent

multitargeted anticancer agents. *Journal of Medicinal Chemistry* **2005,** 48, 5243-5256.

108. Rao, P. N.; Cessac, J. W.; Tinley, T. L.; Mooberry, S. L. Synthesis and antimitotic activity of novel 2-methoxyestradiol analogs. *Steroids* **2002,** 67, 1079-1089.

109. Shiau, A. K.; Barstad, D.; Loria, P. M.; Cheng, L.; Kushner, P. J.; Agard, D. A.; Greene, G. L. The structural basis of estrogen receptor/coactivator recognition and the antagonism of this interaction by tamoxifen. *Cell* **1998,** 95, 927-937.

110. Stauffer, S. R.; Coletta, C. J.; Tedesco, R.; Nishiguchi, G.; Carlson, K.; Sun, J.; Katzenellenbogen, B. S.; Katzenellenbogen, J. A. Pyrazole ligands: Structure-affinity/activity relationships and estrogen receptor-alpha-selective agonists. *Journal of Medicinal Chemistry* **2000,** 43, 4934-4947.

111. Sweet, F.; Boyd, J.; Medina, O.; Konderski, L.; Murdock, G. L. Hydrogen-bonding in steroidogenisis - studies on new heterocyclic-analogs of estrone that inhibit human estradiol 17-beta-dehydrogenase. *Biochemical and Biophysical Research Communications* **1991,** 180, 1057-1063.

112. Vicker, N.; Allan, G. M.; Lawrence, H. R. R.; Day, J. M.; Purohit, A.; Reed, M. J.; Potter, B. V. L. Diaryl Compounds as Non-Steroidal Inhibitors of 17-Beta Hydroxysteroid Dehydrogenase And/Or Steroid Sulphatase for the Treatment of Oestrogen-Related Diseases Such as Hormone Dependent Breast Cancer. PCT Int. Appl. WO2007096647.

113. Allan, G. M.; Vicker, N.; Lawrence, H. R.; Tutill, H. J.; Day, J. M.; Hutchet, M.; Ferandis, E.; Reed, M. J.; Purohit, A.; Potter, B. V. L. P. Novel Inhibitors of 17β-Hydroxysteroid dehydrogenase type 1: Templates for design. *Bioorganic and Medicinal Chemistry* **2008,** 16, 4438-4456.

114. Marchais-Oberwinkler, S.; Kruchten, P.; Frotscher, M.; Ziegler, E.; Neugebauer, A.; Bhoga, U.; Bey, E.; Mueller-Vieira, U.; Messinger, J.; Thole, H.; Hartmann, R. W. Substituted 6-phenyl-2-naphthols. Potent and selective nonsteroidal inhibitors of 17 beta-hydroxysteroid dehydrogenase type 1 (17 beta--HSD1): Design, synthesis, biological evaluation, and pharmacokinetics. *Journal of Medicinal Chemistry* **2008,** 51, 4685-4698.

115. Marchais-Oberwinkler, S.; Frotscher, M.; Ziegler, E.; Werth, R.; Kruchten, P.; Messinger, J.; Thole, H.; Hartmann, R. W. Structure-activity study in the class of 6-(3 '-hydroxyphenyl)naphthalenes leading to an optimization of a pharmacophore model for 17 beta-hydroxysteroid dehydrogenase type 1 (17 beta--HSD1) inhibitors. *Molecular and Cellular Endocrinology* **2009,** 301, 205-211.

116. Bey, E.; Marchais-Oberwinkler, S.; Werth, R.; Al-Soud, Y. A.; Kruchten, P.; Oster, A.; Frotscher, M.; Birk, B.; Hartmann, R. W. Design, Synthesis, Biological Evaluation and Pharmacokinetics of Bis(hydroxyphenyl) substituted Azoles, Thiophenes, Benzenes, and Aza-Benzenes as Potent and Selective Nonsteroidal

Inhibitors of 17 beta-Hydroxysteroid Dehydrogenase Type 1 (17 beta--HSD1). *Journal of Medicinal Chemistry* **2008,** 51, 6725-6739.

117. Al-Soud, Y. A.; Bey, E.; Oster, A.; Marchais-Oberwinkler, S.; Werth, R.; Kruchten, P.; Frotscher, M.; Hartmann, R. W. The role of the heterocycle in bis(hydroxyphenyl)triazoles for inhibition of 17 beta-Hydroxysteroid Dehydrogenase (17 beta--HSD) type 1 and type 2. *Molecular and Cellular Endocrinology* **2009,** 301, 212-215.

118. Bey, E.; Marchais-Oberwinkler, S.; Negri, M.; Kruchten, P.; Oster, A.; Klein, T.; Spadaro, A.; Werth, R.; Frotscher, M.; Birk, B.; Hartmann, R. W. New Insights into the SAR and Binding Modes of Bis(hydroxyphenyl)thiophenes and -benzenes: Influence of Additional Substituents on 17 beta-Hydroxysteroid Dehydrogenase Type 1 (17 beta--HSD1) Inhibitory Activity and Selectivity. *Journal of Medicinal Chemistry* **2009,** 52, 6724-6743.

119. Jeong, E. J.; Liu, X.; Jia, X. B.; Chen, J.; Hu, M. Coupling of conjugating enzymes and efflux transporters: Impact on bioavailability and drug interactions. *Current Drug Metabolism* **2005,** 6, 455-468.

120. Oster, A.; Klein, T.; Werth, R.; Kruchten, P.; Bey, E.; Negri, M.; Marchais-Oberwinkler, S.; Frotscher, M.; Hartmann, R. W. Novel estrone mimetics with high 17 beta--HSD1 inhibitory activity. *Bioorganic and Medicinal Chemistry* **2010,** 18, 3494-3505.

121. Oster, A.; Hinsberger, S.; Werth, R.; Marchais-Oberwinkler, S.; Frotscher, M.; Hartmann, R. W. Bicyclic Substituted Hydroxyphenylmethanones as Novel Inhibitors of 17 beta-Hydroxysteroid Dehydrogenase Type 1 (17 beta--HSD1) for the Treatment of Estrogen-Dependent Diseases. *Journal of Medicinal Chemistry* **2010,** 53, 8176-8186.

122. Vihko, P.; Isomaa, V.; Ghosh, D. Structure and function of 17β-hydroxysteroid dehydrogenase type 1 and type 2. *Molecular and Cellular Endocrinology,* **2001,** 171, 71-76.

123. Lilienkampf, A.; Karkola, S.; Alho-Richmond, S.; Koskimies, P.; Johansson, N.; Huhtinen, K.; Vihko, K.; Wähälä, K. Synthesis and Biological Evaluation of 17β-Hydroxysteroid Dehydrogenase Type 1 (17β--HSD1) Inhibitors Based on a Thieno[2,3-d]pyrimidin-4(3H)-one Core. *Journal of Medicinal Chemistry* **2009,** 52, 6660-6671.

124. Alho-Richmond, S.; Lilienkampf, A.; Wähälä, K. Active site analysis of 17β-hydroxysteroid dehydrogenase type 1 enzyme complexes with SPROUT. *Molecular and Cellular Endocrinology,* **2006,** 248, 208-213.

125. Patton, T. L. ESTROGENS .2. The synthesis of 2-dialkylaminomethylestrogens. *Journal of Organic Chemistry* **1960,** 25, 2148-2151.

126. Pomeroy, J. H.; Craig, C. A. 2 New syntheses of nitriles from aldehydes, using O,N-bis-(trifluoroacetyl)-hydroxylamine or trifluoroacetohydroxamic acid. *Journal of the American Chemical Society* **1959,** 81, 6340-6341.

127. Mappus, E.; Chambon, C.; Fenet, B.; de Ravel, M. R.; Grenot, C.; Cuilleron, C. Y. Synthesis of (5-azido-2-nitrobenzoyl)amido, (4-azido-2-nitrophenyl)amino, and (5-azido-2-nitro-3,4,6-trifluorophenyl)amino derivatives of 17 alpha-methylamino-, 17 alpha-ethylamino-, and 17 alpha-propylamino-5 alpha-dihydrotestosterone as reagents of different linker lengths for the photoaffinity labeling of sex hormone binding globulins and androgen receptors. *Steroids* **2000,** 65, 459-481.

128. Mazza, C.; Breton, R.; Housset, D.; Fontecilla-Camps, J. C. Unusual charge stabilization of NADP(+) in 17 beta-hydroxysteroid dehydrogenase. *Journal of Biological Chemistry* **1998,** 273, 8145-8152.

129. Dunigan, D. D.; Waters, S. B.; Owen, T. C. Aqueous soluble tetrazolium/formazan MTS as an indicator of NADH-dependent and NADPH-dependent dehydrogenase-activity. *Biotechniques* **1995,** 19, 640-649.

130. Puranen, T.; Poutanen, M.; Ghosh, D.; Vihko, P.; Vihko, R. Characterization of structural and functional properties of human 17 beta-hydroxysteroid dehydrogenase type 1 using recombinant enzymes and site-directed mutagenesis. *Molecular Endocrinology* **1997,** 11, 77-86.

131. Sawicki, M. W.; Erman, M.; Puranen, T.; Vihko, P.; Ghosh, D. Structure of the ternary complex of human 17β-hydroxysteroid dehydrogenase type 1 with 3-hydroxyestra-1,3,5,7-tetraen-17-one (equilin) and $NADP^+$ *Prot natl acad sci usa* 1999 96 840-845.

132. Cornish-Bowden, A. Fundamentals of Enzyme Kinetics 3rd Edition. *Portland Press* ISBN: 1-85578-158-1

133. Aka, J. A.; Mazumdar, M.; Chen, C. Q.; Poirier, D.; Lin, S. X. 17 beta-Hydroxysteroid Dehydrogenase Type 1 Stimulates Breast Cancer by Dihydrotestosterone Inactivation in Addition to Estradiol Production. *Molecular Endocrinology* **2010,** 24, 832-845.

134. Han, Q.; Campbell, R. L.; Gangloff, A.; Huang, Y. W.; Lin, S. X. Dehydroepiandrosterone and dihydrotestosterone recognition by human estrogenic 17β-hydroxysteroid dehydrogenase. *Journal of Biological Chemistry* **2000,** 275, 1105-1111.

135. Gangloff, A.; Shi, R.; Nahoum, V.; Lin, S. X. Pseudo-symmetry of C19-steroids, alternative binding orientations and multispecificity in human estrogenic 17 beta-hydroxysteroid dehydrogenase. *FASEB* **2003,** 17, 274-276.

136. Shi, R.; Lin, S. X. Cofactor hydrogen bonding onto the protein main chain is conserved in the short chain dehydrogenase/reductase family and contributes to nicotinamide orientation. *Journal of Biological Chemistry* **2004,** 279, 16778-16785.

137. Mazumdar, M.; Fournier, D.; Zhu, D. W.; Cadot, C.; Poirier, D.; Lin, S. X. Binary and ternary crystal structure analyses of a novel inhibitor with 17 beta--HSD type 1: a lead compound for breast cancer therapy. *Biochemical Journal* **2009,** 424, 357-366.

138. Otwinowski, Z.; Minor, W. Processing of X-ray diffraction data collected in oscillation mode. *Methods in Enzymology* **1997**, 307-326.

139. Chander, S. K.; Purohit, A.; Woo, L. W. L.; Potter, B. V. L.; Reed, M. J. The role of steroid sulphatase in regulating the oestrogenicity of oestrogen sulphamates. *Biochemical and Biophysical Research Communications* **2004,** 322, 217-222.

140. Murshudov, G. N.; Vagin, A. A.; Dodson, E. J. Refinement of macromolecular structures by the maximum-likelihood method. *Acta Crystallographica Section D-Biological Crystallography* **1997,** 53, 240-255.

141. Emsley, P.; Cowtan, K. Coot: model-building tools for molecular graphics. *Acta Crystallographica Section D-Biological Crystallography* **2004,** 60, 2126-2132.

142. Bubert, C.; Leese, M. P.; Mahon, M. F.; Ferrandis, E.; Regis-Lydi, S.; Kasprzyk, P. G.; Newman, S. P.; Ho, Y. T.; Purohit, A.; Reed, M. J.; Potter, B. V. L. 3,17-Disubstituted 2-Alkylestra-1,3,5(10)-trien-3-ol Derivatives: Synthesis, In Vitro and In Vivo Anticancer Activity. *Journal of Medicinal Chemistry* **2007,** 50, 4431-4443.

143. Wong, F. F.; Tseng, W. C.; Chuang, S. H.; Yang, S. C.; Lin, Y. H.; Huang, J. J.; Lin, S. K. One-pot ethynylation and catalytic desilyation in synthesis of mestranol and levonorgestrel. *Tetrahedron* **2010,** 66, 4068 – 4072.

144. Reed, M. J.; Potter, B. V. L. Methods for treating or preventing cancer by preventing, inhibiting, or arresting cell cycling. PCT Int. Appl. US2006/122161A1, Jun 08, 2006.

145. Page, P. C.; Moore, J. P.; Mansfield, I.; McKenzie, M. J.; Bowler, W. B.; Gallagher, J. A. Synthesis of bone-targeted oestrgenic compounds for the inhibition of bone resorption. *Tetrahedron* **2001,** 57, 1837 - 1848

Appendix 1: X-ray Crystallography Data

Table 1: Crystal data and structure refinement.

Identification code	k10farm3
Empirical formula	C22 H27 N O2
Formula weight	337.45
Temperature	150(2) K
Wavelength	0.71073 Å
Crystal system	Triclinic
Space group	P1
Unit cell dimensions	a = 8.2610(1)Å □ = 83.531(1)°
	b = 8.3050(2)Å □ = 75.204(1)°
	c = 14.2860(3)Å □ = 79.068(1)°
Volume	928.30(3) $Å^3$
Z	2
Density (calculated)	1.207 Mg/m^3
Absorption coefficient	0.076 mm^{-1}
F(000)	364
Crystal size	0.45 x 0.40 x 0.35 mm
Theta range for data collection	3.74 to 27.49°
Index ranges	-10<=h<=10; -10<=k<=10; -18<=l<=18
Reflections collected	17910
Independent reflections	7997 [R(int) = 0.0267]
Reflections observed (>2□)	6933
Data Completeness	0.993
Absorption correction	Semi-empirical from equivalents
Max. and min. transmission	0.835 and 0.808
Refinement method	Full-matrix least-squares on F^2
Data / restraints / parameters	7997 / 33 / 498
Goodness-of-fit on F^2	1.038
Final R indices [I>2□(I)]	R1 = 0.0475 wR2 = 0.1185
R indices (all data)	R1 = 0.0587 wR2 = 0.1270
Absolute structure parameter	0.3(10)
Largest diff. peak and hole	0.471 and -0.260 $eÅ^{-3}$

Notes: There are two molecules in the asymmetric unit of this structure. The ethyl and ethoxy groups attached to C2' and C3' (respectively) are disordered over two proximate positions in a 50:50 ratio. Distance and ADP restraints were applied to partial disordered atoms.

Table 2: Atomic coordinates (x 10^4) and equivalent isotropic displacement parameters ($Å^2$ x 10^3). U(eq) is defined as one third of the trace of the orthogonalized Uij tensor.

Atom	x	y	z	U(eq)
O(1)	6012(2)	6256(2)	8722(1)	48(1)
O(2)	12468(2)	-5462(2)	5888(1)	38(1)
O(1')	1313(3)	-1559(3)	3836(2)	66(1)
O(2')	12782(7)	3427(9)	585(5)	53(2)

O(2*)	12714(7)	3814(10)	860(5)	54(2)
N(1)	8467(4)	7638(3)	10268(2)	66(1)
N(1')	-2110(3)	1719(3)	5181(2)	63(1)
C(1)	9475(3)	-1748(2)	6515(1)	31(1)
C(2)	10195(3)	-3256(2)	6140(1)	32(1)
C(3)	11791(3)	-3968(2)	6293(1)	33(1)
C(4)	12597(3)	-3205(2)	6806(2)	33(1)
C(5)	11863(2)	-1665(2)	7169(1)	31(1)
C(6)	12858(3)	-837(3)	7677(2)	39(1)
C(7)	12251(3)	1006(3)	7693(2)	36(1)
C(8)	10321(2)	1363(2)	8076(1)	29(1)
C(9)	9462(2)	804(2)	7355(1)	30(1)
C(10)	10270(2)	-921(2)	7035(1)	29(1)
C(11)	7521(3)	1054(3)	7738(2)	36(1)
C(12)	6779(3)	2861(3)	7946(2)	36(1)
C(13)	7655(2)	3467(2)	8624(1)	31(1)
C(14)	9602(2)	3174(2)	8207(1)	28(1)
C(15)	10258(3)	4190(2)	8817(2)	34(1)
C(16)	8974(3)	5814(2)	8824(1)	34(1)
C(17)	7302(3)	5309(3)	8724(1)	35(1)
C(18)	7109(3)	2697(3)	9670(2)	40(1)
C(19)	14219(3)	-6047(3)	5833(2)	46(1)
C(1')	9684(3)	887(3)	1498(2)	52(1)
C(2')	11195(3)	1444(4)	1067(2)	70(1)
C(3')	11255(3)	3084(4)	1186(2)	57(1)
C(4')	9848(3)	4084(3)	1688(2)	41(1)
C(5')	8340(3)	3488(3)	2105(2)	35(1)
C(6')	6832(3)	4681(3)	2609(2)	46(1)
C(7')	5158(3)	4139(2)	2664(2)	39(1)
C(8')	5221(2)	2355(2)	3082(1)	29(1)
C(9')	6574(3)	1204(2)	2395(1)	32(1)
C(10')	8232(3)	1855(3)	2028(1)	33(1)
C(11')	6726(3)	-559(3)	2856(2)	47(1)
C(12')	5040(3)	-1204(3)	3110(2)	50(1)
C(13')	3615(3)	-16(2)	3723(2)	36(1)
C(14')	3556(2)	1730(2)	3234(1)	31(1)
C(15')	1871(3)	2685(3)	3784(2)	40(1)
C(16')	669(3)	1438(3)	3816(2)	45(1)
C(17')	1811(3)	-291(3)	3811(2)	45(1)
C(19')	12703(15)	5164(10)	530(8)	60(3)
C(19*)	12793(16)	5522(11)	830(7)	53(2)
C(2A)	9392(3)	-4091(3)	5531(2)	40(1)
C(16A)	8695(3)	6836(3)	9638(2)	43(1)
C(17A)	3810(3)	-135(3)	4774(2)	46(1)
C(2A')	12963(5)	565(7)	660(5)	58(2)
C(2A*)	12413(7)	290(6)	318(3)	49(1)
C(2B)	7709(3)	-3188(3)	5377(2)	54(1)
C(2B')	13912(7)	-601(7)	718(4)	53(1)
C(2B*)	12878(8)	-1066(9)	544(5)	71(2)
C(16C)	-877(3)	1581(3)	4592(2)	46(1)

Table 3: Bond lengths [Å] and angles [^{o}].

O(1)-C(17)	1.199(3)	O(2)-C(3)	1.385(2)
O(2)-C(19)	1.421(3)	O(1')-C(17')	1.195(3)
O(2')-C(3')	1.392(4)	O(2')-C(19')	1.425(6)
O(2*)-C(3')	1.402(4)	O(2*)-C(19*)	1.427(6)
N(1)-C(16A)	1.136(3)	N(1')-C(16C)	1.139(3)
C(1)-C(2)	1.384(3)	C(1)-C(10)	1.411(3)
C(1)-H(1)	0.9500	C(2)-C(3)	1.399(3)
C(2)-C(2A)	1.511(3)	C(3)-C(4)	1.377(3)
C(4)-C(5)	1.403(3)	C(4)-H(4)	0.9500
C(5)-C(10)	1.394(3)	C(5)-C(6)	1.519(3)
C(6)-C(7)	1.519(3)	C(6)-H(6A)	0.9900
C(6)-H(6B)	0.9900	C(7)-C(8)	1.529(3)
C(7)-H(7A)	0.9900	C(7)-H(7B)	0.9900
C(8)-C(14)	1.523(3)	C(8)-C(9)	1.544(3)
C(8)-H(8)	1.0000	C(9)-C(10)	1.528(3)
C(9)-C(11)	1.537(3)	C(9)-H(9)	1.0000
C(11)-C(12)	1.541(3)	C(11)-H(11A)	0.9900
C(11)-H(11B)	0.9900	C(12)-C(13)	1.524(3)
C(12)-H(12A)	0.9900	C(12)-H(12B)	0.9900
C(13)-C(17)	1.519(3)	C(13)-C(14)	1.547(3)
C(13)-C(18)	1.548(3)	C(14)-C(15)	1.532(3)
C(14)-H(14)	1.0000	C(15)-C(16)	1.549(3)
C(15)-H(15A)	0.9900	C(15)-H(15B)	0.9900
C(16)-C(16A)	1.461(3)	C(16)-C(17)	1.561(3)
C(16)-H(16)	1.0000	C(18)-H(18A)	0.9800
C(18)-H(18B)	0.9800	C(18)-H(18C)	0.9800
C(19)-H(19A)	0.9800	C(19)-H(19B)	0.9800
C(19)-H(19C)	0.9800	C(1')-C(2')	1.383(4)
C(1')-C(10')	1.402(3)	C(1')-H(1')	0.9500
C(2')-C(3')	1.403(5)	C(2')-C(2A')	1.504(3)
C(2')-C(2A*)	1.547(3)	C(3')-C(4')	1.378(3)
C(4')-C(5')	1.393(3)	C(4')-H(4')	0.9500
C(5')-C(10')	1.395(3)	C(5')-C(6')	1.512(3)
C(6')-C(7')	1.515(3)	C(6')-H(6'1)	0.9900
C(6')-H(6'2)	0.9900	C(7')-C(8')	1.530(3)
C(7')-H(7'1)	0.9900	C(7')-H(7'2)	0.9900
C(8')-C(14')	1.517(3)	C(8')-C(9')	1.541(2)
C(8')-H(8')	1.0000	C(9')-C(10')	1.514(3)
C(9')-C(11')	1.533(3)	C(9')-H(9')	1.0000
C(11')-C(12')	1.529(4)	C(11')-H(11C)	0.9900
C(11')-H(11D)	0.9900	C(12')-C(13')	1.535(3)
C(12')-H(12C)	0.9900	C(12')-H(12D)	0.9900
C(13')-C(17')	1.522(3)	C(13')-C(14')	1.535(3)
C(13')-C(17A)	1.541(3)	C(14')-C(15')	1.532(3)
C(14')-H(14')	1.0000	C(15')-C(16')	1.554(3)
C(15')-H(15C)	0.9900	C(15')-H(15D)	0.9900
C(16')-C(16C)	1.458(3)	C(16')-C(17')	1.561(4)
C(16')-H(16')	1.0000	C(19')-H(19D)	0.9800
C(19')-H(19E)	0.9800	C(19')-H(19F)	0.9800
C(19*)-H(19G)	0.9800	C(19*)-H(19H)	0.9800
C(19*)-H(19I)	0.9800	C(2A)-C(2B)	1.506(3)

C(2A)-H(2A1)	0.9900	C(2A)-H(2A2)	0.9900
C(17A)-H(17A)	0.9800	C(17A)-H(17B)	0.9800
C(17A)-H(17C)	0.9800	C(2A')-C(2B')	1.134(7)
C(2A')-H(2A3)	0.9900	C(2A')-H(2A4)	0.9900
C(2A*)-C(2B*)	1.156(8)	C(2A*)-H(2A5)	0.9900
C(2A*)-H(2A6)	0.9900	C(2B)-H(2B1)	0.9800
C(2B)-H(2B2)	0.9800	C(2B)-H(2B3)	0.9800
C(2B')-H(2B4)	0.9800	C(2B')-H(2B5)	0.9800
C(2B')-H(2B6)	0.9800	C(2B*)-H(2B7)	0.9800
C(2B*)-H(2B8)	0.9800	C(2B*)-H(2B9)	0.9800
C(3)-O(2)-C(19)	116.65(16)	C(3')-O(2')-C(19')	107.1(7)
C(3')-O(2*)-C(19*)	126.5(7)	C(2)-C(1)-C(10)	123.20(18)
C(2)-C(1)-H(1)	118.4	C(10)-C(1)-H(1)	118.4
C(1)-C(2)-C(3)	117.25(17)	C(1)-C(2)-C(2A)	123.11(18)
C(3)-C(2)-C(2A)	119.52(17)	C(4)-C(3)-O(2)	123.93(18)
C(4)-C(3)-C(2)	121.15(18)	O(2)-C(3)-C(2)	114.93(17)
C(3)-C(4)-C(5)	120.94(19)	C(3)-C(4)-H(4)	119.5
C(5)-C(4)-H(4)	119.5	C(10)-C(5)-C(4)	119.52(17)
C(10)-C(5)-C(6)	121.90(17)	C(4)-C(5)-C(6)	118.56(18)
C(7)-C(6)-C(5)	112.14(17)	C(7)-C(6)-H(6A)	109.2
C(5)-C(6)-H(6A)	109.2	C(7)-C(6)-H(6B)	109.2
C(5)-C(6)-H(6B)	109.2	H(6A)-C(6)-H(6B)	107.9
C(6)-C(7)-C(8)	109.88(17)	C(6)-C(7)-H(7A)	109.7
C(8)-C(7)-H(7A)	109.7	C(6)-C(7)-H(7B)	109.7
C(8)-C(7)-H(7B)	109.7	H(7A)-C(7)-H(7B)	108.2
C(14)-C(8)-C(7)	113.98(16)	C(14)-C(8)-C(9)	106.83(15)
C(7)-C(8)-C(9)	109.54(16)	C(14)-C(8)-H(8)	108.8
C(7)-C(8)-H(8)	108.8	C(9)-C(8)-H(8)	108.8
C(10)-C(9)-C(11)	114.49(16)	C(10)-C(9)-C(8)	112.20(15)
C(11)-C(9)-C(8)	111.28(15)	C(10)-C(9)-H(9)	106.1
C(11)-C(9)-H(9)	106.1	C(8)-C(9)-H(9)	106.1
C(5)-C(10)-C(1)	117.91(17)	C(5)-C(10)-C(9)	121.76(16)
C(1)-C(10)-C(9)	120.10(16)	C(9)-C(11)-C(12)	111.49(17)
C(9)-C(11)-H(11A)	109.3	C(12)-C(11)-H(11A)	109.3
C(9)-C(11)-H(11B)	109.3	C(12)-C(11)-H(11B)	109.3
H(11A)-C(11)-H(11B)	108.0	C(13)-C(12)-C(11)	110.71(16)
C(13)-C(12)-H(12A)	109.5	C(11)-C(12)-H(12A)	109.5
C(13)-C(12)-H(12B)	109.5	C(11)-C(12)-H(12B)	109.5
H(12A)-C(12)-H(12B)	108.1	C(17)-C(13)-C(12)	115.86(16)
C(17)-C(13)-C(14)	101.05(15)	C(12)-C(13)-C(14)	110.14(16)
C(17)-C(13)-C(18)	105.00(16)	C(12)-C(13)-C(18)	111.09(17)
C(14)-C(13)-C(18)	113.36(16)	C(8)-C(14)-C(15)	121.82(16)
C(8)-C(14)-C(13)	112.11(15)	C(15)-C(14)-C(13)	104.03(15)
C(8)-C(14)-H(14)	105.9	C(15)-C(14)-H(14)	105.9
C(13)-C(14)-H(14)	105.9	C(14)-C(15)-C(16)	100.72(16)
C(14)-C(15)-H(15A)	111.6	C(16)-C(15)-H(15A)	111.6
C(14)-C(15)-H(15B)	111.6	C(16)-C(15)-H(15B)	111.6
H(15A)-C(15)-H(15B)	109.4	C(16A)-C(16)-C(15)	117.20(18)
C(16A)-C(16)-C(17)	112.62(18)	C(15)-C(16)-C(17)	105.38(16)

C(16A)-C(16)-H(16)	107.0	C(15)-C(16)-H(16)	107.0
C(17)-C(16)-H(16)	107.0	O(1)-C(17)-C(13)	128.5(2)
O(1)-C(17)-C(16)	124.1(2)	C(13)-C(17)-C(16)	107.38(16)
C(13)-C(18)-H(18A)	109.5	C(13)-C(18)-H(18B)	109.5
H(18A)-C(18)-H(18B)	109.5	C(13)-C(18)-H(18C)	109.5
H(18A)-C(18)-H(18C)	109.5	H(18B)-C(18)-H(18C)	109.5
O(2)-C(19)-H(19A)	109.5	O(2)-C(19)-H(19B)	109.5
H(19A)-C(19)-H(19B)	109.5	O(2)-C(19)-H(19C)	109.5
H(19A)-C(19)-H(19C)	109.5	H(19B)-C(19)-H(19C)	109.5
C(2')-C(1')-C(10')	124.3(3)	C(2')-C(1')-H(1')	117.9
C(10')-C(1')-H(1')	117.9	C(1')-C(2')-C(3')	116.8(2)
C(1')-C(2')-C(2A')	132.4(4)	C(3')-C(2')-C(2A')	109.3(3)
C(1')-C(2')-C(2A*)	113.2(4)	C(3')-C(2')-C(2A*)	128.1(3)
C(2A')-C(2')-C(2A*)	31.2(2)	C(4')-C(3')-O(2')	131.9(4)
C(4')-C(3')-O(2*)	114.8(4)	O(2')-C(3')-O(2*)	21.5(3)
C(4')-C(3')-C(2')	120.7(2)	O(2')-C(3')-C(2')	106.4(4)
O(2*)-C(3')-C(2')	124.4(4)	C(3')-C(4')-C(5')	121.0(2)
C(3')-C(4')-H(4')	119.5	C(5')-C(4')-H(4')	119.5
C(4')-C(5')-C(10')	120.39(19)	C(4')-C(5')-C(6')	117.7(2)
C(10')-C(5')-C(6')	121.84(18)	C(5')-C(6')-C(7')	112.41(18)
C(5')-C(6')-H(6'1)	109.1	C(7')-C(6')-H(6'1)	109.1
C(5')-C(6')-H(6'2)	109.1	C(7')-C(6')-H(6'2)	109.1
H(6'1)-C(6')-H(6'2)	107.9	C(6')-C(7')-C(8')	109.51(18)
C(6')-C(7')-H(7'1)	109.8	C(8')-C(7')-H(7'1)	109.8
C(6')-C(7')-H(7'2)	109.8	C(8')-C(7')-H(7'2)	109.8
H(7'1)-C(7')-H(7'2)	108.2	C(14')-C(8')-C(7')	113.65(16)
C(14')-C(8')-C(9')	106.73(15)	C(7')-C(8')-C(9')	110.38(16)
C(14')-C(8')-H(8')	108.7	C(7')-C(8')-H(8')	108.7
C(9')-C(8')-H(8')	108.7	C(10')-C(9')-C(11')	115.27(17)
C(10')-C(9')-C(8')	112.66(16)	C(11')-C(9')-C(8')	109.99(16)
C(10')-C(9')-H(9')	106.1	C(11')-C(9')-H(9')	106.1
C(8')-C(9')-H(9')	106.1	C(5')-C(10')-C(1')	116.8(2)
C(5')-C(10')-C(9')	121.78(17)	C(1')-C(10')-C(9')	121.1(2)
C(12')-C(11')-C(9')	112.56(19)	C(12')-C(11')-H(11C)	109.1
C(9')-C(11')-H(11C)	109.1	C(12')-C(11')-H(11D)	109.1
C(9')-C(11')-H(11D)	109.1	H(11C)-C(11')-H(11D)	107.8
C(11')-C(12')-C(13')	111.35(18)	C(11')-C(12')-H(12C)	109.4
C(13')-C(12')-H(12C)	109.4	C(11')-C(12')-H(12D)	109.4
C(13')-C(12')-H(12D)	109.4	H(12C)-C(12')-H(12D)	108.0
C(17')-C(13')-C(14')	101.14(17)	C(17')-C(13')-C(12')	116.19(19)
C(14')-C(13')-C(12')	110.03(17)	C(17')-C(13')-C(17A)	105.22(18)
C(14')-C(13')-	113.70(18)	C(12')-C(13')-	110.35(19)

C(17A)		C(17A)	
C(8')-C(14')-C(15')	121.75(17)	C(8')-C(14')-C(13')	112.53(16)
C(15')-C(14')-C(13')	104.33(16)	C(8')-C(14')-H(14')	105.7
C(15')-C(14')-H(14')	105.7	C(13')-C(14')-H(14')	105.7
C(14')-C(15')-C(16')	100.11(18)	C(14')-C(15')-H(15C)	111.8
C(16')-C(15')-H(15C)	111.8	C(14')-C(15')-H(15D)	111.8
C(16')-C(15')-H(15D)	111.8	H(15C)-C(15')-H(15D)	109.5
C(16C)-C(16')-C(15')	116.2(2)	C(16C)-C(16')-C(17')	114.0(2)
C(15')-C(16')-C(17')	105.34(19)	C(16C)-C(16')-H(16')	106.9
C(15')-C(16')-H(16')	106.9	C(17')-C(16')-H(16')	106.9
O(1')-C(17')-C(13')	128.5(3)	O(1')-C(17')-C(16')	124.3(2)
C(13')-C(17')-C(16')	107.14(18)	O(2*)-C(19*)-H(19G)	109.5
O(2*)-C(19*)-H(19H)	109.5	H(19G)-C(19*)-H(19H)	109.5
O(2*)-C(19*)-H(19I)	109.5	H(19G)-C(19*)-H(19I)	109.5
H(19H)-C(19*)-H(19I)	109.5	C(2B)-C(2A)-C(2)	115.30(19)
C(2B)-C(2A)-H(2A1)	108.4	C(2)-C(2A)-H(2A1)	108.4
C(2B)-C(2A)-H(2A2)	108.4	C(2)-C(2A)-H(2A2)	108.4
H(2A1)-C(2A)-H(2A2)	107.5	N(1)-C(16A)-C(16)	179.4(3)
C(13')-C(17A)-H(17A)	109.5	C(13')-C(17A)-H(17B)	109.5
H(17A)-C(17A)-H(17B)	109.5	C(13')-C(17A)-H(17C)	109.5
H(17A)-C(17A)-H(17C)	109.5	H(17B)-C(17A)-H(17C)	109.5
C(2B')-C(2A')-C(2')	145.0(7)	C(2B')-C(2A')-H(2A3)	100.6
C(2')-C(2A')-H(2A3)	100.6	C(2B')-C(2A')-H(2A4)	100.6
C(2')-C(2A')-H(2A4)	100.6	H(2A3)-C(2A')-H(2A4)	104.3
C(2B*)-C(2A*)-C(2')	120.8(5)	C(2B*)-C(2A*)-H(2A5)	107.1
C(2')-C(2A*)-H(2A5)	107.1	C(2B*)-C(2A*)-H(2A6)	107.1
C(2')-C(2A*)-H(2A6)	107.1	H(2A5)-C(2A*)-H(2A6)	106.8
C(2A)-C(2B)-H(2B1)	109.5	C(2A)-C(2B)-H(2B2)	109.5
H(2B1)-C(2B)-H(2B2)	109.5	C(2A)-C(2B)-H(2B3)	109.5
H(2B1)-C(2B)-H(2B3)	109.5	H(2B2)-C(2B)-H(2B3)	109.5

C(2A*)-C(2B*)-H(2B7)	109.5	C(2A*)-C(2B*)-H(2B8)	109.5
H(2B7)-C(2B*)-H(2B8)	109.5	C(2A*)-C(2B*)-H(2B9)	109.5
H(2B7)-C(2B*)-H(2B9)	109.5	H(2B8)-C(2B*)-H(2B9)	109.5
N(1')-C(16C)-C(16')	178.0(3)		

Symmetry transformations used to generate equivalent atoms.

Table 4: Anisotropic displacement parameters ($Å^2$ x 10^3). The anisotropic displacement factor exponent takes the form: -2 gpi^2 [h^2 a^{*2} U11 + ... + 2 h k a* b* U

Atom	U11	U22	U33	U23	U13	U12
O(1)	42(1)	39(1)	60(1)	-6(1)	-11(1)	3(1)
O(2)	39(1)	29(1)	45(1)	-10(1)	-6(1)	-3(1)
O(1')	79(1)	56(1)	69(1)	-6(1)	-3(1)	-41(1)
O(2')	28(2)	59(4)	49(4)	7(3)	18(2)	3(2)
O(2*)	30(2)	77(5)	42(3)	-17(2)	14(2)	-3(2)
N(1)	86(2)	49(1)	68(2)	-27(1)	-31(1)	7(1)
N(1')	36(1)	76(2)	69(2)	16(1)	-8(1)	-10(1)
C(1)	33(1)	30(1)	31(1)	1(1)	-8(1)	-6(1)
C(2)	40(1)	28(1)	28(1)	0(1)	-8(1)	-8(1)
C(3)	40(1)	24(1)	32(1)	-1(1)	-2(1)	-7(1)
C(4)	31(1)	27(1)	36(1)	-2(1)	-2(1)	-6(1)
C(5)	31(1)	30(1)	32(1)	-2(1)	-3(1)	-9(1)
C(6)	31(1)	35(1)	55(1)	-12(1)	-12(1)	-4(1)
C(7)	32(1)	34(1)	43(1)	-11(1)	-6(1)	-8(1)
C(8)	31(1)	26(1)	30(1)	-2(1)	-4(1)	-9(1)
C(9)	31(1)	30(1)	28(1)	-2(1)	-5(1)	-6(1)
C(10)	31(1)	26(1)	28(1)	-2(1)	-3(1)	-6(1)
C(11)	31(1)	35(1)	44(1)	-10(1)	-7(1)	-6(1)
C(12)	31(1)	36(1)	41(1)	-6(1)	-9(1)	-3(1)
C(13)	32(1)	29(1)	29(1)	-1(1)	-3(1)	-5(1)
C(14)	33(1)	28(1)	24(1)	-2(1)	-4(1)	-8(1)
C(15)	38(1)	29(1)	36(1)	-4(1)	-7(1)	-7(1)
C(16)	43(1)	27(1)	32(1)	-2(1)	-7(1)	-7(1)
C(17)	40(1)	34(1)	29(1)	-2(1)	-4(1)	-5(1)
C(18)	41(1)	39(1)	32(1)	0(1)	2(1)	-9(1)
C(19)	36(1)	36(1)	62(2)	-15(1)	1(1)	-5(1)
C(1')	47(1)	47(1)	46(1)	-2(1)	6(1)	8(1)
C(2')	44(2)	71(2)	66(2)	15(1)	15(1)	14(1)
C(3')	26(1)	85(2)	47(1)	22(1)	-1(1)	-2(1)
C(4')	32(1)	54(1)	36(1)	4(1)	-8(1)	-10(1)
C(5')	28(1)	43(1)	32(1)	-4(1)	-6(1)	-5(1)
C(6')	35(1)	34(1)	62(1)	-15(1)	5(1)	-9(1)
C(7')	29(1)	27(1)	55(1)	-7(1)	0(1)	-2(1)
C(8')	26(1)	25(1)	34(1)	-5(1)	-6(1)	-1(1)
C(9')	33(1)	29(1)	31(1)	-7(1)	-5(1)	-2(1)
C(10')	30(1)	41(1)	27(1)	-5(1)	-7(1)	2(1)

C(11')	47(1)	29(1)	51(1)	-5(1)	4(1)	3(1)
C(12')	61(2)	28(1)	55(1)	-10(1)	5(1)	-9(1)
C(13')	39(1)	29(1)	38(1)	-4(1)	-5(1)	-7(1)
C(14')	30(1)	32(1)	31(1)	-4(1)	-6(1)	-7(1)
C(15')	27(1)	39(1)	50(1)	1(1)	-7(1)	-5(1)
C(16')	35(1)	61(2)	41(1)	9(1)	-12(1)	-17(1)
C(17')	52(1)	48(1)	39(1)	-3(1)	-6(1)	-22(1)
C(19')	31(3)	83(6)	68(6)	14(4)	-7(4)	-28(4)
C(19*)	37(3)	66(4)	60(5)	13(4)	-18(4)	-23(3)
C(2A)	48(1)	33(1)	42(1)	-5(1)	-15(1)	-10(1)
C(16A)	53(1)	29(1)	46(1)	-7(1)	-15(1)	0(1)
C(17A)	52(1)	44(1)	38(1)	5(1)	-9(1)	-8(1)
C(2A')	31(2)	77(3)	75(3)	-44(3)	-13(2)	-6(2)
C(2A*)	43(2)	59(3)	41(2)	12(2)	-13(2)	-3(2)
C(2B)	48(1)	53(2)	71(2)	-16(1)	-24(1)	-12(1)
C(2B')	40(2)	59(3)	63(3)	-12(2)	-16(2)	-6(2)
C(2B*)	60(3)	77(3)	71(3)	-24(3)	2(3)	-12(3)
C(16C)	33(1)	60(2)	47(1)	13(1)	-16(1)	-14(1)

Table 5: Hydrogen coordinates (x 10^4) and isotropic displacement parameters ($Å^2$ x 10^3).

Atom	x	y	z	U(eq)
H(1)	8392	-1245	6418	38
H(4)	13665	-3729	6915	39
H(6A)	12742	-1322	8351	47
H(6B)	14076	-1050	7339	47
H(7A)	12572	1530	7030	43
H(7B)	12801	1474	8115	43
H(8)	10006	727	8714	35
H(9)	9688	1563	6759	36
H(11A)	7228	347	8341	44
H(11B)	7006	716	7252	44
H(12A)	6931	3552	7328	43
H(12B)	5547	2963	8246	43
H(14)	9795	3732	7540	34
H(15A)	11434	4364	8506	41
H(15B)	10209	3671	9480	41
H(16)	9406	6492	8220	41
H(18A)	7614	3175	10102	60
H(18B)	7498	1506	9679	60
H(18C)	5868	2923	9892	60
H(19A)	14888	-5225	5466	69
H(19B)	14569	-7075	5505	69
H(19C)	14406	-6243	6489	69
H(1')	9626	-225	1430	63
H(4')	9908	5197	1751	49
H(6'1)	6845	5776	2254	55
H(6'2)	6932	4790	3274	55
H(7'1)	4942	4234	2008	47
H(7'2)	4221	4857	3082	47
H(8')	5533	2265	3720	35

H(9')	6120	1186	1811	38
H(11C)	7580	-1288	2400	56
H(11D)	7134	-596	3454	56
H(12C)	5173	-2289	3473	60
H(12D)	4728	-1353	2504	60
H(14')	3410	1641	2569	37
H(15C)	1534	3735	3426	48
H(15D)	1916	2902	4443	48
H(16')	311	1623	3189	54
H(19D)	11705	5708	296	91
H(19E)	13732	5460	81	91
H(19F)	12616	5517	1176	91
H(19G)	11911	6162	529	79
H(19H)	13911	5725	448	79
H(19I)	12609	5850	1491	79
H(2A1)	10192	-4247	4889	48
H(2A2)	9234	-5194	5844	48
H(17A)	2889	624	5158	69
H(17B)	4905	156	4776	69
H(17C)	3761	-1262	5057	69
H(2A3)	12972	622	-38	70
H(2A4)	13639	1405	706	70
H(2A5)	11852	285	-217	59
H(2A6)	13435	804	41	59
H(2B1)	6861	-3151	5999	81
H(2B2)	7344	-3760	4924	81
H(2B3)	7826	-2065	5109	81
H(2B4)	14814	-364	986	80
H(2B5)	14406	-1014	72	80
H(2B6)	13334	-1434	1146	80
H(2B7)	12890	-1168	1232	106
H(2B8)	14027	-1423	153	106
H(2B9)	12110	-1755	437	106

Table 6: Dihedral angles [^{o}]

Atom1 - Atom2 - Atom3 - Atom4	Dihedral
C(10) - C(1) - C(2) - C(3)	-0.1(3)
C(10) - C(1) - C(2) - C(2A)	-176.09(19)
C(19) - O(2) - C(3) - C(4)	-13.4(3)
C(19) - O(2) - C(3) - C(2)	166.32(19)
C(1) - C(2) - C(3) - C(4)	0.8(3)
C(2A) - C(2) - C(3) - C(4)	176.95(19)
C(1) - C(2) - C(3) - O(2)	-178.87(17)
C(2A) - C(2) - C(3) - O(2)	-2.7(3)
O(2) - C(3) - C(4) - C(5)	177.83(18)
C(2) - C(3) - C(4) - C(5)	-1.8(3)
C(3) - C(4) - C(5) - C(10)	2.1(3)
C(3) - C(4) - C(5) - C(6)	-176.39(19)
C(10) - C(5) - C(6) - C(7)	-19.6(3)
C(4) - C(5) - C(6) - C(7)	158.81(18)
C(5) - C(6) - C(7) - C(8)	50.6(2)

C(6) - C(7) - C(8) - C(14)	174.77(17)
C(6) - C(7) - C(8) - C(9)	-65.6(2)
C(14) - C(8) - C(9) - C(10)	171.08(14)
C(7) - C(8) - C(9) - C(10)	47.2(2)
C(14) - C(8) - C(9) - C(11)	-59.17(19)
C(7) - C(8) - C(9) - C(11)	176.93(16)
C(4) - C(5) - C(10) - C(1)	-1.4(3)
C(6) - C(5) - C(10) - C(1)	177.08(19)
C(4) - C(5) - C(10) - C(9)	-175.85(17)
C(6) - C(5) - C(10) - C(9)	2.6(3)
C(2) - C(1) - C(10) - C(5)	0.4(3)
C(2) - C(1) - C(10) - C(9)	174.99(17)
C(11) - C(9) - C(10) - C(5)	-144.74(18)
C(8) - C(9) - C(10) - C(5)	-16.7(2)
C(11) - C(9) - C(10) - C(1)	40.9(2)
C(8) - C(9) - C(10) - C(1)	168.96(16)
C(10) - C(9) - C(11) - C(12)	-174.11(16)
C(8) - C(9) - C(11) - C(12)	57.4(2)
C(9) - C(11) - C(12) - C(13)	-54.1(2)
C(11) - C(12) - C(13) - C(17)	168.04(17)
C(11) - C(12) - C(13) - C(14)	54.2(2)
C(11) - C(12) - C(13) - C(18)	-72.3(2)
C(7) - C(8) - C(14) - C(15)	-54.2(2)
C(9) - C(8) - C(14) - C(15)	-175.35(16)
C(7) - C(8) - C(14) - C(13)	-178.27(16)
C(9) - C(8) - C(14) - C(13)	60.60(19)
C(17) - C(13) - C(14) - C(8)	177.37(15)
C(12) - C(13) - C(14) - C(8)	-59.6(2)
C(18) - C(13) - C(14) - C(8)	65.6(2)
C(17) - C(13) - C(14) - C(15)	43.89(17)
C(12) - C(13) - C(14) - C(15)	166.91(16)
C(18) - C(13) - C(14) - C(15)	-67.93(19)
C(8) - C(14) - C(15) - C(16)	-172.78(16)
C(13) - C(14) - C(15) - C(16)	-45.08(18)
C(14) - C(15) - C(16) - C(16A)	154.63(19)
C(14) - C(15) - C(16) - C(17)	28.47(19)
C(12) - C(13) - C(17) - O(1)	35.5(3)
C(14) - C(13) - C(17) - O(1)	154.5(2)
C(18) - C(13) - C(17) - O(1)	-87.5(3)
C(12) - C(13) - C(17) - C(16)	-143.90(17)
C(14) - C(13) - C(17) - C(16)	-24.92(19)
C(18) - C(13) - C(17) - C(16)	93.16(18)
C(16A) - C(16) - C(17) - O(1)	49.6(3)
C(15) - C(16) - C(17) - O(1)	178.50(19)
C(16A) - C(16) - C(17) - C(13)	-131.00(18)
C(15) - C(16) - C(17) - C(13)	-2.1(2)
C(10') - C(1') - C(2') - C(3')	0.7(4)
C(10') - C(1') - C(2') - C(2A')	165.2(4)
C(10') - C(1') - C(2') - C(2A*)	-165.1(3)
C(19') - O(2') - C(3') - C(4')	-1.0(8)
C(19') - O(2') - C(3') - O(2*)	-43.2(19)
C(19') - O(2') - C(3') - C(2')	167.5(5)
C(19*) - O(2*) - C(3') - C(4')	-13.1(9)

C(19*) - O(2*) - C(3') - O(2')	133(3)
C(19*) - O(2*) - C(3') - C(2')	169.9(6)
C(1') - C(2') - C(3') - C(4')	-1.7(4)
C(2A') - C(2') - C(3') - C(4')	-169.6(4)
C(2A*) - C(2') - C(3') - C(4')	161.7(3)
C(1') - C(2') - C(3') - O(2')	-171.7(4)
C(2A') - C(2') - C(3') - O(2')	20.3(5)
C(2A*) - C(2') - C(3') - O(2')	-8.4(6)
C(1') - C(2') - C(3') - O(2*)	175.2(5)
C(2A') - C(2') - C(3') - O(2*)	7.2(7)
C(2A*) - C(2') - C(3') - O(2*)	-21.5(7)
O(2') - C(3') - C(4') - C(5')	168.2(5)
O(2*) - C(3') - C(4') - C(5')	-176.0(5)
C(2') - C(3') - C(4') - C(5')	1.1(4)
C(3') - C(4') - C(5') - C(10')	0.6(3)
C(3') - C(4') - C(5') - C(6')	-177.5(2)
C(4') - C(5') - C(6') - C(7')	156.6(2)
C(10') - C(5') - C(6') - C(7')	-21.4(3)
C(5') - C(6') - C(7') - C(8')	50.9(3)
C(6') - C(7') - C(8') - C(14')	175.97(17)
C(6') - C(7') - C(8') - C(9')	-64.2(2)
C(14') - C(8') - C(9') - C(10')	169.39(16)
C(7') - C(8') - C(9') - C(10')	45.4(2)
C(14') - C(8') - C(9') - C(11')	-60.5(2)
C(7') - C(8') - C(9') - C(11')	175.54(18)
C(4') - C(5') - C(10') - C(1')	-1.6(3)
C(6') - C(5') - C(10') - C(1')	176.5(2)
C(4') - C(5') - C(10') - C(9')	-174.52(19)
C(6') - C(5') - C(10') - C(9')	3.5(3)
C(2') - C(1') - C(10') - C(5')	0.9(4)
C(2') - C(1') - C(10') - C(9')	173.9(3)
C(11') - C(9') - C(10') - C(5')	-143.1(2)
C(8') - C(9') - C(10') - C(5')	-15.7(3)
C(11') - C(9') - C(10') - C(1')	44.3(3)
C(8') - C(9') - C(10') - C(1')	171.62(19)
C(10') - C(9') - C(11') - C(12')	-173.77(18)
C(8') - C(9') - C(11') - C(12')	57.5(2)
C(9') - C(11') - C(12') - C(13')	-52.4(3)
C(11') - C(12') - C(13') - C(17')	165.3(2)
C(11') - C(12') - C(13') - C(14')	51.2(3)
C(11') - C(12') - C(13') - C(17A)	-75.1(3)
C(7') - C(8') - C(14') - C(15')	-50.9(3)
C(9') - C(8') - C(14') - C(15')	-172.76(18)
C(7') - C(8') - C(14') - C(13')	-175.74(17)
C(9') - C(8') - C(14') - C(13')	62.3(2)
C(17') - C(13') - C(14') - C(8')	178.25(16)
C(12') - C(13') - C(14') - C(8')	-58.4(2)
C(17A) - C(13') - C(14') - C(8')	66.0(2)
C(17') - C(13') - C(14') - C(15')	44.3(2)
C(12') - C(13') - C(14') - C(15')	167.69(19)
C(17A) - C(13') - C(14') - C(15')	-68.0(2)
C(8') - C(14') - C(15') - C(16')	-174.36(18)
C(13') - C(14') - C(15') - C(16')	-45.8(2)

C(14') - C(15') - C(16') - C(16C)	156.31(19)
C(14') - C(15') - C(16') - C(17')	29.1(2)
C(14') - C(13') - C(17') - O(1')	152.9(3)
C(12') - C(13') - C(17') - O(1')	33.8(4)
C(17A) - C(13') - C(17') - O(1')	-88.6(3)
C(14') - C(13') - C(17') - C(16')	-24.6(2)
C(12') - C(13') - C(17') - C(16')	-143.6(2)
C(17A) - C(13') - C(17') - C(16')	94.0(2)
C(16C) - C(16') - C(17') - O(1')	51.0(3)
C(15') - C(16') - C(17') - O(1')	179.5(2)
C(16C) - C(16') - C(17') - C(13')	-131.4(2)
C(15') - C(16') - C(17') - C(13')	-2.9(2)
C(1) - C(2) - C(2A) - C(2B)	-1.6(3)
C(3) - C(2) - C(2A) - C(2B)	-177.5(2)
C(15) - C(16) - C(16A) - N(1)	-174(100)
C(17) - C(16) - C(16A) - N(1)	-52(36)
C(1') - C(2') - C(2A') - C(2B')	-30.0(13)
C(3') - C(2') - C(2A') - C(2B')	135.4(10)
C(2A*) - C(2') - C(2A') - C(2B')	-91.5(11)
C(1') - C(2') - C(2A*) - C(2B*)	-58.5(8)
C(3') - C(2') - C(2A*) - C(2B*)	137.6(7)
C(2A') - C(2') - C(2A*) - C(2B*)	76.6(8)
C(15') - C(16') - C(16C) - N(1')	96(9)
C(17') - C(16') - C(16C) - N(1')	-142(9)

Symmetry transformations used to generate equivalent atoms.